



Rock mass parameters governing the hydraulic erodibility of rock in unlined spillways

By

Lamine Boumaiza

A thesis submitted to *l'Université du Québec à Chicoutimi* in partial fulfillment of the requirements for the degree of Doctor of Philosophy in Earth and Atmospheric Sciences

Department of Applied Sciences, *Université du Québec à Chicoutimi*
Saguenay, Quebec, Canada

© Lamine Boumaiza 2019

ABSTRACT

Among the methods used for evaluating the potential hydraulic erodibility of rock, the most common are those based on the correlation between the force of flowing water and the capacity of a rock to resist erosion. The capacity of a rock to resist erosion is evaluated based on erodibility indices that are determined from specific rock mass parameters, such as the unconfined compressive strength of intact rock, rock block size, joints shear strength, and relative block structure. To quantify the latter parameter, a concept of fractured systems was proposed to develop a mathematical expression that accounted for the rock block's shape and orientation relative to the direction of flow. The initial concept for assessing relative block structure considered that a geological formation is mainly fractured by two joint sets that formed an orthogonal fracture system. In this thesis, an adjusted concept is proposed to determine the relative block structure when the fractured systems are non-orthogonal. An analysis of the proposed relative block structure rating shows that considering a non-orthogonal fracture system has a significant effect on evaluating rock resistance capacity and, as a consequence, assessing the hydraulic erodibility of rock. In this thesis, a review of the existing methods for evaluating the hydraulic erodibility of rock, based on the correlation between the force of flowing water and the capacity of a rock to resist erosion, is undertaken to determine the committed error associated with each existing method. Accordingly, it is identified that there is no clear consensus on which rock mass parameters are indeed relevant for evaluating the hydraulic erodibility of rock, and the key rock mass parameters to be used for assessing the hydraulic erodibility of rock mass remain uncertain. Using a dataset from case studies of eroded unlined spillways, a developed method is proposed for determining the relevant rock mass parameters for evaluating the hydraulic erodibility of rock. The unconfined compressive strength is found to not be a relevant rock mass parameter. Furthermore, using the rock block volume measurement instead of the rock block size parameter improves the quantification of rock block size. The retained rock mass parameters are rock block volume, rock block's shape, and orientation relative to flow direction, as well as the nature of the potentially eroding surface, joints opening, joints shear strength, and rock mass deformation modulus. The other question was related to the degree of importance of these selected rock mass parameters in the erosion mechanism. Accordingly, a method is developed for determining the relative importance of the relevant rock mass parameters for evaluating the hydraulic erodibility of rock. In terms of relative importance, the rock mass parameters are classified in the order of 1) joints shear strength, 2) nature of the potentially eroding surface, 3) rock block volume, 4) joints opening, 5) rock block's shape and orientation relative to the direction of flow, and 6) the rock mass deformation modulus. This order of relative importance agrees largely with that established from field observations.

RÉSUMÉ ÉTENDU

La construction de barrages nécessite la mise en place de structures hydrauliques permettant de contrôler le niveau d'eau et d'assurer ainsi la sécurité des barrages. Ces structures de contrôle pour l'évacuation de l'eau lors des périodes de crues sont quelque part équipées d'un canal déversoir excavé dans le roc, appelé évacuateur de crues. En général, le roc de ces déversoirs est initialement considéré comme étant résistant face à la force érosive de l'eau qui s'y coule. Cependant, l'utilisation réelle des déversoirs rocheux indique que la résistance du roc face à la force de l'écoulement peut être mal évaluée, tel que perçu au déversoir rocheux du barrage de Mokolo en Afrique du Sud, et celui du barrage de Copeton en Australie. Ce phénomène d'érodabilité hydraulique du roc pourrait affecter la stabilité de l'ouvrage hydraulique. Face à ce problème d'érosion hydraulique, plusieurs méthodes ont été proposées pour évaluer l'érodabilité hydraulique du roc. Cependant, une forme spécifique est actuellement utilisée en particulier pour évaluer le potentiel d'érosion hydraulique lors de la conception des déversoirs rocheux. En effet, l'industrie appelle largement aux méthodes du « seuil d'érodabilité ». Ces méthodes, telles que la méthode d'Annandale et celles de Pells, se basent sur une corrélation entre l'énergie hydraulique générée par la force de l'eau qui coule sur le déversoir rocheux (habituellement appelée: puissance hydraulique disponible), et la capacité de résistance du roc étant déterminée à l'aide d'indices d'érodabilité. Ces derniers pourraient être évalués en fonction de certains paramètres caractérisant le massif rocheux, tels que: la résistance matricielle de la roche intacte, la taille des blocs rocheux, la résistance au cisaillement des discontinuités, l'ouverture des joints, la nature de la surface potentiellement érodée, et structure relative des blocs qui prend en compte l'effet de la forme et de l'orientation des blocs rocheux relativement à la direction de l'écoulement de l'eau.

Pour quantifier le paramètre de la structure relative des blocs, une expression mathématique avait été proposée, en assumant que la formation géologique est principalement fracturée par deux familles de joints, formant ainsi un système de fracturation orthogonale. Un angle de 90° est alors maintenu entre les plans des deux familles de joints. Ce concept de fracturation orthogonale est, cependant, appliqué à tout cas, y compris aux systèmes non orthogonaux, en assumant ainsi une certaine imprécision quant à l'évaluation de la capacité de résistance du massif rocheux. Un concept ajusté est proposé dans le cadre de cette thèse pour déterminer la

structure relative des blocs lorsque le système est de fracturation non orthogonale (l'angle entre les plans des deux familles de joints est supérieur ou inférieur à 90°). Deux équations sont proposées dans cette thèse, dont une s'applique lorsque les blocs rocheux sont orientés dans le même sens que celui de la direction de l'écoulement, tandis que la deuxième équation s'applique lorsque les blocs sont orientés contre la direction de l'écoulement. Dans le cadre de cette thèse, une analyse de la nouvelle pondération de la structure relative des blocs pour les systèmes de fracturation non orthogonaux a montré que le fait de considérer un système orthogonal, à la place d'un système réellement non orthogonal, a un effet significatif sur l'évaluation de l'érodabilité hydraulique du roc.

La méthode d'Annandale s'appuie sur un indice d'érodabilité (Indice de Kirsten) initialement développé pour évaluer la capacité d'excavabilité des matériaux. Cet indice inclut certains paramètres qui sont priorisés par une pondération plus élevée comparativement à d'autres. L'une des méthodes de Pells se base sur un indice (*eGSI*) dérivé de l'indice *GSI* initialement développé pour évaluer la compétence des massifs rocheux. Le second indice (appelé : *RMEI*) de la deuxième méthode de Pells est particulièrement développé pour évaluer l'érodabilité hydraulique du roc. Ce deuxième indice peut être déterminé à l'aide d'un système de classification du massif rocheux qui incorpore un certain nombre de paramètres géologiques. Pour l'indice *RMEI*, l'importance relative des paramètres considérés a été déterminée sur la base des observations de terrain effectuées sur des déversoirs rocheux érodés. Il est considéré que les paramètres utilisés pour évaluer l'érodabilité hydraulique du roc reste comme étant une question ouverte, du-même qu'il est difficile de déterminer les paramètres pertinents à l'évaluation de l'érodabilité hydraulique du roc. De plus, l'importance relative attribuée aux paramètres géologiques constitue aussi un point confus contribuant à l'erreur commise lorsque ces méthodes sont utilisées.

En utilisant plus de 100 études de cas sur des déversoirs rocheux érodés, une nouvelle méthode est proposée quant à la détermination des paramètres géologiques pertinents à l'évaluation de l'érodabilité hydraulique du roc. Il est déterminé que la résistance matricielle de la roche intacte ne constitue pas un paramètre pertinent à l'évaluation de l'érodabilité hydraulique du roc. Aussi, il est constaté que l'utilisation de mesure tridimensionnelle du volume des blocs rocheux, à la place du facteur de taille des blocs utilisé dans la méthode d'Annandale, améliore considérablement l'estimation de la taille des blocs rocheux. De plus, le paramètre E_{doa} représentant l'effet de la forme et de l'orientation des blocs rocheux relativement à la direction de

l'écoulement de l'eau, inclut dans l'indice $eGSI$, est déterminé comme étant plus précis que celui adopté dans la méthode d'Annandale. Les paramètres géologiques finalement déterminés comme étant pertinents à l'évaluation de l'érodabilité hydraulique du roc sont : 1) l'ouverture des joints, 2), la résistance au cisaillement des discontinuités 3), la nature de la surface potentiellement érodée 4), le module de déformation du massif rocheux 5) le volume des blocs rocheux, 6) le paramètre E_{doa} représentant la forme et l'orientation du bloc relativement à la direction de l'écoulement.

Vu la confusion établie sur la pondération des paramètres géologiques gouvernant le processus de l'érodabilité hydraulique du roc, une autre nouvelle méthode permettant de déterminer l'importance relative des paramètres est proposée dans le cadre de cette thèse. Cette méthode est dérivée d'une analyse d'une centaine de cas portant sur l'érodabilité hydraulique du roc dans les déversoirs rocheux. Les paramètres étant déterminés pertinents quant à l'évaluation de l'érodabilité hydraulique du roc sont finalement classés (le plus important vers le moins important) selon l'ordre suivant : 1) la résistance au cisaillement des discontinuités, 2) la nature de la surface potentiellement érodée, 3) le volume des blocs rocheux, 4) l'ouverture des joints, 5) le paramètre E_{doa} représentant la forme et l'orientation du bloc relativement à la direction de l'écoulement, et 6) le module de déformation du massif rocheux. Il est constaté que notre ordre de classement en termes d'importance relative des paramètres géologiques analysés concorde largement avec celui établi sur la base des observations de terrain effectuées sur des déversoirs rocheux érodés. Cependant, plus de précision concernant l'importance relative des paramètres géologiques est déterminée selon notre nouvelle méthode, car elle repose sur un processus d'évaluation individuel des paramètres du massif rocheux.

Table of Contents

LIST OF TABLES.....	ix
LIST OF FIGURES	x
LIST OF APPENDICES.....	xiii
LIST OF SYMBOLS AND ABBREVIATIONS.....	xiv
ACKNOWLEDGMENTS	xvi
CHAPTER 1 - INTRODUCTION.....	1
1.1. General concern.....	1
1.2. Statement of the specific problem	4
1.3. Research objectives	7
1.4. Research methodology	8
1.5. Originality and contribution	11
1.6. Thesis outline.....	15
1.7. References	17
CHAPTER 2 - LITERATURE REVIEW	19
2.1. Existing methods based on Kirsten’s index.....	20
2.1.1. Kirsten’s index	22
2.1.1.1. Compressive strength of intact rock rating.....	22
2.1.1.2. Rock block size rating	23
2.1.1.3. Joints shear strength rating	24
2.1.1.4. Relative block structure rating.....	25
2.1.2. Critical observations on the Kirsten’s index	25
2.1.3. Comparative methods based on the Kirsten index.....	27
2.1.3.1. Moore et al.’s scour threshold	28
2.1.3.2. Van Schalkywk et al.’s scour thresholds	29
2.1.3.3. Annandale’s scour threshold	32
2.1.3.4. Kirsten et al.’s scour threshold	33
2.2. Pells’s methods	36
2.2.1. Geological strength index for erodibility (<i>eGSI</i>).....	39
2.2.1.1. Determining <i>GSI</i> from <i>RMR</i> components.....	39
2.2.1.2. Determining <i>GSI</i> from the lookup chart	41
2.2.1.3. Development of the <i>eGSI</i> erodibility index	43
2.2.2. Rock mass erodibility index (<i>RMEI</i>).....	48
2.3. References	52
CHAPTER 3 - DETERMINING RELATIVE BLOCK STRUCTURE RATING FOR ROCK ERODIBILITY EVALUATION IN THE CASE OF NON- ORTHOGONAL	59
JOINT SETS	59
3.1. Introduction	60
3.2. Relative block structure	63
3.2.1. Kinematic possibility of penetration	64
3.2.2. Kinematic possibility of dislodgement.....	66
3.2.3. Relative block structure rating	68
3.3. Methodology.....	76
3.3.1. Principle of the adjusted concept	77
3.3.2. Proposed K_d equation when the block is oriented in direction of flow	80
3.3.3. Proposed K_d equation when the block is oriented against direction of flow	83

3.3.4. Analysis of K_d behavior	85
3.3.5. Proposed equations for determining J_s	87
3.4. Results and discussion	87
3.4.1. Determining J_s when α is larger than 90°	88
3.4.2. Determining J_s when α is less than 90°	94
3.4.3. Steps for determining the value of J_s for non-orthogonal fracture systems.....	99
3.5. Impact of α angle	100
3.6. Conclusion	105
3.7. References	107
CHAPTER 4 - A METHOD TO DETERMINE THE RELEVANT GEOMECHANICAL PARAMETERS FOR EVALUATING THE HYDRAULIC ERODIBILITY OF ROCK	110
4.1. Introduction	111
4.2. Description of the developed method.....	117
4.2.1 Step 1 - Establishing a dataset and an erosion-level scale	117
4.2.2 Step 2 - Selection of a geomechanical parameter	120
4.2.3 Step 3 - Classification of the selected geomechanical parameter	121
4.2.3.1 Classification of the UCS of rock.....	121
4.2.3.2 Classification of rock block size.....	122
4.2.3.3 Classification of joint shear strength	127
4.2.3.4 Classification of a block's shape and orientation parameters.....	128
4.2.3.6 Classification of joint openings	132
4.2.3.7 Classification of NPES	133
4.2.4 Step 4 - Determining mean levels of erosion for given P_a categories	133
4.2.5 Step 5 – Evaluating all geomechanical parameter classes	136
4.2.6 Step 6 - Analysis of sensitivity curves to erodibility	136
4.2.7 Steps 7 and 8 – Analyze of all geomechanical parameters and the selection of the relevant geomechanical parameters.....	137
4.3 Results and discussion	138
4.3.1 Effect of the UCS of rock on erodibility	138
4.3.2 Effect of rock block size on erodibility.....	141
4.3.3 Effect of joint shear strength on erodibility	143
4.3.4 Effect of a block's shape and orientation on erodibility	144
4.3.5 Effect of joint opening on erodibility.....	146
4.3.6 Effect of <i>NPES</i> on erodibility	147
4.4 Validation of developed methodology	149
4.5 Conclusion	153
4.6 References	155
CHAPTER 5 – DEVELOPMENT OF A METHODOLOGY FOR DETERMINING THE RELATIVE IMPORTANCE OF ROCK MASS PARAMETERS THAT CONTROL THE HYDRAULIC ERODIBILITY OF ROCK	160
5.1. Introduction	161
5.2. Background of the comparative methods	164
5.2.1 Background of comparative methods based on Kirsten's index	165
5.2.2 Background of the Pells's methods	167
5.3. Analysis of comparative methods.....	169
5.3.1 Comparing all methods.....	170

5.3.2	Comparing the Van Schalkwyk and Pells methods.....	172
5.3.3	Comparing the Pells methods.....	176
5.3.3.1	Comparisons based on erosion classes.....	176
5.3.3.2	Comparisons based on hydraulic stream power class.....	179
5.4.	Description of the method.....	181
5.4.1	Step 1 - Selecting a rock mass parameter.....	183
5.4.2	Step 2 - Selecting a hydraulic stream power.....	187
5.4.3	Steps 3 and 4 - Determining erosion level based on the selected P_a	188
5.4.4	Steps 5 and 6 - Determining the slope of the hydraulic sensitivity curves to erodibility for the selected rock mass parameters.....	191
5.5	Results and discussion.....	192
5.5.1	Determining the hydraulic sensitivity curves to erodibility.....	192
5.5.2	Determining the relative importance of the selected parameters.....	194
5.5.3	Comparison with field observations.....	197
5.6	Conclusion.....	199
5.7	References.....	200
	CHAPTER 6 – CONCLUSIONS.....	204
6.1	Determining the relative block structure rating for evaluating rock erodibility in the case of non-orthogonal joint sets.....	205
6.2	A method for determining the relevant geomechanical parameters when evaluating the hydraulic erodibility of rock.....	206
6.3	A method to determine the relative importance of rock mass parameters that control the hydraulic erodibility of rock.....	208
6.4	Perspectives for future research.....	209
	APPENDICES.....	211

LIST OF TABLES

Table 2.1. Classification of the degree of erosion (Van Schalkwyk et al. 1994a).	29
Table 2.2. Classification of the degree of erosion (Van Schalkwyk et al. 1994a).	31
Table 2.3. Description of the erosion condition classes (Pells, 2016a).....	37
Table 2.4. Information for determining the factors $F1$ to $F4$ included in Bieniawski's 1976 <i>RMR</i> classification system (Hoek et al., 1995).	40
Table 2.5. Suggested method for estimating LF_{P3} (Pells, 2016a).	49
Table 3.1. The ratio of joint spacing and the angles θ and ψ initially used by Kirsten (Kirsten, personal communication, 2016).	70
Table 3.2. Rating values of the relative block structure (Kirsten 1982, 1988).	74
Table 3.3. Rating values of relative block structures for a non-orthogonal fracture system ($\alpha > 90^\circ$).	93
Table 3.4. Rating values of relative block structures for a non-orthogonal fracture system ($\alpha < 90^\circ$).	98
Table 3.5. Data for the analyzed case studies.....	103
Table 3.6. Calculations of the required hydraulic stream power.....	103
Table 4.1. Summary of the considered geomechanical parameters.	119
Table 4.2. Erosion condition description (Pells, 2016a).	120
Table 4.3. <i>UCS</i> classification of Jennings et al. (1973).	122
Table 4.4. <i>UCS</i> classification adopted from Bieniawski (1989, 1973).	122
Table 4.5. Proposed K_b classification.	124
Table 4.6. Classification of rock block volume (Palmstrom, 1995).....	124
Table 4.7. Proposed K_d classification.	128
Table 4.8. Proposed J_s classification.	129
Table 4.9. Proposed E_{doa} classification.	131
Table 4.10. Joint opening classification (Bieniawski, 1989) with our proposed class.	132
Table 4.11. <i>NPES</i> classification (Pells, 2016a) and our proposed class.	133
Table 4.12. Defined P_a categories.	134
Table 4.13. Example of calculating μ_D	135
Table 4.14. RMSE calculating process according to J_o sensitivity curves to erodibility.	152
Table 4.15. Calculated RMSE and the determined ratio.	153
Table 5.1. Classification of the erosion (Van Schalkwyk et al., 1994a).	165
Table 5.2. Classification of the erosion (Van Schalkwyk et al., 1994b).	165
Table 5.3. Description of erosion conditions (Pells, 2016a).	168
Table 5.4. Committed error calculated based on the various methods.....	172
Table 5.5. Committed error calculated according to the Van Schalkwyk and the Pells's methods (<i>eGSI</i> and <i>RMEI</i>).	175
Table 5.6. Committed error calculated from the <i>RMEI</i> and <i>eGSI</i> methods.	179
Table 5.7. Proposed E_{rm} classification.	185
Table 5.8. Calculated erosion level based on J_o classification.	189
Table 5.9. Determined slopes of hydraulic sensitivity curves to erodibility.	194

LIST OF FIGURES

Figure 1.1. Evolution of erosion at the Rocobayo Dam spillway (Annandale, 2006).	.1
Figure 1.2. Rock erosion at the Copeton Dam spillway, Australia (Pells, 2016a).3
Figure 1.3. Rock erosion at the Mokolo Dam spillway, South Africa (Pells, 2016a).	...3
Figure 2.1. Scour threshold line as determined by Moore et al. (1994).28
Figure 2.2. Scour threshold lines as determined by Van Schalkwyk et al. (1994a).30
Figure 2.3. Scour threshold lines as determined by Van Schalkwyk et al. (1994b).31
Figure 2.4. Scour threshold line as determined by Annandale (1995).33
Figure 2.5. Scour threshold line as determined by Kirsten et al. (2000).34
Figure 2.6. Comparison of determined scour threshold lines.35
Figure 2.7. Lookup chart for determining <i>GSI</i> from field observations (P. Marinos and Hoek, 2000).42
Figure 2.8. Curves to be used for determining E_{doa} factor in the case of horizontal flowing surface submitted to various water flows (Ski-jump flow of 25° relative to flowing surface, and parallel flow relative to flowing surface). 1:1, 1:2, etc. represent the joint set spacing ratios (e.g. 1:2, where 1 represents the width of the block and 2 represents its length) (Pells, 2016a).45
Figure 2.9. Curves to be used for determining E_{doa} factor in the case of inclined flowing surface submitted to various water flows (Ski-jump flow of 25° into adverse inclined flowing surface of 15°, and parallel flow along inclined flowing surface of 15°) (Pells, 2016a).46
Figure 2.10. Interpreted erosion classes using <i>eGSI</i> versus hydraulic power expressed in the figure as II_{UD} (Pells, 2016a).47
Figure 2.11. <i>RMEI</i> classification system for evaluating the hydraulic erodibility of rock (Pells, 2016a).50
Figure 2.12. Interpreted erosion classes using <i>RMEI</i> versus hydraulic power expressed in the Figure as II_{UD} (Douglas et al., 2018).51
Figure 3.1. Model for two joint sets modified from Kirsten (1982). The joint sets in the original figure are not orthogonal. However, Kirsten proposes to consider only orthogonal fracture system. Accordingly, the model here is bit modified to be more representative to an orthogonal fracture system (<i>DA: Dip angle; DD: Dip direction</i>).64
Figure 3.2. The principle of the principal dislodging force.66
Figure 3.3. Representation of the coaxial components as adapted from Kirsten (1982).67
Figure 3.4. Orthogonal fracture system with ratio of joint spacing of 1.72
Figure 3.5. The curve adjustment process (modified from Moore and Kirsten 1988).73
Figure 3.6. Graphical representation of the relative block structure values.73
Figure 3.7. Stereographic representation of two possible situations for a fractured system.76
Figure 3.8. Concept of a delineated blocks oriented in and against the direction of excavation.78

Figure 3.9. Coaxial components for blocks oriented in and against the direction of excavation.....	80
Figure 3.10. Coaxial components for a block oriented in the direction of flow.	81
Figure 3.11. Considered angles when the block is oriented in the direction of flow. .	82
Figure 3.12. Coaxial components for a block oriented against the direction of flow.	83
Figure 3.13. Considered angles when the block is oriented against the direction of flow.....	84
Figure 3.14. Behavior of the kinematic possibility of dislodgment versus θ	86
Figure 3.15. Behavior of the kinematic possibility of dislodgment not expressed in absolute terms.	86
Figure 3.16. Behavior of J_s : (a) $\alpha = 100^\circ$, (b) $\alpha = 110^\circ$, (c) $\alpha = 120^\circ$, (d) $\alpha = 130^\circ$, (e) $\alpha = 140^\circ$, and (f) $\alpha = 150^\circ$	89
Figure 3.17. J_s curves for $r = 8$ when α is larger than 90° : (a) Before adjustment – in the direction of flow; (b) Before adjustment – against the direction of flow; (c) After adjustment – in the direction of flow; and (d) After adjustment – against the direction of flow.	92
Figure 3.18. Behavior of J_s : (a) $\alpha = 80^\circ$, (b) $\alpha = 70^\circ$, (c) $\alpha = 60^\circ$, (d) $\alpha = 50^\circ$, (e) $\alpha = 40^\circ$, and (f) $\alpha = 30^\circ$	95
Figure 3.19. J_s curves when $RJS = 8$: a) Before adjustment-in the direction of flow; b) Before adjustment-against the direction of flow; c) After adjustment-in the direction of flow; d) After adjustment-against the direction of flow.	97
Figure 3.20. Graphical representation of $RMSE$ versus α	101
Figure 3.21. Graphical representation of the required hydraulic stream power versus α	104
Figure 4.1. Algorithm for determining the relevant geomechanical parameters for evaluating the hydraulic erodibility of rock.	118
Figure 4.2. The statistical distribution of K_b values from the case studies of Pells (2016a).....	123
Figure 4.3. The statistical distribution of K_d values from the case studies of Pells (2016a).....	127
Figure 4.4. The statistical distribution of J_s values obtained from the case studies of Pells (2016a).....	129
Figure 4.5. The statistical distribution of E_{doa} values obtained from the case studies of Pells (2016a).....	131
Figure 4.6. Statistical distribution of P_a values from the case studies of Pells (2016a).	134
Figure 4.7. Sensitivity curves to erodibility based on UCS : a) Jenning's UCS classification; b) Bieniawski's UCS classification. Each best-fit line and its equation correspond to the same symbol data points, which are also represented by the same color.....	140
Figure 4.8. Sensitivity curves to erodibility based on rock block size: a) K_b classification; b) V_b classification (V_b calculated according to Method 1); c) V_b classification (V_b calculated according to Method 2); d) V_b classification (V_b calculated according to Method 3). Each best-fit line and its equation correspond	

to the same symbol data points, which are also represented by the same color.	142
Figure 4.9. Sensitivity curves to erodibility based on K_d classification. Each best-fit line and its equation correspond to the same symbol data points, which are also represented by the same color.	144
Figure 4.10. Sensitivity curves to erodibility based on a block's shape and orientation relative to the direction of flow: a) J_s classification; b) E_{doa} classification. Each best-fit line and its equation correspond to the same symbol data points, which are also represented by the same color.	145
Figure 4.11. Sensitivity curves to erodibility based on J_o classification. Each best-fit line and its equation correspond to the same symbol data points, which are also represented by the same color.	147
Figure 4.12. Sensitivity curves to erodibility based on $NPES$ classification. Each best-fit line and its equation correspond to the same symbol data points, which are also represented by the same color.	148
Figure 4.13. Validation based on a) J_o sensitivity curves; b) V_b sensitivity curves; c) K_d sensitivity curves; d) E_{doa} sensitivity curves; and e) $NPES$ sensitivity curves.	150
Figure 5.1. Comparison of scour threshold lines.....	167
Figure 5.2. Erosion classes as determined based on the $eGSI$ index (Pells, 2016). ..	168
Figure 5.3. Erosion classes as determined based on the $RMEI$ index (Douglas et al., 2018).....	169
Figure 5.4. Plots of the 86 case studies according to (a) Kirsten's index, (b) the $eGSI$ index, and (c) the $RMEI$ index.....	171
Figure 5.5. Plotted data based on (a) Kirsten's index, (b) $eGSI$ index, (c) $RMEI$ index by considering three erosion classes.	174
Figure 5.6. Plotted data based on the (a) $eGSI$ index and (b) $RMEI$ index with five classes.	177
Figure 5.7. Committed errors within the different erosion classes.	179
Figure 5.8. Committed errors for the various P_a classes.	180
Figure 5.9. Algorithm for determining the relative importance of selected parameters.	182
Figure 5.10. Sensitivity curves to erodibility based on E_{rm} classification. It should be mentioned that each best-fit line corresponds to symbol data points of the same color and shape (e.g., the best-fit blue line corresponds to the blue circles), and the associated equation is also of the same color.	186
Figure 5.11. Sensitivity curves to erodibility based on J_o classification (Boumaiza et al., 2019a).	188
Figure 5.12. J_o hydraulic sensitivity curves to erodibility.....	190
Figure 5.13. Hydraulic sensitivity curves for (a) K_d , (b) V_b , (c) E_{doa} , (d) $NPES$, and (e) E_{rm} . Note that for the hydraulic sensitivity curves of K_d , V_b , E_{doa} , and E_{rm} , the x-axis values are presented from higher to lower values.....	193
Figure 5.14. Slope variation curves of the selected parameters.	195
Figure 5.15. Extended slope variation curves of the selected parameters.....	196

LIST OF APPENDICES

- Appendix A. Description of rock mass parameters rating (Kirsten 1982)
- Appendix B. Relative block structure rating (Annandale 1995, 2006)
- Appendix C. Curves before and after adjustment for a RJS of 4, 2 and 1 ($\alpha > 90^\circ$)
- Appendix D. Curves before and after adjustment for a RJS of 4, 2 and 1 ($\alpha < 90^\circ$)
- Appendix E. Summary of the data used in this study (Chapter 4)
- Appendix F. Summary of V_b calculating according to the three used methods
- Appendix G. Summary of the data used in this study (Chapter 5)
- Appendix H. Sensitivity curves to erodibility based on (a) K_d , (b) V_b , (c) E_{doa} , (d) *NPES* classifications (Boumaiza et al., 2019b)

LIST OF SYMBOLS AND ABBREVIATIONS

- A, A', B and B' : the coaxial components of force
- a : Ripping efficiency coefficient ($a = 5$)
- a_1 : Longest dimension of a rock block (m)
- a_3 : Shortest dimension of a rock block (m)
- b : Ripping efficiency coefficient ($b = 5$)
- D : Disturbance factor
- D_i : Erosion level
- E_{doa} : Erosion, discontinuity orientation adjustment
- $eGSI$: Erodibility geological strength index
- E_i : Young's modulus of intact rock (GPa)
- E_{rm} : Rock mass deformation modulus (GPa)
- GSI : Geological strength index
- i : Erosion level class
- J_a : Joint surface alteration number
- J_n : Joint set number
- J_o : Joint opening (mm)
- J_r : Joint roughness number
- J_s : Relative block structure
- J_v : Number of joints intersecting a volume of 1 m³
- J_s^p : Required penetration effort
- J_s^d : Required dislodging effort
- K_b : Rock block size
- K_d : Discontinuity shear strength
- K_d : Kinematic possibility of dislodgment
- K_p : Kinematic possibility of penetration
- LF : Likelihood factor
- MR : Modulus ratio
- M_s : Compressive strength number
- N : Kirsten's index

n_i : Number of study cases of a given erosion level
 $NPES$: Nature of the potentially eroding surface
 n_t : Total number of study cases
 P_a : Available hydraulic stream power (kW/m^2)
 P_i : Probability of erosion
 P_r : Required hydraulic stream power
 RF : Relative importance factor
 RJS : Ratio of joint spacing (expressed in an equation as $r = S_\Psi/S_\theta$)
 RMR : Rock mass rating system
 $RMEI$: Rock mass erosion index
 RMi : Rock mass index
 $RMSE$: Root mean square error (%)
 RQD : Rock quality designation
 S_a : Average joint spacing (m)
 S : Slope ($^\circ$)
 S_l : Spacing in joint set (m)
 S_θ : Joint spacing of the first joint set
 S_Ψ : Joint spacing of the second joint set
 UCS : Unconfined compressive strength (MPa)
 V_b : Rock block volume (m^3)
 μ_D : Mean erosion level for a given hydraulic steam power category
 γ_l : Angles between joint sets ($^\circ$)
 β : Block shape factor
 λ_n : Joint frequency
 σ_{ci} : Uniaxial compressive strength (MPa)
 θ : Dip angle of the first joint set
 Ψ : Dip angle of the second joint set
 α : Angle between the planes of two joint sets
 λ_θ : Joint frequency of the first joint set
 λ_Ψ : Joint frequency of the second joint set

ACKNOWLEDGMENTS

I would like to express my sincerest appreciation and gratitude to my supervisor, Professor Ali Saeidi, and my co-supervisor, Dr. Marco Quirion, for their valuable supervision, kindness, precious advice, and suggestions. I would like to also thank Professors Alain Rouleau and Pierre Cousineau (*Université du Québec à Chicoutimi (UQAC) – Canada*), as well as Professor Patrice Rivard (*Université de Sherbrooke - Canada*) for agreeing to examine my Ph.D. thesis. I am grateful to all the organizations that have funded my research project, namely the Natural Sciences and Engineering Research Council of Canada, Hydro-Québec, and the Mitacs Accelerate Program. Furthermore, I would like to thank *la Fondation de l'Université du Québec à Chicoutimi*, *la Fondation de l'Université du Québec*, the Canadian Geotechnical Society, and the Canadian Dam Association from which I received the cited excellence scholarships and awards:

1. “Denis W. Roy Excellence Scholarship - Geology”, 2019 Edition
2. “Gary Salmon Memorial Award - Geosciences”, 2019 Edition
3. “Pierre La-Rochelle Award - Geotechnics”, 2019 Edition
4. “RBC Royal Bank Excellence Scholarship - Earth Sciences”, 2019 Edition
5. “Desjardins Bank Scholarship - Voluntary involvement”, 2019 Edition
6. “Graduate Studies Excellence Award - Engineering”, 2019 Edition
7. “Federation of Professional Staff of Universities Scholarship”, 2019 Edition
8. “Globalink Research Award”, 2018 Edition
9. “RBC Royal Bank Excellence Scholarship - Earth Sciences”, 2018 Edition
10. “Lucien Bouchard Excellence Scholarship - Geology”, 2018 Edition
11. “Denis W. Roy Excellence Scholarship - Geology”, 2017 Edition

I would also like to acknowledge the financial support of many organizations: *Bureau de l'International*, *Service de la Vie Étudiante*, *MAGE-UQAC*, and the *Décanat de la recherche et la création*. These UQAC-based organizations financed my travels to conferences in Canada and abroad. Throughout my Ph.D. project, I had many extremely positive discussions with experts in rock scour, including Dr. George Annandale, Dr. Hendrik Kirsten, Dr. Steven Pells, Dr. Michael George, Professor Monte Van Schalkwayk, and Mrs. Amanda Rock. I would like to acknowledge their useful assistance and advice. I would also like to thank Dr. Rock Flamand from Hydro-Québec (Chicoutimi Office) for the welcome into his team during my Mitacs-training. I also appreciated all my colleagues in the R2eau research group (*Groupe de recherche Risque Ressource Eau*), as well as all professors involved in this research group, including Professors Romain Chesnaux and Julien Walter. Their suggestions and advice during meetings and presentation sessions were very useful to improve my oral presentation skills. Above all, I want to express my deepest appreciation, my full gratitude, and my sincerest acknowledgement to my wife Hiba for her full and complete support. Each time when I was facing difficulties, the members of my close family (Hiba and my two children, Karim and Rym) were key to keep me going forward and remembering the well-known proverb “*Rise and rise again until lambs become lions*”. This work is dedicated first to my close family for their kindness and endless moral support and second to all members of my larger family in Algeria, especially my mother, Fatima, and my father, Bachir.

CHAPTER 1 - INTRODUCTION

1.1. General concern

The construction of dams requires the building of hydraulic structures to control the water level and thus ensure the safety of dams during flood events. These control structures for evacuating water are equipped with a channel excavated in the rock; these channels are referred to as unlined spillways. Generally, the rock mass of these spillways is assumed to be resistant to the erosive force of flowing water. However, the actual use of the spillways indicates that the initial rock resistance to erosive force of flowing water may be evaluated incorrectly. This may lead to rock erosion that can potentially affect the stability of hydraulic structures, as observed for the case of the Ricobayo Dam spillway in Spain (Figure 1.1). Within two years of operation, multiple flood events, despite having power flowing water energy well below the maximum designed flow, caused significant deterioration of the unlined spillway and raised concerns regarding the safety of the dam (George, 2015).



Figure 1.1. Evolution of erosion at the Ricobayo Dam spillway (Annandale, 2006).

Furthermore, there are several hydropower stations in Sweden where the unlined spillways have been subjected to extensive scour¹, even though none of the spillways have experienced any long-term high water flows (Mörén and Sjöberg, 2007). Other spectacular erosion events have occurred in unlined spillways; for example, the Copeton Dam spillway, in Australia, saw the formation of a 20-m deep erosion hole (Figure 1.2), and the Mokolo Dam spillway in South Africa (Figure 1.3) was marked by the creation of a 30-m deep erosion hole (Pells, 2016a). For these two unlined spillways, the erosive force of flowing water was much lower than the initial evaluated rock resistance capacity calculated according to existing methods for evaluating hydraulic rock scour.

The rock scour of unlined spillway may result in the failure of the spillway structure, loss of the stored water, serious damage to property and infrastructure, and negative impacts on communities located immediately downstream from these structures (Sawadogo, 2010). In the case of many eroded dam spillways, the repair costs of the unlined channel can be quite high. The California Department of Water Resources revealed that the cost of the emergency response and the subsequent repair work at the Oroville Dam spillway has reached \$1.1 billion (CDWR, 2019).

¹ The terms “scour”, “erodibility”, and “hydraulic erosion” are considered in this thesis as synonymous technical terms to describe significant localized erosion of rock that occurs when the rock is submitted to the force of flowing water.

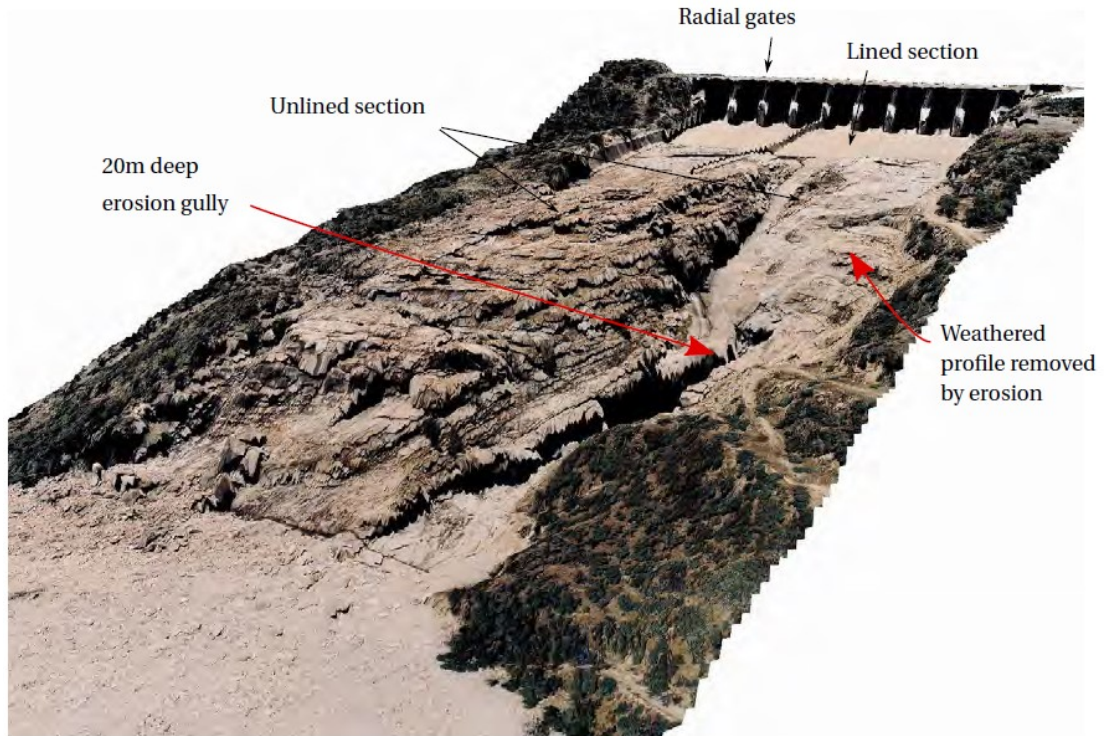


Figure 1.2. Rock erosion at the Copeton Dam spillway, Australia (Pells, 2016a).

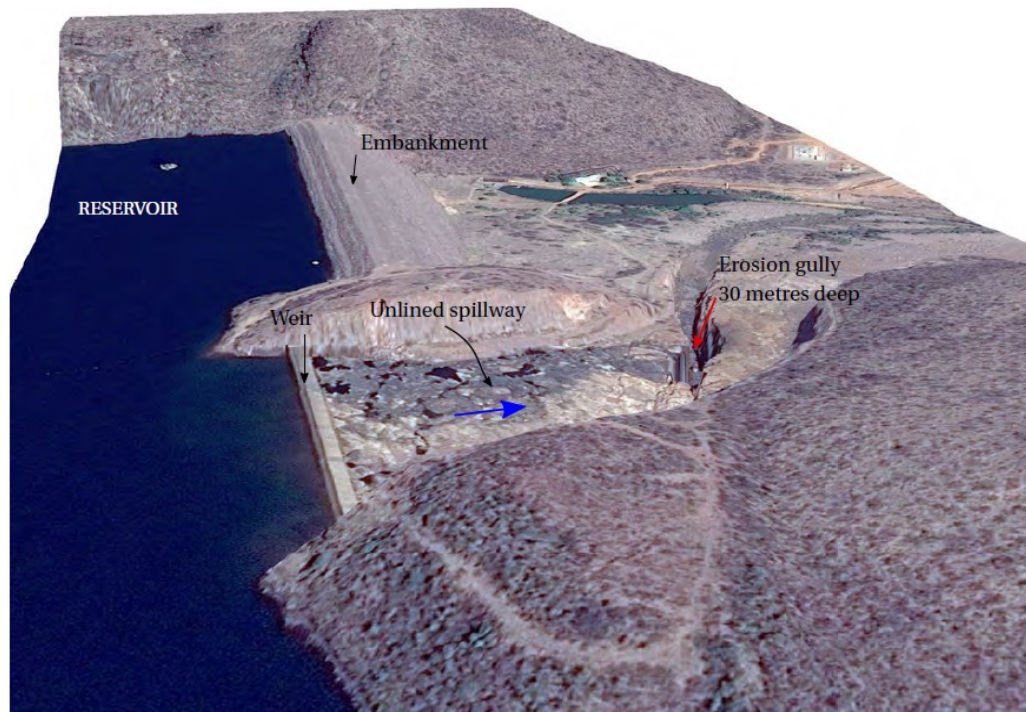


Figure 1.3. Rock erosion at the Mokolo Dam spillway, South Africa (Pells, 2016a).

Global climate change will certainly result in some areas experiencing increased precipitation, in intensity and/or amount, which will increase the flooding of rivers. Consequently, the stored water in dam reservoirs will have to be evacuated using the existing unlined spillways. This raises a question of how the unlined spillway will resist these flood conditions that may exceed flood levels of the original design. Rock scour is a highly complex mechanism that is governed by both rock mass and erosive flowing water (Bollaert and Schleiss, 2003). As such, reliable spatial and temporal estimates of rock scour require a thorough understanding of the fundamental mechanisms that govern the process; this full understanding has proven to be a challenge (George, 2015). Several studies have focused on characterizing and analysing the force of flowing water based on experimentation of hydraulic concepts (Bollaert, 2002; Castillo et al., 2014, 2007; Ervine et al., 1997; Ervine and Falvey, 1987). However, only a few studies have tried to understand rock mass behaviour when submitted to hydraulic forces (George, 2015; Pells, 2016a).

1.2. Statement of the specific problem

The structural features and mechanical properties of a rock mass are of critical importance for determining the hydraulic erodibility of rock. The most commonly used methods for evaluating the potential hydraulic erodibility of rock are based on the correlation between the force of flowing water (P_a) and the capacity of the rock to resist the flow energy (e.g. Annandale 1995, 2006; Pells 2016). In these methods,

rock resistance to flow is evaluated using erodibility indices that are determined from specific rock mass parameters, such as (1) the unconfined compressive strength of intact rock, (2) rock block size, (3) joints shear strength, (4) relative block structure, (5) joints opening, and (6) the nature of the potentially eroded surface. The relative block structure parameter (number 4 in the list above) was initially proposed by Kirsten (1982) to quantify the effect of rock block's shape and orientation relative to the direction of the ripping action.

An analogy between the mechanical ripping and hydraulic flow action led to the adoption of the relative block structure parameter to properly evaluate hydraulic rock scour (Moore and Kirsten 1988). Kirsten (1982) proposed a simplified overview in which he assumed that geological formations are mainly fractured by two intersecting joint sets, where a 90° angle is maintained between the planes of the two joint sets (orthogonal fracture system). In practice, however, Kirsten's assumption of an orthogonal fracture set being applied to all cases, including non-orthogonal fracture systems, results in a certain lack of precision when assessing rock resistance capacity.

Furthermore, rock resistance capacity in the Annandale method (Annandale 1995, 2006) is evaluated using Kirsten's index (Kirsten 1982); an index that is determined using the following rock mass parameters: (1) the unconfined compressive strength of intact rock, (2) rock block size, (3) joints shear strength, and (4) relative block structure. Recently, Pells (2016) proposed two other indices for assessing the capacity of rock to resist flowing water. The first one, *eGSI*, represents a modification of *GSI* (Geological Strength Index) previously proposed by Hoek et al.

(1995) to characterize the rock mass. The second one, rock mass erosion index (*RMEI*), incorporates a set of rock mass parameters, including the kinematically viable mechanism for block detachment, the nature of the potentially eroding surface, the nature of the joints, the joints spacing, and the rock block shape. There is, however, no clear consensus on which rock mass parameters are indeed relevant for evaluating the hydraulic erodibility of rock, and the key rock mass parameters to be used for assessing rock resistance capacity remain uncertain.

Moreover, the rock mass parameters included in Kirsten's index and *RMEI* are weighted differently. Some parameters in Kirsten's index are prioritized using a higher rating compared to other parameters. However, each one of the parameters is determined using a specific approach. The compressive strength rating is determined using an unconfined compressive test; rock block size and the joints shear strength ratings are both established using field judgment experience, and the relative block structure rating is quantified mathematically. For this purpose, Pells (2016) assumed that Kirsten's index does not represent the mechanism of hydraulic erosion given that initially it was proposed for evaluating the excavatability of earth materials. Hence, Pells (2016) proposed the *RMEI* system to represent the rock mass parameters that govern erosion; the weighting (relative importance) of these parameters is based on field observations of the eroded spillways. However, the field observations can be influenced greatly by the judgment of the specific analyst; thus, determining the relative importance of rock mass parameters using an objectively accurate method remains a challenge.

1.3. Research objectives

The general objective of this thesis is to understand the process of rock erodibility and identify those rock mass parameters that govern the hydraulic erodibility of rock. To achieve this goal, the specific objectives of this study are summarized as follows.

- (1) Identify and understand the concepts surrounding the most commonly used methods for evaluating the hydraulic erodibility of rock;
- (2) Develop a new rating of the relative block structure that corresponds to non-orthogonal fracture systems based on Kirsten's initial concept of an orthogonal fracture system;
- (3) Adopt or develop a classification system for the analysis of selected rock mass parameters, and develop a method to determine the relevant rock mass parameters for evaluating the hydraulic erodibility of rock;
- (4) Perform a comparative analysis of the most commonly used methods for evaluating the hydraulic erodibility of rock to assess the reliability of each method;
- (5) Develop a method to determine the relative importance of individual rock mass parameters that govern the hydraulic erodibility of rock.

1.4. Research methodology

The methodologies used to meet the objectives listed in the previous section are summarized as follows.

(1) This objective involves an extensive literature review of the specific methods currently applied to dam spillway designs and that are used for assessing hydraulic rock scour. This review allows studying the rationale behind the various erodibility indices used to evaluate the rock resistance capacity; the rationale includes i) the framework in which the erodibility indices were proposed; ii) the practical limitations and origin of the adopted rock mass parameters; iii) the methods adopted to weigh the various rock mass parameters within the erodibility indices; and iv) the principles underlying the equations of the developed erodibility indices.

(2) Kirsten's concept for assessing the relative block structure parameter considers that the geological formation is mainly fractured by two joint sets that form an orthogonal fracture system, meaning that there is an angle of 90° between the planes of the two considered joints. To quantify the relative block structure parameter, Kirsten developed a sole mathematical expression to evaluate the effect of rock block's shape and orientation relative to the flow direction. Kirsten's expression is based on a concept of a rock block that is oriented against the direction of flow. When the rock block is oriented in the direction of flow, Kirsten changed only the sign of the considered angles in his expression. Instead of using one

concept as done by Kirsten, two concepts are proposed in this thesis. The first is used when the blocks are inclined in the direction of flow, while the second involves cases when blocks are inclined against the direction of flow. For each concept, a specific equation is proposed. Using the two proposed equations and varying the angle between the two joint sets (greater or less than 90°) makes it possible to generate a rating for the relative block structure parameter when the fractured system is non-orthogonal.

(3) The methodology, to achieve the third objective stated in the previous section, consists of collecting data from existing case studies of eroded unlined spillways. These data include rock mass parameters, the (P_a), and the observed erosion that are ranked as a function of depth and extent of eroded area (1: negligible, 2: minor, 3: moderate, 4: large, and 5: extensive). Each of the analysed rock mass parameters can be classified, and, for each class, it is possible to perform a series of calculations involving the mean of the observed erosion versus the mean of a specific P_a rang. The same calculations are then run for the other classes of rock mass parameter. The best-fit curves, representing the calculated mean of the observed erosion versus the average P_a , can be considered as the sensitivity curves to erodibility. The evaluation of the rock mass parameters is based on the analysis of the sensitivity curves to erodibility. Those showing a logical sequence can be considered as sensitivity curves to erodibility that are associated with a relevant rock mass parameter for evaluating the hydraulic erodibility of rock. If not, the analyzed rock mass parameter is deemed as not being a relevant parameter.

(4) The “scour threshold” of the comparative methods, used for evaluating the hydraulic rock scour, can be determined from different scour conditions that can be distinguished based on the plotted data of rock resistance capacity versus P_a . Using a considerable number of erosion case studies, the comparative analysis of these methods involves determining, for each method, the number of case studies where scour conditions are poorly evaluated. As existing methods do not always apply the same scales of scour conditions, the various developed erosion classes must be harmonized. The comparative process will also be undertaken by comparing the plotting of the case studies based on the different erosion classes.

(5) The methodology to be used for determining the relative importance of the rock mass parameters consists of selecting a given P_a value to establish the corresponding erosion level based on sensitivity curves to erodibility. This process will determine the erosion level when various sequential classes of the rock mass parameter are submitted to the same P_a . The same process is then repeated, using other sequential P_a values, to determine the erosion level behaviour when sequential classes of rock mass are submitted to sequential P_a values. The best-fit curves of the calculated erosion level versus the classes of rock mass parameter will have an inclined shape as the erosion condition is proportional to the rock mass classes. Other best-fit curves can be produced based on other selected sequential P_a . The slopes of the hydraulic sensitivity curves, associated with other individual rock mass parameters, can be plotted together to determine the classified order, and provide insight to the degree of relative importance of the all considered rock mass parameters.

1.5. Originality and contribution

The originality of this research work is summarized through the following points.

a) The “relative block structure” parameter is included in Kirsten’s index; this index is used for assessing rock resistance capacity. Kirsten, in his initial concept, assumed that geological formations are fractured mainly by two intersecting joint sets, where an angle of 90° is maintained between the planes constituting their “orthogonal fracture system.” The originality of this research is the refinement of the “relative block structure” parameter to be applied to a “non-orthogonal fracture system”. An adjusted concept is proposed with a corresponding rating and illustrates the effect of assuming an orthogonal fracture system in cases represented by a non-orthogonal fracture system.

b) As there is no clear consensus on which rock mass parameters are indeed relevant for evaluating the hydraulic erodibility of rock, the originality in this work is the identification of a set of relevant rock mass parameters for evaluating the hydraulic erodibility of rock by developing a method from the analyses of case studies from eroded unlined spillways. No previous study has proposed a method that can determine the relevant rock mass parameters for evaluating the hydraulic erodibility of rock.

c) Although field observations are very helpful for determining the relative importance of the rock mass parameters that govern rock hydraulic scour, it remains

that this field evaluation can be greatly influenced by the analyst. The originality in this work is the determination of the relative importance of a set of rock mass parameters through the analysis of case studies of eroded unlined spillways. No previous work has proposed a method that can determine the relative importance of the rock mass parameters governing the rock hydraulic erodibility process.

The contributions cited below are realized in this Ph.D. project framework. All these contributions are co-authored by Prof. Ali Saeidi (Professor at *Université du Québec à Chicoutimi*) as supervisor, and Dr. Marco Quirion (Rock mechanics Engineer at *Hydro-Québec*) as co-supervisor of this thesis.

Articles published and submitted in refereed international journals

- Boumaiza, L., Saeidi, A., and Quirion, M. (2019). A method to determine the relative importance of rock mass parameters controlling the hydraulic erodibility of rock. *Journal of Rock Mechanics and Geotechnical Engineering* (Submitted).
- Boumaiza, L., Saeidi, A. and Quirion, M. (2019). A method to determine the relevant geomechanical parameters for evaluating the hydraulic erodibility of rock. *Journal of Rock Mechanics and Geotechnical Engineering*, 11(5), 1004-1018 pp.
- Boumaiza, L., Saeidi, A. and Quirion, M. (2019). Determining relative block structure rating for rock erodibility evaluation in the case of non-orthogonal joint sets. *Journal of Rock Mechanics and Geotechnical Engineering*, 11(1), 72-87 pp.

Articles peer-reviewed and published in conference proceedings

- Boumaiza, L., Saeidi, A. and Quirion, M. (2019). Determining the most representative parameter for quantifying the rock block size used for evaluating the hydraulic erodibility of rock. Proceedings of the 72nd Canadian Geotechnical Conference (GeoSt-John's-2019), St-John's, Newfoundland, Canada, 6 p.
- Boumaiza, L., Saeidi, A. and Quirion, M. (2019). Determining geomechanical parameters controlling the hydraulic erodibility of rock in dam unlined spillways. Proceedings of the 87th Annual Meeting of the International Commission on Large Dams, Ottawa, Ontario, Canada, 13 p.
- Boumaiza, L., Saeidi, A. and Quirion, M. (2018). Determining rock erodibility parameter « relative block structure » for non-perpendicular hydraulic flow. Proceedings of the 71st Canadian Geotechnical Conference and the 13th Joint CGS/IAH-CNC Groundwater Conference (GeoEdmonton-2018), Edmonton, Alberta, Canada, 7 p.
- Boumaiza, L., Saeidi, A. and Quirion, M. (2017). Improving the assessment of the Kirsten's rock hydraulic erodibility index. Proceedings of the International Workshop on Overflowing Erosion of Dams and Dikes, Aussois, France, 6 p.
- Boumaiza, L., Saeidi, A. and Quirion, M. (2017). Evaluation of the impact of the geomechanical factors of the Kirsten's index on the shifting-up of rock mass erodibility class. Proceedings of the 70th Canadian Geotechnical Conference and the 12th Joint CGS/IAH-CNC Groundwater Conference (GeoOttawa-2017), Ottawa, Ontario, Canada, 8 p.

Communications with published abstract

- Boumaiza, L., Saeidi, A. and Quirion, M. (2019). Impact of rock block's shape and orientation on the hydraulic erodibility process. The Joint AGC/AMC/IAH-CNC Conference (May 12 to 15, 2019), Quebec City, (Quebec), Canada.
- Boumaiza, L., Saeidi, A. and Quirion, M. (2019). Determining rock mass parameters governing the hydraulic erodibility of rock. Earth Sciences Meeting (*Carrefour des Sciences de la Terre*), March 28 - 29, 2019, Université du Québec à Chicoutimi (Quebec), Canada.
- Boumaiza, L., Saeidi, A. and Quirion, M. (2018). Overview of methods used to assess hydraulic rock scour in unlined spillways. Dam Safety Interest Group Workshop on Rock Erosion at Unlined Spillways. 2018, October 3rd, Atlanta (Georgia) USA.
- Boumaiza, L., Saeidi, A. and Quirion, M. (2018). Geomechanical parameters controlling the hydraulic erodibility of rock in unlined spillways. Dam Safety Interest Group Workshop on Rock Erosion at Unlined Spillways. 2018, October 3rd, Atlanta (Georgia) USA.
- Boumaiza, L., Saeidi, A. et Quirion, M. (2018). *Perspective d'amélioration de l'évaluation de l'érodabilité hydraulique du roc dans les canaux d'évacuation de crues des barrages*. Congrès annuel de l'Association francophone pour le savoir (ACFAS, 7 - 11 mai 2018), Université du Québec à Chicoutimi, (Québec), Canada.
- Boumaiza, L., Saeidi, A. et Quirion, M. (2018). *Impact de la direction de l'écoulement sur l'érodabilité hydraulique du roc*. Journée des Sciences de la

Terre et de l'Environnement (JSTE, 15 mars 2018), INRS-ETE, Québec, (Québec), Canada.

- Boumaiza, L., Saeidi, A. et Quirion, M. (2017). *Évaluation de l'effet de la résistance matricielle de la roche intacte dans le processus de l'érodabilité hydraulique du roc*. Congrès de Québec-Mines (21 - 24 novembre 2017), Québec, (Québec), Canada.
- Boumaiza, L., Saeidi, A. et Quirion, M. (2017). *Analyse des fondements de l'indice d'excavabilité utilisé pour l'évaluation de l'érodabilité hydraulique du roc*. Earth Sciences Meeting (*Carrefour des Sciences de la Terre*), March 22 - 24, 2019, Université du Québec à Chicoutimi (Quebec), Canada.

1.6. Thesis outline

This Ph.D. thesis is a collection of three manuscripts of scientific papers (Chapters 3, 4, and 5) that have been published or submitted in international peer-reviewed journals. The first author of these articles is the author of this thesis that contains six chapters as summarized below:

- Chapter 1 (this chapter) is an introduction that includes the general concern, the statement of the research problem, the research objectives, the adopted research methodology to reach the defined objectives, the introduction of the novelty of the research project, and the thesis outline.

- Chapter 2 is written to address Objective 1, which aims to identify and understand the concepts of the most methods used in dam spillway design that assess the hydraulic erodibility of rock. This chapter contains a literature review of the existing comparative methods, as well as a description of different erodibility indices used in these methods to evaluate the rock resistance capacity.
- Chapter 3 has been published as a paper in a refereed journal. After the initial literature review, it became evident that assuming an orthogonal fracture system in cases of non-orthogonal fracture systems can produce considerable error when determining the rock resistance capacity. Accordingly, Chapter 3 is written to achieve Objective 2 of this thesis. This chapter presents an extensive review of Kirsten's concept concerning the "relative block structure" parameter as well as the introduced adjustments to Kirsten's original concept for assessing the required effort to remove a rock block in non-orthogonal joint set systems. An analysis of the proposed relative block structure rating for non-orthogonal fracture systems is also introduced to illustrate the effect of the proposed rating on Kirsten's index.
- Chapter 4 has been published as a paper in a refereed journal. Another element that I retained from the literature review was that there existed no clear consensus on the actual rock mass parameters that most govern the rock scour mechanism. This chapter thus addresses Objective 3 of this thesis. It presents a novel method developed in this thesis for determining the relevant rock mass parameters for evaluating the hydraulic erodibility of rock. Using a

dataset of more than 100 case studies of eroded unlined spillways, existing systems are adapted to classify the selected analyzed parameters. Otherwise, rock mass parameter classification systems are proposed in this study based on the statistical analyses of the considered case studies.

- Chapter 5 has been submitted in manuscript form to a refereed journal. Once the rock mass parameters controlling the rock scour process were determined (Chapter 4), it was appropriate to establish the relative order of the selected parameters, as no clear consensus exists in regard to the weighting (relative importance) of these parameters within the existing erodibility indices used to evaluate the rock resistance capacity. This chapter achieves Objective 5 of this thesis. We propose a novel method for determining the relative importance of rock mass parameters that control the hydraulic erodibility of rock. Chapter 5 also includes a comparative analysis of the methods used for evaluating the hydraulic erodibility of rock (Objective 4 of this thesis).
- Chapter 6 includes the conclusions, recommendations, and future research perspectives.

1.7. References

- Annandale, G.W. 1995. Erodibility. *Journal of Hydraulic Research*, **33**(4): 471–494.
- Annandale, G.W. 2006. *Scour Technology, Mechanics and Engineering in Practice*. McGraw-Hill, New York.
- Bollaert, E. 2002. Transient water pressures in joints and formation of rock scour due to high-velocity jet impact. PhD thesis, École Polytechnique Fédérale de Lausanne, Lausanne, Switzerland.

- Bollaert, E., and Schleiss, A. 2003. Scour of rock due to the impact of plunging high velocity jets Part I: A state-of-the-art review. *Journal of Hydraulic Research*, **41**(5): 451–464.
- Castillo, L.G., Carrillo, J.M., and Sordo-Ward, Á. 2014. Simulation of overflow nappe impingement jets. *Journal of Hydroinformatics*, **16**(4): 922–940.
- Castillo, L.G., Puertas, J., and Dolz, J. 2007. Scour of rock due to the impact of plunging high velocity jets Part I: A state-of-the-art review. *Journal of Hydraulic Research*, **45**(6): 853–858.
- CDWR, (California Department of Water Resources). 2019. <http://www.water.ca.gov/oroville-spillway/> (Consulted in 2019).
- Ervine, D.A., and Falvey, H.T. 1987. Behaviour of turbulent water jets in the atmosphere and in plunge pools. *Proceedings of the Institution of Civil Engineers*, **2**(83): 295–314.
- Ervine, D.A., Falvey, H.T., and Withers, & W. 1997. Pressure fluctuations on plunge pool floors. *Journal of Hydraulic Research*, **35**(2): 257–279.
- George, M.F. 2015. 3D block erodibility: Dynamics of rock-water interaction in rock scour. Ph.D thesis, University of California at Berkeley, USA.
- Hoek, E., Kaiser, P.K., and Bawden, W.F. 1995. Support of underground excavations in hard rock. A.A. Balkema/Rotterdam/Brookfield
- Kirsten, H.A.D. 1982. A classification system for excavation in natural materials. *The Civil Engineer in South Africa*, **24**(7): 292–308.
- Kirsten, H.A.D. 1988. Case histories of groundmass characterization for excavatability. *Rock Classification Systems for Engineering Purposes*. American Society for Testing and Materials, STP 984,: 102–120.
- Moore, J.S., and Kirsten, H.A.D. 1988. Discussion – Critique of the rock material classification procedure. *In Rock classification systems for engineering purposes*. American Society for Testing and Materials, STP-984, L. Kirkaldie Ed, Philadelphia. pp. 55–58.
- Mörén, L., and Sjöberg, J. 2007. Rock erosion in spillway channels – A case study of the Ligga spillway. *In Proceedings of 11th Congress of the International Society for Rock Mechanics*, Lisbon, Portugal. pp. 87–90.
- Pells, S.E. 2016. Erosion of rock in spillways. Ph.D thesis, University of New South Wales, Australia.
- Sawadogo, O. 2010. Scour of unlined dam spillways. Master’s thesis, Stellenbosch University, South Africa.

CHAPTER 2 - LITERATURE REVIEW

The hydraulic erodibility of earth materials was assessed initially for problems associated with the erosion of earth materials under bridges (Keaton, 2013). However, it has been since adopted for dams given that erosion phenomena can occur on the downstream rocks of spillways during flood spill periods, such as observed in 1976 at the Tarbela Dam in Pakistan (Lowe et al., 1979) and in 1962 at the Kariba Dam in Zambia (Bollaert et al., 2012). Since the 1930s, several methods have been proposed to evaluate the hydraulic erodibility of earth materials. However, these approaches are not applicable to a wide range of earth materials (Annandale, 2006), and some methods relate poorly to the interaction of many phenomena during hydraulic erosion (Simoes and Vargas, 2001). Bollaert and Schleiss (2003) cited various developed methods for evaluating the hydraulic erosion of earth materials. An overview of existing scour evaluation methods distinguished between empirical formulae that are based on field or laboratory observations (Mason and Armugam, 1985; Veronese, 1937), analytical-empirical methods that combine empiricism with some physical background (Fahlbusch, 1994; Mirtskhulava et al., 1967), methods that consider extreme values of fluctuating pressures on rock blocks (Armengou, 1991; Puertas, 1994), and methods based on time-averaged or instantaneous pressure differences over and under the rock blocks (Fiorotto and Salandin, 2000; Reinius, 1986). Most methods cited in Bollaert and Schleiss (2003) consider two specific conditions: 1) a hydraulic plunging jet into a plunge pool and 2) flowing water parallel to the spillway channel. For the latter case, there are, however, few methods

available. A specific form is currently used for dam spillway design to assess the hydraulic erosion potential; industry relies largely on “scour threshold line” methods (Hahn and Drain, 2010; Mören and Sjöberg, 2007; Pells et al., 2015). These methods take the form of a correlation between hydraulic energy and the rock resistance capacity. The hydraulic energy (expressed in kW/m^2) generated by flowing water (Henderson, 1966) is usually named the available hydraulic stream power (P_a), and the rock resistance capacity is determined as a value representing an erodibility index, such as Kirsten’s index (Kirsten, 1988, 1982). Examples of such an approach include the Pells (Pells, 2016a) and Annandale methods (Annandale, 1995).

2.1. Existing methods based on Kirsten’s index

Many rock mass classification systems used in engineering were developed during the last century. The most common are the rock mass rating (*RMR*) system (Bieniawski, 1973), the Q-system, also known as the Norwegian Geotechnical Institute classification (Barton et al., 1974), the geological strength index (*GSI*) proposed by Hoek et al. (1995), and the rock mass index (*RMi*) system (Palmstrom, 1996). These classification systems were developed for multiple rock engineering purposes, including underground excavation and slope stability, as well as support design in mines (Hudson and Harrison, 2005; USACE, 1997). Furthermore, some classifications have been used to develop related indices to evaluate the excavatability of earth materials, such as Weaver’s classification (Weaver, 1975), which is based on

the *RMR* system, and Kirsten's index (Kirsten, 1982), which includes several parameters used in the Q-system. During the Cincinnati Symposium (Kirkaldie, 1988), which focused on engineering rock mass classification systems, it was argued that the mechanical excavatability and the hydraulic erodibility of earth materials could be considered as similar processes (Moore and Kirsten, 1988). Van Schalkwyk (1989), Pitsiou (1990), and Moore (1991) then demonstrated that the existing rock mass systems used for evaluating the mechanical excavatability of rock mass incorporate most parameters that affect the hydraulic erodibility of rock. For evaluating the hydraulic erodibility of rock, Van Schalkwyk et al. (1994a) tested several rock mass characterization indices, such as the *RMR* system (Bieniawski, 1973), the Q-system (Barton et al., 1974), and Kirsten's index (Kirsten, 1988, 1982). They found that the tested indices generated similar results; however, Kirsten's index (*N*) was more accurate. This index, developed initially to evaluate the excavatability of earth materials, has since been adopted for assessing the hydraulic erodibility of earth materials, where the "direction of excavation" of the original index has been replaced by the "direction of flow" (Annandale, 1995; Annandale and Kirsten, 1994; Dooge, 1993; Kirsten et al., 1996; Moore et al., 1994; Van-Schalkwyk et al., 1994b, 1994a). The terms "direction of excavation" and the "direction of flow" that correspond to the direction of the acting force, are considered as synonymous in this thesis.

2.1.1.1. **Kirsten's index**

Kirsten's index is expressed as follows:

$$N = M_s \cdot K_b \cdot K_d \cdot J_s \quad (2.1)$$

where:

N : Kirsten's index

M_s : Compressive strength rating

K_b : Rock block size rating

K_d : Joint shear strength rating

J_s : Relative block structure rating

2.1.1.1.1. **Compressive strength of intact rock rating**

The compressive strength of intact rock is determined by performing an unconfined compressive stress (*UCS*) test on a rock sample. Then, knowing the *UCS* value, Equations 2.2 and 2.3 can determine the compressive strength rating number of the intact rock (M_s). Kirsten (1982) also proposed a descriptive chart (Appendix A - Table A.1) having a corresponding M_s rating (0.87 to 280) adapted from the classification of Jennings et al. (1973).

$$\text{For } UCS \leq 10 \text{ MPa} \quad M_s = 0.78 C_r (UCS)^{1.05} \quad (2.2)$$

$$\text{For } UCS \geq 10 \text{ MPa} \quad M_s = C_r (UCS) \quad (2.3)$$

where C_r is a density coefficient (Equation 2.4) defined as a function of the volumetric weight of the rock (γ_r , expressed in kN/m^3).

$$C_r = \frac{\gamma_r}{27} \quad (2.4)$$

2.1.1.2. Rock block size rating

The rock block size factor (K_b) was initially introduced by Cecil (1970) who combined the *RQD* (rock quality designation) index (Deere 1968, Deere and Deere 1988) with the joint sets rating (J_n). This factor (Equation 2.5) was later adopted by Barton et al. (1974) into the Q-system to classify rock masses for the design of underground excavation support and by Kirsten (1982) for his N index.

$$K_b = \frac{RQD}{J_n} \quad (2.5)$$

For our purposes, the *RQD* varies between 5% and 100%, and it is determined following the guidelines of Barton et al. (1974). For its part, the J_n value is determined by a compilation and interpretation of the structural geology of the site.

Knowing the number of joint sets, the corresponding J_n rating is determined following the classification of Kirsten (1982) presented in Appendix A-Table A.2. It should be noted that the J_n ratings proposed by Kirsten were calculated using the same approach as that proposed by Barton et al. (1974). However, the maximum value of 20 calculated by Barton et al. (1974) was found by Kirsten to be unsuitable for the excavatability of earth material. Kirsten (1982, 1988) therefore proposed a maximum value of 5. The rating of J_n as proposed by Kirsten (1982, 1988) varies from 1 to 5.

2.1.1.3. Joints shear strength rating

Kirsten (1982) also adopted the K_d quotient proposed by Barton et al. (1974), which represents the joints shear strength. It is expressed as the ratio of the rating corresponding to joints roughness (J_r) and the value corresponding to the alteration degree of the joints' surface (J_a) as presented in Equation 2.6.

$$K_d = \frac{J_r}{J_a} \quad (2.6)$$

The rating of J_r and J_a can be determined from the visual evaluation of joint conditions in the field and then applying the corresponding rating that was established from the field experience (Barton et al. 1974). The J_r rating for various joint conditions ranges from 0.5 to 4 (Appendix A-Table A.3). The rating proposed for joint alteration (J_a) for different gouge materials is presented in Appendix A-Table

A.4. Although presented in a different format, the values of J_a as defined by Kirsten (1982) are identical to those as defined by Barton et al. (1974), except that the latter proposed a maximum rating of 20 for J_a , whereas Kirsten (1982) reduced it to a maximum value of 18 but maintained the same minimum of 0.75.

2.1.1.4. **Relative block structure rating**

The relative block structure parameter (J_s) corresponds to the effort required to remove a rock block from the rock mass. It was developed mathematically by considering the rock block's shape and orientation relative to the direction of flow (Kirsten, 1982). In practice, the J_s rating is determined as a function of dip and dip direction of the rock block, as well as the joints spacing ratio (Appendix A-Table A.5). Comparing the J_s values initially proposed by Kirsten (1982) to evaluate the mechanical excavatability of earth materials and the J_s values presented in Annandale (1995, 2006) to evaluate the hydraulic erodibility of earth materials (Appendix B), there are slight differences that likely occurred due to minor adjustments.

2.1.2. **Critical observations on Kirsten's index**

Using Kirsten's index to evaluate the excavatability of earth materials faced criticism in regards to its reliability. Braybrooke (1988) mentions issues regarding the

accuracy of Kirsten's index that led to contractual disputes. These disputes were related to a contractor's inability to excavate rock that was initially assessed to be excavatable or from sites having low excavation productivity. As well, MacGregor et al. (1994) found, based on their datasets for excavation productivity, that Kirsten's method is a conservative method of prediction, i.e., rock masses predicted to be extremely hard were determined to be medium to hard in the field. On the other hand, Palmstrom et al. (2002), discussing the limitations of the Q-system (Barton et al., 1974), argued that the block size factor K_b , included in Kirsten's index, provided no meaningful quantification of rock block size. Palmstrom (2005) and Palmstrom and Broch (2006) stated that using rock block volume (V_b) instead of the K_b parameter would improve the quality of Q-system results. Grenon and Hadjigeorgiou (2003) also concluded, from in-situ investigations in Canadian mines, that K_b is an inaccurate parameter for characterizing block size. Furthermore, Pells et al. (2017a) argued that at the time of its development, the RQD index, used as a part of the K_b factor, was developed for a specific application, and it is sometimes applied inconsistently in practice.

In the context of the hydraulic erodibility of rock, Pells (2016) argued that none of the published rock mass indices, including Kirsten's index, was developed specifically to evaluate the hydraulic erodibility of earth materials. Furthermore, he maintained that the UCS , as a parameter included in Kirsten's index, is not appropriate for representing the hydraulic erodibility process. Spectacular erosion events have occurred in rocks having high UCS values, such as those observed in the Copeton Dam spillway in Australia and the Mokolo Dam spillway in South Africa

where 20-m and 30-m deep erosion holes were formed, respectively (Pells, 2016a). Compared to other considered parameters, Kirsten's index is determined to a great extent by the *UCS* rating, which has values ranging from 0.87 to 280 MPa. Furthermore, it is assumed by certain researchers that rock mass strength is controlled mainly by joint systems that could create significant weaknesses in the rock mass (Bieniawski, 1973; Goodman, 1993).

Nonetheless, the J_s parameter included in Kirsten's index was mathematically quantified based on the effect of a block's shape and orientation relative to the direction of excavation. This parameter was adopted subsequently into other systems developed to evaluate the excavatability of earth materials (Hadjigeorgiou and Poulin, 1998; Scoble et al., 1987). Pells (2016) argued, based on the field observations of multiple eroded spillways and laboratory experiments, that the J_s values proposed by Kirsten (1982) for assessing the mechanical excavatability of earth materials were not intuitively representative when assessing the hydraulic erodibility of rock.

2.1.3. Comparative methods based on the Kirsten index

Using the correlation relationship between water flow energy (P_a) and Kirsten's index, it was observed, from the plotted data of the various case studies, that case studies exhibiting scour conditions could be distinguished from those showing no scour. These two groups can be separated by "scour threshold lines."

2.1.3.1. Moore et al.'s scour threshold

Using field data collected by the U.S. Department of Agriculture, Moore et al. (1994) and Temple and Moore (1994) proposed a scour threshold line that was a function of Kirsten's index and P_a . However, their P_a was calculated for a specific flowing water condition known as "headcut²" (Henderson, 1966), expressed in kW/m. Annandale (2006) mentioned that the number of no-scour events that Moore et al. (1994) used was insufficient (only six no-scour events – Figure 2.1) to clearly demarcate the zone between scour and no-scour events (Annandale, 2006).

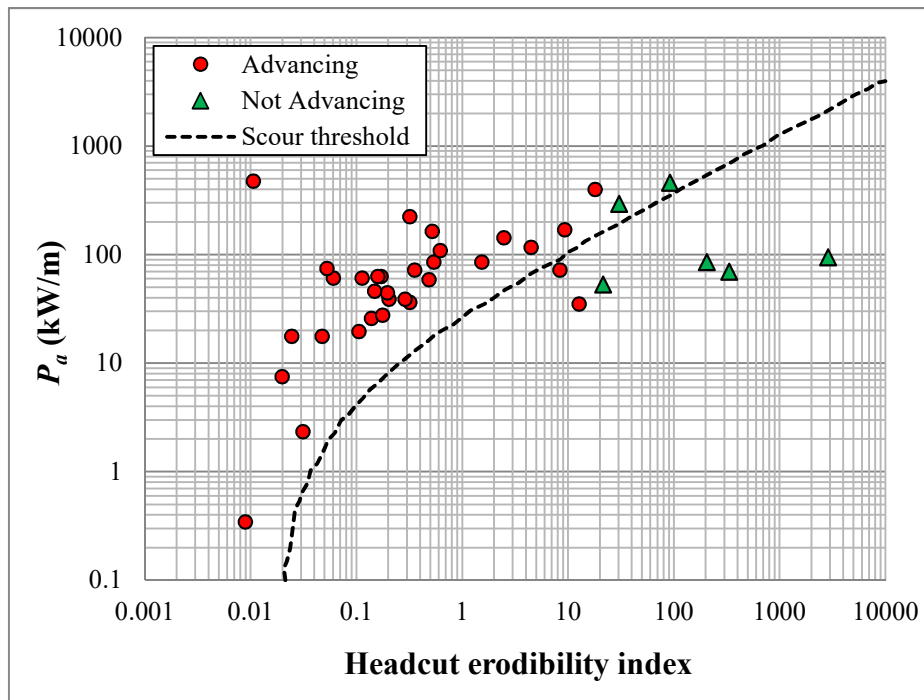


Figure 2.1. Scour threshold line as determined by Moore et al. (1994).

² Headcutting is the removal of earth material by the combined effect of the erosive power of a jet discharging over an edge and mass wasting.

2.1.3.2. Van Schalkwyk et al.'s scour thresholds

Pitsiou (1990) and Dooge (1993) reviewed hydraulic erosion case studies of several rocky unlined spillways of dams in South Africa. In these reviews, the geological conditions were characterized using Kirsten's index and P_a calculated in kW/m^2 . Van Schalkwyk et al. (1994a) compiled the findings from 18 selected unlined spillways of these two cited works. In contrast to the initial work conducted by Moore et al. (1994), Van Schalkwyk et al. (1994a) stated that categorizing the erosion condition in multiple classes, rather than two classes (scour and no-scour), could predict more accurately the scour risk. Consequently, multiple scour threshold lines were proposed as a function of erosion depth (Table 2.1). These scour thresholds lines are shown in Figure 2.2. Note that the two erosion classes "little" and "moderate" in Table 2.1 are grouped together in Figure 2.2 and are illustrated as a single erosion class named "little to moderate".

Table 2.1. Classification of the degree of erosion (Van Schalkwyk et al. 1994a).

Depth of erosion (m)	Erosion class
0	None
0–1	Little
1–5	Moderate
>5	Extensive

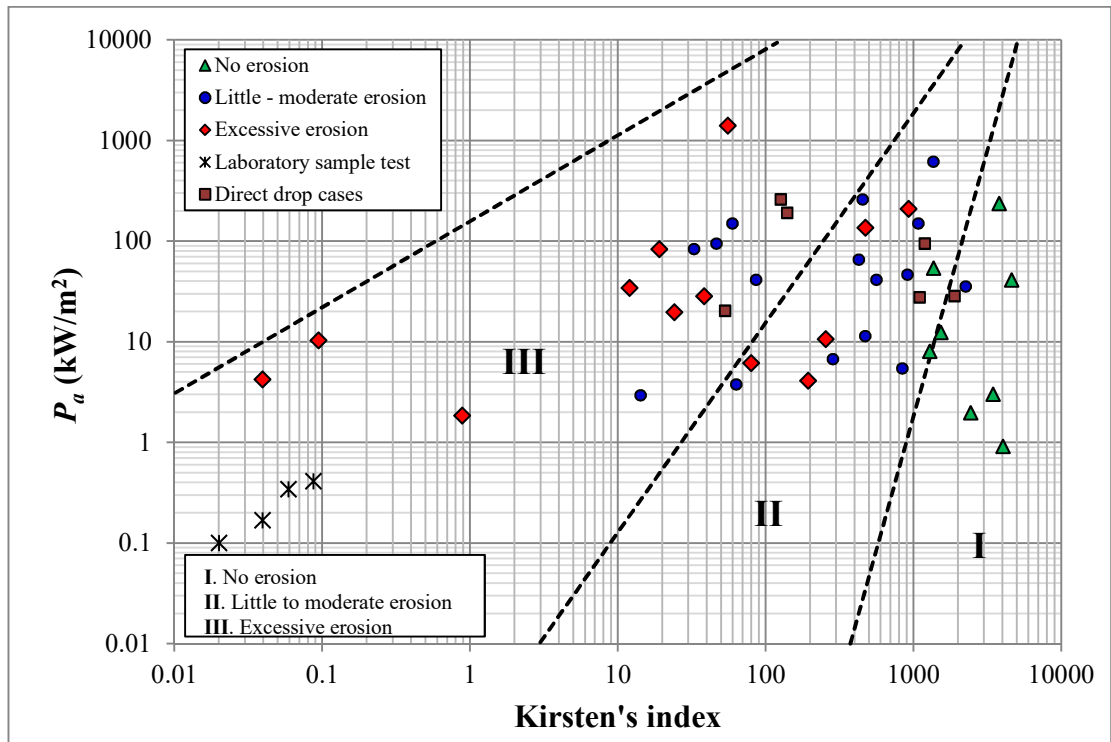


Figure 2.2. Scour threshold lines as determined by Van Schalkwyk et al. (1994a).

Van Schalkwyk et al. (1994b) updated their findings by including additional data used by Moore et al. (1994). The new perceived scour threshold lines were then altered (Figure 2.3) by adding these new data points and adopting the new erosion classification presented in Table 2.2. Note again that the two erosion classes “minor” and “moderate” in Table 2.2 are combined in Figure 2.3 and are illustrated as a single erosion class “minor to moderate”.

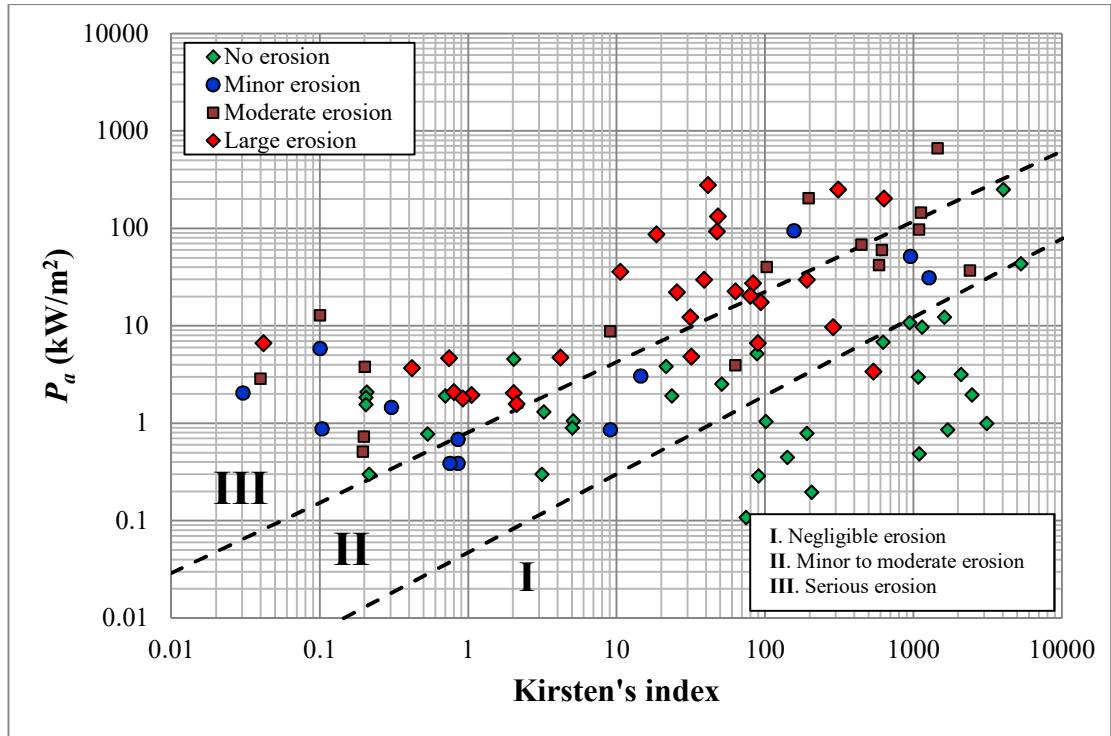


Figure 2.3. Scour threshold lines as determined by Van Schalkwyk et al. (1994b).

Table 2.2. Classification of the degree of erosion (Van Schalkwyk et al. 1994a).

Depth of erosion (m)	Erosion class
<0.2	Negligible
0.2–0.5	Minor
0.5–2	Moderate
>2	Large

2.1.3.3. Annandale's scour threshold

Annandale (1995), using Kirsten's index, analysed the collected data of Moore et al. (1994), some data of Van Schalkwyk et al. (1994a), and scour data from the Bartlett Dam (Arizona). By plotting this data in relation to P_a (kW/m²), Annandale (1995) proposed a scour threshold line that demarcated the separation of scour and no-scour events (Figure 2.4). This scour threshold line was also validated via near-prototype experiments undertaken at the Engineering Research Center of Colorado State University, Fort Collins (Annandale et al., 1998; Kuroiwa et al., 1998). Annandale considered an erosion depth greater than 2 m to be exhibiting a scour condition. His justification for this 2 m limit was that less than 2 m of erosion in rock is considered to be relatively inconsequential and most probably the result of the removal of loose blocks of rock at the stratum surface (Annandale, 2006).

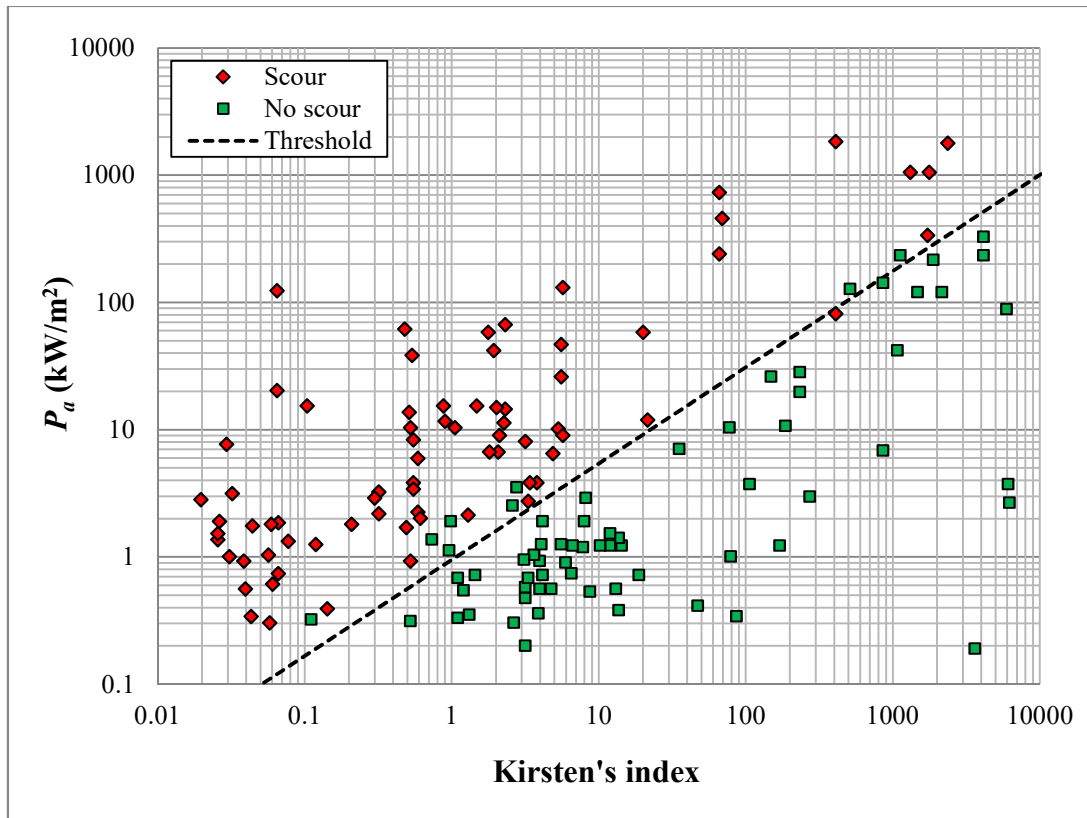


Figure 2.4. Scour threshold line as determined by Annandale (1995).

2.1.3.4. Kirsten et al.'s scour threshold

Considering the same concept of Annandale (1995) in terms of scour condition (>2 m = scour; <2 m = no scour), Kirsten et al. (1996, 2000) used data from Dooge (1993) and Moore et al. (1994) to propose another scour threshold line (Figure 2.5); the scour conditions in this data set were not specified in the original chart version of Kirsten et al. (1996, 2000). Kirsten et al. (1996, 2000) and Annandale (1995, 2006) have attempted to produce extensive analyses that involve various earth

materials, ranging from non-cohesive silt material to soft and resistant materials such as rock. This wide-ranging approach aimed to develop a single relationship for all materials by relating Kirsten's index to P_a . The scour thresholds shown in Figures 2.4 and 2.5 present only the soft and resistant materials characterized by a Kirsten's index of >0.01 (Annandale, 2006; Kirsten et al., 2000).

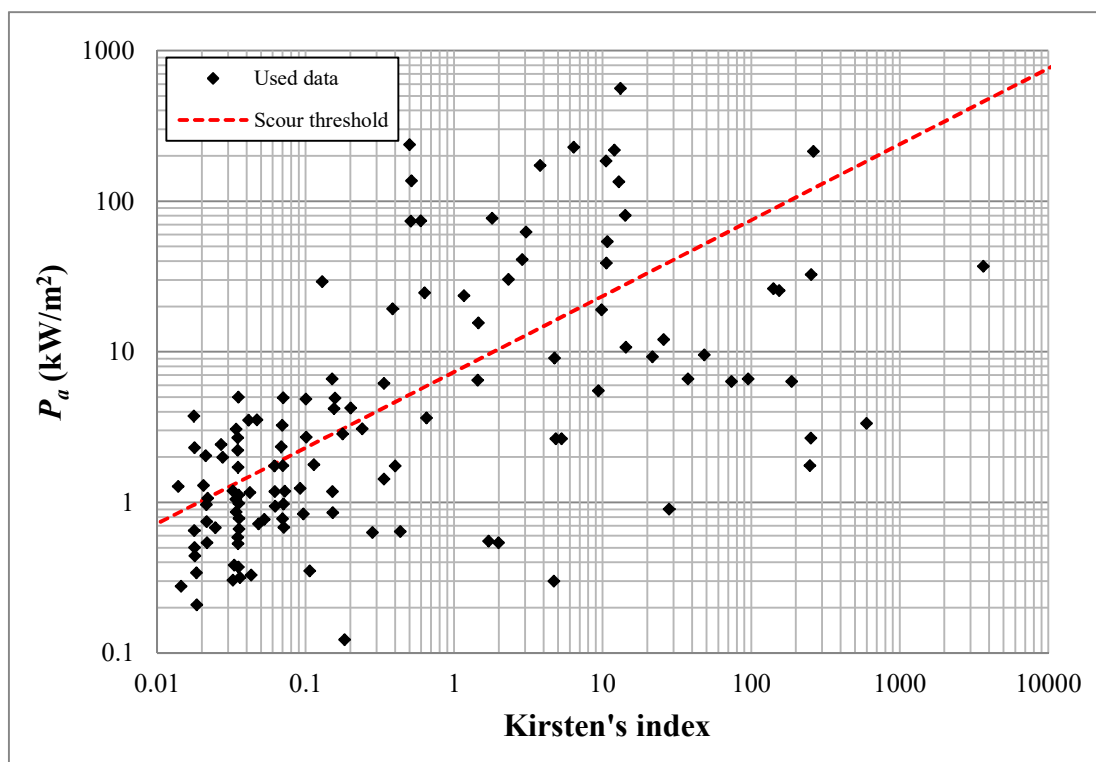


Figure 2.5. Scour threshold line as determined by Kirsten et al. (2000).

Considering that the scour threshold lines proposed by Annandale (1995) and Kirsten et al. (1996) are based on an identical limit for erosion (>2 m = scour; <2 m = no scour), they can be plotted together. The concept proposed by Van Schalkwyk et

al. (1994a) cannot be compared in this framework because it does not consider an erosion limit depth of 2 m (Table 2.1). However, the erosion conditions proposed by Van Schalkwyk et al. (1994b) can be compared with those of Annandale (1995) and Kirsten et al. (1996) by considering the classes of “negligible”, “minor”, and “moderate” (Table 2.2) as no-scour conditions (<2 m), while the erosion class of “large”, as presented in Table 2.2, represents scour conditions (>2 m). The lines demarcating the interpreted onset of scour based on Kirsten’s index versus P_a are presented in Figure 2.6. The scour threshold proposed by Moore et al. (1994) is not included in this comparison because the hydraulic energy was expressed in kW/m rather than kW/m².

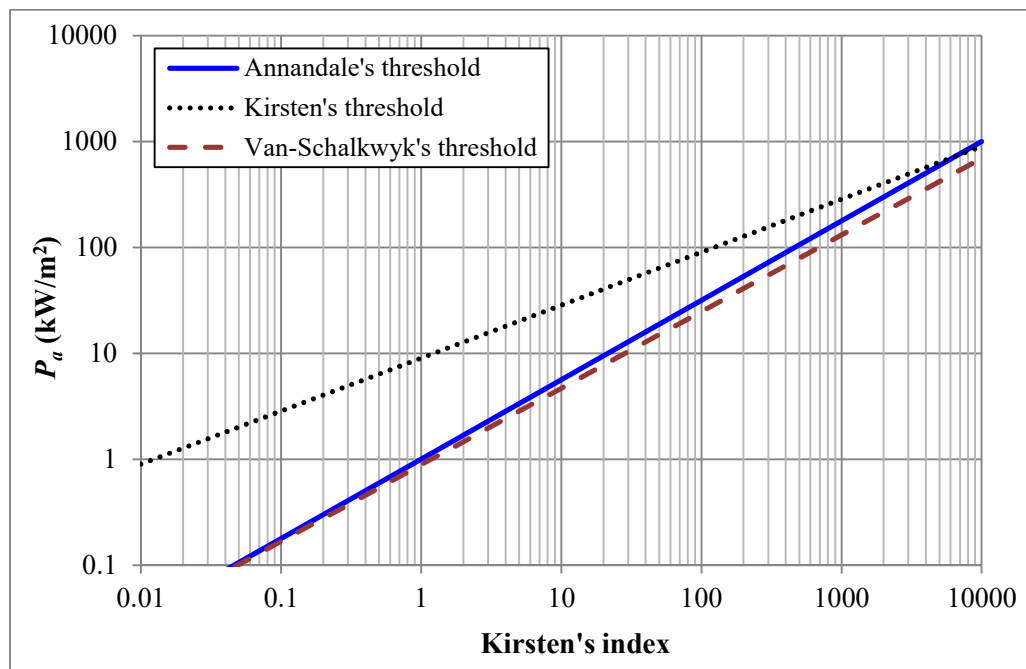


Figure 2.6. Comparison of determined scour threshold lines.

As the comparative methods are all based on Kirsten's index, Figure 2.6 shows a good correlation between Annandale's and Van Schalkwyk's thresholds, although Kirsten's threshold differs slightly. This difference could be explained by the independent field assessment of the earth materials when the data was interpreted. Industry, however, relies largely on Annandale's threshold (Castillo and Carrillo, 2016; George and Annandale, 2006; Hahn and Drain, 2010; Laugier et al., 2015; Monfette, 2004; Mören and Sjöberg, 2007; Pells et al., 2015; Rock, 2015). Using Annandale's chart (Figure 2.4), the calculated value of Kirsten's index for earth material can be plotted on the abscissa axis. By projecting this value on the threshold line, a hydraulic power expressed in kW/m^2 , usually called the "required hydraulic power (P_r)" is then determined on the ordinate axis. P_r represents the maximum hydraulic power that the rock could support during a flood period. If the rock is subjected to $P_a > P_r$, there will be a possibility of rock erosion.

2.2. Pells's methods

In seeking to develop an appropriate rock mass index for evaluating the hydraulic erodibility of rock, Steven Pells characterized an extensive set of rock masses from unlined rocky spillways of selected dams in Australia, South Africa, and the USA (Pells, 2016a; Pells et al., 2017b, 2016, 2015). These case studies of eroded unlined spillways included the characterization of the amount of erosion, the interpretation of rock mass geology, and the analysis of historical floods and

hydraulic conditions. In most of the South Africa spillways, care was taken to also review the same locations of erosion investigated previously by Van Schalkwyk et al. (1994b) to provide an independent assessment of erosion, geology, and hydraulic conditions. Erosion was then classified qualitatively within five classes (Table 2.3). This classification differed somewhat to that of Van Schalkwyk et al. (1994a, 1994b) (Tables 2.1 and 2.2) by dividing erosion >2 m depth into two classes (“large” and “extensive”) and including the size of the eroded hole (Table 2.3). A complete detailed summary of the collected data (observed erosion, rock mass geology, and hydraulic conditions) is available in Pells (2016).

Table 2.3. Description of the erosion condition classes (Pells, 2016a).

Max. depth (m)	General extent (m ³ /100 m ²)	Descriptor	Erosion class
<0.3	<10	Negligible	I
0.3–1	1–30	Minor	II
1–2	30–100	Moderate	III
2–7	100–350	Large	IV
>7	>350	Extensive	V

Based on the correlation between the erosive force of flowing water and rock resistance capacity, Pells (2016a) tested the rock mass indices that are used widely in the analysis of underground excavation stability and support design. These indices

include the Q-system of Barton et al. (1974) and the geological strength index (*GSI*) proposed by Hoek et al. (1995). The *GSI* index was calculated from the *RMR* components system (Bieniawski, 1976) and also estimated from a lookup chart of Marinos and Hoek (2000). Pells (2016) also tested Kirsten's index (Kirsten, 1982) as it is commonly used to evaluate the hydraulic erodibility of rock.

Pells (2016) observed that increased erosion was associated with an increase in hydraulic loading and a decrease in rock mass quality based on the tested indices. However, the “goodness” of the correlation was not noticeably superior for any one of the tested rock mass indices. This stands to reason as none of the tested indices was developed to represent the hydraulic erodibility mechanism (Pells, 2016a). On the other hand, it was verified that *GSI*, estimated from the *GSI* chart of Marinos and Hoek (2000), is of compatible accuracy to erosion estimated through calculating the various sub-parameters of the *RMR* system (Bieniawski, 1976). This was one of the reasons Pells (2016) proposed his first alternative erodibility index, derived from *GSI* estimated using the Marinos and Hoek's lookup chart. This *GSI* index was then modified to make it more amenable for evaluating the hydraulic erodibility of rock. The erodibility index “Rock Mass Erosion Index (*RMEI*)” was also developed as an attempt to represent most erosion mechanisms observed in the field.

2.2.1. Geological strength index for erodibility (*eGSI*)

To modify the intact rock Hoek-Brown failure criteria (Hoek and Brown, 1980a, 1980b), so as to represent rock mass, Hoek et al. (1995) altered their initial equations by incorporating some of Bieniawski's *RMR* system components (Bieniawski, 1989, 1976) to create the *GSI*. Marinos and Hoek (2001) then produced a lookup chart for determining the *GSI* of heterogeneous rock masses. Pells (2016) examined the two proposed alternative means of determining *GSI* (from the *RMR* system and the *GSI* lookup chart) and then modified the *GSI* to develop an erodibility index (*eGSI*) that was more amenable to evaluating the hydraulic erodibility of rock. However, before discussing the developed *eGSI* index, the two methods for determining *GSI* (from *RMR* system and from *GSI* lookup chart) are first summarized below.

2.2.1.1. Determining *GSI* from *RMR* components

The *RMR* classification system was initially proposed by Bieniawski (1973). However, it has since been modified to be more accurate when applied to rock mass engineering design (Bieniawski, 1989, 1976). The *RMR* value can be calculated using Equation 2.7, where the factors *F1* to *F6* are, respectively: the *UCS* of intact rock, *RQD*, joints spacing, joints conditions, groundwater conditions, and joints orientation.

$$RMR = F1 + F2 + F3 + F4 + F5 + F6 \quad (2.7)$$

Using the *RMR* from Bieniawski (1976), Table 2.4 should be applied to calculate factors *F1* to *F4*. The rock mass is assumed to be completely dry by assigning rating of 10 to the groundwater factor (*F5*). Also, very favourable joints orientations are assumed and the adjustment for joints orientation value is set at zero (Hoek et al., 1995). The final *RMR*, usually called *RMR*₇₆, is therefore determined as:

$$RMR_{76} = F1 + F2 + F3 + F4 + 10 \quad (2.8)$$

Table 2.4. Information for determining the factors *F1* to *F4* included in Bieniawski's 1976 *RMR* classification system (Hoek et al., 1995).

Parameter		Range of values							
<i>F1</i>	Strength of intact rock material	Point-load strength index	>8 MPa	4 – 8 MPa	2 – 4 MPa	1 – 2 MPa	For this low rang uniaxial compressive test is preferred		
		Uniaxial compressive strength	>200 MPa	100 – 200 MPa	50 – 100 MPa	25 – 50 MPa	10-25 MPa	3-10 MPa	1-3 MPa
	Rating	15	12	7	4	2	1	0	
<i>F2</i>	Drill core quality RQD	90 – 100 %	75 – 90 %	50 – 75 %	25 – 50 %	<25 %			
	Rating	20	17	13	8	3			
<i>F3</i>	Spacing of joints	>3 m	1 – 3 m	0.3 – 1 m	50 - 300 mm	<50 mm			
	Rating	30	25	20	10	5			
<i>F4</i>	Condition of joints	Very rough surfaces Not continuous No separation Hard joint wall contact	Slightly rough surfaces Separation <1 mm Hard joint wall contact	Slightly rough surfaces Separation <1 mm Soft joint wall contact	Slickensided surfaces OR Gouge <5 mm thick OR Joints open 1-5 mm Continuous joints	Soft gouge >5 mm thick OR Joints open >5 mm Continuous joints			
		Rating	25	20	12	6	0		

When the *RMR*₇₆ >18, *GSI* has the same value as *RMR*₇₆ (Equation 2.8). For *RMR*₇₆ <18, Bieniawski's 1976 classification cannot be used to estimate *GSI*. Hoek et al. (1995) recommended instead Equation 2.9 based on the Q-system of Barton et al. (1974), but they modified (Q') for non-groundwater conditions (Equation 2.10).

$$GSI = 9 \ln Q' + 44 \quad (2.9)$$

$$Q' = K_b \cdot K_d \quad (2.10)$$

2.2.1.2. Determining *GSI* from the lookup chart

Later, Marinos and Hoek (2000, 2001) proposed a lookup chart for the *GSI* for heterogeneous rock masses (Figure 2.7). It is based on an assessment of the lithology, structure, and condition of joints surfaces in the rock mass and is estimated from visual examination of the rock mass exposed in outcrops and surface excavations, such as road cuts, tunnel faces, and borehole cores. It is based on two fundamental parameters of the geological process (the blockiness of the mass and joints condition); hence, it takes into account the main geological constraints that govern a geological formation. It is thus a geologically sound index that is simple to apply in the field (Marinos et al., 2007; Tsiambaos and Saroglou, 2010).





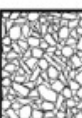





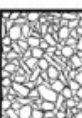

<p>GEOLOGICAL STRENGTH INDEX FOR JOINTED ROCKS (Hoek and Marinos, 2000)</p> <p>From the lithology, structure and surface conditions of the discontinuities, estimate the average value of GSI. Do not try to be too precise. Quoting a range from 33 to 37 is more realistic than stating that GSI = 35. Note that the table does not apply to structurally controlled failures. Where weak planar structural planes are present in an unfavourable orientation with respect to the excavation face, these will dominate the rock mass behaviour. The shear strength of surfaces in rocks that are prone to deterioration as a result of changes in moisture content will be reduced if water is present. When working with rocks in the fair to very poor categories, a shift to the right may be made for wet conditions. Water pressure is dealt with by effective stress analysis.</p>		<p>SURFACE CONDITIONS</p> <p>VERY GOOD Very rough, fresh unweathered surfaces</p> <p>GOOD Rough, slightly weathered, iron stained surfaces</p> <p>FAIR Smooth, moderately weathered and altered surfaces</p> <p>POOR Slickensided, highly weathered surfaces with compact coatings or fillings or angular fragments</p> <p>VERY POOR Slickensided, highly weathered surfaces with soft clay coatings or fillings</p> <p>STRUCTURE DECREASING SURFACE QUALITY →</p>				
<p>STRUCTURE</p> <p> INTACT OR MASSIVE - intact rock specimens or massive in situ rock with few widely spaced discontinuities</p> <p> BLOCKY - well interlocked undisturbed rock mass consisting of cubical blocks formed by three intersecting discontinuity sets</p> <p> VERY BLOCKY- interlocked, partially disturbed mass with multi-faceted angular blocks formed by 4 or more joint sets</p> <p> BLOCKY/DISTURBED/SEAMY - folded with angular blocks formed by many intersecting discontinuity sets. Persistence of bedding planes or schistosity</p> <p> DISINTEGRATED - poorly interlocked, heavily broken rock mass with mixture of angular and rounded rock pieces</p> <p> LAMINATED/SHEARED - Lack of blockiness due to close spacing of weak schistosity or shear planes</p> <p>← DECREASING INTERLOCKING OF ROCK PIECES</p>		<p>DECREASING INTERLOCKING OF ROCK PIECES</p> <p>90</p> <p>80</p> <p>70</p> <p>60</p> <p>50</p> <p>40</p> <p>30</p> <p>20</p> <p>10</p> <p>N/A N/A</p>				
<p> INTACT OR MASSIVE - intact rock specimens or massive in situ rock with few widely spaced discontinuities</p>		90	80	70	60	N/A
<p> BLOCKY - well interlocked undisturbed rock mass consisting of cubical blocks formed by three intersecting discontinuity sets</p>		80	70	60	50	40
<p> VERY BLOCKY- interlocked, partially disturbed mass with multi-faceted angular blocks formed by 4 or more joint sets</p>		70	60	50	40	30
<p> BLOCKY/DISTURBED/SEAMY - folded with angular blocks formed by many intersecting discontinuity sets. Persistence of bedding planes or schistosity</p>		60	50	40	30	20
<p> DISINTEGRATED - poorly interlocked, heavily broken rock mass with mixture of angular and rounded rock pieces</p>		50	40	30	20	10
<p> LAMINATED/SHEARED - Lack of blockiness due to close spacing of weak schistosity or shear planes</p>		N/A	N/A	10	20	30

Figure 2.7. Lookup chart for determining *GSI* from field observations (P. Marinos and Hoek, 2000).

2.2.1.3. Development of the *eGSI* erodibility index

The case studies of the eroded spillways documented by Pells (2016) produced *RMR* values >18 ; for these values, Equation 2.8 is used to determine *GSI*. *GSI* can also be determined using the lookup chart (*GSI-Chart*). The data points are classified according to the interpreted erosion categories presented in Table 2.3. There exists a correlation between both *GSI* and the interpreted erosion categories; however, a stronger correlation is noted when the *GSI-Chart* is used (Pells, 2016a). As such, Pells (2016) proposed an erodibility index *eGSI* derived from the *GSI-Chart*. Furthermore, use of the *GSI-Chart* is of considerable interest because:

- 1) The values determined from the lookup chart (Figure 2.7) are substantially easier to obtain than values obtained via calculation from *RMR*;

- 2) The lookup chart is not encumbered with the problematic *RQD*, as is the *GSI-RMR*. Indeed, Pells et al. (2017a) argued that at the time of its development, the *RQD* index was developed for a specific application and that this parameter is sometimes applied inconsistently in practice;

- 3) The lookup chart is also not dominated by the substance strength value of *UCS*, as occurs with *GSI-RMR*. In fact, Pells (2016) considered that the *UCS* of rock plays a very limited, if not negligible, role in the erodibility of fractured rock masses.

Factor F_6 , representing the discontinuity orientation adjustment, can be removed from RMR_{76} (Section 2.2.1.1), and a new erosion-discontinuity orientation adjustment factor (E_{doa}), which represents the vulnerability of a rock mass to erodibility, can be added (Pells 2016). Therefore, the proposed erodibility index (Equation 2.11) takes the form of the original RMR equation (Equation 2.7).

$$eGSI = GSI + E_{doa} \quad (2.11)$$

The E_{doa} factor can be determined from the curves presented in Figures 2.8 and 2.9. As reported by Pells (2016), the process of deriving these curves was inspired from the graphical presentation of Kirsten's J_s factor (Moore and Kirsten, 1988). Various pictograms were drawn for rock masses having two orthogonal joint sets at various orientations relative to the direction of flow and marked by various relative spacing (Figures 2.8 and 2.9). For the pictograms, the surface was defined primarily along joints observed at spillway sites. The surface formed in this manner creates a roughness and block shape that reflects joint structure. The E_{doa} values were derived purely by thought-experiment with the pictograms, assessing vulnerability to significant and ongoing erosion and considering the kinematics of block removal as well as the nature and direction of hydraulic loading, as intuited from field observation and the analysis of the numerous model tests. The process was also undertaken for non-orthogonal joint sets; however, the appraised values were not significantly different (Pells, 2016a).

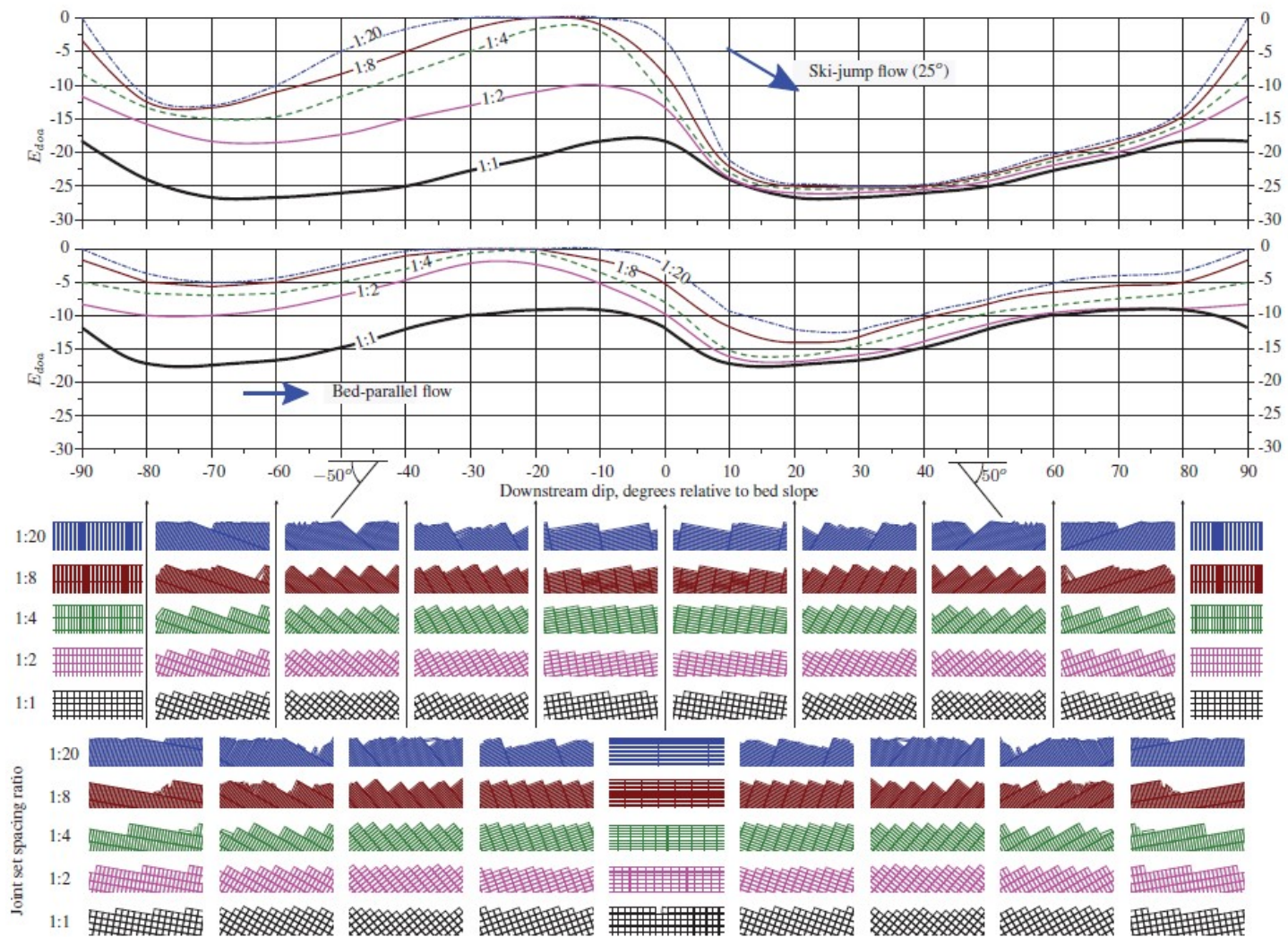


Figure 2.8. Curves used for determining the E_{doa} factor in the case of horizontal flowing surface as subjected to various water flows (ski-jump flow of 25° relative to flowing surface and parallel flow relative to flowing surface). 1:1, 1:2, etc. represent the joint set spacing ratios (e.g., 1:2, where 1 represents the width of the block, and 2 represents its length) (Pells, 2016a).

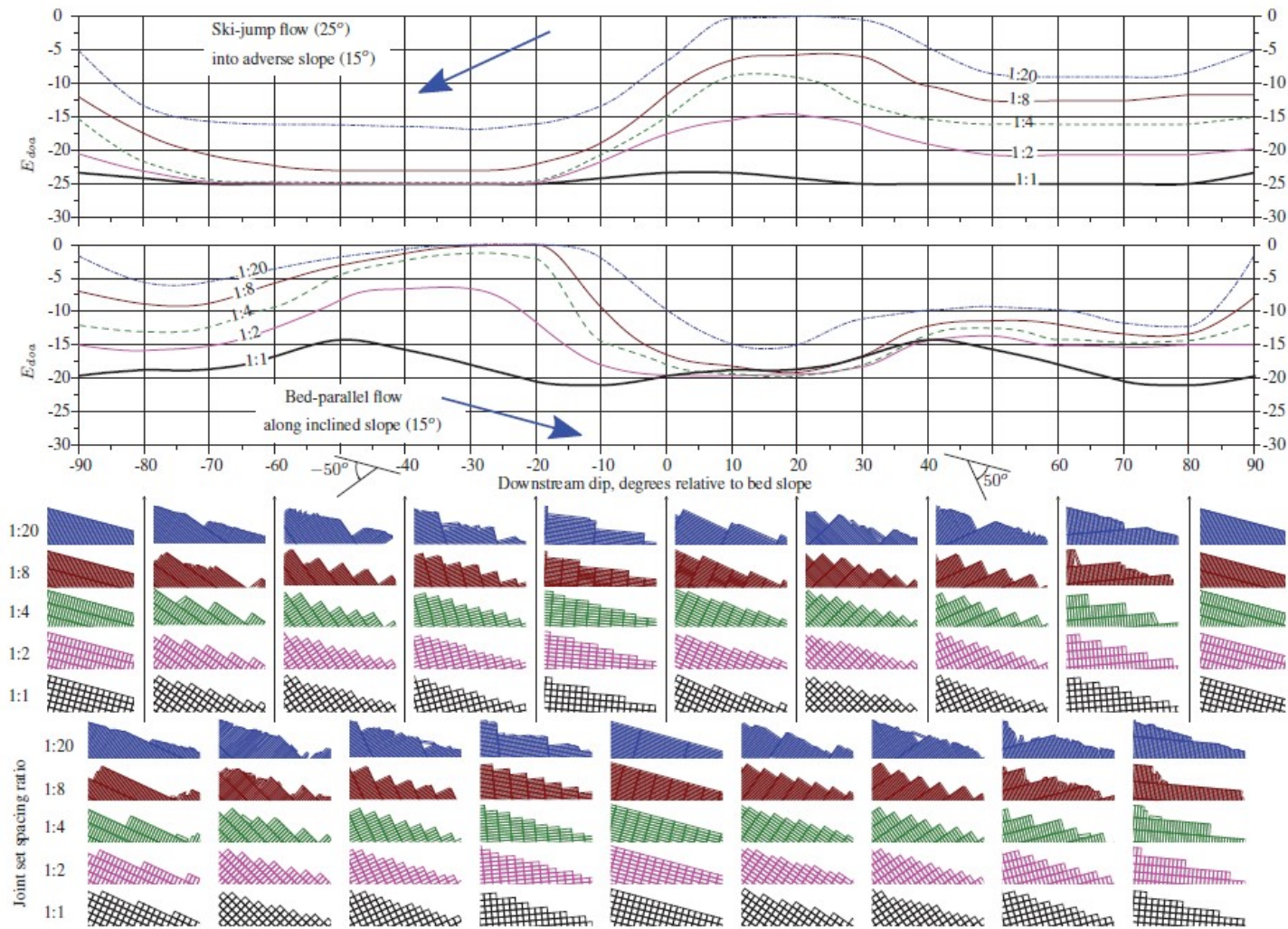


Figure 2.9. Curves used for determining the E_{doa} factor in the case of inclined flowing surface subjected to various water flows (ski-jump flow of 25° into an adverse inclined flowing surface of 15° and parallel flow along an inclined flowing surface of 15°) (Pells, 2016a).

The plotting of the force of flowing water versus the $eGSI$ index is shown in Figure 2.10. The data points are classified according to the interpreted erosion classes presented in Table 2.3, and the erosion classes boundaries are contoured manually. Pells (2016) stated that the inclusion of the factor E_{doa} , representing the erosion vulnerability due to rock block's shape and orientation relative to the flow direction, increased the “spread” of the data and provided a subtle improvement in the correlation with erosion. Consequently, the $eGSI$ index becomes more amenable for evaluating the hydraulic erodibility of rock (Pells 2016). It should be noted, however, that the GSI lookup chart remains semi-qualitative, and any subsequent evaluation can be greatly influenced by the judgment of the analyst in the field. Furthermore, it was not developed specifically to assess the hydraulic erodibility of rock; for example, it does not incorporate details related to joints opening that could play a determining role in the hydraulic erodibility process.

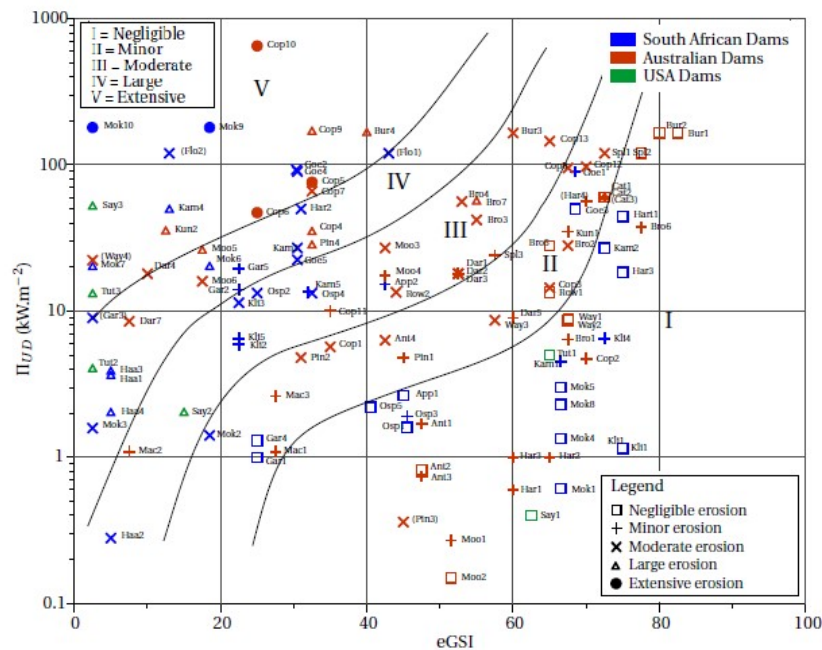


Figure 2.10. Interpreted erosion classes using $eGSI$ versus hydraulic power expressed in the figure as Π_{UD} (Pells, 2016a).

2.2.2. Rock mass erodibility index (*RMEI*)

The *RMEI* classification system was developed as alternative to represent the most important geological factors controlling the erosion mechanism. It is based on field observations of eroded case studies (Pells 2016). Pells (2016) conceived the *RMEI* classification system as the existing rock mass indices, including Kirsten's index, did not represent the erosion actually observed during field investigations. The valuable addition to the *RMEI* classification system was the representation of the geological factors controlling the erosion mechanism, where the relative importance of each factor is based on the field observations of eroded spillway case studies.

The structure of the *RMEI* classification system was inspired from that used in Fell et al. (2008); the subsequent classification system combines multiple factors (Pells, 2016a). For the *RMEI* system, the factors combining was applied to represent the likelihood factor (*LF*) concerning the detachment of rock blocks from the spillway floor. The *RMEI* classification system is also based on the relative importance factor (*RF*). This factor places the greatest weight to those factors judged to be most important in controlling detachment and down-weights those judged least important (Pells, 2016a). The *RMEI* classification system is presented in Figure 2.11. The value of *RMEI* is determined based on *RF* and *LF* as presented in Equation 2.12. The prefixes *P1* to *P5* are various sets of parameters that represent, respectively, the kinematically viable mechanism for detachment, the nature of the potentially eroding surface, the nature of the joints, the joints spacing, and the block shape.

$$RMEI = (RF_{P1}.LF_{P1}).(RF_{P2}.LF_{P2}).[(RF_{P3}.LF_{P3})+(RF_{P4}.LF_{P4})+(RF_{P5}.LF_{P5})] \quad (2.12)$$

To define the parameter of the nature of the joints (Figure 2.11), Pells (2016) grouped three rock mass characteristics (joints roughness, joints aperture, and the *UCS* of joints). On the other hand, Pells (2016) provided a suggested method for estimating the likelihood factor for this parameter as presented in Table 2.5. However, this table does not consider the *UCS* of joints.

Table 2.5. Suggested method for estimating LF_{P3} (Pells, 2016a).

Aperture	Joint roughness coefficient (JRC)				Smooth and/or slickensided
	>12	8 to 10	4 to 8	<4	
Tight	1	1	1	2	2
<1 mm	1	1	2	3	3
1 to 2 mm	1	2	3	4	4
2 to 5 mm	2	3	4	5	5
>5 mm	3	4	5	5	5

Erosion vulnerability parameter	RF ¹	Likelihood factor (LF)				
		Very unlikely	Unlikely	Likely	Highly likely	Almost certain
		1	2	3	4	5
P1: Kinematically viable mechanism for detachment ²	3	Rock with three defects, basal defect subparallel to spillway floor, and no day lighting basal release surface	Rock with three or more defects with: basal defect subparallel to spillway floor, Joint 2 protruding from surface	Rock with three or more defects with persistent basal defect dip 10°–30° upstream relative to the spillway floor	Rock with three or more defects, with persistent basal defect dip ≤10° upstream relative to the spillway floor	Persistent basal defect subparallel to the spillway floor, day lighting upstream or downstream
		or Massive rock with effectively only two defect sets and no basal release surface	or Basal defect inclined upstream or downstream at >30° relative to spillway floor	or Persistent basal defect dip 10°–30° downstream relative to the spillway floor	or Persistent basal defect dip ≤10° downstream relative to the spillway floor	or Persistent shear and/or closely jointed rock which erodes readily forming a release surface into the shear
P2: Nature of the potentially eroding surface	3	Smooth water or glacier worn, with no protrusions of joint 2, no opening of defects	Bedding surface with protrusions of joint 2 <1 mm, and little or no opening of defects	Relatively small protrusions and defect openings (e.g. pre-split, or ripped and bulldozed)	Irregular surface following defects, little opening of defects (e.g. blasted rock).	Irregular surface following defects, extensive defect opening (e.g. heavily blasted rock)
P3: Nature of the defects ³	2	Very rough surfaces, e.g. JRC ≥12	Rough surfaces, e.g. JRC 8–10	Slightly rough surfaces, e.g. JRC 4–8	Smooth surfaces e.g. JRC <4	Smooth or slickensided surfaces
		No separation	Aperture <1 mm	Aperture 1–2 mm	Aperture 2–5 mm	Aperture >5 mm
		UCS >50MPa	UCS 20 to 50MPa	UCS 5 to 20MPa	UCS 1 to 5MPa	UCS <1MPa, or Soft gouge >5mm thick
P4: Spacing of basal defect ⁴	1	>3 m	1–3 m	0.3–1m	0.1–0.3m	<0.1m
P5: Block shape ⁵	1	≤0.5	0.5–1	1–2	2–5	>5
Notes: 1. Relative importance factor 2. Defects include joints, bedding surfaces, shears, and foliation partings. 3. Select class which best fits the data taking into account the kinematically viable mechanism and those defects that control the displacement of the block of rock from the spillway. Use Table 2.5 to assist in making this assessment but use best judgment to make the assessment. 4. Joint 1 is the basal defect of a block or region (bedding or joint). 5. Block shape = Joint 2 spacing/Joint 1 spacing; Joint 2 is sub-vertical defect normal to the flow in the spillway.						

Figure 2.11. *RMEI* classification system for evaluating the hydraulic erodibility of rock (Pells, 2016a).

The plotting of the force of flowing water versus *RMEI* is shown in Figure 2.12. The data points are classified according to the interpreted erosion classes presented in Table 2.3, and the erosion classes boundaries are contoured manually. It should be mentioned that Figure 2.12 was originally proposed by Pells (2016) and was modified slightly by Douglas et al. (2018); however, it is not clear whether an optimizing process was used for updating the threshold lines.

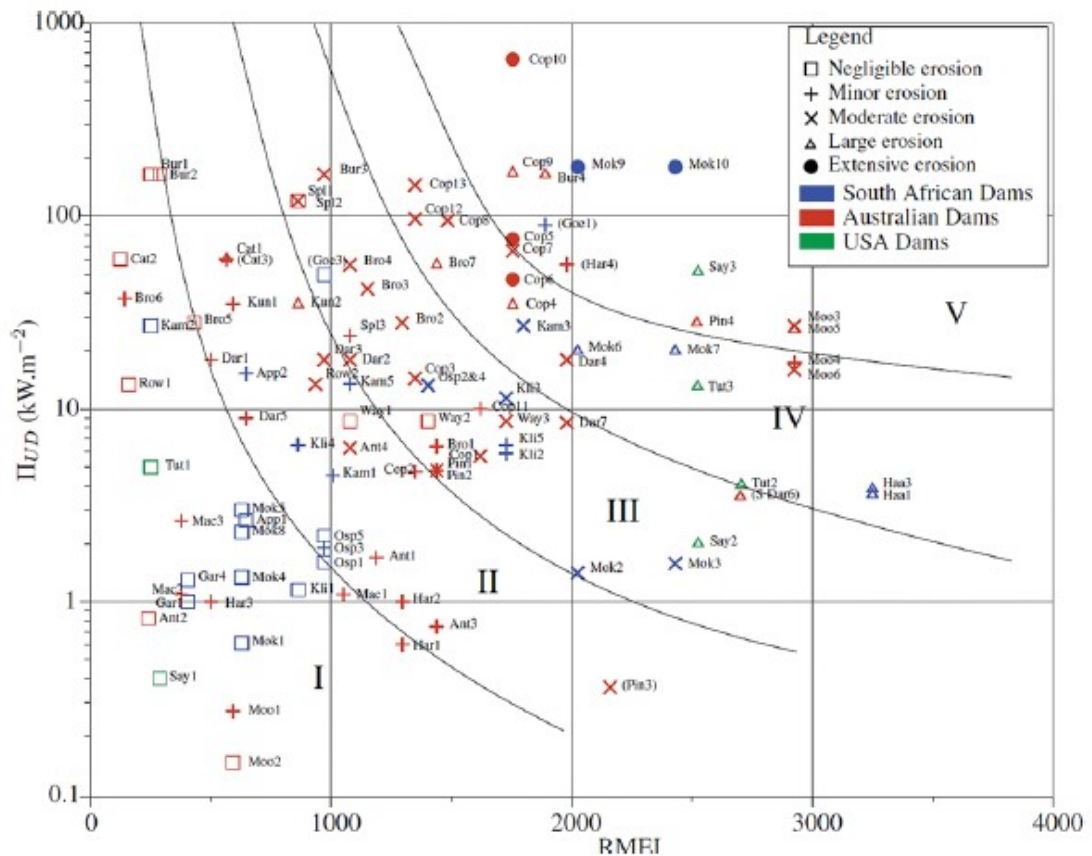


Figure 2.12. Interpreted erosion classes using *RMEI* versus hydraulic power expressed in the Figure as Π_{UD} (Douglas et al., 2018).

The *RMEI* classification system for evaluating hydraulic erosion can also be considered as a method inspired from the engineering rock mass classification systems developed for assessing underground excavation stability and tunnel support design, such as the Q-system (Barton et al., 1974) similarly developed based on the field investigation. The Q-system, however, gives the most important rating to the K_b factor (rating ranges from 1–100), which is an indication of the rock block size, as compared with the K_d factor (rating ranges from 0.03–5.33) that represents the joints shear strength (Barton et al., 1974). In the *RMEI* classification system, rock block size is not included directly. However, joints spacing can provide an idea of rock block size given that greater spacing of joints generate a larger rock block volume than a tighter spacing of joints. Also, the joints shear strength is not included in the *RMEI* classification system; however, the nature of joints factor can be considered as synonymous given that this factor incorporates the natural condition of joints. In contrast to the Q-system, the *RMEI* classification system considers the joints spacing factor as being less important ($RF = 1$) than the nature of joints factor weighted at $RF = 2$. This comparison demonstrates how the field evaluation is influenced highly by the judgment of the analyst.

2.3. References

- Annandale, G.W. 1995. Erodibility. *Journal of Hydraulic Research*, **33**(4): 471–494.
- Annandale, G.W. 2006. *Scour Technology, Mechanics and Engineering in Practice*. McGraw-Hill, New York.

- Annandale, G.W., and Kirsten, H.A.D. 1994. On the erodibility of rock and other earth materials. *Hydraulic Engineering*, **1**: 68–72.
- Annandale, G.W., Ruff, J.F., Wittler, R.J., and T.M., L. 1998. Prototype validation of erodibility index for scour in fractured rock media. *In Proceedings of the International Water Resources Engineering Conference, Memphis, Tennessee, American Society*. pp. 1096–1101.
- Armengou, J. 1991. Disipacion de energia hidraulica a pie de presa en presas boveda. Ph.D thesis, Universitat Politecnica de Catalunya, Barcelona Spain.
- Barton, N., Lien, R., and Lunde, J. 1974. Engineering classification of rock masses for the design of tunnel support. *Rock Mechanics*, **6**(4): 189–236.
- Bieniawski, Z.T. 1973. Engineering Classification of Jointed Rock Masses. *The Civil Engineer in South Africa*, **15**(12): 343–353.
- Bieniawski, Z.T. 1976. Rock mass classification in rock engineering. In *Exploration for rock engineering, procedures of the symposium*. Z.T. Bieniawski, Cape Town: Balkema,; 97–106.
- Bieniawski, Z.T. 1989. *Engineering rock mass classifications : a complete manual for engineers and geologists in mining, civil, and petroleum engineering*. Wiley, New York.
- Bollaert, E., Munodawafa, M.C., and Mazvidza, D.Z. 2012. Kariba Dam Plunge Pool Scour : quasi-3D Numerical Predictions. *In Proceeding of 6th International Conference on Scour and Erosion, Paris*. pp. 627–634.
- Bollaert, E., and Schleiss, A. 2003. Scour of rock due to the impact of plunging high velocity jets Part I: A state-of-the-art review. *Journal of Hydraulic Research*, **41**(5): 451–464.
- Braybrooke, J.C. 1988. The state of the art of rock cuttability and rippability prediction. *In Proceedings of the Fifth Australia New Zealand Conference on Geomechanics*. pp. 13–42.
- Castillo, L.G., and Carrillo, J.M. 2016. Scour, velocities and pressures evaluations produced by spillway and outlets of dam. *Water*, **8**(3): 1–21.
- Cecil, O.S. 1970. Correlations of rock bolt-shotcrete support and rock quality parameters in Scandinavian tunnels. Ph.D thesis., Urbana, University of Illinois (cited in Barton et al. 1974).
- Deere, D.U. 1968. Geological considerations, *Rock Mechanics in Engineering Practice*. KG Stagg and Zienkiewicz, John Wiley and Sons, London,; 1–20 (cited in Deere and Deere 1988).

- Deere, D.U., and Deere, D.W. 1988. The Rock Quality Designation (RQD) Index in Practice; In *Rock Classification Systems for Engineering Purposes*, Ed. L. Kirkaldie (West Conshohocken, PA: ASTM International), 91-101.
- Dooge, N. 1993. Die hidrouliese erodeerbaarheid van rotmassas in onbelynde oorlope met spesiale verwysing na die rol van naatvulmateriaal. Master's thesis, University of Pretoria, South Africa (cited in Pells 2016).
- Douglas, K., Pells, S., Fell, R., and Peirson, W. 2018. The influence of geological conditions on erosion of unlined spillways in rock. *Quarterly Journal of Engineering Geology and Hydrogeology*, **51**(1): 219–228.
- Fahlbusch, F.E. 1994. Scour in rock riverbeds downstream of large dams. *Hydropower & Dams*,: 30–32.
- Fell, R., Foster, M., Cyganiewicz, J., Sills, G., Vroman, N., and Davidson, R. 2008. A unified method for estimating probabilities of failure of embankment dams by internal erosion and piping. Technical Report No. 446, School of Civil and Environmental Engineering, University of New South Wales, Sydney, Australia (cited in Pells 2016).
- Fiorotto, V., and Salandin, P. 2000. Design of anchored slabs in spillway stilling basins. *Journal of hydraulic engineering*, **126**(7): 502–512.
- George, M.F., and Annandale, G.W. 2006. Dam failure by rock scour: Evaluation and prevention (A Case Study). *In* The 41st U.S. Symposium on Rock Mechanics (USRMS), 17-21 June, Golden, Colorado, USA. p. 8.
- Goodman, R.E. 1993. *Engineering geology-Rock in engineering construction*. John Wiley & Sons, New York.
- Grenon, M., and Hadjigeorgiou, J. 2003. Evaluating discontinuity network characterization tools through mining case studies. *Soil Rock America*, **1**: 137–142.
- Hadjigeorgiou, J., and Poulin, R. 1998. Assessment of ease of excavation of surface mines. *Journal of Terramechanics*, **35**(3): 137–153.
- Hahn, W.F., and Drain, M.A. 2010. Investigation of the erosion potential of kingsley dam emergency spillway. *In* Proceeding of the joint Annual Meeting and Conference of AIPG, AGWT, and the Florida Section of AIPG, Orlando, Florida, USA. pp. 1–10.
- Henderson, F.M. 1966. *Open Channel Flow*. Macmillan. New York.
- Hoek, E., and Brown, E.T. 1980a. Empirical strength criterion for rock masses. *Journal of the geotechnical engineering division*, **106**(GT9): 1013–1035.

- Hoek, E., and Brown, E.T. 1980b. *Underground Excavations in Rock*. London: Institution of Mining and Metallurgy.
- Hoek, E., Kaiser, P.K., and Bawden, W.F. 1995. Support of underground excavations in hard rock. A.A. Balkema/Rotterdam/Brookfield.
- Hudson, J.A., and Harrison, J.P. 2005. *Engineering rock mechanics: an introduction to the principles*. Tarrytown, N.Y: Pergamon.
- Jennings, J.E., Brink, A.B.A., and Williams, A.A.B. 1973. Revised guide to soil profiling for civil engineering purposes in South Africa. *Civil Engineering in South Africa*, **15**(1): 3–12.
- Keaton, J.R. 2013. Estimating erodible rock durability and geotechnical parameters for scour analysis. *Environmental & Engineering Geoscience*, **4**: 319–343.
- Kirkaldie, L. 1988. Rock classification systems for engineering purposes. American Society for Testing and Materials, ASTM STP-984, Philadelphia, PA, (cited in Annandale 2006).
- Kirsten, H.A.D. 1982. A classification system for excavation in natural materials. *The Civil Engineer in South Africa*, **24**(7): 292–308.
- Kirsten, H.A.D. 1988. Case histories of groundmass characterization for excavatability. *Rock Classification Systems for Engineering Purposes*. American Society for Testing and Materials, STP 984,: 102–120.
- Kirsten, H.A.D., Moore, J.S., Kirsten, L.H., and Temple, D.M. 1996. Erodibility criterion for auxiliary spillways of dams. *In ASAE International Meeting, Phoenix, Arizona, No. 962099*.
- Kirsten, H.A.D., Moore, J.S., Kirsten, L.H., and Temple, D.M. 2000. Erodibility criterion for auxiliary spillways of dams. *International Journal of Sediment Research*, **15**: 93–107.
- Kuroiwa, J., Ruff, J.F., Wittler, R.J., and Annandale, G.W. 1998. Prototype Scour Experiment in Fractured rock media. *In Proceedings of International Water Resources Engineering Conference and Mini-Symposia, ASCE, Memphis, TN*.
- Laugier, F., Leturcq, T., and Blancet, B. 2015. Stabilité des barrages en crue : Méthodes d'estimation du risque d'érodabilité aval des fondations soumises à déversement par-dessus la crête. *In Proceeding de la Fondation des barrages. Chambéry, France*. pp. 125–136.
- Lowe, J., Chao, P.C., and Luecker, A.R. 1979. Tarbela service spillway plunge pool development. *Water power dam construction*, **31**(11): 85–90.

- MacGregor, F., Fell, R., Mostyn, G.R., Hocking, G., and McNally, G. 1994. The estimation of rock rippability. *Quarterly Journal of Engineering Geology*, **27**: 123–144.
- Marinos, P., and Hoek, E. 2000. GSI: A geologically friendly tool for rock mass strength estimation. *In Proceedings of GeoEng2000 Conference, Melbourne, Australia*. pp. 1422–1446.
- Marinos, P., and Hoek, E. 2001. Estimating the geotechnical properties of heterogeneous rock masses such as flysch. *Bulletin of Engineering Geology and the Environment*, **60**: 85–92.
- Marinos, V., Marinos, P., and Hoek, E. 2007. Geological Strength Index (GSI). A characterization tool for assessing engineering properties for rock masses. *In Underground works under special conditions*. pp. 13–21.
- Mason, P.J., and Armugam, K. 1985. Jet scour below dams and flip buckets. *Journal of Hydraulic Engineering*, **111**(2): 220–235.
- Mirskhulava, T.E., Dolidze, I.V., and Magomeda, A.V. 1967. Mechanism and computation of local and general scour in non-cohesive, cohesive soils and rock beds. *In Proceedings of the 12th IAHR Congress Fort Collins, Colorado, USA*. pp. 169–176.
- Monfette, M. 2004. Comprehensive review of plunge pool performance at four of BC Hydro dam sites and assessment of scour extent. Master's thesis, University of British Columbia. Vancouver, British Columbia, Canada.
- Moore, J.S. 1991. The characterization of rock for hydraulic erodibility. SCS Technical Release - 78, Northeast National Technical Center, Chester. PA.
- Moore, J.S., and Kirsten, H.A.D. 1988. Discussion – Critique of the rock material classification procedure. *In Rock classification systems for engineering purposes*. American Society for Testing and Materials, STP-984, L. Kirkaldie Ed, Philadelphia. pp. 55–58.
- Moore, J.S., Temple, D.M., and Kirsten, H.A.D. 1994. Headcut advance threshold in earth spillways. *Bulletin of the Association of Engineering Geologists*, **31**(2): 277–280.
- Mörén, L., and Sjöberg, J. 2007. Rock erosion in spillway channels – A case study of the Ligga spillway. *In Proceedings of 11th Congress of the International Society for Rock Mechanics, Lisbon, Portugal*. pp. 87–90.
- Palmstrom, A. 1996. Characterizing rock masses by the RMI for Use in Practical Rock Engineering. Part 1: The development of the Rock Mass index (RMI). *Tunnelling and Underground Space Technology*, **11**(2): 175–188.

- Palmstrom, A. 2005. Measurements of and correlations between block size and rock quality designation (RQD). *Tunnelling and Underground Space Technology*, **20**(4): 362–377.
- Palmstrom, A., Blindheim, O.T., and Broch, E. 2002. The Q-system – possibilities and limitations (in Norwegian). *In Norwegian National Conference on Tunnelling*. Norwegian Tunnelling Association, Oslo, Norway. p. 41.1-41.43.
- Palmstrom, A., and Broch, E. 2006. Use and misuse of rock mass classification systems with particular reference to the Q-system. *Tunnelling and Underground Space Technology*, **21**(6): 575–593.
- Pells, S.E. 2016. Erosion of rock in spillways. Ph.D Thesis, University of New South Wales, Australia.
- Pells, S.E., Bieniawski, Z.T., Hencher, S., and Pells, P.J.N. 2017a. RQD: Time to Rest in Peace. *Canadian Geotechnical Journal*, **54**(6): 825–834.
- Pells, S.E., Douglas, K., Pells, P.J.N., Fell, R., and Peirson, W.L. 2017b. Rock mass erodibility. Technical Note: *Journal of Hydraulic Engineering*, **43**(5): 1–8.
- Pells, S.E., Pells, P.J.N., Peirson, W.L., Douglas, K., and Fell, R. 2015. Erosion of unlined spillways In Rock - does a “scour threshold” exist? *In Proceeding of Australian National Committee on Large Dams* . Brisbane, Queensland, Australia. pp. 1–9.
- Pells, S.E., Pells, P.J.N., and Van Schalkwyk, A. 2016. A tale of two spillways. *In Proceedings of the International Symposium on “Appropriate Technology to Ensure Proper Development, Operation and Maintenance of Dams in Developing Countries”*, SANCOLD, Johannesburg, South Africa. pp. 279–288.
- Pitsiou, S. 1990. The effect of discontinuities of the erodibility of rock in unlined spillways of dams. Master’s thesis, University of Pretoria, South Africa.
- Puertas, J. 1994. Criterios hidraulicos para el diseno de cuencos de disipacion de energia en presas boveda con vertido libre por coronacion. Ph.D thesis, Universitat Politecnica de Catalunya, Barcelona, Spain.
- Reinius, E. 1986. Rock erosion. *Water power and dam construction*, **38**(6): 43–48.
- Rock, A.J. 2015. A semi-empirical assessment of plung pool scour: Two-dimensional application of Annandale’s Erodibility Method on four dams in British Columbia, Canada. Master’s thesis, University of British Columbia. Vancouver, British Columbia, Canada.

- Scoble, M.J., Hadjigeorgiou, J., and Nenonen, L. 1987. Development of an excavating equipment selection expert system, based on geotechnical considerations. *In Proceedings of the 40th Canadian Geotechnical Conference, Regina.* pp. 67–78.
- Simoes, G.F., and Vargas, E. do. A. 2001. Analysis of erosion processes downstream of spillways in large dams. *In Proceeding of the 38th U.S. Rock Mechanis Symposium Held in Washigton, D.C.* pp. 959–966.
- Temple, D.M., and Moore, J.S. 1994. Headcut advance prediction for earth spillways. *In ASAE Internation Winter Meeting, Atlanta, Georgia, No. 942540.*
- Tsiambaos, G., and Saroglou, H. 2010. Excavatability assessment of rock masses using the Geological Strength Index (GSI). *Bulletin of Engineering Geology and the Environment*, **69**(1): 13–27.
- USACE, (United States Army Corps of Engineers). 1997. Engineering and design, tunnels and shafts in rock. Engineering manual 1110-2-2901.
- Van-Schalkwyk, A. 1989. Watenavorsingskommissie: Verslag oor loodsondersoek: Die erodeerbaarheid van verskillende rotsformasies in onbeklede damoorlope., Unpublished report, University of Pretoria, South Africa.
- Van-Schalkwyk, A., Jordaan, J.M., and Dooge, N. 1994a. Erosion of rock in unlined spillways. *In Proceeding of International Commission on Large Dams, Paris, 71 (37).* pp. 555–571.
- Van-Schalkwyk, A., Jordaan, J.M., and Dooge, N. 1994b. Die Erodeerbaarheid van Verskillende Rotsformasies Onder Varierende Vloeitoestande. Tech. Rep. WNK Verslag No. 302/1/95, verslag aan die waternavorsingskommissie deur die Departement of Geologie, Universiteit van Pretoria, South Africa.
- Veronese, A. 1937. Erosion of a bed downstream from an outlet. Colorado A&M College, Fort Collins, Colorado, USA.
- Weaver, J.M. 1975. Geological factors significant in the assessment of rippability. *The Civil Engineer in South Africa*, **17**: 313–316.

CHAPTER 3 - DETERMINING RELATIVE BLOCK STRUCTURE RATING FOR ROCK ERODIBILITY EVALUATION IN THE CASE OF NON-ORTHOGONAL JOINT SETS³

Abstract

The most commonly used method for assessing the hydraulic erodibility of rock is Annandale's method. This method is based on a correlation between the erosive force of flowing water and the capacity of rock resistance. This capacity is evaluated using Kirsten's index, which was initially developed to evaluate the excavatability of earth materials. For rocky material, this index is determined according to certain geomechanical factors related to the intact rock and the rock mass, such as the compressive strength of intact rock, the rock block size, the discontinuity shear strength and the relative block structure. To quantify the relative block structure, Kirsten developed a mathematical expression that accounted for the shape and orientation of the blocks relative to the direction of flow. Kirsten's initial concept for assessing relative block structure considers that the geological formation is mainly fractured by two joint sets forming an orthogonal fracture system. An adjusted concept is proposed to determine the relative block structure when the fracture system is non-orthogonal where the angle between the planes of the two joint sets is greater or less than 90°. An analysis of the proposed relative block structure rating shows that considering a non-orthogonal fracture system has a significant effect on Kirsten's index and, as a consequence, on the assessment of the hydraulic erodibility of rock.

Keywords: Fractured rock, Blocky rock, Dip angle, Dip direction, Joint spacing, Relative ground structure, Hydraulic erodibility of rock, Annandale's method, Kirsten's index.

³ Boumaiza, L., Saeidi, A. and Quirion, M. (2019). Determining relative block structure rating for rock erodibility evaluation in the case of non-orthogonal joint sets. *Journal of Rock Mechanics and Geotechnical Engineering*, 11(1), 72-87 pp.

3.1. Introduction

The assessment of the hydraulic erodibility of earth materials was studied initially for problems associated with the erosion of earth materials under bridges (Keaton, 2013). It has since been adopted for dams given that erosion phenomena can occur on downstream rocks during flood spill periods, as observed at the Tarbela Dam in Pakistan (Lowe et al., 1979) and the Kariba Dam in Zambia (Bollaert et al., 2012). Annandale's method (Annandale 1995, 2006) is the most commonly used method for assessing the hydraulic erodibility of earth materials (Castillo and Carrillo, 2016; Hahn and Drain, 2010; Laugier et al., 2015; Mören and Sjöberg, 2007; Pells et al., 2015; Rock, 2015). This method is based on a correlation between the erosive force of flowing water, namely the available hydraulic stream power, and the capacity of rock to resist the flow energy. This capacity is evaluated using Kirsten's index (Kirsten, 1982, 1988), which was initially developed to evaluate the excavatability of earth materials but has since been adopted to assess the hydraulic erodibility of earth materials. The interest of using Kirsten's index was first mentioned at a symposium focused on rock mass classification systems (ASTM STP-984, 1988), where it was argued that the processes of mechanical excavatability and hydraulic erodibility of earth materials could be considered as similar processes (Moore and Kirsten 1988). Since then, many researchers have analyzed the hydraulic erodibility of earth materials by using the excavatability index, where the "direction of excavation" of the original index has been replaced by the "direction of flow"

(Annandale, 1995; Annandale and Kirsten, 1994; Dooge, 1993; Kirsten et al., 2000; Moore et al., 1994; Pitsiou, 1990; Van-Schalkwyk et al., 1994a). Hereinafter, the terms “direction of excavation” and “direction of flow” are considered as synonymous and the term corresponds to the direction of the acting force. For rock material, Kirsten’s index (N) is determined according to certain geomechanical factors related to the intact rock and the rock mass, such as the compressive strength of intact rock (M_s), the rock block size (Kb), the discontinuity shear strength (Kd) and the relative block structure (J_s). Kirsten’s index can be calculated according to the following equation:

$$N = M_s \cdot Kb \cdot Kd \cdot J_s \quad (3.1)$$

There are many indices developed for assessing the excavatability of earth materials (Basarir and Karpuz, 2004; Clark, 1996; Hadjigeorgiou and Poulin, 1998; MacGregor et al., 1994). The choice of adopting Kirsten’s index is mainly based on its wide range of applications ranging from cohesive and non-cohesive soils to rock (Kirsten et al., 2000). In addition, Van Schalkwyk et al. (1994) tested several rock mass characterization indices and found that they generated similar results, but better accuracy was obtained with Kirsten's index (Pells, 2016). To improve the evaluation of bedrock erosion, Huang et al. (2013) proposed a modification of the erodibility index, and developed a new equation for determining the RQD (rock quality designation) that is included in the factor Kb . However, the other factors included in Kirsten’s index have not had any modifications.

As reported by Pells (2016), Kirsten considered the orientation of a block relative to the direction of flow as an important parameter to be considered in assessing the hydraulic erodibility of rock. Thus, Kirsten has included the “relative block structure” parameter in his index. This parameter represents the required effort to excavate the rock, and it has been quantified mathematically. Kirsten assumed that geological formations are mainly fractured by two intersecting joint sets, where an angle of 90° is kept between the planes of the two joint sets (orthogonal fracture system). Given that a bulldozer’s bucket needs to penetrate the ground surface and then dislodge the blocks of rock during the excavation process, the excavatability of the rock mass can be determined according to the action of ground surface penetration and the dislodging of rocky blocks. For the latter, Kirsten (1982) developed a concept for blocks oriented against the direction of excavation, and he then generated a mathematical expression for determining the required effort to dislodge the block. It should be noted that Kirsten (1982)’s concept is only truly valid for an orthogonal fracture system. However, in practice, Kirsten’s index is applied to all cases, including non-orthogonal fracture systems, by assuming a certain lack of precision in terms of the assessment of erodibility. As part of this study, adjustments are introduced to the initial “relative block structure” concept proposed by Kirsten. The introduced adjustments produce two equations for assessing the required effort to dislodge rocky blocks for a non-orthogonal joint set system. No previous works have proposed adjustments for a non-orthogonal joint set system. One equation is applied when the blocks are oriented in the direction of flow. The second equation is applicable when the blocks are oriented against the direction of flow. This paper first describes the initial “relative block structure” concept of Kirsten. Then the second

part of this paper describes the proposed equations, the initial results obtained from these equations, and the adjustments made to produce the final J_s rating for non-orthogonal fracture systems. Given that two joint sets are intersected by both larger and smaller angles compared to the single 90° angle considered by Kirsten, this paper also presents the effect of a non-orthogonal joint sets system on Kirsten's index and, consequently, on the assessment of the hydraulic erodibility of rock.

3.2. Relative block structure

Our modifications of Kirsten's index focus on the relative block structure factor. This section describes the initial "relative block structure" concept of Kirsten, but we include a large review of the underlying concepts that were not included in the initial Kirsten paper. According to Kirsten (1982), the relative orientation of blocks and the spacing of joints affect the possibilities of both penetrating the ground surface and dislodging the individual blocks. Accordingly, Kirsten (1982) determined the effect of orientation and shape of blocks on the excavatability process by considering the kinematic possibility of penetration (K_p) and the kinematic possibility of dislodgment (K_d). The following first and second subsections describe K_p and K_d , respectively, while the third subsection describes the methodology followed by Kirsten to develop the relative block structure rating.

3.2.1. Kinematic possibility of penetration

To represent a rock block volume, at least three joint sets are required to be intersected (3D representation). In this work, a block is represented in 2D and consequently considered to be delineated by only two joint sets. K_p is directly related to the inclination of the joints bounding blocks. The respective dips of these two joint sets relative to the ground surface are labeled as θ and ψ , while S_θ and S_ψ represent their respective spacing (Kirsten, 1982) (Figure 3.1). As the reciprocal of the joint spacing provides the number of joints per unit length, defined as the joint frequency (λ), λ_θ can be given as $1/S_\theta$ and λ_ψ can be given as $1/S_\psi$. Accordingly, the dip weighted by the number of joints of the first joint set can be defined as $\lambda_\theta \tan \theta$ and as $\lambda_\psi \tan \psi$ for the second joint set. As the geological formation is assumed to be fractured by two intersected joint sets, the combined kinematic possibility of penetration is the arithmetic average of the relative dips weighted by the number of joints of joint sets (Eq. 3.2).

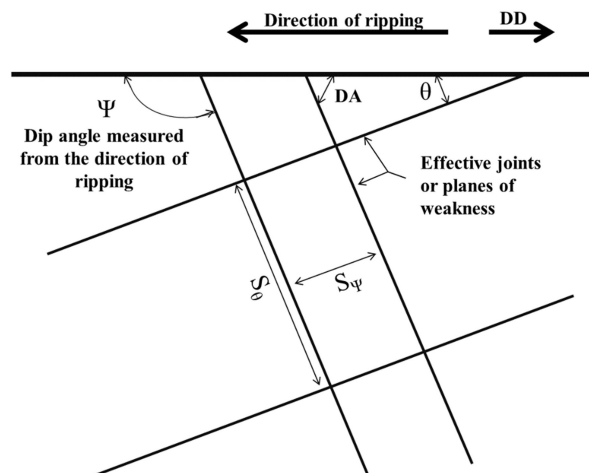


Figure 3.1. Model for two joint sets as modified from Kirsten (1982). The joint sets in the original figure are not orthogonal; however, Kirsten considers only the orthogonal fracture system. Accordingly, the model here is slightly modified to be more representative of an orthogonal fracture system (DA : dip angle; DD : dip direction).

$$K_p = \frac{\tan \theta \lambda_\theta + \tan \psi \lambda_\psi}{\lambda_\theta + \lambda_\psi} \quad (3.2)$$

As λ_θ and λ_ψ can be given as $1/S_\theta$ and $1/S_\psi$, respectively, K_p can be expressed according to Eq. 3.3:

$$K_p = \frac{S_\psi \tan \theta + S_\theta \tan \psi}{S_\psi + S_\theta} \quad (3.3)$$

Given that the ratio of joint spacing (RJS), named r , is equal to S_ψ/S_θ , Eq. 3.3 can be expressed as:

$$K_p = \frac{r \tan \theta + \tan \psi}{a (r + 1)} \quad (3.4)$$

The value of a in Eq. 3.4 is 5 based on empirical assessments of the effects of the direction of ripping on the efficiency of ripping (Kirsten, 1982). Furthermore, it is considered by Kirsten (1982) that the sum of K_p and the required penetration effort (J_s^P) is equal to 1 (i.e. $K_p + J_s^P = 1$). Therefore, J_s^P can be expressed as follows:

$$J_s^P = \left[1 - \frac{r \tan \theta + \tan \psi}{a (r + 1)} \right] \quad (3.5)$$

3.2.2. Kinematic possibility of dislodgement

Once there is penetration into the ground (Figure 3.2 depicts a bulldozer, which is moving from right to left), excavatability occurs according to the digging process of angle θ , followed by the riding process of angle ψ (Figure 3.2). The action of block dislodgement can be represented by a horizontal force behind the block while this block is free to move in a perpendicular direction to the ground surface (Kirsten, 1982). As a result, K_d shown in Figure 3.3 can be obtained by the vector product of the principal dislodging force and the principal degree of freedom. The vectors of the principal dislodging force and the principal degree of freedom can be decomposed into parallel coaxial components along the sides of the block (Kirsten, 1982). The coaxial components are identified as A , B , B' and A' in Figure 3.3.

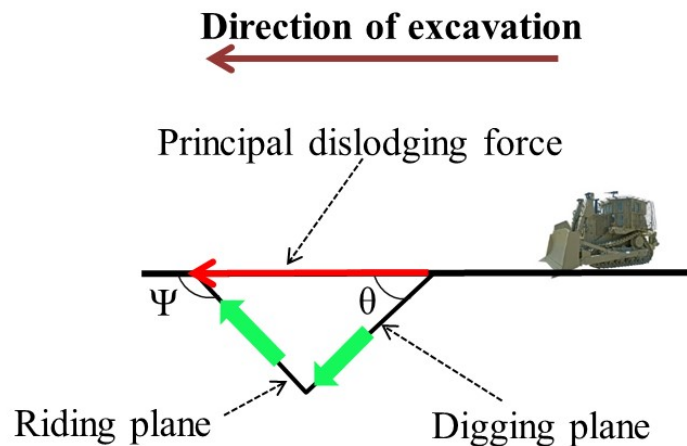


Figure 3.2. The principle of the principal dislodging force.

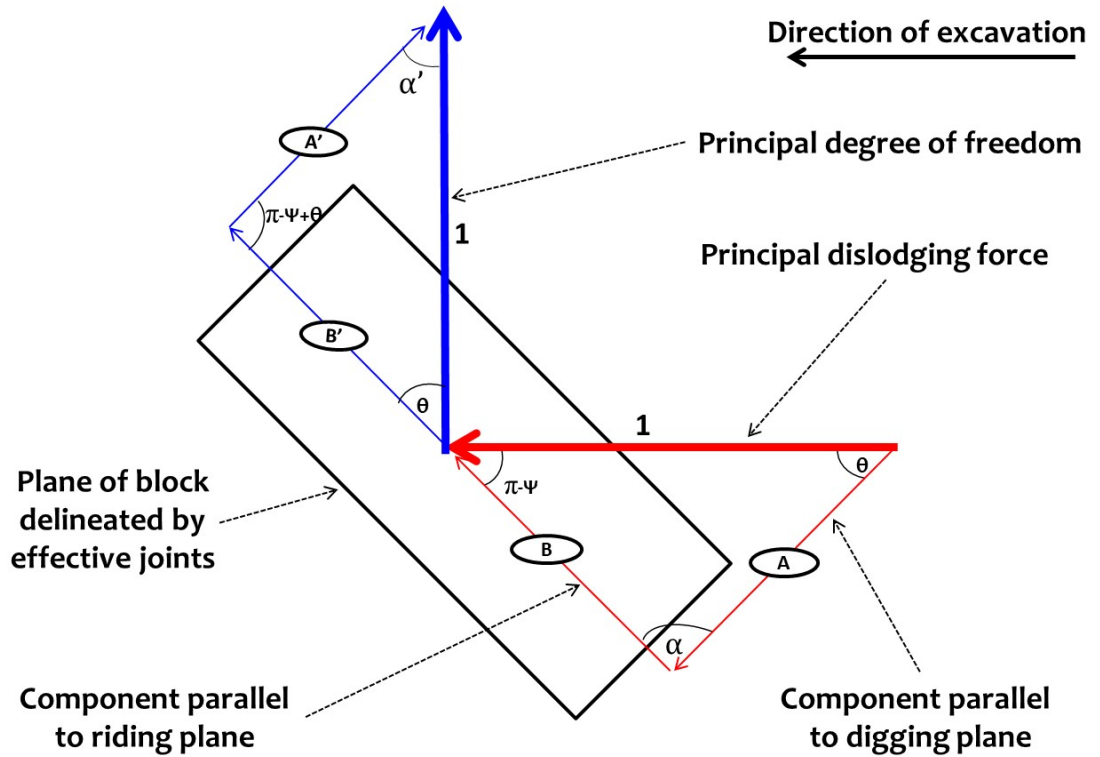


Figure 3.3. Representation of the coaxial components as adapted from Kirsten (1982).

The coaxial component identified as A in Figure 3.3, is in the opposite direction of the coaxial component, identified as A' in Figure 3.3. Accordingly, K_d can be expressed as a function of the other two coaxial components identified as B and B' , respectively (Figure 3.3). These two coaxial components can be determined according to the following equation:

$$\left. \begin{aligned} B &= \frac{\sin \theta}{\sin (\psi - \theta)} \\ B' &= \frac{\cos \theta}{\sin (\psi - \theta)} \end{aligned} \right\} \quad (3.6)$$

Thus, the final equation of K_d is given by the product of the two components of B and B'. This equation is expressed as follows:

$$K_d = \frac{\cos \theta \cdot \sin \theta}{b \sin^2(\psi - \theta)} \quad (3.7)$$

The value of b in Eq. 3.7 is 1 based on empirical assessments of the effects of the direction of ripping on the efficiency of ripping (Kirsten, 1982). Furthermore, it is assumed that the sum of K_d and the required dislodging effort (J_s^d) is equal to 1 (i.e. $K_d + J_s^d = 1$). Therefore, J_s^d can be expressed as:

$$J_s^d = \left[1 - \frac{\cos \theta \cdot \sin \theta}{b \sin^2(\psi - \theta)} \right] \quad (3.8)$$

3.2.3. Relative block structure rating

Eqs. 3.5 and 3.8 were combined to obtain the following equation representing the product of J_s^p and J_s^d , which has been used to determine the relative block structure rating (J_s):

$$J_s = \left[1 - \frac{r \tan \theta + \tan \psi}{a (r + 1)} \right] \cdot \left[1 - \left| \frac{\cos \theta \cdot \sin \theta}{b \sin^2(\psi - \theta)} \right| \right] \quad (3.9)$$

The values of J_s were determined by Kirsten (1982) using four values of RJS ($r = S_{\psi}/S_{\theta}$), i.e. $r = 1:1$, $1:2$, $1:4$ and $1:8$ (e.g. $1:2 = 2/1 = 2$, where 1 represents the width of the block and 2 represents its length). Beyond a RJS value of 8 (1:8), the values of J_s do not show any significant change. For this reason, the maximum RJS adopted was $r = 8$. The initial results, derived from Eq. 3.9, are presented in Table 3.1. However, published J_s values presented by Kirsten (1982) do not generally match the results obtained using Eq. 3.9. Kirsten graphically represented the results obtained using Eq. 3.9. He then adjusted the obtained curves to determine, from the final adjusted curves, the J_s rating. It should be noted that no determination can be performed when $\theta = 0^\circ$ or 90° as Kirsten considered K_d and K_p to be zero when the joints are sub-horizontal (dip = 0°) or sub-vertical (dip = 90°). For these cases, Kirsten assigned a J_s value of 1 for the four values of RJS. Indeed, when $K_p = 0$ and $K_d = 0$, Eq. 3.9 calculates J_s value as the product of $1 \times 1 = 1$, explaining the J_s values of 1 when dips are 0° or 90° . For excavatability, Kirsten supposed that the ground would not be excavated when $J_s = 1$, as the sub-horizontal or sub-vertical joints, relative to the ground surface, would not constitute a situation favorable for excavation.

Table 3.1. The ratio of joint spacing and the angles θ and ψ initially used by Kirsten (Kirsten, personal communication, 2016).

Direction of excavation ¹	θ (°)	ψ (°)	Ratio of joint spacing			
			1	2	4	8
In the direction of excavation	89	179	-4.64	-6.52	-8.02	-9.02
	85	175	-0.12	-0.47	-0.75	-0.94
	80	170	0.37	0.21	0.08	0.00
	75	165	0.49	0.39	0.31	0.26
	70	160	0.52	0.45	0.39	0.35
	65	155	0.51	0.46	0.42	0.39
	60	150	0.50	0.46	0.42	0.40
	55	145	0.49	0.45	0.42	0.40
	50	140	0.49	0.46	0.43	0.41
	45	135	0.50	0.47	0.44	0.42
	40	130	0.53	0.49	0.46	0.45
	35	125	0.57	0.53	0.50	0.48
	30	120	0.63	0.59	0.55	0.53
	25	115	0.72	0.67	0.62	0.60
	20	110	0.84	0.77	0.71	0.68
	15	105	1.01	0.91	0.83	0.78
	10	100	1.28	1.12	0.99	0.91
	5	95	1.95	1.60	1.32	1.13
	0,5	90,5	12.35	8.56	5.53	3.51
	Against the direction of excavation	-5	85	-0.12	0.23	0.51
-10		80	0.37	0.54	0.66	0.75
-15		75	0.49	0.59	0.67	0.72
-20		70	0.52	0.59	0.64	0.68
-25		65	0.51	0.57	0.61	0.64
-30		60	0.50	0.55	0.58	0.60
-35		55	0.49	0.53	0.56	0.58
-40		50	0.49	0.52	0.55	0.57
-45		45	0.50	0.53	0.56	0.58
-50		40	0.53	0.56	0.59	0.61
-55		35	0.57	0.61	0.64	0.66
-60		30	0.63	0.68	0.71	0.73
-65		25	0.72	0.77	0.82	0.85
-70		20	0.84	0.91	0.97	1.00
-75		15	1.01	1.11	1.19	1.24
-80		10	1.28	1.45	1.58	1.66
-85		5	1.95	2.30	2.58	2.77
-89		1	6.61	8.49	9.99	10.99

1: This column was added to better explain the presented concepts.

On the other hand, a ground characterized by a J_s of 1 would have a representative value of its excavatability being determined according to the factors included in Kirsten's index. However, it is practically non-excavatable. Accordingly, the curve adjusting process was undertaken by considering that the curves must be plotted with a J_s of 1 when the dip is 0° or 90° . From this, two conditions have been respected during the adjusting of curves. The first condition is imposed to avoid negative determinations of J_s , and the second condition is imposed to have a constant behavior of the J_s curves.

Furthermore, when $RJS = 1$, the joint spacing is of the same order for the two considered joint sets. This means that the length and the width of the blocks are of the same order. For this situation, it is impossible to determine which of the two joint sets represents the closer spaced joint set. Consequently, determining the orientation of the blocks relative to the direction of flow has two possible options: the blocks can be considered as being oriented in or against the direction of flow. The RJS in Figure 3.4 is 1. If the first joint set is considered to be the closer spaced joint set, the block is oriented accordingly in the direction of flow (dip angle is 30°). If the second joint set is considered to be the closer spaced joint set, the block is oriented accordingly against the direction of flow (dip angle is 60°). Consequently, when the blocks are oriented in the direction of flow with a dip of 30° , J_s is of the same order as the one in the case when the blocks are oriented against the direction of flow with a dip of 60° . This principle, indicated hereinafter as the "same required effort principle", was adopted by Kirsten.

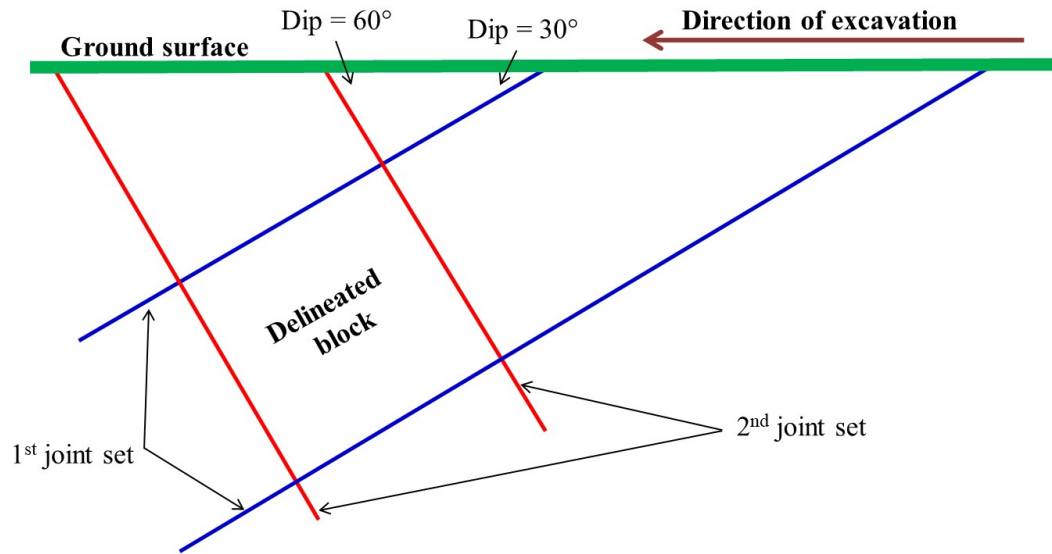


Figure 3.4. Orthogonal fracture system with ratio of joint spacing of 1.

The adjustment process, run based on $r = 1:1$ and $1:8$, is presented in Figure 3.5 (the adjustment is represented by dashed lines). The final adjusted curves, according to the four RJS values, are shown in Figure 3.6. Accordingly, J_s values determined from these final curves are presented in Table 3.2 (Kirsten, 1982, 1988). Comparing the J_s values initially proposed by Kirsten (1982, 1988) to evaluate the mechanical excavatability of earth materials and those proposed by Annandale (1995, 2006) to evaluate the hydraulic erodibility of earth materials, slight differences are observed, which are likely to occur due to another adjustment process.

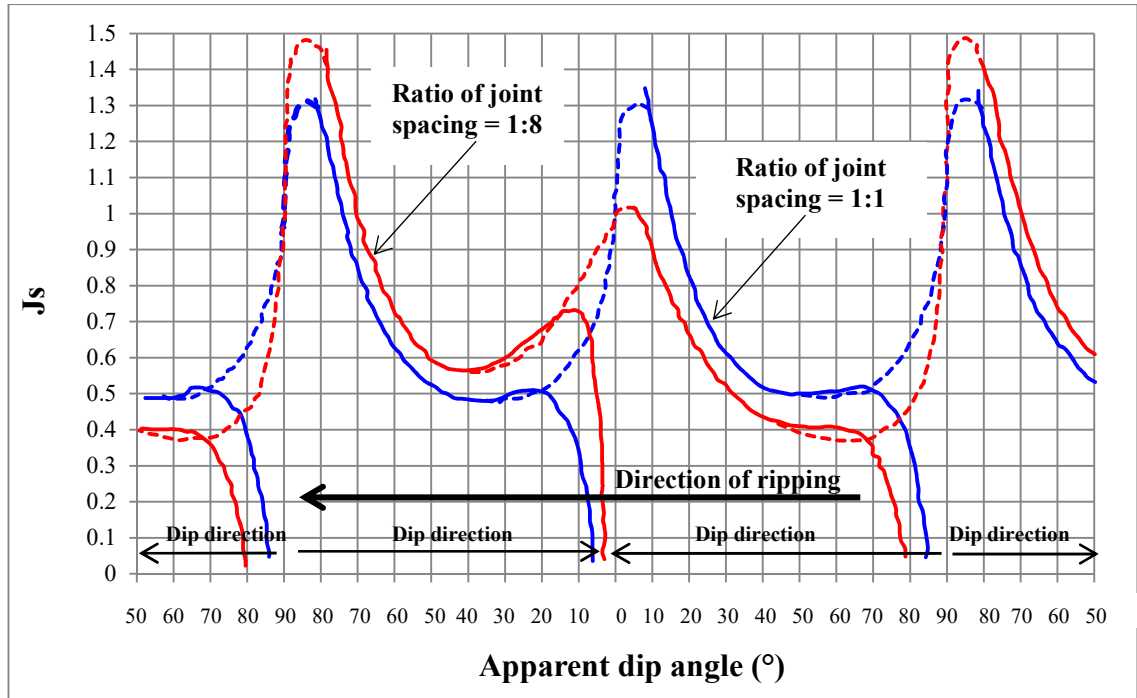


Figure 3.5. The curve adjustment process (modified from Moore and Kirsten 1988).

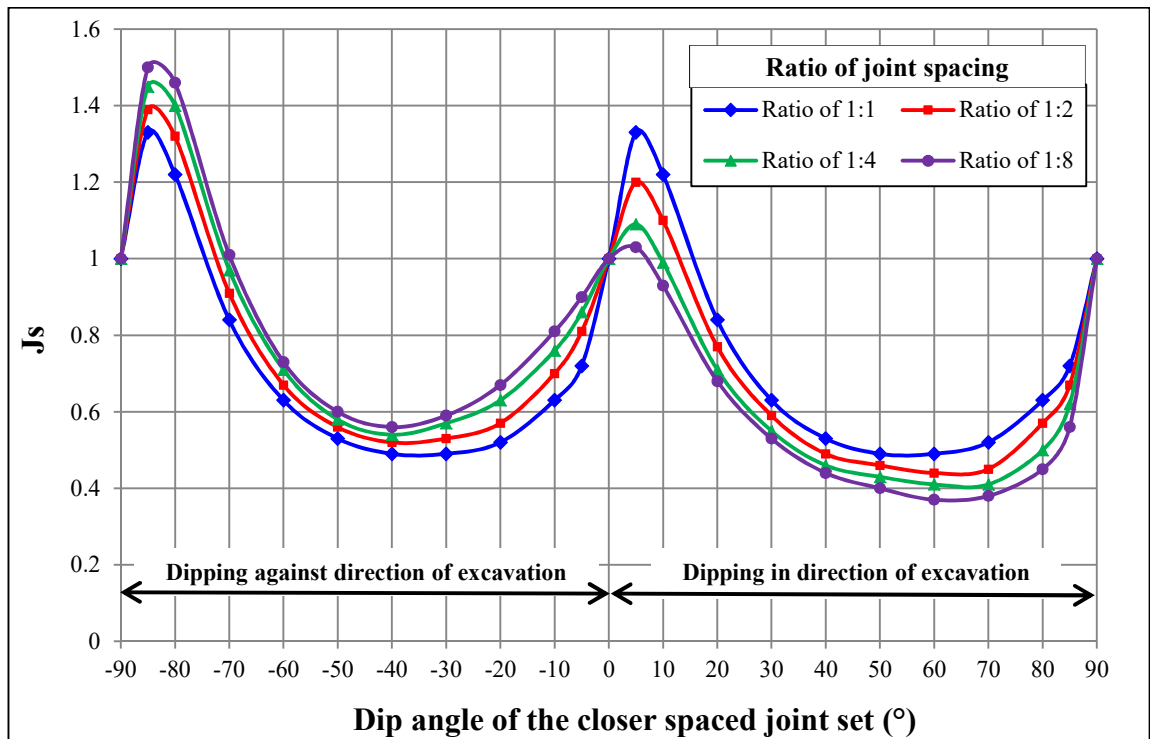


Figure 3.6. Graphical representation of the relative block structure values.

Table 3.2. Rating values of the relative block structure (Kirsten 1982, 1988).

Dip direction ¹ of the closer spaced joint set (°)	Dip angle ² of the closer spaced joint set (°)	Ratio of joint spacing (<i>r</i>)			
		1:1	1:2	1:4	1:8
		Values of relative block structure (<i>J_s</i>)			
180/0	90	1	1	1	1
	85	0.72	0.67	0.62	0.56
	80	0.63	0.57	0.5	0.45
	70	0.52	0.45	0.41	0.38
	60	0.49	0.44	0.41	0.37
	50	0.49	0.46	0.43	0.4
	40	0.53	0.49	0.46	0.44
	30	0.63	0.59	0.55	0.53
	20	0.84	0.77	0.71	0.68
	10	1.22	1.1	0.99	0.93
0/180	0	1	1	1	1
	5	0.72	0.81	0.86	0.9
	10	0.63	0.7	0.76	0.81
	20	0.52	0.57	0.63	0.67
	30	0.49	0.53	0.57	0.59
	40	0.49	0.52	0.54	0.56
	50	0.53	0.56	0.58	0.6
	60	0.63	0.67	0.71	0.73
	70	0.84	0.91	0.97	1.01
	80	1.22	1.32	1.4	1.46
Against the direction of excavation	85	1.33	1.39	1.45	1.5
	90	1	1	1	1

1: Dip direction of the closer spaced joint set relative to the direction of excavation

2: Apparent dip of the closer spaced joint set in the vertical plane containing the direction of excavation

3: For intact material, $J_s = 1$

4: For values of r less than 0.125, take J_s as for $r = 0.125$

In practice, the dip angle of the closer spaced joint set and its dip direction relative to the direction of flow are used to determine J_s values. The dip angle is between 0° and 90°, while the dip direction is determined as a function of the direction of flow. In the example shown in Figure 3.7a, the direction of flow is 320°. If the closer spaced joint set has a dip direction between 230° (320°–90°) and 50° (320°+ 90°), it is considered to be in the same direction as that of the flow.

Otherwise, it is against the direction of flow. If the closer spaced joint set in Figure 3.7a is the first joint set, the dip direction will be taken as being in the direction of flow. Thus, the dip of the closer spaced joint set should be evaluated to determine the J_s value. Kirsten (1982) considered the geological formation to be fractured by an orthogonal system. Thus, he always maintained an angle of 90° between the planes of the two joint sets (this angle is indicated hereinafter as α). It should be noted that this situation only occurs when the direction of flow is perpendicular to the azimuth of the closer spaced joint set. If the direction of flow is not perpendicular, Kirsten suggested taking the apparent dip of the closer spaced joint set, in the vertical plane containing the direction of flow, to determine the J_s value (Table 3.2).

In Figure 3.7a, the two joint sets constitute an orthogonal fracture system. The dip and dip direction of the first joint set are 30° and 270° , respectively; those of the second joint set are 60° and 90° , respectively. The first joint set is considered as the closer spaced joint set, and the direction of flow is 320° . The apparent dip used to determine J_s would therefore be 20° . However, it is found that α , on the plane containing the direction of flow, is 112° (Figure 3.7a). Remembering that the J_s value, when the dip is 20° , was initially proposed by Kirsten with $\alpha = 90^\circ$ (orthogonal fracture system), it does not seem appropriate to only consider the apparent dip in such situations. The change of the angle between (1) the joint sets and (2) the vertical plane containing the direction of flow should also be considered. Such a situation, where α differs from 90° (on the vertical plane containing the direction of flow), is equivalent to a flow having a direction that is perpendicular to the strike of the closer spaced joint set, but in a non-orthogonal fracture system with an α angle of 112°

rather than 90° as shown in Figure 3.7b. For this second situation, the first joint set has a dip of 20° , while the dip of the second joint set is 48° . Our work aims to determine the J_s rating for non-orthogonal fracture systems, which includes the J_s rating when the direction of flow is not perpendicular to the azimuth of the closer spaced joint set.

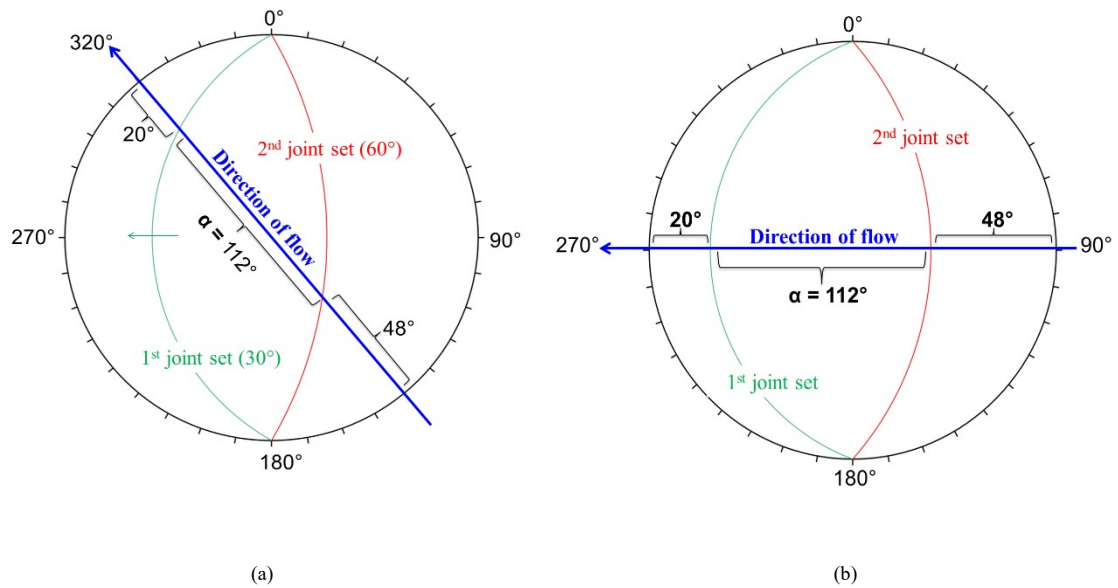


Figure 3.7. Stereographic representation of two possible situations for a fractured system.

3.3. Methodology

As already mentioned, the block dislodging action is controlled by K_p and K_d , while the α angle for non-orthogonal fracture systems could be larger or smaller than 90° . Kirsten's J_s equation (Eq. 3.9) could be used for this purpose. However, his

initial relative block structure concept must be adjusted. As a modification of α angle in the equation for K_d subsequently modifies the equation for K_p , only K_d is adjusted. This section describes the principle of the adjusted relative block structure concept that is used to develop a new set of equations for determining K_d . These new equations are then included as part of the equation for J_s to propose a rating of J_s for non-orthogonal fracture systems.

3.3.1. Principle of the adjusted concept

The RJS values, as well as angles θ and ψ initially used by Kirsten to determine J_s values, are presented in Table 3.1. Based on these unpublished data, a representation of two blocks is produced in this thesis (Figure 3.8). The planes of the joints associated with θ and ψ are plotted in blue and red, respectively (Figure 3.8). When the block is oriented in the direction of excavation, Kirsten considered θ to be positive (e.g. $\theta = 30^\circ$), while ψ is determined by adding an angle of 90° to θ (e.g. $\theta = 30^\circ$, thus $\psi = 30^\circ + 90^\circ = 120^\circ$). On the other hand, when the block is oriented against the direction of excavation, Kirsten considered θ to be negative (e.g. $\theta = -30^\circ$), while ψ is determined by again adding an angle of 90° to θ (e.g. $\theta = -30^\circ$, thus $\psi = -30^\circ + 90^\circ = 60^\circ$). For these two orientations of block relative to direction of excavation, Kirsten always kept $\alpha = 90^\circ$ between the planes of the joints associated to θ and ψ to consider this as an orthogonal fracture system.

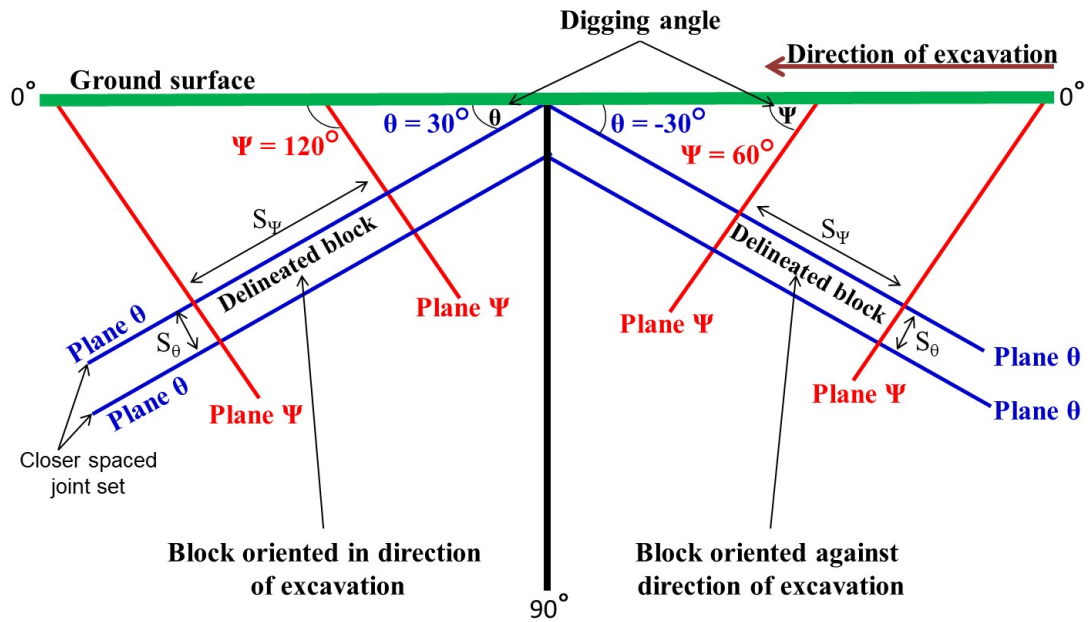


Figure 3.8. Concept of a delineated blocks oriented in and against the direction of excavation

Based on the concept presented in Figure 3.8, when the block is oriented in or against the direction of excavation, the joint spacing S_ψ is always greater than S_θ . Therefore, the RJS (i.e. $r = S_\psi/S_\theta$) is of the same order for both blocks, although their orientations differ (Figure 3.8). This explains why Kirsten always used the same fixed RJS values ($1 = 1:1$, $2 = 1:2$, $4 = 1:4$, $8 = 1:8$) for both directions of the block (in and against the direction of excavation). On the other hand, in Kirsten's initial representation, as shown in Figure 3.1 where a block is oriented against the direction of excavation, the joint spacing S_ψ is smaller than S_θ . For this, the corresponding RJS should not be of the same order as that presented in Table 3.1. If, for example, $S_\psi = 1$ and $S_\theta = 2$, the RJS would be $1/2 = 0.5$. In addition, as stated in Table 3.2, for r

>0.125 , J_s is determined according to $r = 0.125$. This value of 0.125 represents the ratio of 1/8, rather than 8/1 as presented in Table 3.1. The value of 0.125 has also been noted by Kirsten (1988) and the USDA (1997). Annandale (1995, 2006) has corrected this by indicating that beyond a RJS value of 8 ($1:8 = 8/1 = 8$), J_s could be considered to have a RJS of 8. However, the initial concept presented in Figure 3.1 could be adjusted. Indeed, when the block is oriented against the direction of excavation, the digging angle is ψ (Figure 3.8), while Kirsten (1982) represented this angle as θ , as shown in Figure 3.1. Given that the two coaxial components considered for K_d are obtained by having the digging angle as θ (Section 3.2.1), the equation of K_d (Eq. 3.7) presented by Kirsten (1982) must be adjusted if the digging angle is considered to be ψ (Figure 3.8). This is also taken into account when the block is oriented in the direction of excavation. Indeed, the digging angle for this situation would be θ (Figure 3.8). Consequently, two equations of K_d will be proposed according to the adopted digging angles.

Furthermore, it should be noted that the orientation of the block can be changed depending on the rotation center being the convergence point between the principal dislodging force and the principal degree of freedom (Figure 3.9). The concepts of the principal dislodging force and the principal degree of freedom can be seen as being the same concept for a block oriented in and against the direction of excavation, as shown in Figure 3.9. Therefore, the two components of opposite directions (identified as A and A' in Figure 3.9) will not be considered, whatever the orientation of the block, and consequently K_d will be determined according to the other coaxial components, namely those identified as B and B' in Figure 3.9.

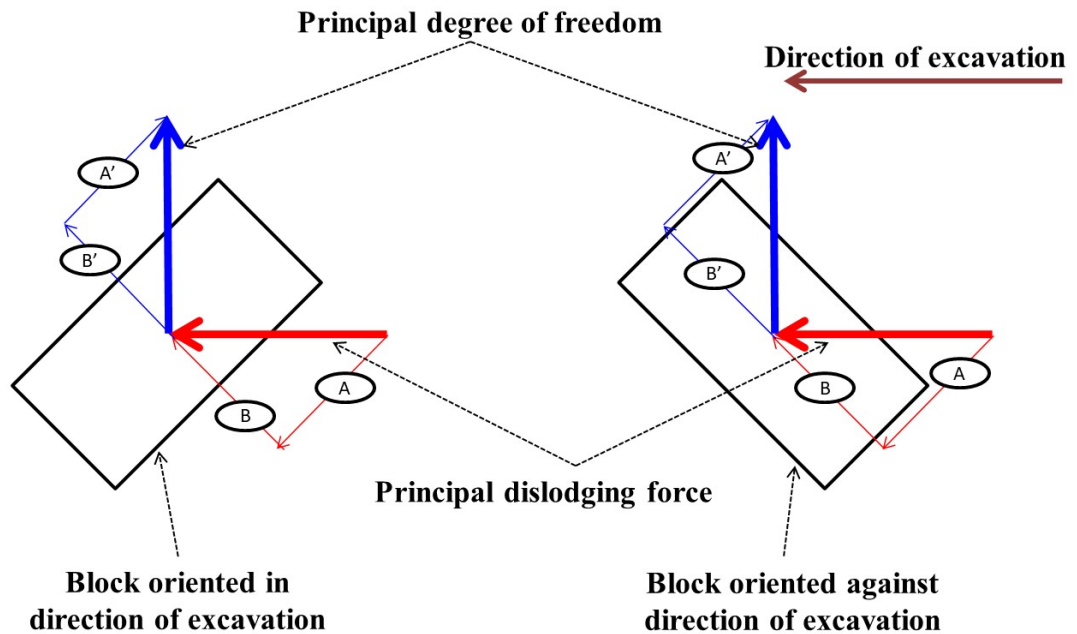


Figure 3.9. Coaxial components for blocks oriented in and against the direction of excavation.

3.3.2. Proposed K_d equation when the block is oriented in direction of flow

The concept of a block oriented in the direction of flow is shown in Figure 3.10. According to the determination of the coaxial components of the principal dislodging force and the principal degree of freedom for a block oriented in the direction of flow (Figure 3.10), the unknown angle (considered as α), as well as the coaxial components (B and B') can be determined according to the following equation:

$$\left. \begin{aligned} \alpha &= \psi - \theta \\ B &= \frac{\sin \theta}{\sin (\psi - \theta)} \\ B' &= \frac{\sin \left(\frac{\pi}{2} - \theta\right)}{\sin (\psi - \theta)} \end{aligned} \right\} \quad (3.10)$$

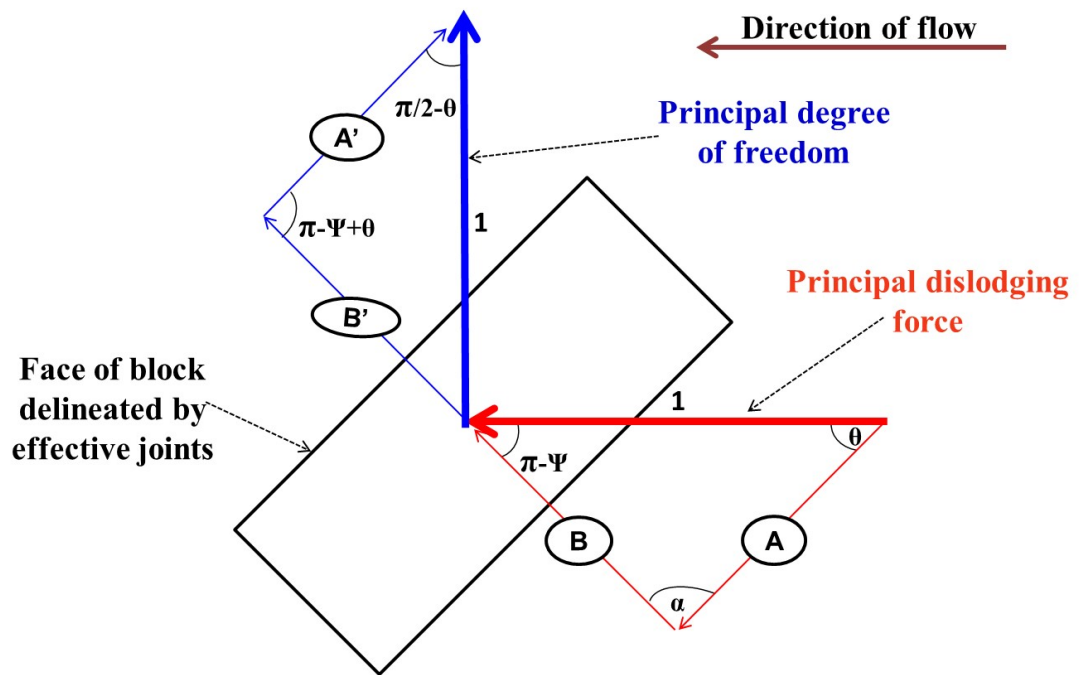


Figure 3.10. Coaxial components for a block oriented in the direction of flow.

The final equation of K_d when the block is oriented in the direction of flow is given by the product of the two components B and B' . This final equation is expressed as follows:

$$K_d = \frac{\sin \theta \cdot \cos \theta}{\sin^2(\psi - \theta)} \quad (3.11)$$

It should be mentioned that Eq. 3.11 can be applied under the following conditions:

$$\left. \begin{array}{l} \psi = \alpha + \theta \\ 0^\circ < \theta < 90^\circ \\ 90^\circ < \psi < 180^\circ \end{array} \right\} \quad (3.12)$$

The angles of α , ψ and θ are schematically shown in Figure 3.11.

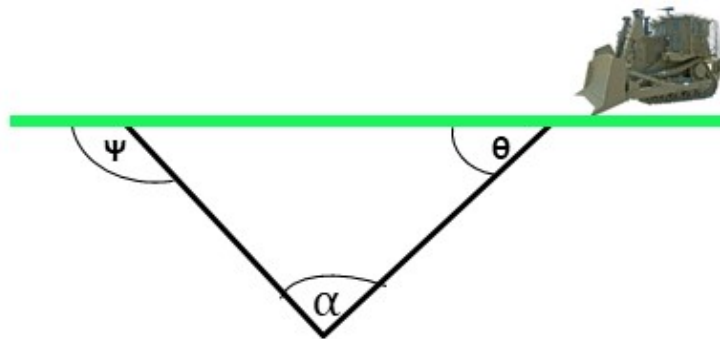


Figure 3.11. Considered angles when the block is oriented in the direction of flow.

3.3.3. Proposed K_d equation when the block is oriented against direction of flow

The concept of a block oriented against the direction of flow is shown in Figure 3.12. According to the determination of the coaxial components of the principal dislodging force and the principal degree of freedom for a block oriented in the direction of flow (Figure 3.12), the unknown angle (considered as α) and the coaxial components (B and B') could be determined according to the following equation:

$$\left. \begin{aligned} \alpha &= \theta - \psi \\ B &= \frac{\sin \psi}{\sin (\theta - \psi)} \\ B' &= \frac{\sin \left(\frac{\pi}{2} - \psi\right)}{\sin (\theta - \psi)} \end{aligned} \right\} \quad (3.13)$$

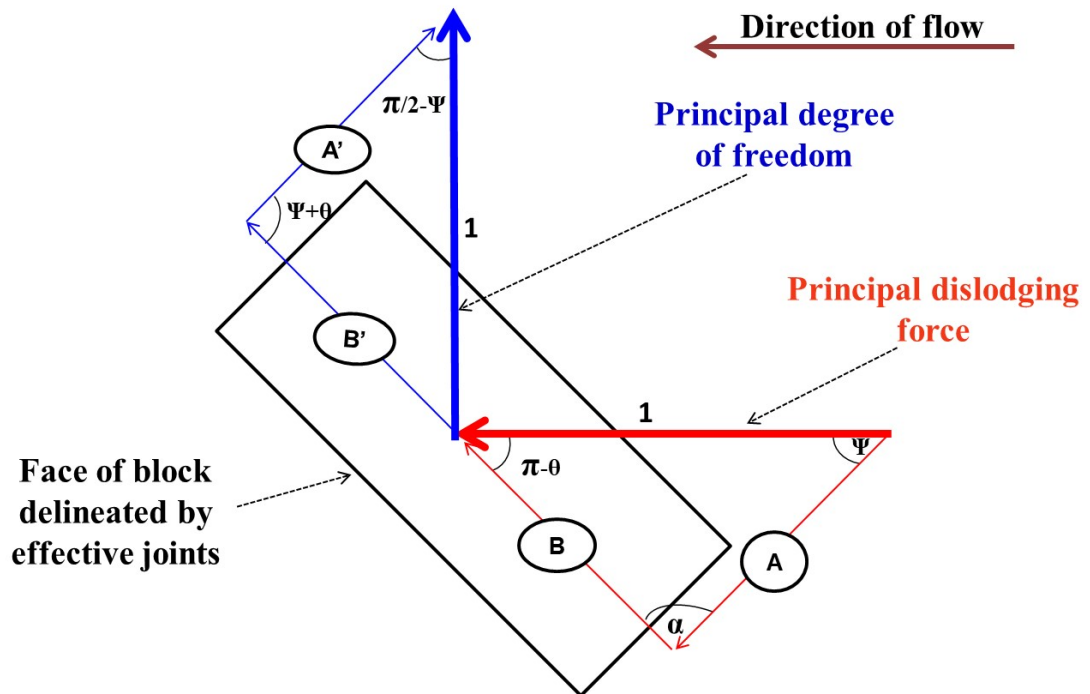


Figure 3.12. Coaxial components for a block oriented against the direction of flow.

The final equation of K_d when the block is oriented against the direction of flow is given by the product of the two components B and B' , which is expressed as follows:

$$K_d = \frac{\sin \psi \cdot \cos \psi}{\sin^2(\theta - \psi)} \quad (3.14)$$

It should be mentioned that Eq. 3.14 can be applied under the following conditions:

$$\left. \begin{array}{l} \psi = \theta - \alpha \\ 90^\circ < \theta < 180^\circ \\ 0^\circ < \psi < 90^\circ \end{array} \right\} \quad (3.15)$$

In this situation, the angles of α , ψ and θ are schematically shown in Figure 3.13.

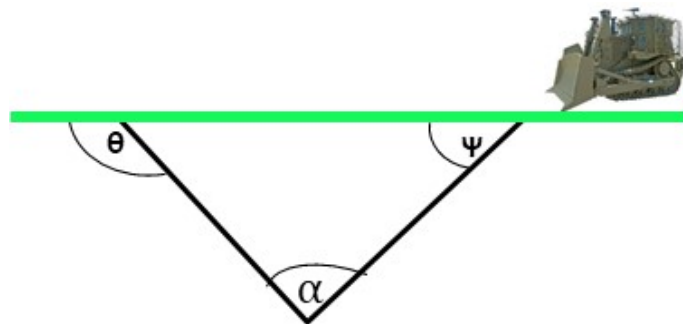


Figure 3.13. Considered angles when the block is oriented against the direction of flow.

3.3.4. Analysis of K_d behavior

The behavior of K_d is assessed according to Eqs. 3.11 and 3.14 that represent K_d when the block is oriented in and against the direction of flow, respectively. The results of K_d are shown in Figure 3.14. For blocks oriented against the direction of flow, θ is represented as dips ranging from 0° to 90° . Thus, for example, a value of $\theta = 175^\circ$ used for calculating K_d is represented on the curve as an angle of 5° . According to Figure 3.14, K_d presents the same behavior when the block is oriented in or against the direction of flow. Since the orientation of the block changes depending on the rotation center, the concepts of the principal dislodging force and the principal degree of freedom are always maintained regardless of the block's orientation relative to the direction of flow. Thus K_d , for the same dip, is of the same value when the block is oriented in or against the direction of flow. This is confirmed by the proposed equations.

The results obtained from the proposed equations are in perfect agreement with those obtained through Kirsten's concept. Thus, the proposed equations provide reliable estimates of K_d without these equations being forced to be expressed in absolute terms, as proposed by Kirsten (1982). It should be noted that the K_d values determined according to Kirsten's concept, when the block is oriented against or in the direction of excavation, are not equal, as shown in Figure 3.15. For example, $K_d = -0.09$ for $\theta = 5^\circ$ oriented against the direction of excavation, while it is 0.09 for $\theta = 5^\circ$ oriented in the direction of excavation. Consequently, Kirsten expressed K_d in

absolute terms (Eq. 3.8) and produced identical K_d values when the block is oriented in or against the direction of excavation.

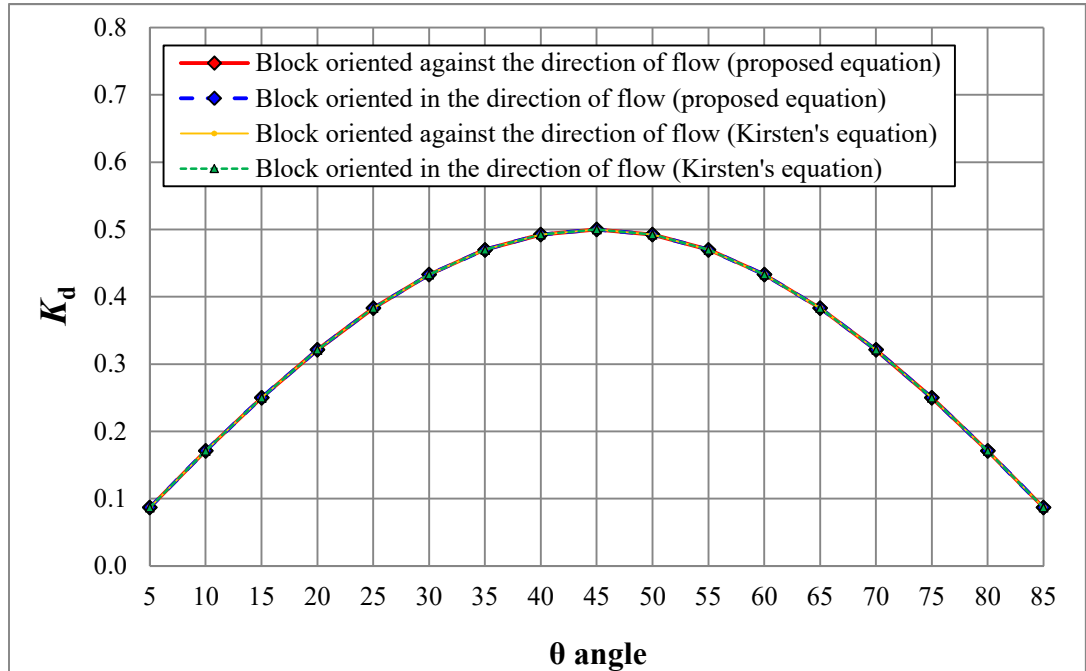


Figure 3.14. Behavior of the kinematic possibility of dislodgment versus θ .

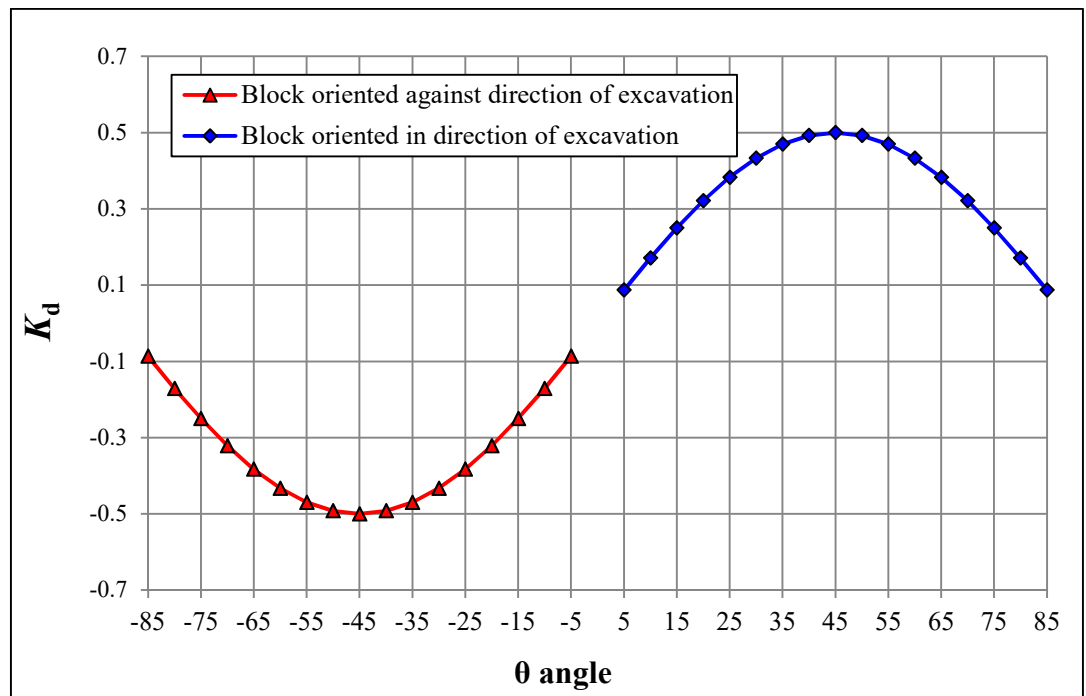


Figure 3.15. Behavior of the kinematic possibility of dislodgment not expressed in absolute terms.

3.3.5. Proposed equations for determining J_s

Considering that the required effort is equal to 1 minus the kinematic possibility as proposed by Kirsten (1982), J_s values can be determined by the proposed equations (Eqs. 3.16 and 3.17). Eq. 3.16 is applied when the blocks are oriented in the direction of flow (Eq. 3.11 for K_d is introduced), while Eq. 3.17 is used when the blocks are oriented against the direction of flow (Eq. 3.14 for K_d is introduced). It should be noted that no change is introduced into the equation for K_p (Eq. 3.4).

$$J_s = \left[1 - \frac{r \tan \theta + \tan \psi}{a (r + 1)} \right] \cdot \left[1 - \frac{\sin \theta \cdot \cos \theta}{\sin^2 (\psi - \theta)} \right] \quad (3.16)$$

$$J_s = \left[1 - \frac{r \tan \theta + \tan \psi}{a (r + 1)} \right] \cdot \left[1 - \frac{\sin \psi \cdot \cos \psi}{\sin^2 (\theta - \psi)} \right] \quad (3.17)$$

3.4. Results and discussion

Determining J_s values for the non-orthogonal fracture systems is carried out according to the proposed equations (Eqs. 3.16 and 3.17) using RJSs of 1:1, 1:2, 1:4 and 1:8 for the case of blocks oriented in and against the direction of flow. It should be noted that when $\theta = 0^\circ$, 90° and 180° , the J_s value is 1 (Section 3.2.3). Therefore, no analyses are performed for these angles.

3.4.1. Determining J_s when α is larger than 90°

For non-orthogonal fracture systems, α may be greater than 90° (from 91° to 179°). To determine the effect of α in this range on J_s , a series of angles is evaluated (100° , 110° , 120° , 130° , 140° and 150°). In geomechanics, planes are usually considered as parallel when the angle between the planes is less than 20° . Examples of this case include the angle between the joint's dip direction and the direction of excavation when determining the orientation factor in the rock mass classification system (*RMR*) of Bieniawski (1989) and the angle of the joint's dip direction and the direction of slope surface during the analysis of possible planar failure (Wyllie and Mah, 2004). Consequently, the α angle for non-orthogonal fracture systems is limited to a maximum of 150° .

The behavior of J_s as a function of θ (considered as the dip of the closer spaced joint set) when $\alpha = 100^\circ$, 110° , 120° , 130° , 140° and 150° is shown in Figure 3.16. When the block is oriented in the direction of flow, θ ranges from 0° to 90° , whereas θ ranges from 90° to 180° when the block is oriented against the direction of flow (Eq. 3.14). However, the latter angles are represented as angles varying from 0° to 90° marked by a negative sign. For example, $\theta = 150^\circ$ corresponds to an angle of -30° ($\theta = 180^\circ - 150^\circ = 30^\circ$) in Figure 3.16.

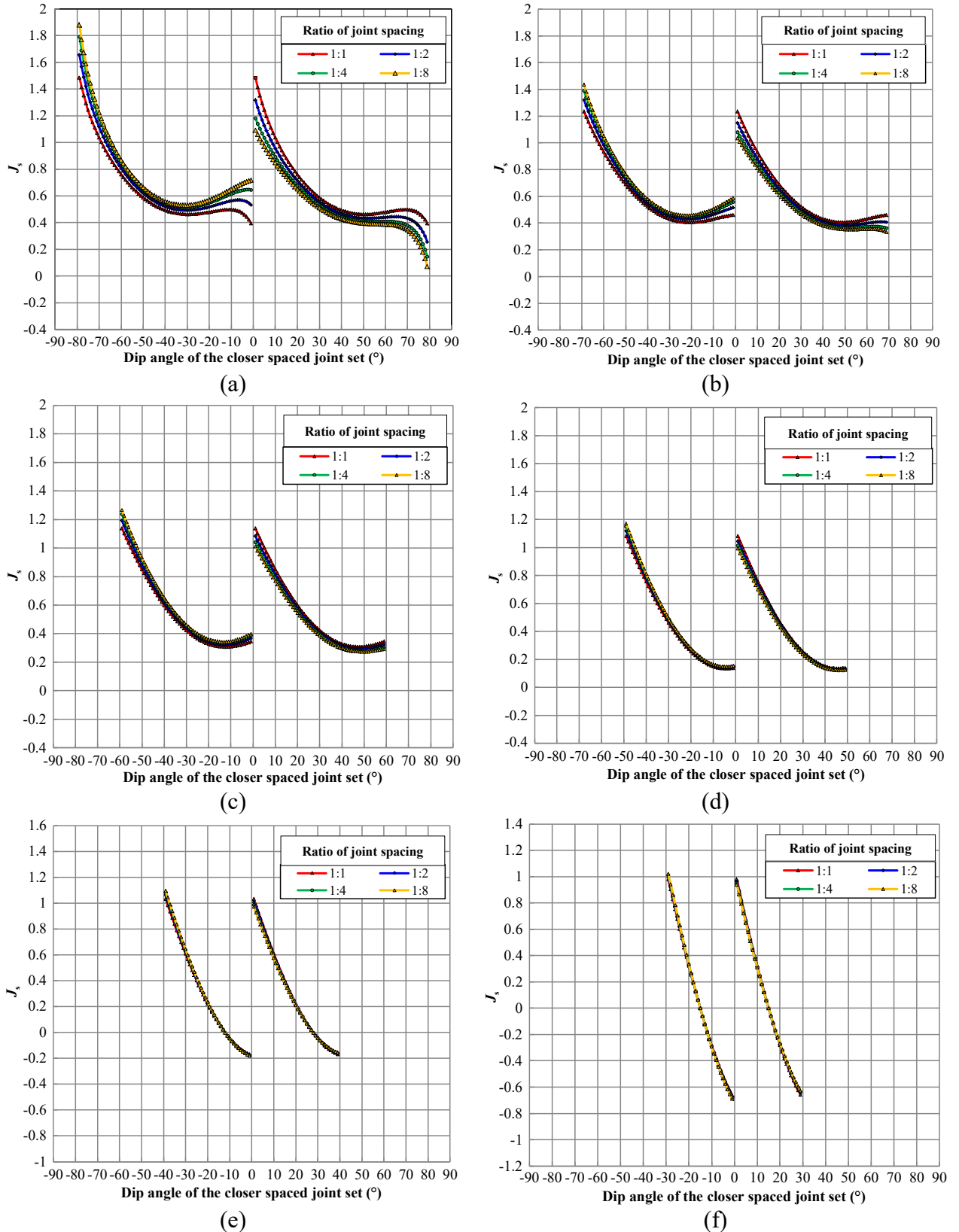


Figure 3.16. Behavior of J_s : (a) $\alpha = 100^\circ$, (b) $\alpha = 110^\circ$, (c) $\alpha = 120^\circ$, (d) $\alpha = 130^\circ$, (e) $\alpha = 140^\circ$, and (f) $\alpha = 150^\circ$.

When $\alpha = 100^\circ$ (Figure 3.16a), J_s is not calculated for $\theta \geq 80^\circ$. This is explained by a non-favorable geometry applying to the conditions as indicated in Eqs. 12 and 15. Similar situations are noted with the pairings $\alpha = 110^\circ$ and $\theta \geq 70^\circ$ (Figure 3.16b), $\alpha = 120^\circ$ and $\theta \geq 60^\circ$ (Figure 3.16c), $\alpha = 130^\circ$ and $\theta \geq 50^\circ$ (Figure 3.16d), $\alpha = 140^\circ$ and $\theta \geq 40^\circ$ (Figure 3.16e) and $\alpha = 150^\circ$ and $\theta \geq 30^\circ$ (Figure 3.16f). Moreover, when $\alpha = 100^\circ, 110^\circ, 120^\circ$ and 130° , the J_s behavior curves vary according to the RJS. However, when $\alpha = 140^\circ$ or 150° , the J_s behavior curves do not vary with the RJS. Thus, the RJS has no effect when $\alpha > 130^\circ$. Accordingly, the proposed J_s values can be assigned for any RJS when $\alpha = 140^\circ$. This process is also valid when $\alpha = 150^\circ$.

Although the dip of the closer spaced joint set can vary from 0° to 90° , to keep the same considerations as Kirsten (1982), only dip angles used by Kirsten (1982) are used in the adjustment process. These dips correspond to $5^\circ, 10^\circ, 20^\circ, 30^\circ, 40^\circ, 50^\circ, 60^\circ, 70^\circ, 80^\circ, 85^\circ$ and 90° . Moreover, the adjustment process is performed for $r = 1:1, 1:2, 1:4$ and $1:8$. However, only the adjustment process for $r = 1:8$ is discussed in this paper. For the other RJSs, the same method is applied⁴.

When the blocks are oriented in the direction of flow, the initial results obtained by using Eq. 3.16 are represented in Figure 3.17a, and the results for blocks oriented against the direction of flow, derived from Eq. 3.17, are

⁴ Curves before and after adjustment for a RJS of 4, 2, and 1 ($\alpha > 90^\circ$) are presented in Appendix C of this thesis, but they were not included in the published paper.

represented in Figure 3.17b. Adopting the same adjusting method as Kirsten (explained in Section 3.2.3), the curve adjusting process considers that all the curves must be plotted with J_s of 1 when the dip angles are 0° and 90° . On the other hand, the adjusting process is performed to avoid having negative determinations of J_s , as exemplified by the dip angle/ α pairing of $30^\circ/140^\circ$ where the J_s value is modified from -0.04 to 0.11 (Figure 3.17a and c) or the pairing of $5^\circ/140^\circ$ where the J_s value is modified from -1.15 to 0.11 (Figure 3.17b and d). Furthermore, as it is considered that the J_s values can be of the same order for a given dip, regardless of the RJS when $\alpha = 140^\circ$ or 150° , the “same required effort principle” is applied during the adjustment process as when a RJS of 1 is used. Thus, in the case of $\alpha = 140^\circ$, the same required effort principle is applied for a dip of 20° oriented in or against the direction of flow. In the case of $\alpha = 150^\circ$, the same required effort principle is applied for the dip pairings of $20^\circ/10^\circ$ and $10^\circ/20^\circ$ (the first dip of each pairing is oriented in the direction of flow, and the second dip is oriented against the direction of flow). The final adjusted curves when the blocks are oriented in and against the direction of flow are shown in Figure 3.17c and d, respectively. The final adopted J_s values are presented in Table 3.3.

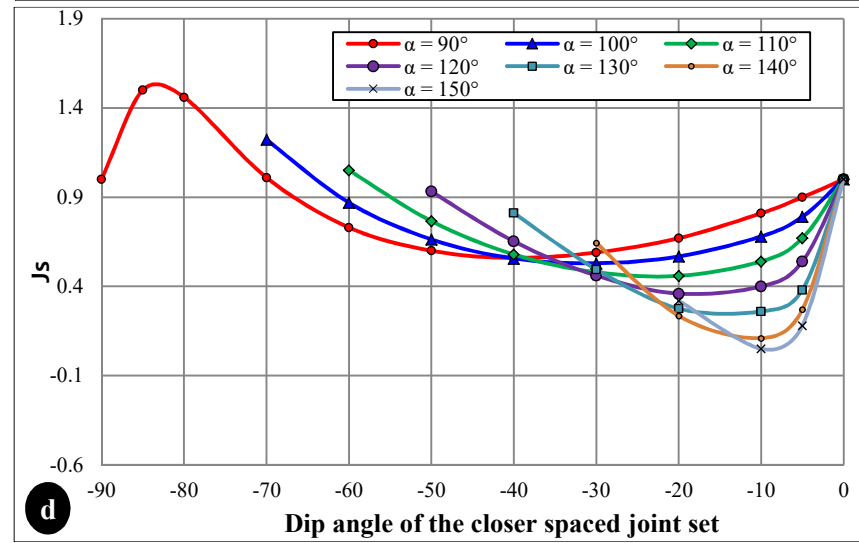
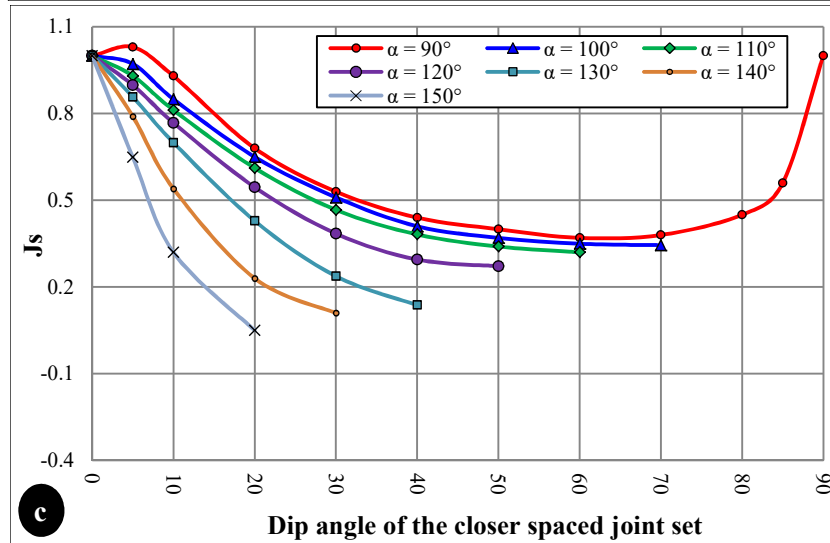
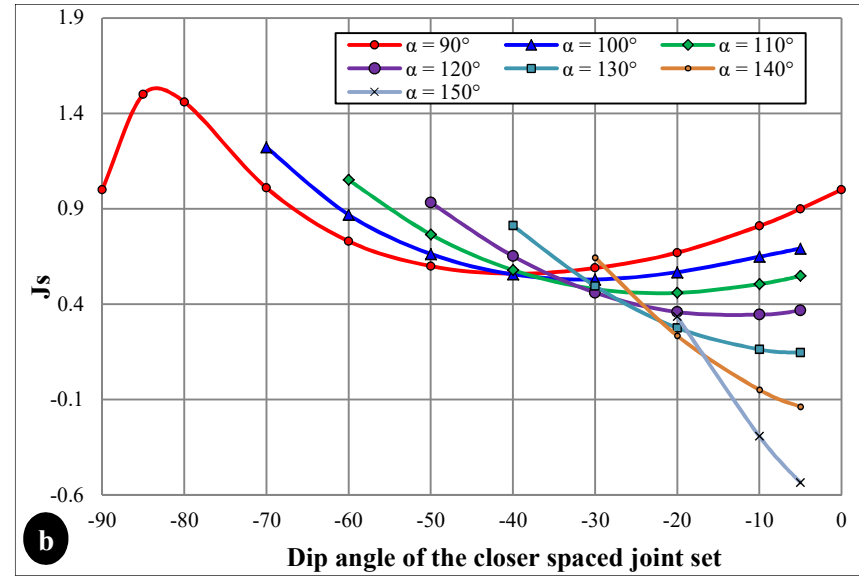
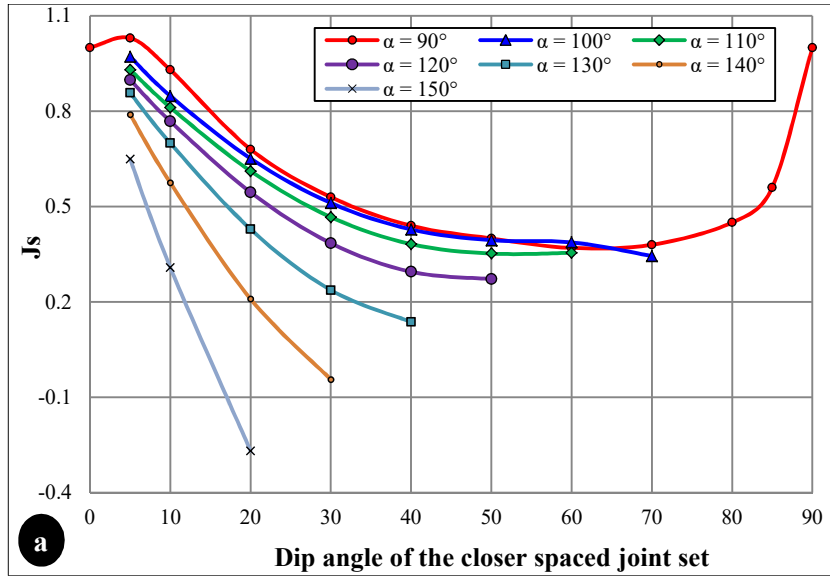


Figure 3.17. J_s curves for $r = 8$ when α is larger than 90° : (a) Before adjustment – in the direction of flow; (b) Before adjustment – against the direction of flow; (c) After adjustment – in the direction of flow; and (d) After adjustment – against the direction of flow.

Table 3.3. Rating values of relative block structures for a non-orthogonal fracture system ($\alpha > 90^\circ$).

	Angle of the closer spaced joint set ¹	Angle between the two planes (α)																140°	150°
		100°				110°				120°				130°					
		Ratio of joint spacing (r)																	
	1:1	1:2	1:4	1:8	1:1	1:2	1:4	1:8	1:1	1:2	1:4	1:8	1:1	1:2	1:4	1:8	For any r	For any r	
Dip direction of the closer spaced joint set is in the direction of flow	70°	0.50	0.42	0.38	0.34	-	-	-	-	-	-	-	-	-	-	-	-	-	
	60°	0.46	0.41	0.38	0.35	0.42	0.37	0.35	0.32	-	-	-	-	-	-	-	-	-	
	50°	0.46	0.42	0.40	0.37	0.41	0.38	0.36	0.34	0.31	0.29	0.28	0.27	-	-	-	-	-	
	40°	0.49	0.45	0.43	0.41	0.43	0.41	0.39	0.38	0.33	0.31	0.30	0.30	0.15	0.14	0.14	0.14	-	
	30°	0.59	0.55	0.52	0.51	0.52	0.50	0.48	0.47	0.42	0.41	0.39	0.38	0.26	0.25	0.24	0.24	0.11	
	20°	0.76	0.71	0.67	0.65	0.69	0.66	0.63	0.61	0.60	0.58	0.56	0.55	0.46	0.45	0.44	0.43	0.23	
	10°	1.04	0.99	0.91	0.85	0.93	0.90	0.84	0.81	0.85	0.82	0.79	0.77	0.76	0.73	0.71	0.70	0.54	
	5°	1.24	1.13	1.03	0.97	1.09	1.02	0.97	0.93	0.99	0.96	0.92	0.90	0.93	0.90	0.87	0.86	0.79	
Dip direction of the closer spaced joint set is against the direction of flow	5°	0.68	0.72	0.75	0.79	0.56	0.60	0.63	0.67	0.44	0.48	0.51	0.54	0.29	0.31	0.34	0.38	0.27	
	10°	0.50	0.60	0.64	0.68	0.42	0.48	0.50	0.54	0.31	0.36	0.36	0.40	0.15	0.21	0.22	0.26	0.11	
	20°	0.46	0.52	0.55	0.57	0.41	0.43	0.45	0.46	0.33	0.34	0.35	0.36	0.26	0.26	0.27	0.28	0.23	
	30°	0.46	0.49	0.51	0.53	0.43	0.45	0.47	0.48	0.42	0.44	0.45	0.46	0.46	0.48	0.49	0.50	0.64	
	40°	0.49	0.52	0.54	0.56	0.52	0.55	0.57	0.58	0.60	0.62	0.64	0.65	0.76	0.78	0.80	0.81	-	
	50°	0.59	0.62	0.65	0.66	0.69	0.72	0.75	0.77	0.85	0.89	0.91	0.93	-	-	-	-	-	
	60°	0.76	0.81	0.84	0.87	0.93	0.98	1.02	1.05	-	-	-	-	-	-	-	-	-	
	70°	1.04	1.12	1.18	1.22	-	-	-	-	-	-	-	-	-	-	-	-	-	

1: Apparent dip angle of the closer spaced joint set in a vertical plane containing direction of flow

3.4.2. Determining J_s when α is less than 90°

A series of α angles (30° , 40° , 50° , 60° , 70° and 80°) are adopted to evaluate the J_s rating when α is less than 90° . Cases where $\alpha = 10^\circ$ and 20° are excluded as they represent situations where the planes of the joints are parallel (Bieniawski, 1989). The behavior of J_s with $\alpha = 80^\circ$, 70° , 60° , 50° , 40° and 30° are presented in Figure 3.18. The θ angles in these Figures, which originally varied from 90° to 180° (Eq. 3.14) when the block is oriented against the direction of flow, are represented by an angle varying from 0° to 90° with a negative sign.

When $\alpha = 80^\circ$ and $\theta = 10^\circ$ (Figure 3.18a), the J_s value cannot be determined as Eqs. 16 and 17 generate abnormal values by using $\psi = 90^\circ$, $\alpha = 80^\circ$ and $\theta = 10^\circ$. Such a situation occurred also for the α/θ pairings of $70^\circ/20^\circ$ (Figure 3.18b), $60^\circ/30^\circ$ (Figure 3.18c), $50^\circ/40^\circ$ (Figure 3.18d), $40^\circ/50^\circ$ (Figure 3.18e) and $30^\circ/60^\circ$ (Figure 3.18f). On the other hand, when $\alpha = 80^\circ$ and $\theta < 10^\circ$, the J_s value was not valid as the ψ angle here would have a value beyond that of the validated tuned interval (see the application conditions of Eqs. 3.12 and 3.15). Such a situation also occurred for the α/θ pairings of $70^\circ/<20^\circ$ (Figure 3.18b), $60^\circ/<30^\circ$ (Figure 3.18c), $50^\circ/<40^\circ$ (Figure 3.18d), $40^\circ/<50^\circ$ (Figure 3.18e) and $30^\circ/<60^\circ$ (Figure 3.18f). According to Figure 3.18, J_s curves vary as a function of RJS, except for those at $\alpha = 30^\circ$ (Figure 3.18f). Thus, the RJS has no impact when $\alpha = 30^\circ$.

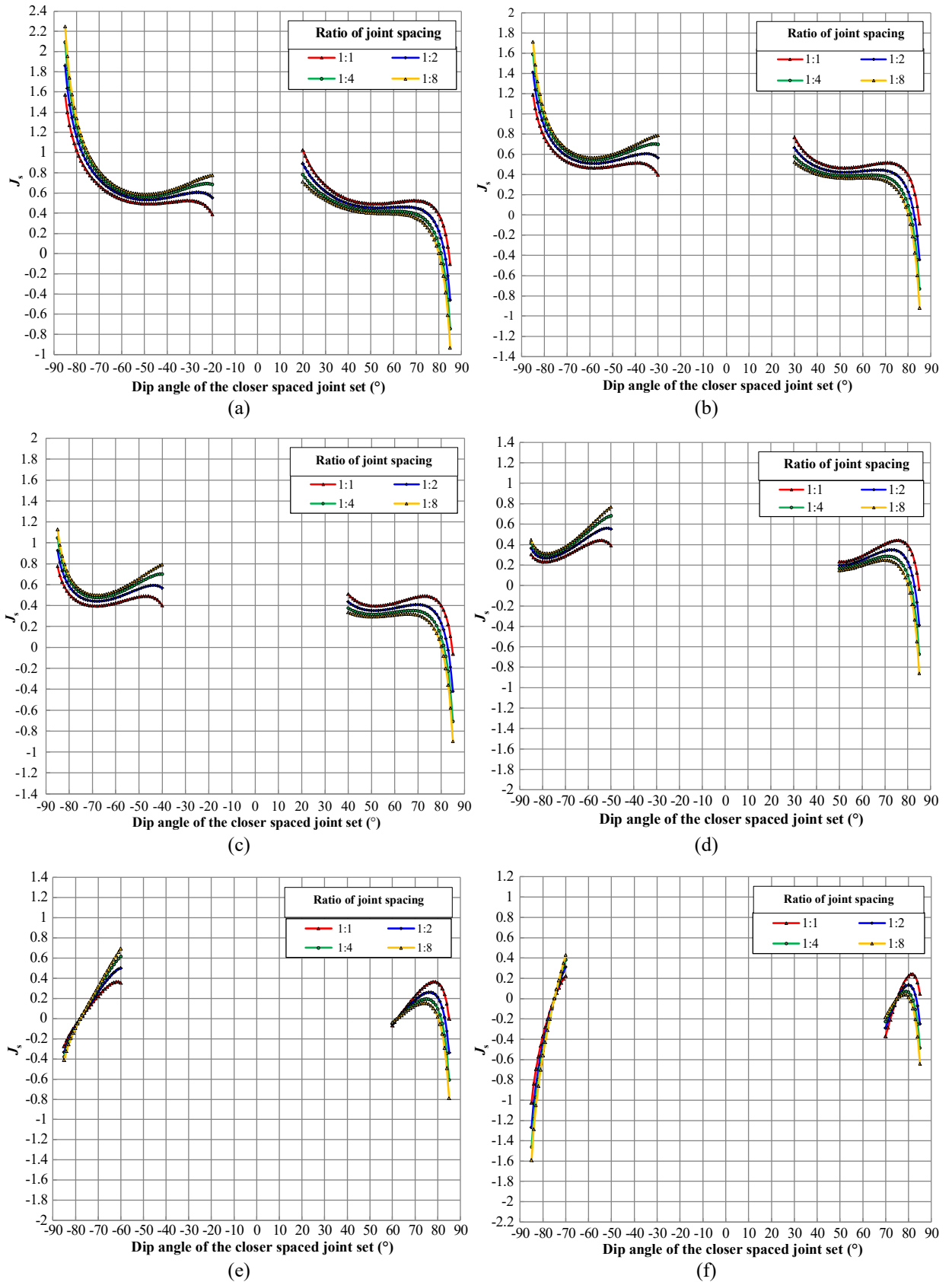


Figure 3.18. Behavior of J_s : (a) $\alpha = 80^\circ$, (b) $\alpha = 70^\circ$, (c) $\alpha = 60^\circ$, (d) $\alpha = 50^\circ$, (e) $\alpha = 40^\circ$, and (f) $\alpha = 30^\circ$.

The outcomes for J_s when the blocks are oriented against the direction of flow are presented in Figure 3.19a, while J_s values when the blocks are oriented in the direction of flow are shown in Figure 3.19b. It should be mentioned that the obtained curves are based on the same adjustment process as Kirsten's (explained in Section 3.2.3). The curve adjustment process is undertaken (1) to ensure that all curves are plotted with $J_s = 1$ when the dip = 0° or 90° and (2) to avoid negative determinations of J_s , as exemplified by the dip/ α pairing of $80^\circ/30^\circ$ where the J_s value of -0.56 (see Figure 3.19b) is modified to 0.14 (see Figure 3.19d). Furthermore, the "same required effort principle" is applied during the adjustment process, as demonstrated by a dip angle of 70° oriented in the direction of flow and a dip angle of 80° oriented against the direction of flow (and vice versa). The final adjusted curves when the blocks are oriented in and against the direction of flow are shown in Figure 3.19c and Figure 3.19d, respectively⁵. The final adopted J_s values are presented in Table 3.4.

⁵ Curves before and after adjustment for a RJS of 4, 2, and 1 ($\alpha < 90^\circ$) are presented in Appendix D of this thesis, but they were not included in the published paper.

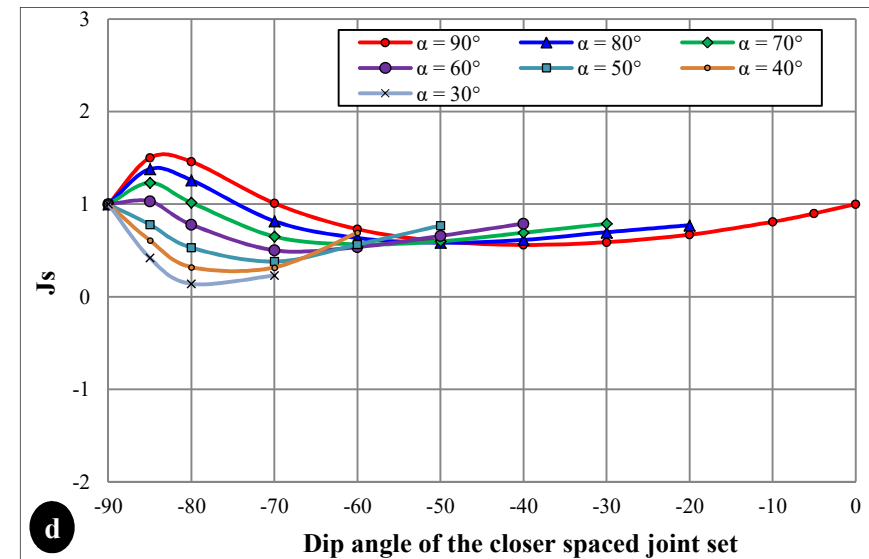
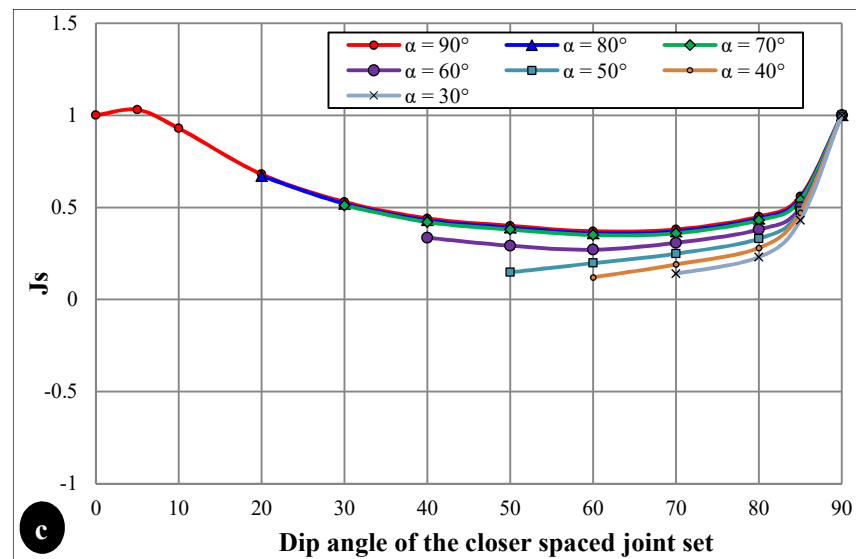
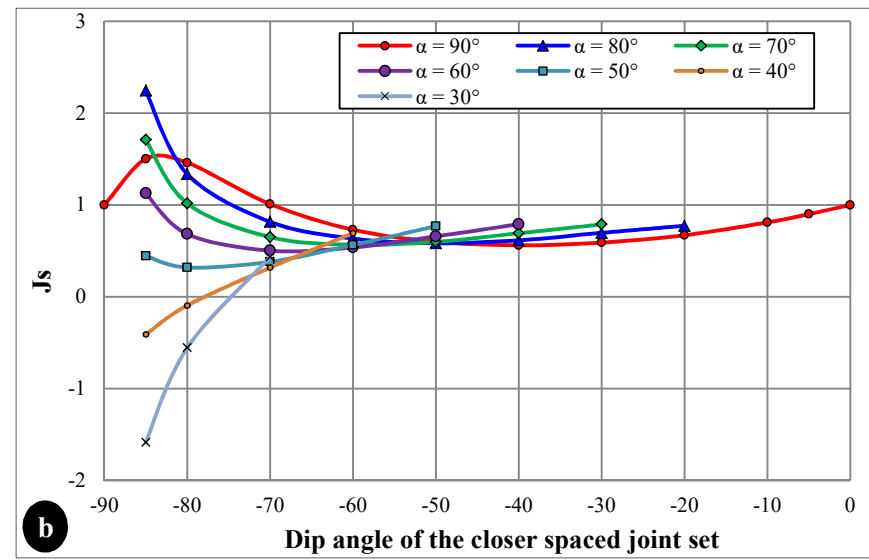
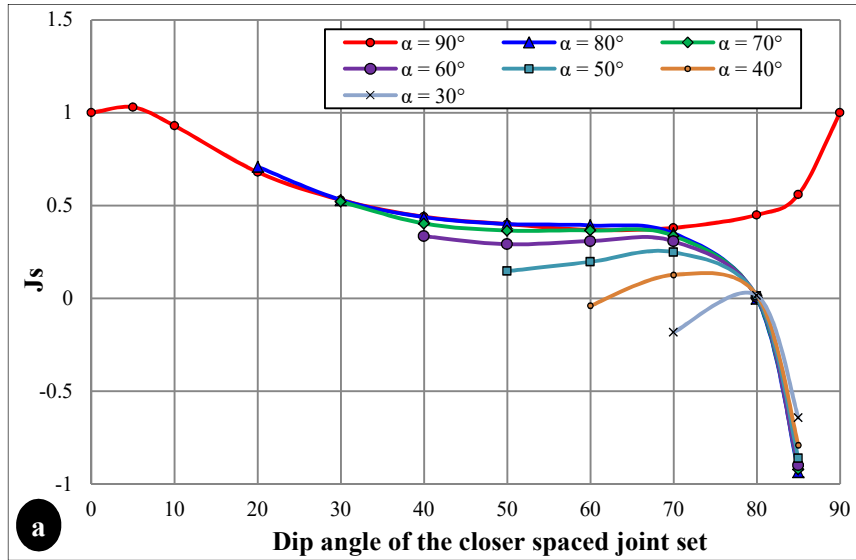


Figure 3.19. J_s curves when $RJS = 8$: a) Before adjustment-in the direction of flow; b) Before adjustment-against the direction of flow; c) After adjustment-in the direction of flow; d) After adjustment-against the direction of flow.

Table 3.4. Rating values of relative block structures for a non-orthogonal fracture system ($\alpha < 90^\circ$).

Angle of closer spaced joint set ¹	Angle between the two planes (α)																				For any r	
	80°				70°				60°				50°				40°					
	Ratio of joint spacing (r)																					
	1:1	1:2	1:4	1:8	1:1	1:2	1:4	1:8	1:1	1:2	1:4	1:8	1:1	1:2	1:4	1:8	1:1	1:2	1:4	1:8		
Dip direction of the closer spaced joint set is in the direction of flow	85°	0.71	0.66	0.61	0.55	0.70	0.65	0.60	0.54	0.63	0.59	0.55	0.50	0.54	0.52	0.50	0.48	0.44	0.45	0.46	0.47	0.43
	80°	0.62	0.56	0.49	0.44	0.61	0.55	0.48	0.43	0.54	0.48	0.44	0.38	0.42	0.42	0.38	0.33	0.27	0.26	0.27	0.28	0.23
	70°	0.51	0.44	0.40	0.37	0.50	0.43	0.39	0.36	0.46	0.39	0.35	0.31	0.34	0.31	0.28	0.25	0.18	0.17	0.18	0.19	0.14
	60°	0.48	0.43	0.40	0.36	0.47	0.42	0.39	0.35	0.42	0.35	0.31	0.27	0.29	0.25	0.22	0.20	0.09	0.10	0.11	0.12	-
	50°	0.48	0.45	0.42	0.39	0.47	0.44	0.41	0.38	0.40	0.36	0.32	0.29	0.23	0.21	0.17	0.15	-	-	-	-	-
	40°	0.52	0.48	0.45	0.43	0.51	0.47	0.44	0.42	0.41	0.38	0.35	0.34	-	-	-	-	-	-	-	-	-
	30°	0.62	0.58	0.54	0.52	0.61	0.57	0.53	0.51	-	-	-	-	-	-	-	-	-	-	-	-	-
	20°	0.81	0.76	0.70	0.67	-	-	-	-	-	-	-	-	-	-	-	-	-	-	-	-	-
Dip direction of the closer spaced joint set is against the direction of flow	20°	0.62	0.55	0.68	0.77	-	-	-	-	-	-	-	-	-	-	-	-	-	-	-	-	-
	30°	0.51	0.60	0.66	0.70	0.61	0.56	0.70	0.79	-	-	-	-	-	-	-	-	-	-	-	-	-
	40°	0.48	0.55	0.59	0.61	0.50	0.59	0.65	0.69	0.54	0.57	0.70	0.79	-	-	-	-	-	-	-	-	-
	50°	0.48	0.53	0.56	0.58	0.47	0.53	0.57	0.60	0.46	0.56	0.62	0.66	0.42	0.55	0.68	0.77	-	-	-	-	-
	60°	0.52	0.58	0.61	0.63	0.47	0.51	0.54	0.57	0.42	0.47	0.51	0.54	0.34	0.47	0.53	0.56	0.27	0.27	0.62	0.69	-
	70°	0.62	0.73	0.78	0.82	0.51	0.58	0.62	0.65	0.40	0.44	0.48	0.50	0.29	0.33	0.36	0.38	0.18	0.18	0.30	0.32	0.23
	80°	0.81	1.14	1.20	1.26	0.61	0.94	0.98	1.02	0.41	0.74	0.76	0.78	0.23	0.49	0.51	0.53	0.09	0.24	0.28	0.32	0.14
	85°	1.23	1.28	1.33	1.38	1.08	1.13	1.18	1.23	0.97	0.99	1.01	1.03	0.66	0.70	0.74	0.78	0.46	0.51	0.56	0.61	0.42

1: Apparent dip angle of the closer spaced joint set in a vertical plane containing direction of flow

3.4.3. Steps for determining the value of J_s for non-orthogonal fracture systems

Assuming a geological formation mainly fractured by two joint sets, data collected from the field can be interpreted by stereographic projection to determine the mean planes of dip and dip direction of each joint set. The J_s value can then be determined as follows:

- Draw the two planes representing the two joint sets;
- Draw the vector representing the direction of flow;
- Determine the α angle between the two planes of joint sets along the flow direction vector;
- Determine the closer spaced joint set according to the joint spacing of both joint sets;
- Determine the apparent dip of the closer spaced joint sets along the flow direction vector;
- Determine the dip direction of the closer spaced joint set relative to the direction of flow (in or against the direction of flow);
- Determine the RJS of the two joint sets.

Since the α angle, the apparent dip of the closer spaced joint set, the dip direction of the closer spaced joint set relative to the direction of flow and the RJS are determined, Table 3.3 (if $\alpha > 90^\circ$) and Table 3.4 (if $\alpha < 90^\circ$) can be used to determine the J_s value.

3.5. Impact of α angle

The root mean square error (*RMSE*) is used as a standard statistical measure of model performance in meteorology, air quality, climate research studies, etc. In the field of geosciences, the *RMSE* is often used to assess modeling quality both in terms of accuracy and precision (Gokceoglu and Zorlu, 2004; Jones et al., 2003; Wise, 2000; Zimmerman et al., 1999). As shown in Eq. 3.18, the *RMSE* parameter corresponds to the mean of the differences between the J_s obtained by considering the modification associated to α and the standard J_s proposed by Kirsten for an orthogonal system. For this study, the *RMSE* value indicates the importance of the error produced when the used J_s does not correspond to that of the studied case. A higher *RMSE* value indicates a considerable difference between our proposed values of J_s and the standard values proposed by Kirsten.

$$RMSE = \left(\frac{1}{n} \sum_{i=1}^n (J_{s_{orthogonal}} - J_{s_{\alpha angle}})^2 \right)^{1/2} \quad (3.18)$$

The produced *RMSE* results are shown in Figure 3.20. The *RMSE* value (expressed in %) for a given α angle is the average value of *RMSE* determined according to all considered angles of the closer spaced joints set. According to Figure 3.20, the *RMSE* is proportional to the difference between the α angle and the 90° angle used by Kirsten. The *RMSE* values when $\alpha < 90^\circ$ are greater than those when $\alpha > 90^\circ$. Given the obtained *RMSE*, assuming an orthogonal fracture system rather than a non-orthogonal fracture system can produce considerable error when determining the erodibility index.

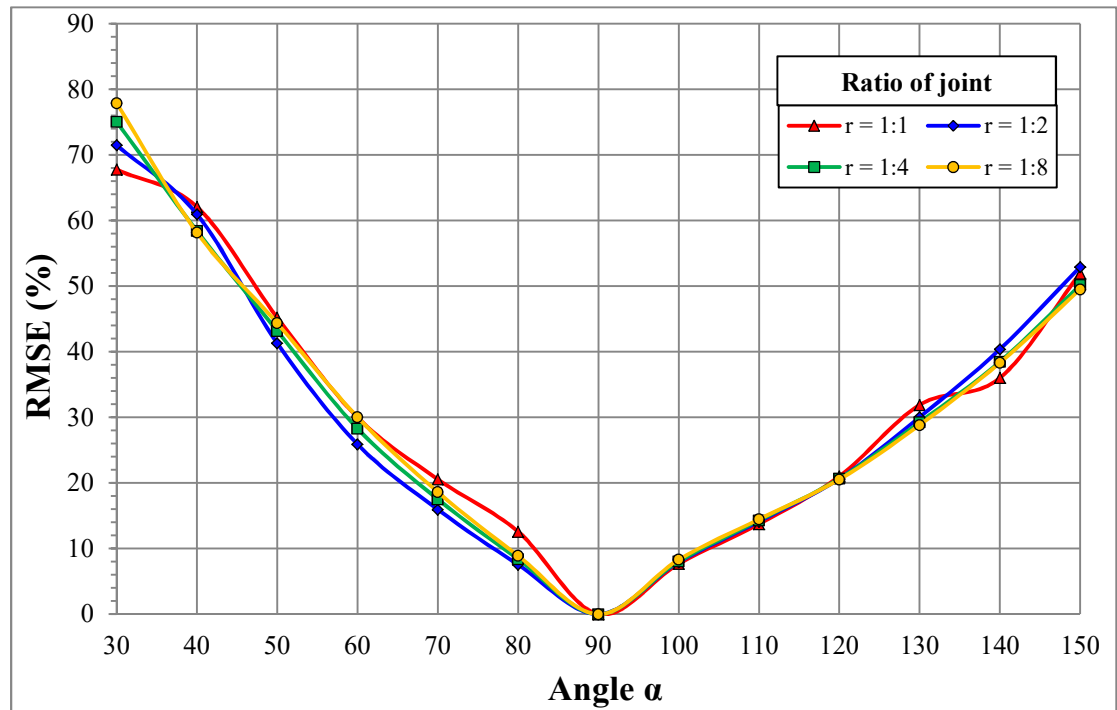


Figure 3.20. Graphical representation of *RMSE* versus α .

To illustrate these findings, three cases examined by Pells (2016) and originally studied by Van Schalkwyk et al. (1994) are analyzed with the J_s values proposed in this study for a non-orthogonal fracture system. The three case studies are from the spillways of dams located in South Africa: the rock mass section 8E-1 of the Mokolo Dam, the rock mass section 9E-2 of the Hartebeespoort Dam and the rock mass section 13E-3 of the Marico-Bosved Dam. The data for the examined sections, as related to Kirsten's index factors, include the compressive strength of intact rock (M_s), the rock block size (Kb), the discontinuity shear strength (Kd) and the relative block structure (J_s) (Table 3.5). The J_s values adopted by Van Schalkwyk et al. (1994) assumed an orthogonal fracture system ($\alpha = 90^\circ$). From the adopted J_s value of each examined section, the RJS, the dip direction of the closer spaced joint set relative to the direction of flow and the dip of the closer spaced joint set are determined using Table 3.2 (Kirsten, 1982). This information is then used to calculate the corresponding J_s when $\alpha > 90^\circ$ (from 100° to 150°) by considering the proposed J_s rating as presented in Table 3.3. The corresponding J_s values are presented in Table 3.5. Subsequently, Kirsten's index is calculated according to the corresponding J_s values (Table 3.6).

The values obtained for Kirsten's index for the three examined sections, calculated as a function of α , are converted into required hydraulic stream power (P_r) using Eq. 3.19 as proposed by Annandale (1995, 2006). Note that all examined case studies of Annandale (1995, 2006) are considered to be orthogonal fracture systems. The determined P_r values for the three examined sections are presented in Table 3.6 and shown in Figure 3.21.

$$P_r = N^{0.75} \quad (3.19)$$

where P_r is the required hydraulic stream power, and N is Kirsten's index.

Table 3.5. Data for the analyzed case studies.

Case study	M_s	K_b	K_d	J_s (90°)	r ¹ -Direction ² - Dip ³	α angle					
						100°	110°	120°	130°	140°	150°
8E-1	140	25.45	0.94	0.81	2-against-5°	0.72	0.6	0.48	0.31	0.27	0.18
9E-2	70	16.47	1.00	1.20	2-in-5°	1.13	1.02	0.96	0.90	0.79	0.65
13E-3	140	26.95	1.68	0.69	4-against-10°	0.64	0.50	0.36	0.22	0.11	0.05

The information below are determined using data from Table 3.2 of Kirsten (1982) based on the J_s value

1: Ratio of joint spacing.

2: Dip direction of closer spaced joint set relative to the direction of flow, either in or against direction of flow.

3: Dip angle of the closer spaced joint set.

Table 3.6. Calculations of the required hydraulic stream power.

Case study	8E-1		9E-2		13E-3	
α angle	N	P_r	N	P_r	N	P_r
90°	2713	376	1380	226	4752	572
100°	2411	344	1303	217	4056	508
110°	2009	300	1176	201	3169	422
120°	1608	254	1107	192	2282	330
130°	1038	183	1037	183	1394	228
140°	904	165	911	166	697	136
150°	603	122	749	143	317	75

N : Kirsten's index

P_r : Required hydraulic steam power

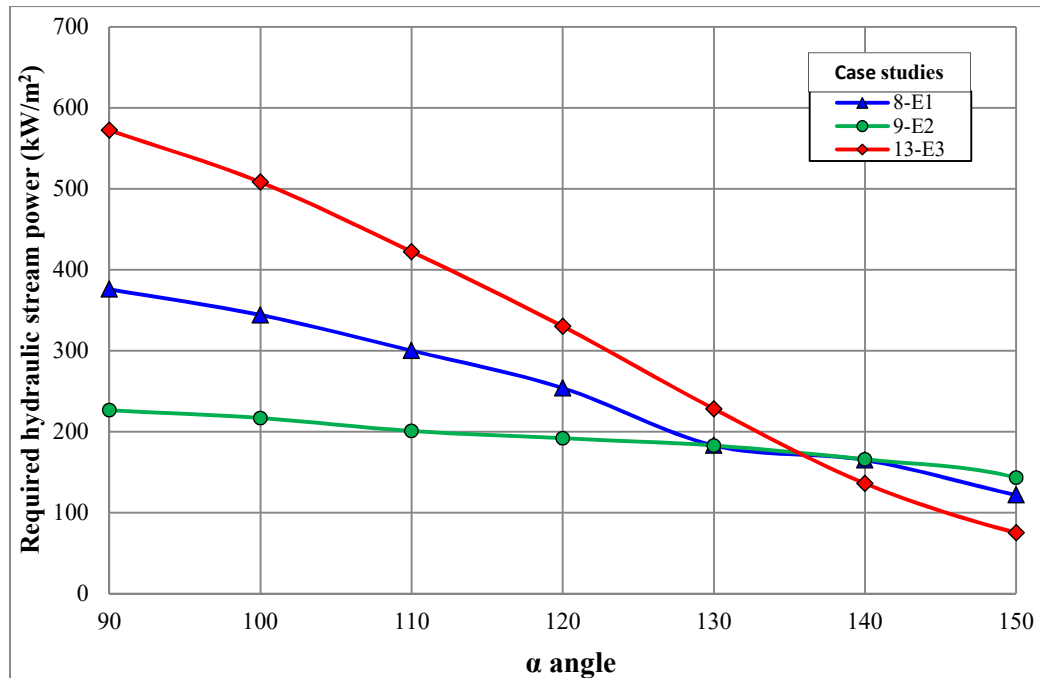


Figure 3.21. Graphical representation of the required hydraulic stream power versus α .

According to Figure 3.21, the required hydraulic stream power for the three examined sections has an inversely proportional relationship to α . Thus, when $\alpha > 90^\circ$, there is a decreasing trend of the required hydraulic stream power. Indeed, the greatest difference in terms of the required hydraulic stream power occurs between the standard angle of 90° and the α of 150° . This confirms the previously established findings regarding *RMSE*, where the largest error (when $\alpha > 90^\circ$) is observed at $\alpha = 150^\circ$. Moreover, the required hydraulic stream power, using $\alpha = 150^\circ$ for the 13-E3, 8-E1 and 9-E2 case studies, is reduced by an order of 7, 3 and 1.5 times, respectively, when compared to the required hydraulic stream power when $\alpha = 90^\circ$ (see Figure 3.21 and Table 3.6). Although the rock mass section 13E-3 has the highest factor values for M_s , K_b and K_d (Table 3.5), there is a marked decreasing curve of the required hydraulic stream power. This is explained by the effect of J_s . Indeed, the lowest J_s

values, according to α , are noted for rock mass section 13E-3 (Table 3.5). These findings highlight the importance of considering α when determining Kirsten's index to calculate the required hydraulic stream power.

3.6. Conclusion

Adjustments are introduced into Kirsten's initial concept concerning the relative block structure parameter. Thus, equations are proposed to determine the relative block structure parameter when the fractured system is non-orthogonal, where the angle between the planes of the two joint sets is larger or smaller than the 90° angle considered by Kirsten. Two equations are proposed: the first assesses the relative block structure when the blocks are oriented in the direction of flow, while the second is used when blocks are oriented against the direction of flow. The use of the two proposed equations, by varying the angle between the two joint sets (α angle), makes it possible to propose a rating for the relative block structure parameter when α is larger or smaller than the standard angle of 90° .

According to our analyses, assuming an orthogonal fracture system in cases represented by a non-orthogonal fracture system can create discrepancies in the determination of the erodibility index and, consequently, in the assessment of the hydraulic erodibility of rock. The non-orthogonal fracture systems reflect cases that can be found in the field where rock's vulnerability to erosion will differ if one

assumes an orthogonal fracture system. Accordingly, our proposed rating of J_s for non-orthogonal fracture systems can provide a more accurate assessment of the hydraulic erodibility of rock.

Conflict of interest

The authors wish to confirm that there are no known conflicts of interest associated with this publication and there has been no significant financial support for this work that could have influenced its outcome.

Acknowledgement

The authors would like to thank the organizations that have funded this project: Natural Sciences and Engineering Research Council of Canada (Grant No 498020-16), Hydro-Quebec (NC-525700) and Mitacs Accelerate program (Grant Ref. IT10008). The authors would acknowledge the useful assistance of Dr Hendrik Kirsten and Professor Monte Van Schalkwayk.

3.7. References

- Annandale GW. Erodibility. *Journal of Hydraulic Research* 1995;33:471–94.
- Annandale GW. *Scour Technology, Mechanics and Engineering in Practice*. McGraw-Hill, New York; 2006.
- Annandale GW, Kirsten HAD. On the erodibility of rock and other earth materials. *Hydraulic Engineering* 1994;1:68–72.
- Basarir H, Karpuz C. A rippability classification system for marls in lignite mines. *Engineering Geology* 2004;74:303–18.
- Bieniawski ZT. *Engineering rock mass classifications: a complete manual for engineers and geologists in mining, civil, and petroleum engineering* 1989:251.
- Bollaert E, Munodawafa MC, Mazvidza DZ. Kariba Dam Plunge Pool Scour : quasi-3D Numerical Predictions. *Proceeding of 6th International Conference on Scour and Erosion, Paris, 2012*, p. 627–34.
- Castillo LG, Carrillo JM. Scour, velocities and pressures evaluations produced by spillway and outlets of dam. *Water* 2016;8:1–21.
- Clark PB. *Rock mass and rippability evaluation for a proposed open pit mine at Globe-Progress, near Reefton. Master of Science in Engineering Geology, University of Canterbury, New Zealand; 1996.*
- Doog N. Die hidrouliese erodeerbaarheid van rotmassas in onbelynde oorlope met spesiale verwysing na die rol van naatvulmateriaal. *Master thesis in Afrikaans language, University of Pretoria, South Africa (cited in Pells, 2016).; 1993.*
- Gokceoglu C, Zorlu K. A fuzzy model to predict the uniaxial compressive strength and the modulus of elasticity of a problematic rock. *Engineering Applications of Artificial Intelligence* 2004;17:61–72.
- Hadjigeorgiou J, Poulin R. Assessment of ease of excavation of surface mines. *Journal of Terramechanics* 1998;35:137–53.
- Hahn WF, Drain MA. Investigation of the erosion potential of kingsley dam emergency spillway. *Proceeding of the joint Annual Meeting and Conference of AIPG, AGWT, and the Florida Section of AIPG, Orlando, Florida, USA., 2010*, p. 1–10.

- Huang MW, Liao JJ, Pan YW, Cheng MH. Modifications of the erodibility index method for the evaluation of the soft bedrock erosion. 47th US Rock Mechanics / Geomechanics Symposium, 2013, p. 7.
- Jones NL, Davis RJ, Sabbah W. A comparison of three-dimensional interpolation techniques for plume characterization. *Ground Water* 2003;41:411–9.
- Keaton JR. Estimating erodible rock durability and geotechnical parameters for scour analysis. *Environmental & Engineering Geoscience* 2013;4:319–43.
- Kirkaldie L. Rock classification systems for engineering purposes. American Society for Testing and Materials, ASTM STP-984, Philadelphia, PA 1988.
- Kirsten HAD. Case histories of groundmass characterization for excavatability. *Rock Classification Systems for Engineering Purposes American Society for Testing and Materials, STP 984* 1988:102–120.
- Kirsten HAD. A classification system for excavation in natural materials. *The Civil Engineer in South Africa* 1982;24:292–308.
- Kirsten HAD, Moore JS, Kirsten LH, Temple DM. Erodibility criterion for auxiliary spillways of dams. *International Journal of Sediment Research* 2000;15:93–107.
- Laugier F, Leturcq T, Blancet B. Stabilité des barrages en crue: Méthodes d'estimation du risque d'érodabilité aval des fondations soumises à déversement par-dessus la crête. *Proceeding de la Fondation des barrages. Chambéry, France, 2015*, p. 125–36.
- Lowe J, Chao PC, Luecker AR. Tarbela service spillway plunge pool development. *Water Power Dam Construction* 1979;31:85–90.
- MacGregor F, Fell R, Mostyn GR, Hocking G, McNally G. The estimation of rock rippability. *Quarterly Journal of Engineering Geology* 1994;27:123–44.
- Moore JS, Kirsten HAD. Discussion – Critique of the rock material classification procedure. *Rock classification systems for engineering purposes. American Society for Testing and Materials, STP-984, L. Kirkaldie Ed, Philadelphia, 1988*, p. 55–8.
- Moore JS, Temple DM, Kirsten HAD. Headcut advance threshold in earth spillways. *Bulletin of the Association of Engineering Geologists* 1994;31:277–80.
- Mörén L, Sjöberg J. Rock erosion in spillway channels – A case study of the Ligga spillway. *Proceedings of 11th Congress of the International Society for Rock Mechanics, Lisbon, Portugal, 2007*, p. 87–90.

- Pells SE. Erosion of rock in spillways. Ph.D thesis, University of New South Wales, Australia; 2016.
- Pells SE, Pells PJN, Peirson WL, Douglas K, Fell R. Erosion of unlined spillways In Rock - does a “scour threshold” exist? Proceeding of Australian National Committee on Large Dams . Brisbane, Queensland, Australia, 2015, p. 1–9.
- Pitsiou S. The effect of discontinuities of the erodibility of rock in unlined spillways of dams. Master’s Thesis, University of Pretoria, South Africa; 1990.
- Rock A.J. A semi-empirical assessment of plung pool scour: Two-dimensional application of Annandale’s Erodibility Method on four dams in British Columbia, Canada. Master’s Thesis, University of British Columbia. Vancouver, British Columbia, Canada; 2015.
- United States Department of Agriculture (USDA). Field procedures guide for the headcut erodibility index, Chapter 52, Part 628 Dams. vol. 628. 1997.
- Van Schalkwyk A, Jordaan J, Dooge N. Erosion of rock in unlined spillways. Proceeding of International Commission on Large Dams, Paris, 71 (37), 1994, p. 555–71.
- Wise S. Assessing the quality for hydrological applications of digital elevation models derived from contours. *Hydrological Processes* 2000;14:1909–29.
- Wyllie C, Mah W. Rock slope engineering civil and mining. In: Hoek, E. and Bray, J.W., Eds., *Rock slope Engineering*, Taylor & Francis Group, London and New York; 2004.
- Zimmerman D, Pavlik C, Ruggles A, Armstrong MP. An experimental comparison of ordinary and universal kriging and inverse distance weighting. *Mathematical Geology* 1999;31:375–90.

CHAPTER 4 - A METHOD TO DETERMINE THE RELEVANT GEOMECHANICAL PARAMETERS FOR EVALUATING THE HYDRAULIC ERODIBILITY OF ROCK⁶

Abstract

Among the methods used for evaluating the potential hydraulic erodibility of rock, the most common are those based on the correlation between the force of flowing water and the capacity of a rock to resist erosion, such as Annandale's and Pells's methods. The capacity of a rock to resist erosion is evaluated based on erodibility indices that are determined from specific geomechanical parameters of a rock mass. These indices include the unconfined compressive strength (UCS) of rock, rock block size, joint shear strength, a block's shape and orientation relative to the direction of flow, joint openings, and the nature of the surface to be potentially eroded. However, it is difficult to determine the relevant geomechanical parameters for evaluating the hydraulic erodibility of rock. The assessment of eroded unlined spillways of dams has shown that the capacity of a rock to resist erosion is not accurately evaluated. Using more than 100 case studies, we develop a method to determine the relevant geomechanical parameters for evaluating the hydraulic erodibility of rock in unlined spillways. The UCS of rock is found not to be a relevant parameter for evaluating the hydraulic erodibility of rock. On the other hand, we find that the use of three-dimensional block volume measurements, instead of the block size factor used in Annandale's method, improves the rock block size estimation. Furthermore, the parameter representing the effect of a rock block's shape and orientation relative to the direction of flow, as considered in Pells's method, is more accurate than the parameter adopted by Annandale's method.

Keywords: Rock mass, Hydraulic erodibility, Geomechanical parameters, Rock block size, Annandale's method, Pells's method, Kirsten's index, Erosion level.

⁶ Boumaiza, L., Saeidi, A. and Quirion, M. (2019). A method to determine the relevant geomechanical parameters for evaluating the hydraulic erodibility of rock. *Journal of Rock Mechanics and Geotechnical Engineering*, 11(5), 1004-1018 pp.

4.1. Introduction

Many rock mass classification systems used in engineering were developed during the last century. The most common are the rock mass rating (*RMR*) system (Bieniawski, 1973), the Q-system, also known as the Norwegian Geotechnical Institute classification (Barton et al., 1974), the geological strength index (*GSI*) proposed by Hoek et al. (1995), and the rock mass index (*RMI*) system (Palmstrom, 1996). These classification systems were developed for multiple purposes, including underground excavation stability and support design. Furthermore, some have been used to develop related indices to evaluate the excavatability of earth materials, such as Weaver's classification (Weaver, 1975), which was based on the *RMR* system, and Kirsten's index (Kirsten, 1982), which includes several of parameters used in the Q-system.

During the Cincinnati Symposium (Kirkaldie, 1988) that focused on engineering rock mass classification systems, it was proposed that the mechanical excavatability and the hydraulic erodibility of earth materials could be considered as similar processes (Moore and Kirsten 1988). Van Schalkwyk (1989), Pitsiou (1990), and Moore (1991) then demonstrated that the existing rock mass classification systems used for evaluating the mechanical excavatability of rock incorporate most of parameters that affect the hydraulic erodibility of rock. The term "erodibility" is used here to describe significant localized erosion of rock that occurs when the rock is submitted to hydraulic erosive power. Van Schalkwyk et al. (1994) tested several rock mass characterization indices for evaluating the hydraulic erodibility of rock,

and they found that the indices generated similar results. However, Kirsten's index is more accurate (Pells, 2016a). This index, initially developed to evaluate the excavatability of earth materials, has since been adopted for assessing the hydraulic erodibility of earth materials where the “direction of excavation” of the original index has been replaced by the “direction of flow” (Annandale, 1995; Annandale and Kirsten, 1994; Dooge, 1993; Kirsten et al., 2000; Moore et al., 1994; Pitsiou, 1990; Van-Schalkwyk et al., 1994a). In these cited works, the assessment of hydraulic erodibility is based on a correlation between the erosive force of flowing water and the capacity of the rock to resist the erosive force⁷. The erosive force generated by the flowing water is the hydraulic energy, expressed in kW/m², generated by the flowing water. This erosive force is usually called the available hydraulic stream power (P_a). For its part, the resistance capacity of rock can be evaluated using the Kirsten’s index (Kirsten, 1988, 1982), which is determined according to certain geomechanical factors related to the intact rock and the rock mass, such as the unconfined compressive strength (UCS) of rock (M_s), the rock block size (K_b), the joint shear strength (K_d), and the relative block structure (J_s), which considers the effect of a block’s shape and orientation relative to the direction of excavation. Kirsten’s index (N) can be calculated according to Eq. 4.1:

$$N = M_s \cdot K_b \cdot K_d \cdot J_s \quad (4.1)$$

⁷ As noted in Pells (2016a), methods to characterize the “erosive capacity” of a flow and relate it to the “erosive resistance” of the earth or rock material date back many centuries; Rouse and Ince (1957) provide evidence of such a pursuit by Domenico Guglielmini in 1697.

Although there are several developed methods using this correlation approach, Annandale's method (Annandale, 2006, 1995) is the most common (Castillo and Carrillo, 2016; Hahn and Drain, 2010; Laugier et al., 2015; Mören and Sjöberg, 2007; Pells et al., 2015; Rock, 2015), and this method has been validated in a series of laboratory tests (Annandale et al., 1998; Kuroiwa et al., 1998; Wittler et al., 1998). Recently, Pells (2016a) proposed two other indices to assess the capacity of rock to resist flowing water. The first, $eGSI$, represents a modification of GSI previously proposed by Hoek et al. (1995) to characterize the rock mass environment. When the GSI index is determined using the RMR system, the discontinuity orientation factor is removed from RMR (Bieniawski, 1976). Pells (2016a) proposed the $eGSI$ index to include a new discontinuity orientation adjustment factor (E_{doa}) to represent the effect of a rock block's shape and orientation relative to the direction of flow Eq. 4.2.

$$eGSI = GSI + E_{doa} \quad (4.2)$$

The second index proposed by Pells (2016a) is the $RMEI$ (rock mass erosion index). It can be determined based on the relative importance factor (RF) and likelihood factor (LF) as presented in Eq. 4.3. The prefixes P1 to P5 in Eq. 4.3 are various sets of parameters that represent, respectively, the kinematically viable mechanism for detachment, the nature of the potentially eroding surface, the nature of the joints, the joints spacing, and the block shape (Pells 2016a).

$$RMEI = (RF_{P1}.LF_{P1}).(RF_{P2}.LF_{P2}).[(RF_{P3}.LF_{P3})+(RF_{P4}.LF_{P4})+(RF_{P5}.LF_{P5})] \quad (4.3)$$

Bieniawski (1973) showed that rock mass strength is controlled mostly by joint intensity and joint spacing. Even though the rock substance itself may be strong, impermeable, or both, systems of joints create significant weaknesses and favor fluid conductivity (Goodman 1993). Boumaiza et al. (2017) argued that the *UCS* of rock could beget a less important impact on the shifting-up of erodibility class. Pells (2016a) considered that the *UCS* of rock plays a very limited role in the erodibility of fractured rock masses. For example, spectacular erosion events occurred in rock having high *UCS* values at the Copeton Dam in Australia, where a 20 m deep erosion gully was formed, and at the Mokolo Dam in South Africa, where a 30 m deep erosion gully was produced (Pells, 2016a). However, compared to other considered parameters, Kirsten's index is determined to a great extent by the *UCS* rating having values ranging from 0.87 to 280 MPa.

Pells et al. (2017a) argued that at the time of its development, the *RQD* (rock quality designation) parameter, used as a part of the K_b factor, was developed for a specific application and that this parameter is sometimes applied inconsistently in practice. Accordingly, Pells (2016a) recommended use of the Marinos and Hoek (2000) chart to determine *GSI* (also used to determine the *eGSI* index), as it considers neither *UCS* of the rock nor the *RQD*. However, this chart remains semi-qualitative, and any subsequent evaluation can be greatly influenced by the judgment of the analyst. Furthermore, it was not developed to assess the hydraulic erodibility of rock.

It does not incorporate details on joint openings (J_o) that can play a determining role in the hydraulic erodibility process. Pells (2016a) included J_o and other geological parameters, such as the nature of the potentially eroding surface (*NPES*), within the *RMEI* classification. *NPES* is deemed as an important parameter in *RMEI* classification, more so than other considered parameters, such as joint spacing and block shape (Pells 2016a). Nonetheless, these existing rock mass indices fail to represent the mechanisms of erosion observed in field investigations.

The J_s parameter included in Kirsten's index is mathematically quantified based on the effect of a block's shape and orientation relative to the direction of excavation. This parameter was, furthermore, adopted by other systems developed to evaluate the excavatability of earth materials (Scoble et al. 1987, Hadjigeorgiou and Poulin 1998). Pells (2016a) argued, based on the field observations of multiple eroded spillways and laboratory experiments, that the J_s values proposed by Kirsten (1982) for assessing mechanical excavatability of earth materials are not intuitively representative of an assessment of hydraulic erodibility. Furthermore, as set by Kirsten, its rating from 0.37–1.5 has only a subtle impact on the value of Kirsten's index compared to the *UCS* rating of rock that ranges from 0.87–280. For this purpose, Pells (2016a) proposed the E_{doa} factor to represent the effect of the block's shape and orientation relative to the direction of hydraulic flow. Palmstrom et al. (2002), discussed the limitations of the Q-system (Barton et al., 1974) and argued that the block size factor K_b , which is included in Kirsten's index, provides no meaningful quantification of rock block size. Accordingly, Palmstrom (2005) and Palmstrom and Broch (2006) stated that using block volume (V_b) instead of the K_b parameter would

improve the quality of Q-system results. Grenon and Hadjigeorgiou (2003) have also concluded, from in-situ investigations in Canadian mines, that K_b is an inaccurate parameter for characterizing block size.

In summary, the key geomechanical parameters to be used for assessing the hydraulic erodibility of rock remain uncertain. The *UCS* of rock, favored by Kirsten (1982) as a relevant parameter of rock mass competence, is deemed as being less relevant by Pells (2016a) and others. The K_b parameter used in Kirsten's index as an indication of block size is also deemed as inappropriate by some researchers, including Grenon and Hadjigeorgiou (2003). Although J_o could have an important role in the assessment of the hydraulic erodibility of rock, this parameter was not considered directly by Kirsten's index, and it was ignored completely by the *eGSI* index when *GSI* is determined using Marinos and Hoek's (2000) chart. As well, values for the J_s parameter, as proposed by Kirsten (1982) for assessing the mechanical excavatability of earth materials, are considered by Pells (2016a) as having no intuitively representative values for assessing hydraulic erodibility. Furthermore, *NPES* is deemed to be a relevant parameter for evaluating the hydraulic erodibility of rock. In short, there exists no clear consensus on what geomechanical parameters are indeed relevant for evaluating the hydraulic erodibility of rock.

This paper presents a method for determining the relevant geomechanical parameters when evaluating the hydraulic erodibility of rock. This method is described in the second section where several geomechanical parameters, such as *UCS*, K_b , K_d , J_s , J_o , *NPES*, V_b , and E_{doa} , are evaluated based on the developed method. Field data obtained from more than 100 existing case studies and coupled with our

novel approach demonstrate those geomechanical parameters that are relevant for evaluating the hydraulic erodibility of rock (Section 4.3). Section 4.4 presents a validation process of the selected parameters.

4.2. Description of the developed method

The proposed method for determining the relevant geomechanical parameters for evaluating the hydraulic erodibility of rock is summarized in Figure 4.1. Each methodological step is described in the following subsections.

4.2.1 Step 1 - Establishing a dataset and an erosion-level scale

Step 1, establishing a dataset (Figure 4.1), consists of collecting the data from case studies conducted on rocky dam spillways. These data include all available information related to the geomechanical parameters that characterize rock mass, the P_a , and the observed condition of erosion. Table 4.1 summarizes the geomechanical parameters used by Pells (2016a) to develop the two erodibility indices of $eGSI$ and $RMEI$. Some of the geomechanical parameters considered in Pells's erodibility indices are also included in Kirsten's index. Consequently, we also selected geomechanical parameters considered in Kirsten's index (Kirsten, 1982) for our dataset. For their parts, J_o and $NPES$ are also included in the dataset, although they are not directly included in Kirsten's index. As K_b is an inaccurate parameter for characterizing block size (Palmstrom, 2005), we retained V_b as a parameter to be

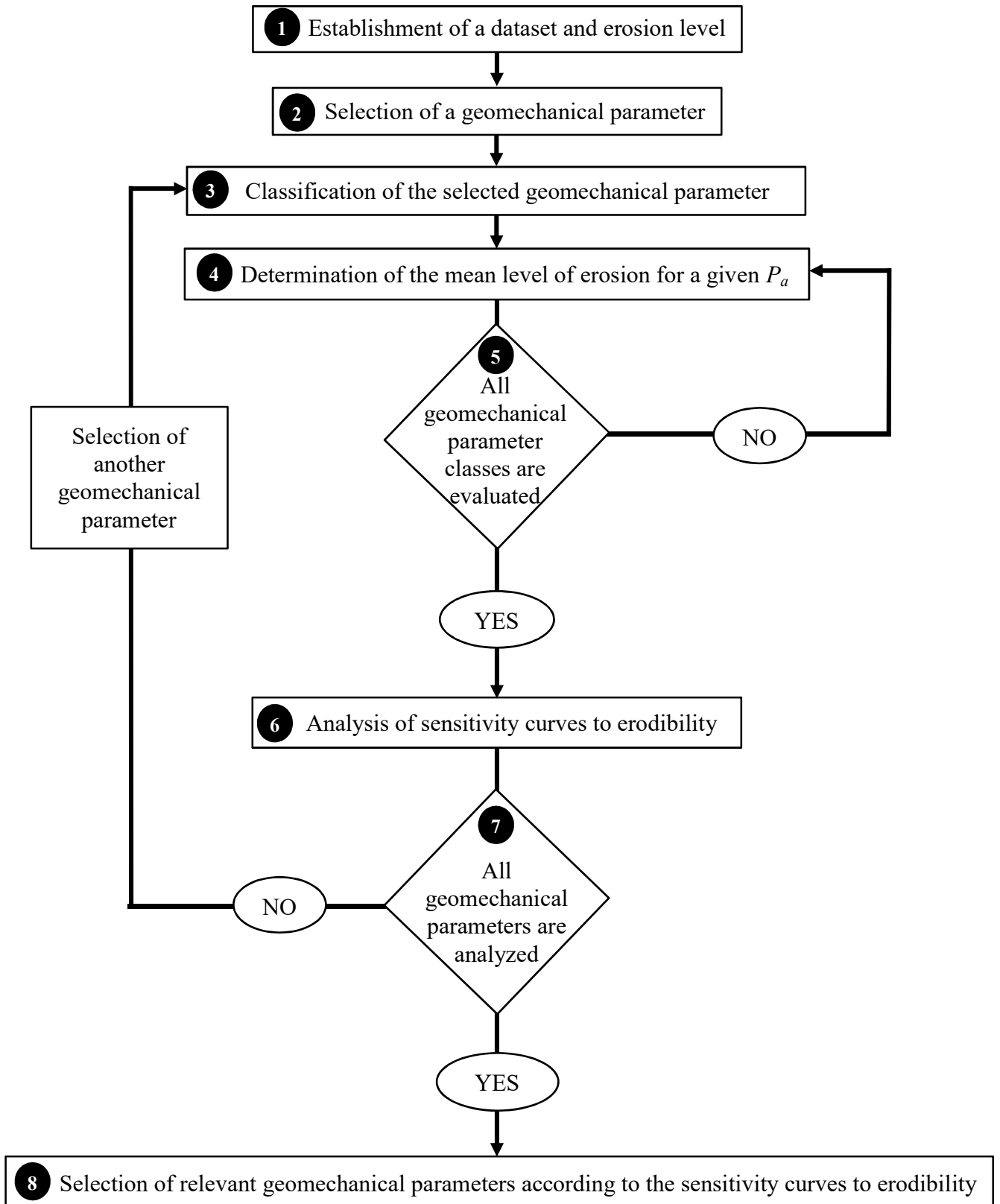


Figure 4.1. Algorithm for determining the relevant geomechanical parameters for evaluating the hydraulic erodibility of rock.

analyzed. Finally, E_{doa} is deemed synonymous to J_s for determining the effect of a rock block's shape and orientation relative to the direction of flow (Pells, 2016b; Pells et al., 2017b); we therefore included this parameter to verify its effectiveness compared to that of J_s . In summary, we retained the geomechanical parameters of M_s , K_b , K_d , J_s , J_o , $NPES$, V_b , and E_{doa} . These parameters will be analyzed for determining the relevant parameters for the evaluating the hydraulic erodibility of rock.

Table 4.1. Summary of the considered geomechanical parameters.

Index	Conditions	Parameters
$eGSI$ ¹	Strength of rock	UCS
	Joints condition	RQD
		Joint spacing
		Joint opening
Rock block condition ²	Roughness	
	Infilling gouge	
	Weathering	
$RMEI$	Joint condition	Shape
		Dipping
		Orientation
		Number of joint sets
	Rock block condition	Dipping
		Orientation
		Roughness
Nature of the potentially eroding surface	UCS of joints	
	Joint opening	
	Joint spacing	
N	Strength of rock	Shape
	Joint condition	Protrusion of joints
		Opening of joints
		Weathering
	Rock block condition	UCS
RQD		
Number of joint sets		
Rock block condition	Roughness	
	Infilling gouge	
	Orientation	

1: $eGSI$ parameters are specified according to the RMR system.

2: Considered as part of the E_{doa} parameter.

The field data collected from more than 100 case studies conducted by Pells (2016a) are presented in the Appendix E. These case studies, conducted on unlined rocky spillways of selected dams in Australia and South Africa, were selected as they provide complete data for the retained geomechanical parameters (M_s , K_b , K_d , J_s , J_o , $NPES$, V_b , and E_{doa}), the P_a , and the observed condition of erosion.

The erosion-level scale used in this study, as part of Step 1 (Figure 4.1), is based on the description of the erosion condition as defined by Pells (2016a). Erosion condition is determined using the maximum depth and extension of the eroded gully (Table 4.2).

Table 4.2. Erosion condition description (Pells, 2016a).

Max. depth (m)	General extent (m ³ /100 m ²)	Descriptor	Erosion level
<0.3	<10	Negligible	1
0.3–1	1–30	Minor	2
1–2	30–100	Moderate	3
2–7	100–350	Large	4
>7	>350	Extensive	5

4.2.2 Step 2 - Selection of a geomechanical parameter

The retained geomechanical parameters (M_s , K_b , K_d , J_s , J_o , $NPES$, V_b , and E_{doa}) are assessed individually. Therefore, Step 2 (Figure 4.1) consists of selecting one geomechanical parameter from the set of retained parameters. This selected

parameter is then analyzed in Steps 3–7 (Figure 4.1). This process is repeated for each of the retained parameters.

4.2.3 Step 3 - Classification of the selected geomechanical parameter

Once a geomechanical parameter is considered for analysis (Step 2, Figure 4.1), this parameter is then classified in Step 3. The objective of Step 3 is to verify the level of erosion (1 to 5; Table 4.2) when a given rock mass is submitted to various P_a . The classification of the geomechanical parameters relies on existing classifications from the literature or our proposed statistical classifications. In the following subsections, we describe the classifications of all retained geomechanical parameters (M_s , K_b , K_d , J_s , J_o , $NPES$, V_b , and E_{doa}).

4.2.3.1 Classification of the UCS of rock

M_s included in Kirsten's index is determined according to the *UCS* of rock, which can be estimated by performing an unconfined compression test on an intact rock sample (Annandale, 2006). We use two common *UCS* scales (Tables 4.3 and 4.4).

Table 4.3. *UCS* classification of Jennings et al. (1973).

Class	<i>UCS</i> (MPa)	Description
1	1.7–3.3	Very soft rock
2	3.3–13.2	Soft rock
3	13.2–26.4	Hard rock
4	26.4 –106	Very hard rock
5	>106	Extremely hard rock

Table 4.4. *UCS* classification adopted from Bieniawski (1989, 1973).

Class	<i>UCS</i> (MPa)	Description
1	1–5	Very low strength
2	5–25	Low strength
3	25 –50	Medium strength
4	50–100	High strength
5	100–250	Very high strength
6	>250	Extremely high strength

4.2.3.2 Classification of rock block size

Classification of K_b

Block size is an extremely important parameter for evaluating rock mass behavior (Barton, 1990; ISRM, 1978). The most common indicator of block size was introduced by Cecil (1970) who combined the *RQD* index with the joint set number (J_n) to create the quotient K_b (RQD/J_n). This quotient was later adopted by Barton et al. (1974) into the Q-system and by Kirsten (1982) for his excavatability index.

However, RQD measurements have several limitations (Grenon and Hadjigeorgiou, 2003; Palmstrom et al., 2002; Pells et al., 2017a). This parameter is included in our analyzed geomechanical parameters to verify if it can be retained as a relevant parameter for evaluating the hydraulic erodibility of rock (as previously maintained). As RQD can vary from 5% to 100% and J_n values vary from 1 to 5 (Kirsten, 1988, 1982), consequently the K_b values range from 1 to 100. However, there is no existing classification system for K_b . The K_b classification framework proposed in this study is based on the statistical distribution of K_b that was established through evaluating the case studies. The most representative normal distribution of K_b data is obtained based on the interval values presented in Figure 4.2. Accordingly, five classes of K_b are defined (Table 4.5).

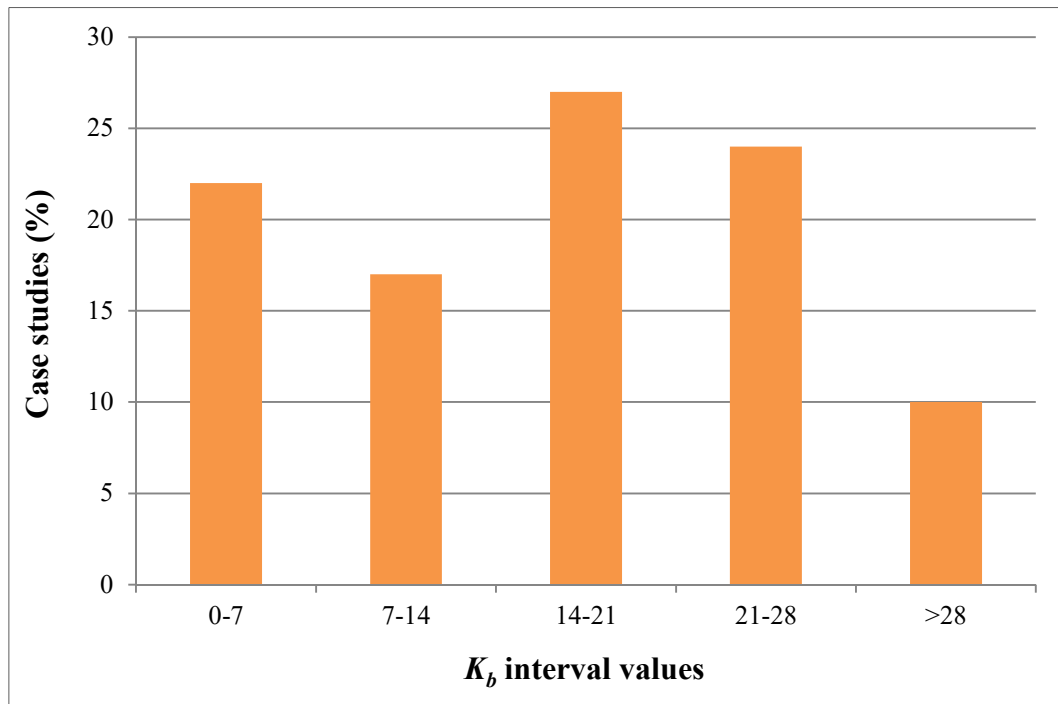


Figure 4.2. The statistical distribution of K_b values from the case studies of Pells (2016a).

Table 4.5. Proposed K_b classification.

Class	K_b
1	0–7
2	7–14
3	14–21
4	21–28
5	>28

Classification of V_b

Palmstrom (2005) stated that using three-dimensional (3D) block volume measurements improves the characterization of block size. The block volume classification of Palmstrom (1996, 1995), presented in Table 4.6, is adopted for this study. Furthermore, we apply three methods (Methods 1, 2, and 3) to characterize rock block volume (Palmstrom, 2005).

Table 4.6. Classification of rock block volume (Palmstrom, 1995).

V_b (m ³)	Description
0.0002–0.01	Small
0.01–0.2	Moderate
0.2–10	Large
>10	Very large

Method 1

When the average joint spacing is used rather than the abundance of joint sets, the following expression is used to determine V_b (m^3):

$$V_b = Sa^3 \quad (4.4)$$

where Sa is the average joint spacing equal to $(S_1+S_2+S_3+S_n)/n$, where $S_1, S_2, S_3 \dots S_n$ is the average spacing for each of the joint sets.

Method 2

When three joint sets occur, the following expression may be used to determine V_b (m^3):

$$V_b = \frac{S_1 \cdot S_2 \cdot S_3}{\sin \gamma_1 \cdot \sin \gamma_2 \cdot \sin \gamma_3} \quad (4.5)$$

where S_1 , S_2 , and S_3 represent the spacing of the three joint sets, and γ_1 , γ_2 , γ_3 represent the angles between the joint sets.

Method 3

The block volume may be determined according to:

$$V_b = \beta \cdot J_V^{-3} \quad (4.6)$$

where β is the block shape factor obtained through the following equation:

$$\beta = 20 + (7a_3/a_1) \quad (4.7)$$

where a_3 and a_1 are the shortest and longest dimensions of a block, respectively. J_V is defined as the number of joints intersecting a volume of 1 m³, as determined using $J_V = \lambda_1 + \lambda_2 + \lambda_3 + \lambda_n$ (where λ_1 is the joint frequency of joint set 1).

4.2.3.3 Classification of joint shear strength

In his index, Kirsten (1982) included K_d , as proposed by Barton et al. (1974); this quotient represents joint shear strength and is expressed as the ratio J_r/J_a , where J_r is the rating number corresponding to joint roughness, while J_a is the rating number corresponding to joint surface alteration. The J_r rating for joint conditions ranges from 0.5 to 4, whereas the J_a rating varies from 0.75 to 18 (Kirsten, 1982). Accordingly, K_d varies from 0.03 to 5.33; however, there is no existing classification of K_d . Based on the statistical distribution of K_d (Figure 4.3), we determined four classes (Table 4.7). The maximum K_d value obtained from the case study data is 3.

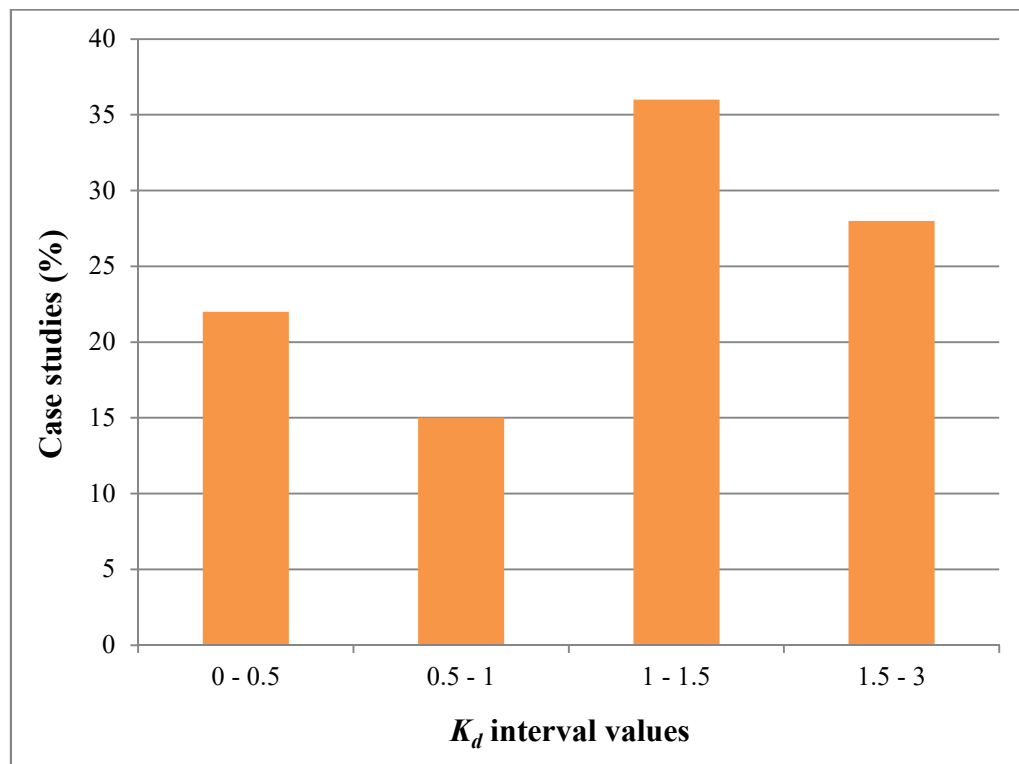


Figure 4.3. The statistical distribution of K_d values from the case studies of Pells (2016a).

Table 4.7. Proposed K_d classification.

Class	K_d
1	0–0.5
2	0.5–1
3	1–1.5
4	1.5–3

4.2.3.4 Classification of a block's shape and orientation parameters

Classification of J_s

The J_s parameter included in Kirsten's index was mathematically quantified according to the effect of a block's shape and orientation relative to the direction of excavation. Its rating, as proposed by Kirsten, ranges from 0.37 to 1.5. As there is no existing classification of J_s , we performed a statistical distribution of the case studies data (Figure 4.4). We determined five classes for J_s (Table 4.8). Class 4 (Table 4.8) is defined by the value of 1 given that there are multiple case studies having a J_s value of 1.

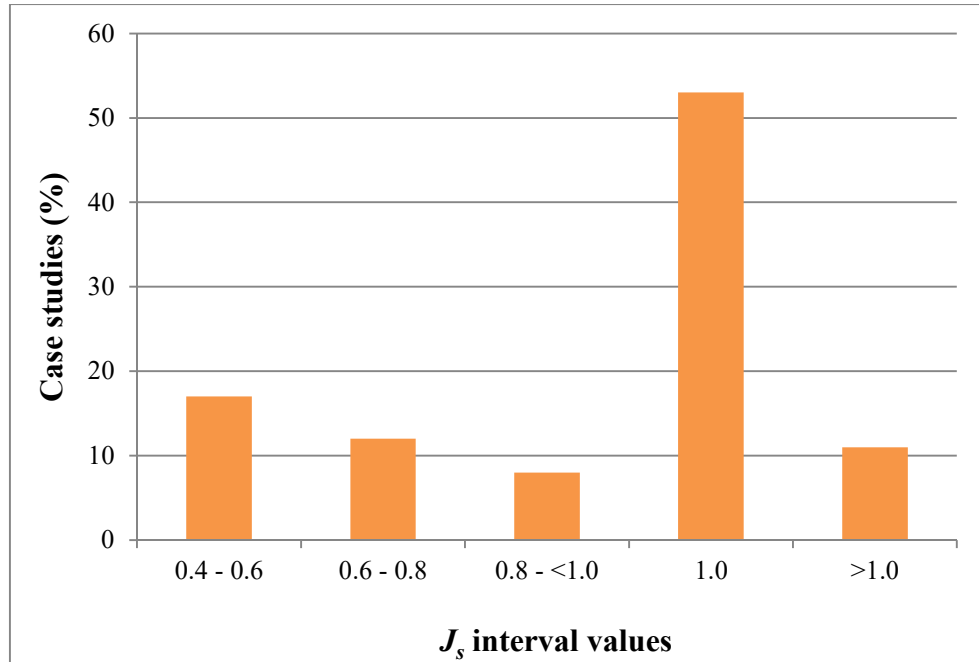


Figure 4.4. The statistical distribution of J_s values obtained from the case studies of Pells (2016a).

Table 4.8. Proposed J_s classification.

Class	J_s	Description
1	0.4–0.6	Highly vulnerable to erosion
2	0.6–0.8	Very vulnerable to erosion
3	0.8–<1	Moderately vulnerable to erosion
4	1	Less vulnerable to erosion
5	>1	Minimally vulnerable to erosion

Classification of E_{doa}

Pells (2016a) proposed the *eGSI* index to include a new discontinuity orientation adjustment factor (E_{doa}) to represent the effect of a rock block's shape and orientation relative to the direction of flow (Eq. 4.2). The process of deriving values for E_{doa} was inspired from Kirsten's J_s parameter. However, values were derived purely by a thought experiment. A rock's vulnerability to significant and ongoing erosion was assessed by taking into consideration the kinematics of block removal and the nature and direction of hydraulic loading, as derived from the observation at sites and the analysis of numerous tested models (Pells, 2016a). As the values of E_{doa} present the discontinuity orientation factor, they are presented as negative values, such as those included in the *RMR* system (Bieniawski, 1976).

The E_{doa} parameter is included in our list of analyzed geomechanical parameters to verify whether E_{doa} can be retained as a relevant parameter and to compare the results with those for J_s . This comparison will confirm which parameter is the most representative of the effect of the block's shape and orientation. According to Pells (2016a), E_{doa} values vary from 0 to -30.

Given that there is no existing classification of E_{doa} , we assessed a statistical distribution of data from the case studies (Figure 4.5), and we determined four classes for the E_{doa} parameter (Table 4.9). Lower values of E_{doa} , such as those included in Class 4, indicate that a rock is more vulnerable to erosion and, consequently, could be susceptible to forms of aggressive erosion.

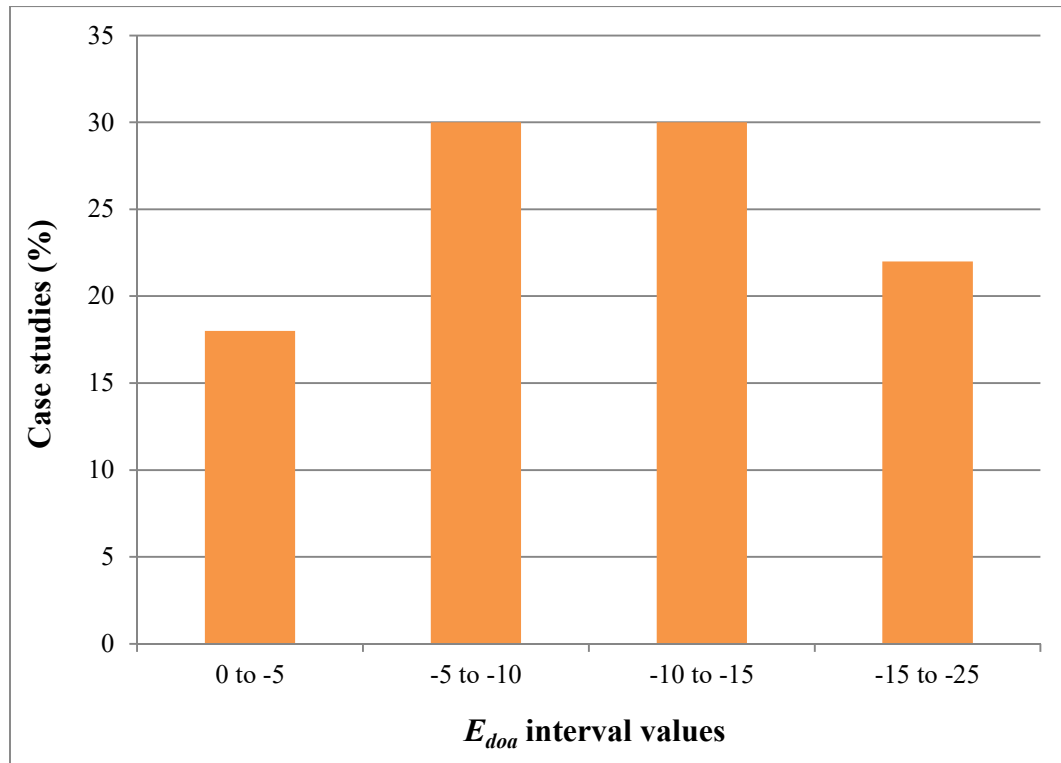


Figure 4.5. The statistical distribution of E_{doa} values obtained from the case studies of Pells (2016a).

Table 4.9. Proposed E_{doa} classification.

Class	E_{doa}	Description
1	0 to -5	Minimally vulnerable to erosion
2	-5 to -10	Less vulnerable to erosion
3	-10 to -15	Moderately vulnerable to erosion
4	-15 to -25	Highly vulnerable to erosion

4.2.3.6 Classification of joint openings

Here, we adopt the joint opening classification of Bieniawski (1989), as presented in Table 4.10. As some case studies contain more than three joint sets, characterized by different joint opening dimensions, we use the joint opening of the joint set most sensitive to hydraulic erodibility (the joint set most oriented with the flow direction). As presented in the Appendix E, some joint set dimensions are characterized by an interval, such as 0.1–0.5 mm. For such cases, the maximum value of the interval is retained for classification purposes.

Table 4.10. Joint opening classification (Bieniawski, 1989) with our proposed class.

Opening (mm)	Description	Proposed class
<0.1	Very tight	1
0.1–0.25	Tight	2
0.25–0.5	Partly open	3
0.5–2.5	Open	4
2.5–10	Widely open	5
10–100	Very widely open	6
100–1000	Extremely widely open	7
>1000	Cavernous	8

4.2.3.7 Classification of NPES

Our classification of nature of the potentially eroding surface (*NPES*) in Table 4.11 is adopted from the *RMEI* classification (Pells, 2016a). Spillways characterized as Class 5 in Table 4.11 are the most sensitive to erosion.

Table 4.11. *NPES* classification (Pells, 2016a) and our proposed class.

Likelihood	Description	Proposed class
Very unlikely	Smooth water or glacier worn, no protrusions of joint 2, no opening of joints	1
Unlikely	Bedding surface with protrusions of joint 2 <1 mm, little or no opening of joints	2
Likely	Relatively small protrusions and joints openings (e.g. pre-split, or ripped and bulldozed)	3
Highly likely	Irregular surface following joints, little opening of joints (e.g. blasted rock)	4
Almost certain	Irregular surface following joints, extensive joints opening (e.g. heavily blasted rock)	5

4.2.4 Step 4 - Determining mean levels of erosion for given P_a categories

In Step 4, the objective is to verify erosion levels when the same rock mass class (rock mass classes are defined in Tables 4.3–4.11) is subjected to various P_a . As there are several case studies within the same geomechanical class, we determine in Step 4 the mean level of erosion for a given P_a category (Figure 4.1). However, there

is no existing classification of P_a . Accordingly, we performed a statistical distribution of data from the case studies (Figure 4.6), and defined six P_a categories (Table 4.12).

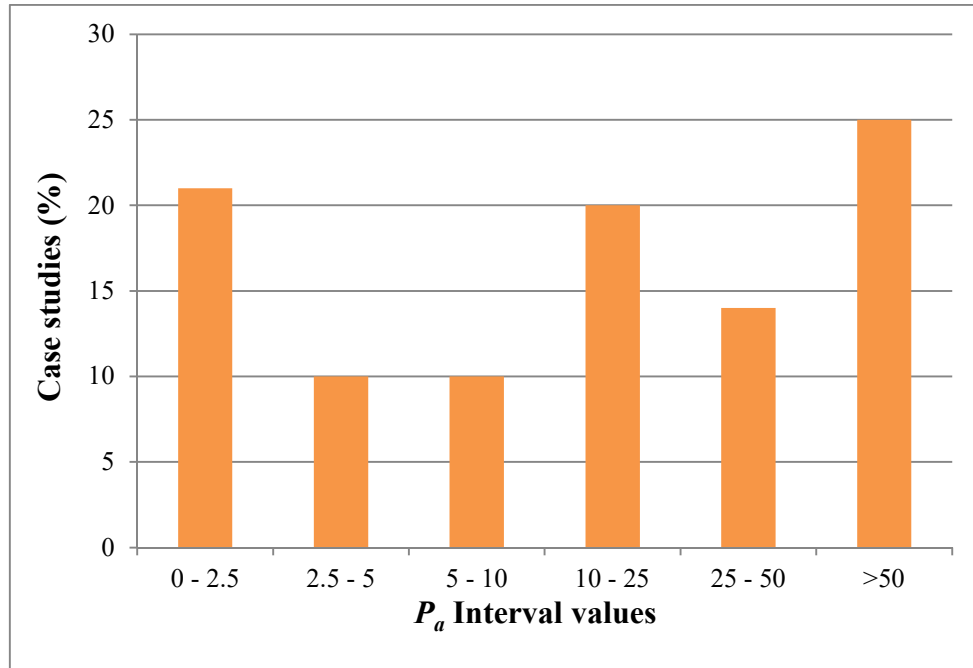


Figure 4.6. Statistical distribution of P_a values from the case studies of Pells (2016a).

Table 4.12. Defined P_a categories.

Category	P_a (kW/m ²)
1	0–2.5
2	2.5–5
3	5–10
4	10–25
5	25–50
6	>50

The mean level of erosion for a given P_a category is calculated using Eq. 4.8 (Saeidi et al., 2012, 2009), where, in this study, μ_D represents the mean erosion level for a given hydraulic steam power category, and P_i is the probability of erosion level D_i , where i is ranking of the erosion level classes from 1 to 5 (Table 4.2). P_i is calculated according to Eq. 4.9, where n_i is the number of case studies of erosion level D_i , and n_t is the total number of case studies, both considered for each P_a category. An example of how the mean erosion level is calculated is presented in Table 4.13.

$$\mu_D = \sum_{i=1}^5 P_i \cdot D_i \quad (4.8)$$

$$P_i = \frac{n_i}{n_t} \quad (4.9)$$

Table 4.13. Example of calculating μ_D

Erosion class	D_i	n_i
Negligible	1	3
Minor	2	3
Moderate	3	1
Large	4	1
Extensive	5	0
	n_t	8
	μ_D	2

4.2.5 Step 5 – Evaluating all geomechanical parameter classes

After calculating the mean level of erosion for a P_a category (e.g. for Category 1 in Table 4.12; $P_a = 0\text{--}2.5 \text{ kW/m}^2$), the identical process for calculations is then run for all P_a categories listed in Table 4.12. Each series of calculations for the P_a categories is run for only a single geomechanical parameter class (e.g. Class 1 of the *NPES* classification in Table 4.11) at a time. Accordingly, a best-fit curve representing the calculated mean level of erosion versus the average of all considered P_a categories are then plotted for this single class of geomechanical parameter. Step 5 (Figure 4.1) aims to run the identical process of calculations for each class of a single geomechanical parameter (e.g. the calculating process for classes 1 to 5 of *NPES* classification as indicated in Table 4.11).

4.2.6 Step 6 - Analysis of sensitivity curves to erodibility

A best-fit curve here is the line representing the considered points of the calculated mean level of erosion versus the average of all considered P_a categories. For each class of a single geomechanical parameter, a best-fit curve is traced. These best-curves are considered as the sensitivity curves to erodibility that could produce a synthetic value for the potential level of erosion at a given value of P_a for a specific geomechanical parameter class. These best-fit curves are used in our subsequent analyses. The main objective of Step 6 (Figure 4.1) is to analyze the obtained sensitivity curves. For a geomechanical parameter, the obtained sensitivity curves to

erodibility showing a logical sequence can be considered as curves associated with a relevant geomechanical parameter for evaluating the hydraulic erodibility of rock. Otherwise, it can be concluded that the analyzed geomechanical parameter cannot be considered as a relevant parameter.

4.2.7 Steps 7 and 8 – Analyze of all geomechanical parameters and the selection of the relevant geomechanical parameters

Step 7 consists of analyzing all retained geomechanical parameters (M_s , K_b , K_d , J_s , J_o , $NPES$, V_b , and E_{doa}) via the process described in the previous steps. Each retained parameter will have a specific sensitivity curves to erodibility. Step 8 is to select the relevant geomechanical parameters for evaluating the hydraulic erodibility of rock based on the obtained sensitivity curves to erodibility. For this purpose, the sensitivity curves showing a logical sequence can be considered as the curves associated with a relevant geomechanical parameter.

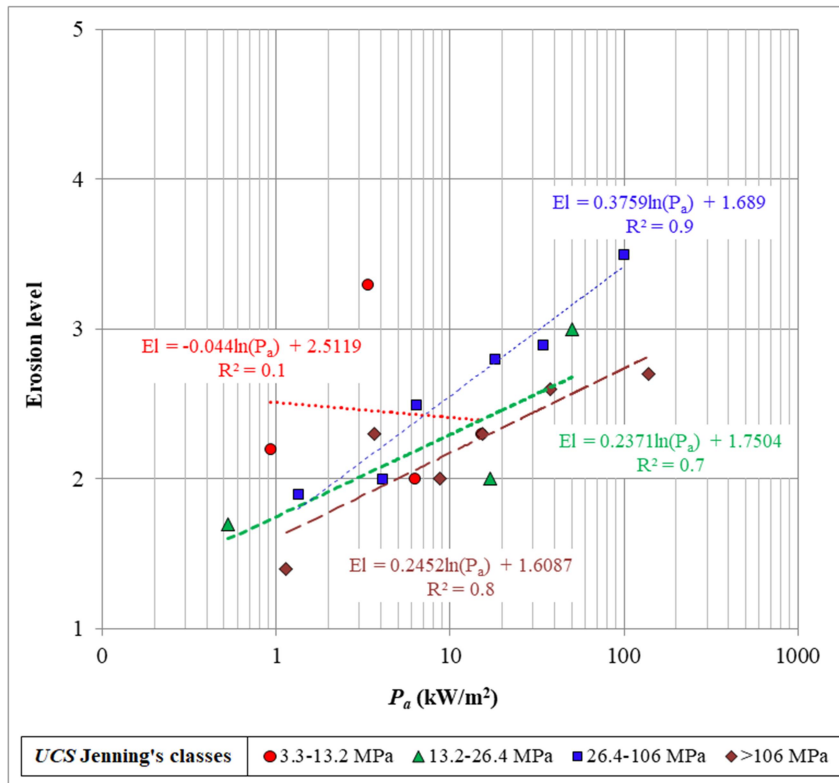
4.3 Results and discussion

4.3.1 Effect of the UCS of rock on erodibility

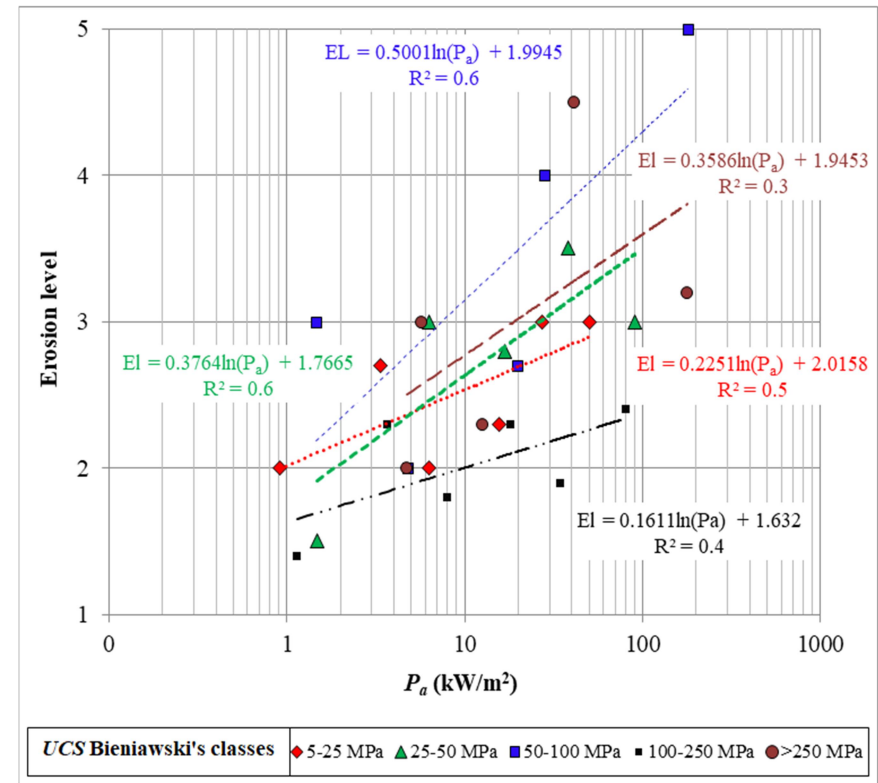
Sensitivity curves to erodibility based on the *UCS* classifications are shown in Figure 4.7. For Jennings's *UCS* classification (Figure 4.7a), if *UCS* controls the hydraulic erodibility process, rock masses having the highest *UCS*, such as the extremely hard rock class in Table 4.3 (>106 MPa), should produce the least sensitive erodibility curves, whereas a lower *UCS*, such as the hard rock class in Table 4.3 (13.2–26.4 MPa), should generate the most sensitive erodibility curve. As expected, the extremely hard rock class (>106 MPa) produces the least sensitive curve; however, the very hard rock class (26.4–106 MPa) has the most sensitive erodibility curve, rather than the hard rock class (Figure 4.7a) that has a lower *UCS* interval (13.2–26.4 MPa). Given this inversion of the generated sensitivity curves to erodibility for hard and very hard rock classes, it is difficult to justify using *UCS* in assessing the hydraulic erodibility process.

Sensitivity curves to erodibility based on Bieniawski's *UCS* classification (Table 4.4) are shown in Figure 4.7b. Rock masses characterized by the highest *UCS* values, such as the extremely strength class in (>250 MPa, Table 4.4), should produce the least sensitive curve to erodibility, whereas rock masses having the lowest *UCS* values, such as the low-strength class (5–25 MPa, Table 4.4), should generate the most sensitive curve. However, we observe (Figure 4.7b) that the most sensitive

erodibility curve is obtained for the high strength rock class (50–100 MPa), whereas the least sensitive curve to erodibility is for the very high strength rock class (100–250 MPa). Surprisingly, the sensitivity curve to erodibility for the extremely high strength class (>250 MPa) is the second-most sensitive curve. Furthermore, sensitivity curves to erodibility of the low-strength class and medium strength class are misplaced from the expected pattern (Figure 4.7b). These two sensitivity curves to erodibility should be placed at the top as the more sensitive erodibility curves according to their *UCS* of 5–25 MPa and 25–50 MPa, respectively, rather than being placed as moderately sensitive curves. As *UCS* sensitivity curves to erodibility, according to Bieniawski's *UCS* classification, show a random sequence (and a similar pattern is observed using Jennings's *UCS*), *UCS* cannot be considered as a relevant parameter for evaluating the hydraulic erodibility of rock.



(a)



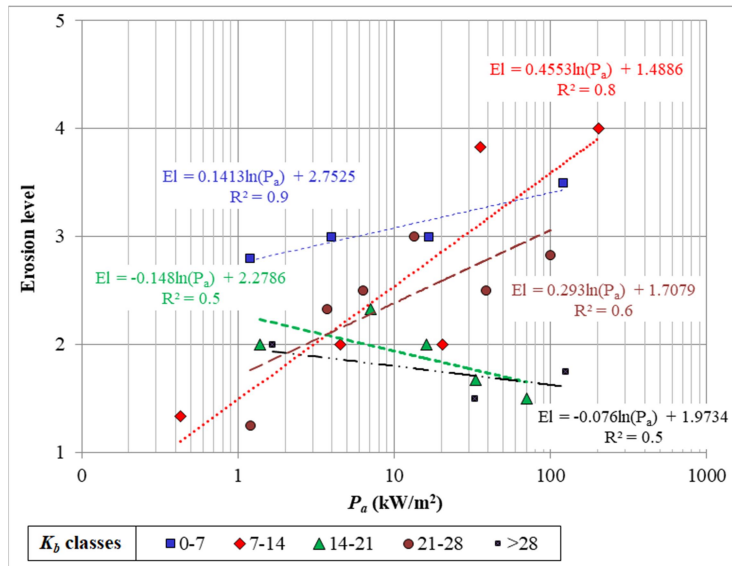
(b)

Figure 4.7. Sensitivity curves to erodibility based on *UCS*: a) Jenning's *UCS* classification; b) Bieniawski's *UCS* classification. Each best-fit line and its equation correspond to the same symbol data points, which are also represented by the same color.

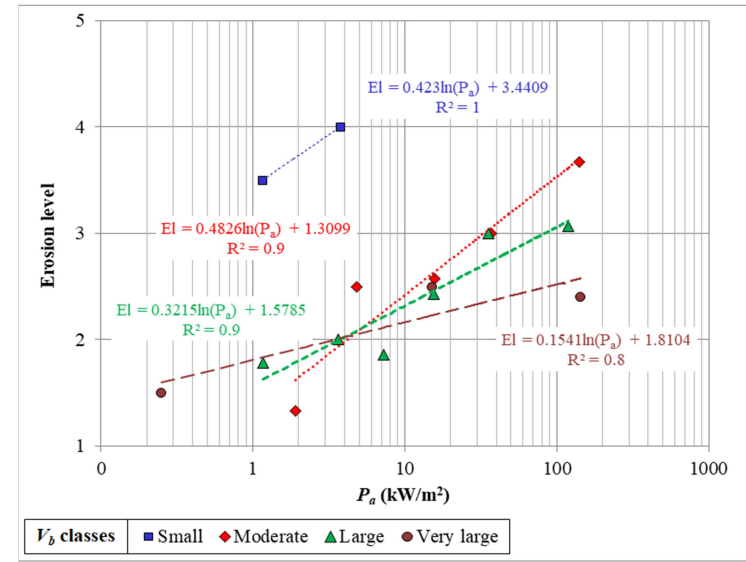
4.3.2 Effect of rock block size on erodibility

Rock block volume V_b was calculated using the three described methods in Section 4.2.2.2 (Calculates are presented in Appendix F). Sensitivity curves to erodibility according to rock block size (K_b and V_b) are shown in Figure 4.8. Sensitivity curves to erodibility based on K_b show that a rock mass characterized by a K_b of Class 1 ($K_b = 0-7$) is, as expected, the most sensitive to erodibility (Figure 4.8a). However, this curve is intersected by the curve representing Class 2 ($K_b = 7-14$) when $P_a = 60 \text{ kW/m}^2$. Accordingly, Class 2 becomes subsequently more sensitive than Class 1 as P_a increases. On the other hand, the sensitivity curves to erodibility for classes 3 and 5 decrease as P_a increases. This is not logical as an increased P_a should beget an increase in the amount of erosion. Also, the sensitivity curve to erodibility representing Class 2 ($K_b = 7-14$) is more sensitive than the Class 4 sensitivity curve to erodibility ($K_b = 21-18$); however, this pattern is only observed when P_a is $>4 \text{ kW/m}^2$. Below this threshold, Class 4 is more sensitive to erodibility than Class 2, rendering this behavior invalid. Given these patterns, K_b cannot be selected as a relevant parameter for evaluating the hydraulic erodibility of rock.

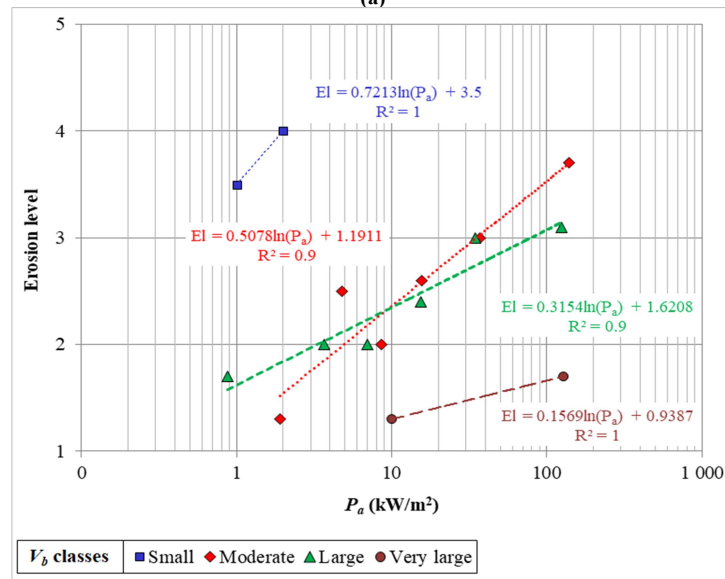
Sensitivity curves to erodibility based on V_b , when V_b is calculated according to Method 1, show that for moderate, large, and very large classes, very large volumes ($>10 \text{ m}^2$) are the least sensitive to erodibility, and sensitivity is subsequently more important as V_b decreases (Figure 4.8b). However, this is only noted when P_a is $>6 \text{ kW/m}^2$. Method 1 thus provides a good evaluation for a large range of P_a values; however, at values $<6 \text{ kW/m}^2$, Method 1 produces invalid results. Similar patterns are



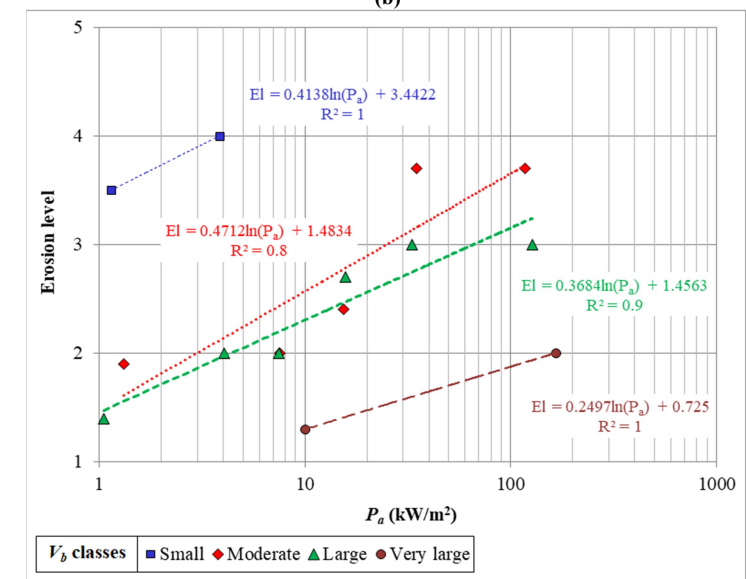
(a)



(b)



(c)



(d)

Figure 4.8. Sensitivity curves to erodibility based on rock block size: a) K_b classification; b) V_b classification (V_b calculated according to Method 1); c) V_b classification (V_b calculated according to Method 2); d) V_b classification (V_b calculated according to Method 3). Each best-fit line and its equation correspond to the same symbol data points, which are also represented by the same color.

observed when V_b is calculated via Method 2 (Figure 4.8c) and Method 3 (Figure 4.8d). Methods 2 and 3 provide a good evaluation, although only when P_a values are $>10 \text{ kW/m}^2$ and $>1 \text{ kW/m}^2$, respectively.

Overall, use of the 3D block volume measurement, rather than the K_b parameter, provides a better characterization of the rock block size. Palmstrom (2005) argued that their method (Palmstrom 1995, 1996), based on volumetric joint count (Method 3), provides the best characterization of the block volume. We also select this method as it provides a good evaluation for much of the range for P_a relative to methods 1 and 2.

4.3.3 Effect of joint shear strength on erodibility

As K_d indicates the joints shear strength, rock mass characterized by a K_d of Class 1 ($K_d = 0-0.5$), as described in Table 4.7, should be more sensitive to erodibility than other rock masses characterized, for example, by a K_d of Class 4 ($K_d = 1.5-3$). Sensitivity curves to erodibility based on the K_d classification (Table 4.7) follow the K_d categories perfectly (Figure 4.9). Case studies of Class 4 ($K_d = 1.5-3$) are the least sensitive to erodibility, and sensitivity is subsequently greater as K_d decreases. With a P_a value of 10 kW/m^2 , for example, a Class 4 rock mass ($K_d = 1.5-3$) would have negligible to minor erosion, whereas a Class 1 rock mass ($K_d = 0-0.5$) would have moderate erosion. As K_d sensitivity curves to erodibility show a logical sequence having a proportional relationship between the joints shear strength and the level of erosion (when the joints shear strength decreases, erosion is greater), K_d can be retained as a relevant parameter for evaluating the hydraulic erodibility of rock.

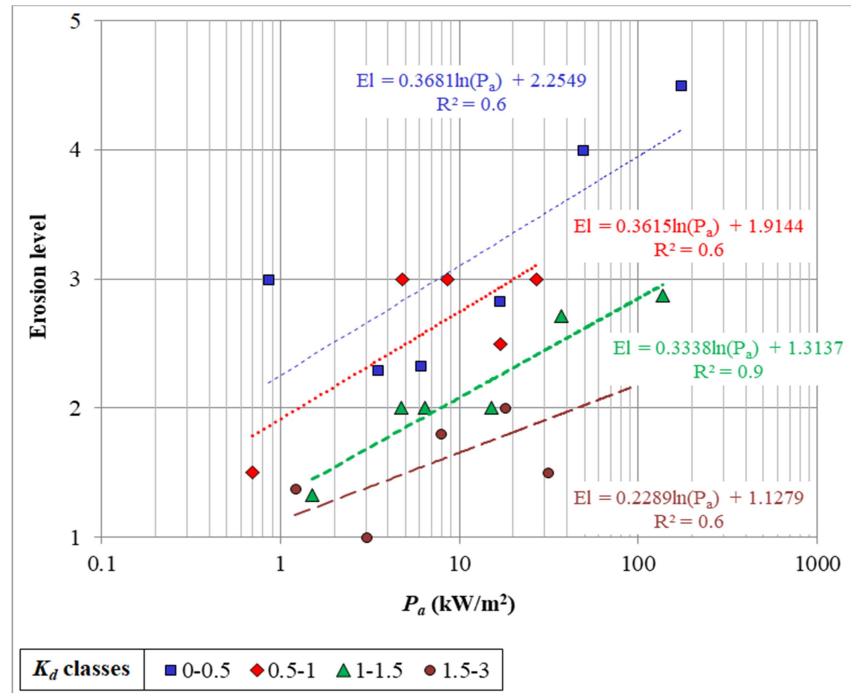
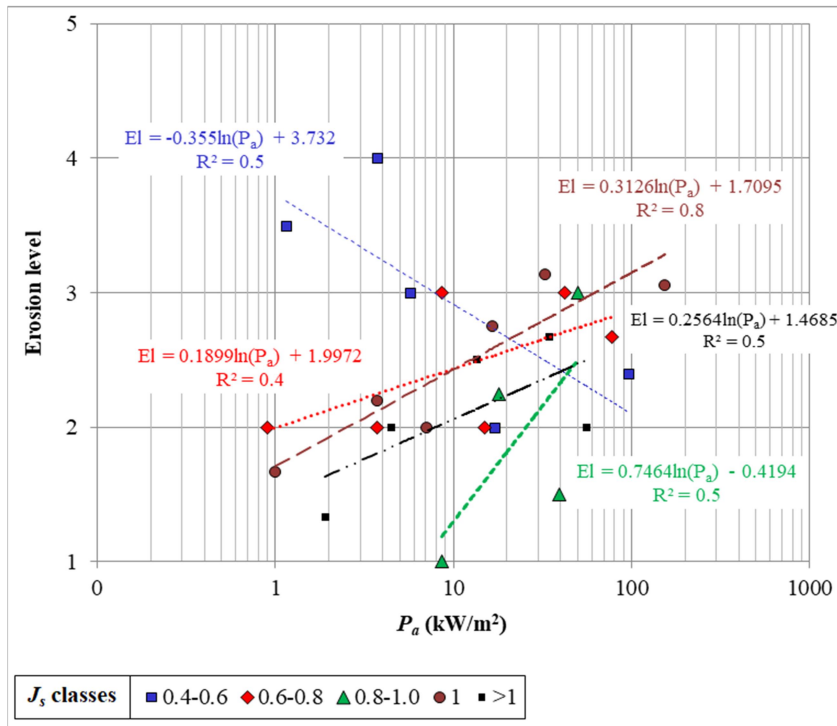


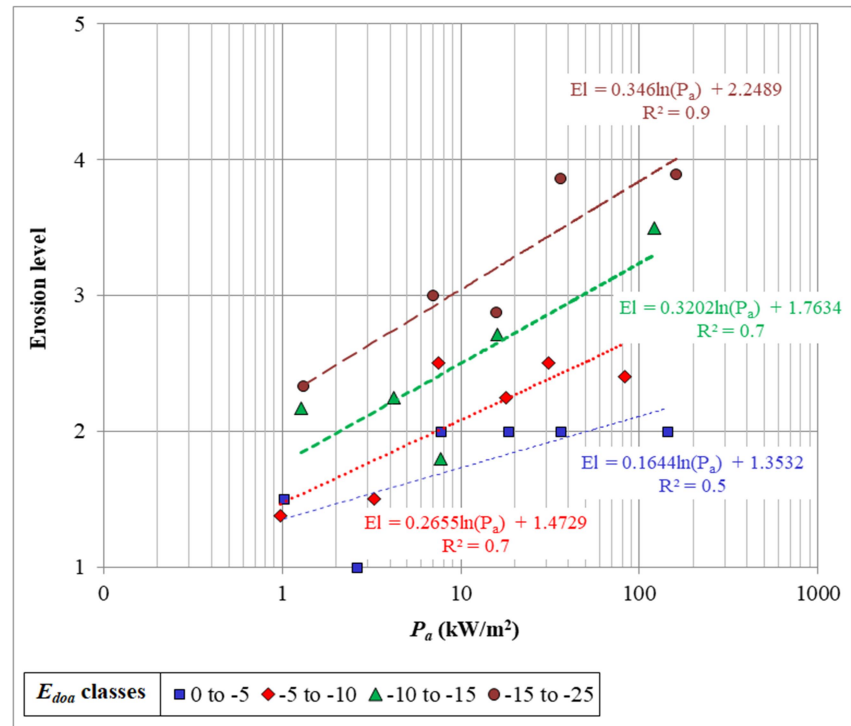
Figure 4.9. Sensitivity curves to erodibility based on K_d classification. Each best-fit line and its equation correspond to the same symbol data points, which are also represented by the same color.

4.3.4 Effect of a block's shape and orientation on erodibility

Sensitivity curves to erodibility based on J_s classification (Table 4.8) show that the curves of Class 1 ($J_s = 0.4\text{--}0.6$) decreases as P_a increases (Figure 4.10a). This is considered as a random pattern as increased P_a should beget increased levels of erosion. Also, multiple intersecting points are noted between the sensitivity curves to erodibility; for example, the Class 2 sensitivity curve ($J_s = 0.6\text{--}0.8$) intersects with the Class 4 curve ($J_s = 1$) at $P_a = 10 \text{ kW/m}^2$. This confusing observation is also noted for classes 3 and 5 at a P_a of 50 kW/m^2 . Random patterns of the J_s sensitivity curves complicate the use of J_s as a relevant parameter for evaluating the hydraulic erodibility of rock.



(a)



(b)

Figure 4.10. Sensitivity curves to erodibility based on a block's shape and orientation relative to the direction of flow: a) J_s classification; b) E_{doa} classification. Each best-fit line and its equation correspond to the same symbol data points, which are also represented by the same color.

The E_{doa} parameter is proposed as an indicator of the effect of a rock block's shape and its orientation relative to the direction of flow. The lowest values of E_{doa} , such as those included of Class 4 ($E_{doa} = -15$ to -25), indicate that the rock mass would be greatly susceptible to erosion. Based on the sensitivity curves to erodibility in Figure 4.10b, Class 1 rock masses ($E_{doa} = 0$ to -5) are the least sensitive, and sensitivity increases as E_{doa} decreases. At a P_a of 100 kW/m^2 , for example, a Class 1 rock mass ($E_{doa} = 0$ to -5) would have undergone minor levels of erosion, whereas a Class 4 rock mass ($E_{doa} = -15$ to -25) would have experienced marked erosion. As E_{doa} sensitivity curves to erodibility show a logical sequence having a proportional relationship between E_{doa} and the level of erosion (as E_{doa} decreases, erosion increases), E_{doa} is retained as a relevant parameter for evaluating the hydraulic erodibility of rock.

4.3.5 Effect of joint opening on erodibility

Sensitivity curves to erodibility based on J_o classification (Table 4.10) are aligned according to J_o (Figure 4.11). Case studies having a tight joint opening ($J_o < 0.25 \text{ mm}$) are the least sensitive to erosion, and sensitivity to erodibility increases as J_o increases. At a P_a of 100 kW/m^2 , for example, a rock mass having tight joint openings ($< 0.25 \text{ mm}$) would experience minor erosion, whereas a rock mass having widely open joints ($2.5\text{--}10 \text{ mm}$) would experience marked erosion. As J_o sensitivity curves to erodibility show a logical pattern and have a proportional relationship between joint opening and the level of erosion (as J_o increases, erosion is greater), J_o is considered as a relevant parameters for evaluating the hydraulic erodibility of rock.

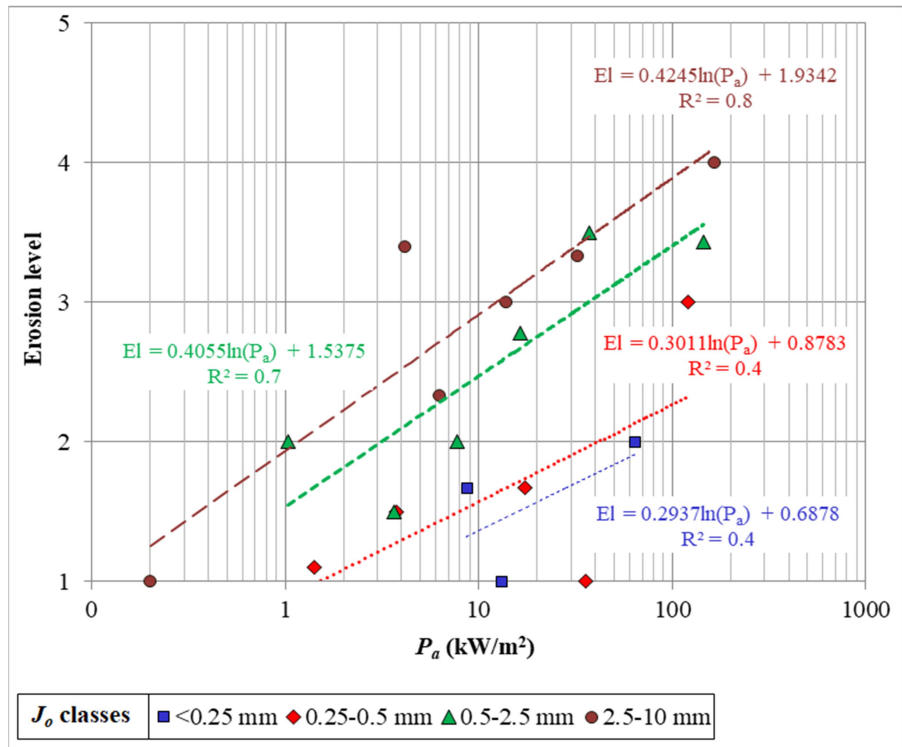


Figure 4.11. Sensitivity curves to erodibility based on J_o classification. Each best-fit line and its equation correspond to the same symbol data points, which are also represented by the same color.

4.3.6 Effect of NPES on erodibility

Sensitivity curves to erodibility based on NPES classification show that this parameter has a proportional relationship with erosion (Figure 4.12). Class 2 rock mass (Class 2 includes a flowing surface with an unlikely potential for erosion, Table 4.11) is the least sensitive to erosion, while Class 5 rock mass (Class 5 includes a flowing surface having an almost certain potential for erosion, Table 4.11) is most sensitive. Transmitted flow energy, in the case of an irregular flowing surface, can be greater than that for a smooth flowing surface (Annandale, 2006). Other sensitivity

curves to erodibility associated with classes 3, 4, and 5 are also plotted (Figure 4.12) and show a similar relationship with P_a . As $NPES$ sensitivity curves to erodibility show a logical relationship with P_a , $NPES$ is retained as a relevant parameter for evaluating the hydraulic erodibility of rock.

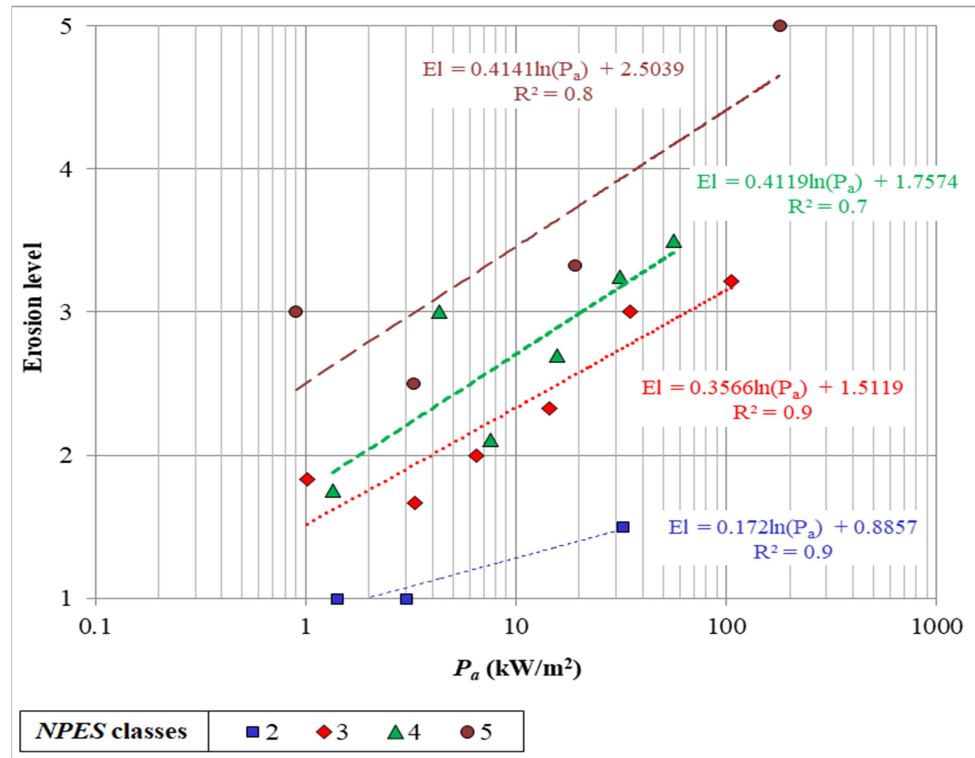
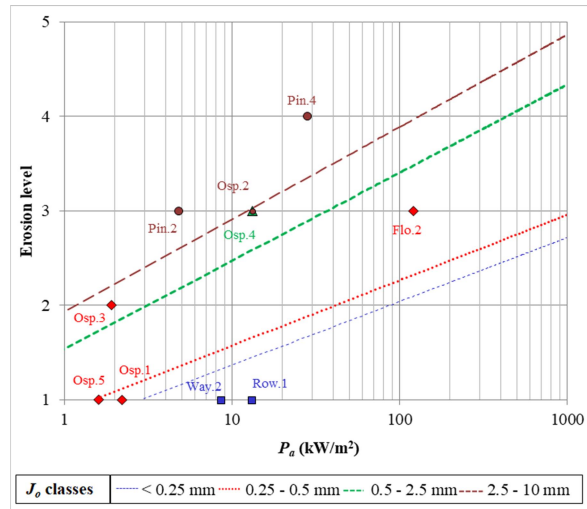


Figure 4.12. Sensitivity curves to erodibility based on $NPES$ classification. Each best-fit line and its equation correspond to the same symbol data points, which are also represented by the same color.

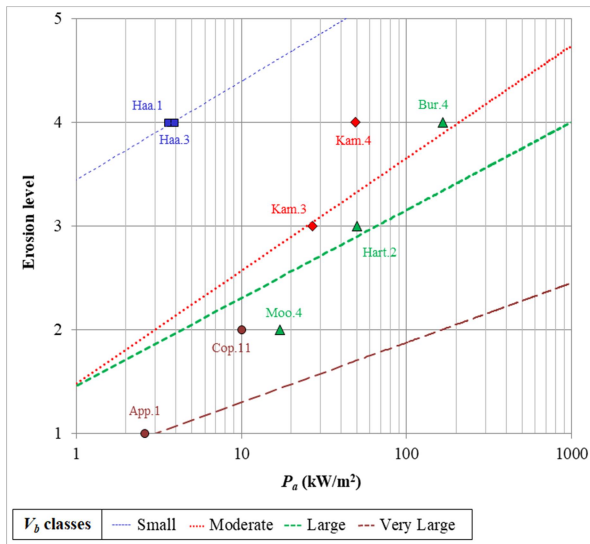
From our analysis of the sensitivity curves to erodibility, five parameters (J_o , K_d , V_b , E_{doa} , and $NPES$) are retained as relevant parameters for evaluating the hydraulic erodibility of rock (Step 8 - Figure 4.1). UCS , K_b , and J_s present some random or illogical patterns related to the erosion condition and, consequently, are not considered further. The selected parameters can be used for developing new erodibility index for evaluating the hydraulic erodibility of rock.

4.4 Validation of developed methodology

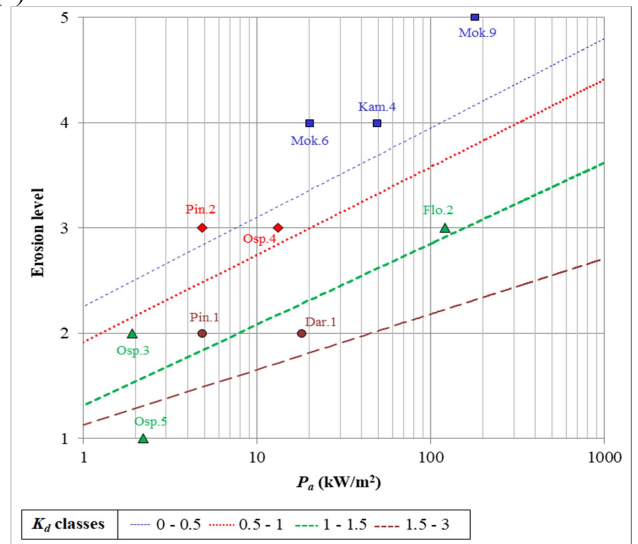
We can determine the individual effect of each geomechanical parameter. However, the selected geomechanical parameters (J_o , V_b , K_d , E_{doa} , and $NPES$) could interact with regard to their effect on the level of erosion. Accordingly, it is important to validate whether the obtained sensitivity curves to erodibility for a given parameter provide a reliable prediction of erosion level when all selected parameters are considered. To validate the J_o sensitivity curves to erodibility for this purpose, we selected from the existing case studies those cases having the same geomechanical parameter class for V_b , K_d , E_{doa} , and $NPES$, while the parameter J_o is omitted from this selection. If this subset of case studies having identical geomechanical parameter classes (except for J_o) are characterized by differing levels of erosion, then the differences in the degree of erosion are influenced by J_o . Erosion level and P_a associated with this subset of case studies (where V_b , K_d , E_{doa} , and $NPES$ values are similar) are plotted on J_o sensitivity curves to erodibility (Fig. 4.11) to verify whether the observed erosion agrees with the J_o sensitivity curves to erodibility. This approach is then repeated for each of the selected parameters (each parameter is isolated from the other four parameters), and the obtained results are shown in Fig. 4.13. For each parameter validation, ten case studies were used. The exception was the validation process of V_b where nine case studies were used (Fig. 4.13). In Fig. 4.13, the colored dashed lines represent the sensitivity curves to erodibility for the selected parameters, as explained in the previous section. The individual symbols are the observed case studies data that are plotted on Fig. 4.13a to 4.13e (e.g. for the validation of the $NPES$



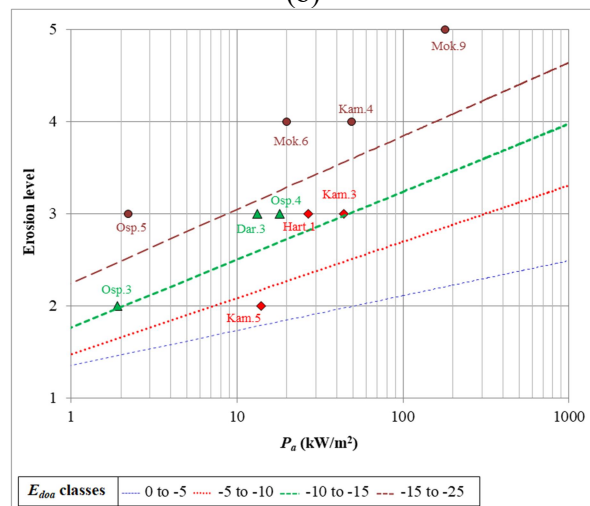
(a)



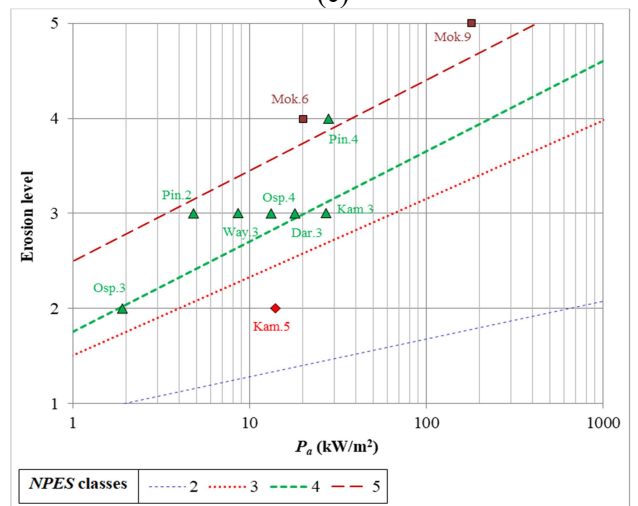
(b)



(c)



(d)



(e)

Figure 4.13. Validation based on a) J_o sensitivity curves; b) V_b sensitivity curves; c) K_d sensitivity curves; d) E_{doa} sensitivity curves; and e) $NPES$ sensitivity curves.

parameter presented in Fig. 4.13e, the colored dashed lines are the sensitivity curves to erodibility developed for this parameter. The associated symbols are the data from the observed case studies, and their color corresponds to their class).

Some case studies agree perfectly with the developed sensitivity curves to erodibility, including the case study Osp.2 introduced to validate J_o sensitivity curves (Figure 4.13a), Haa.1, Haa.3, Kam.3, and Opp.1 used to validate the V_b curves (Figure 4.13b), Flo.2 plotted on the K_d sensitivity curves (Figure 4.13c), Osp.3 used to validate the E_{oda} curves (Figure 4.13d), and Dar.3 and Osp.3 plotted on the $NPES$ sensitivity curves to erodibility (Figure 4.13e). Nonetheless, certain case studies do not agree perfectly with the developed sensitivity curves to erodibility (Figure 4.13). To determine the efficiency of the obtained results, we use the root mean square error (RMSE). In geosciences, RMSE is often used to assess modeling quality both in terms of accuracy and precision (Boumaiza et al., 2019b; Gokceoglu and Zorlu, 2004; Wise, 2000; Zimmerman et al., 1999). In this study, as shown in Eq. 4.10, RMSE corresponds to the mean of differences between the theoretical level of erosion ($El_{Supposed}$) as determined via the developed sensitivity curves to erodibility, and the actual level of erosion (El_{Real}) observed in the field. The calculated RMSE (named Real RMSE) indicates the produced error according to the obtained result.

$$RMSE = \left(\frac{1}{n} \sum_{i=1}^n (El_{Supposed} - El_{Real})^2 \right)^{1/2} \quad (4.10)$$

To determine the maximum possible error (named Max RMSE), the actual erosion level (El_{Real}) is replaced, in a second step, by the level of erosion that produces a Max RMSE. The maximum level of erosion that could be eventually produced, according to Table 4.2, represents the extensive erosion corresponding to a value of 5. An example of the calculations is presented in Table 4.14.

Table 4.14. RMSE calculating process according to J_o sensitivity curves to erodibility.

ID	Theoretical level of erosion ¹	Actual level of erosion	Max. level of erosion
Pin.4	3	4	5
Osp.2	3	3	5
Pin.2	3	3	5
Osp.4	3	3	5
Flo.2	2	3	5
Osp.3	1	2	5
Osp.5	1	1	5
Osp.1	1	1	5
Way.2	1	1	5
Row.1	1	1	5
Real RMSE		0.49	
		Max RMSE	3.13

¹: Rounded values determined from sensitivity curves shown in Fig. 4.13a.

The ratio of real RMSE to max RMSE indicates the magnitude associated to the actual produced error compared to the maximum possible produced error. Table 4.15 presents Real and Max RMSE values, calculated based on sensitivity curves to

erodibility for each of the selected parameters presented in Figure 4.13, and the determined ratio (%). Real RMSE is always lower than Max RMSE, where the determined ratio of Real RMSE to Max RMSE varies from 16% (for J_o sensitivity curves to erodibility) to 42% (for E_{doa} and $NPES$ sensitivity curves to erodibility) (Table 4.15). Consequently, the real produced error according to our method can be considered acceptable compared to the maximum produced error, and this verification confirms the efficiency of the proposed methodology.

Table 4.15. Calculated RMSE and the determined ratio.

Parameter	J_o	V_b	K_d	E_{doa}	$NPES$
Real RMSE	0.49	1.12	1.07	1.33	1.33
Max RMSE	3.13	3.13	3.18	3.18	3.18
Ratio (%)	16	36	34	42	42

4.5 Conclusion

Our method for determining relevant rock mass parameters in the evaluation of the hydraulic erodibility of rock is derived from case studies of erosion in unlined rocky spillways of selected dams in Australia and South Africa. As the hydraulic erodibility of rock is a physical process controlled by a group of rock mass geomechanical parameters, several geomechanical parameters of rock mass (UCS , K_b ,

K_d , J_s , J_o , $NPES$, V_b , and E_{doa}) were analyzed to determine those parameters that are relevant for evaluating the hydraulic erodibility of rock. We found that the UCS of rock does not have a significant effect on hydraulic erodibility. The K_b parameter, defined to represent rock block size in the context of hydraulic erodibility, can be improved by replacing it with the V_b parameter. Given the importance of a block's orientation and shape relative to the direction of flow in the erodibility process, the E_{doa} parameter is determined as a more relevant parameter than J_s . For their part, parameters associated with joint conditions (K_d and J_o) and $NPES$ parameter are retained as relevant geomechanical parameters for evaluating the hydraulic erodibility of rock.

Kirsten's index includes some parameters (UCS , K_b and J_s) that our method deemed to be non-relevant parameters for evaluating the hydraulic erodibility of rock, and it was concluded that the use of the 3D block volume measurement (V_b), rather than the K_b parameter, could improve the characterization of rock block size. Furthermore, the J_o and V_b parameters are determined as relevant parameters for evaluating the hydraulic erodibility of rock. However, $eGSI$ index does not consider them when GSI is determined from Marinos and Hoek (2000) chart. Finally, it was concluded that determining the relevant geomechanical parameters for evaluating the hydraulic erodibility of rock, as determined in this study, could be very useful key-step to develop a new hydraulic erodibility index, one that could be used to provide a more accurate assessment of the hydraulic erodibility of rock.

Conflict of interest

The authors confirm that there are no known conflicts of interest associated with this publication, and there has been no significant financial support for this work that could have influenced its outcome.

Acknowledgments

The authors would like to thank the organizations that have funded this project: Natural Sciences and Engineering Research Council of Canada (Grant No. 498020-16), Hydro-Quebec (NC-525700), and the Mitacs Accelerate program (Grant Ref. IT10008).

4.6 References

- Annandale GW. Erodibility. *Journal of Hydraulic Research* 1995;33:471–94.
- Annandale GW. *Scour Technology, Mechanics and Engineering in Practice*. McGraw-Hill, New York; 2006.
- Annandale GW, Kirsten HAD. On the erodibility of rock and other earth materials. *Hydraulic Engineering* 1994;1:68–72.
- Annandale GW, Ruff JF, Wittler RJ, T.M. L. Prototype validation of erodibility index for scour in fractured rock media. *Proceedings of the International Water Resources Engineering Conference, Memphis, Tennessee, American Society, 1998, p. 1096–101.*

- Barton N. Scale effects or sampling bias. Proceeding of International Workshop Scale Effects in Rock Masses, Balkema Publication, Rotterdam, 1990, p. 31–55.
- Barton N, Lien R, Lunde J. Engineering classification of rock masses for the design of tunnel support. *Rock Mechanics* 1974;6:189–236.
- Bieniawski ZT. Engineering rock mass classifications : a complete manual for engineers and geologists in mining, civil, and petroleum engineering 1989:251.
- Bieniawski ZT. Rock mass classification in rock engineering. In Exploration for rock engineering, procedures of the symposium. ZT Bieniawski, Cape Town: Balkema 1976:97–106.
- Bieniawski ZT. Engineering Classification of Jointed Rock Masses. *The Civil Engineer in South Africa* 1973;15:343–53.
- Boumaiza L, Saeidi A, Quirion M. Determining relative block structure rating for rock erodibility evaluation in the case of non-orthogonal joint sets. *Journal of Rock Mechanics and Geotechnical Engineering* 2019;11:72–87.
- Boumaiza L, Saeidi A, Quirion M. Evaluation of the impact of the geomechanical factors of the Kirsten's index on the shifting-up of rock mass erodibility class. Proceeding of The 70th Canadian Geotechnical Conference and the 12th Joint CGS/IAH-CNC Groundwater Conference, Ottawa, Ontario, Canada, 2017, p. 8.
- Castillo LG, Carrillo JM. Scour, velocities and pressures evaluations produced by spillway and outlets of dam. *Water* 2016;8:1–21.
- Cecil OS. Correlations of rock bolt-shotcrete support and rock quality parameters in Scandinavian tunnels. Ph.D Thesis., Urbana, University of Illinois, (cited in Barton et al., 1974); 1970.
- Doog N. Die hidrouliese erodeerbaarheid van rotmassas in onbelynde oorlope met spesiale verwysing na die rol van naatvulmateriaal. Master thesis in Afrikaans language, University of Pretoria, South Africa; 1993.
- Gokceoglu C, Zorlu K. A fuzzy model to predict the uniaxial compressive strength and the modulus of elasticity of a problematic rock. *Engineering Applications of Artificial Intelligence* 2004;17:61–72.
- Goodman RE. Engineering geology-Rock in engineering construction. John Wiley & Sons, New York; 1993.
- Grenon M, Hadjigeorgiou J. Evaluating discontinuity network characterization tools through mining case studies. *Soil Rock America* 2003;1:137–142.
- Hadjigeorgiou J, Poulin R. Assessment of ease of excavation of surface mines. *Journal of Terramechanics* 1998;35:137–153.

- Hahn WF, Drain MA. Investigation of the erosion potential of kingsley dam emergency spillway. Proceeding of the joint Annual Meeting and Conference of AIPG, AGWT, and the Florida Section of AIPG, Orlando, Florida, USA., 2010, p. 1–10.
- Hoek E, Kaiser PK, Bawden WF. Support of underground excavations in hard rock. A.A. Balkema/Rotterdam/Brookfield.; 1995.
- ISRM (International Society for Rock Mechanics). Suggested methods for the quantitative description of discontinuities in rock masses. International Journal of Rock Mechanics and Mining Sciences & Geomechanics Abstracts 1978;15:319–68.
- Jennings JE., Brink ABA, Williams AAB. Revised guide to soil profiling for civil engineering purposes in South Africa. Civil Engineering in South Africa 1973;15:3–12.
- Kirkaldie L. Rock classification systems for engineering purposes. American Society for Testing and Materials, ASTM STP-984, Philadelphia, PA 1988.
- Kirsten HAD. Case histories of groundmass characterization for excavatability. Rock Classification Systems for Engineering Purposes American Society for Testing and Materials, STP 984 1988:102–120.
- Kirsten HAD. A classification system for excavation in natural materials. The Civil Engineer in South Africa 1982;24:292–308.
- Kirsten HAD, Moore JS, Kirsten LH, Temple DM. Erodibility criterion for auxiliary spillways of dams. International Journal of Sediment Research 2000;15:93–107.
- Kuroiwa J, Ruff JF, Wittler RJ, Annandale GW. Prototype Scour Experiment in Fractured rock media. Proceedings of International Water Resources Engineering Conference and Mini-Symposia, Americal Society of Civil Engineering, Memphis, TN., 1998.
- Laugier F, Leturcq T, Blancer B. Stabilité des barrages en crue: Méthodes d'estimation du risque d'érodabilité aval des fondations soumises à déversement par-dessus la crête. Proceeding de la Fondation des barrages. Chambéry, France, 2015, p. 125–36.
- Marinos P, Hoek E. GSI: A geologically friendly tool for rock mass strength estimation. Proc. GeoEng2000 Conference, 2000, p. 1422–42.
- Moore JS. The characterization of rock for hydraulic erodibility. SCS Technical Release - 78, Northeast National Technical Center, Chester. PA. (Cited in Van Schalkway et al., 1994); 1991.

- Moore JS, Kirsten HAD. Discussion – Critique of the rock material classification procedure. Rock classification systems for engineering purposes. American Society for Testing and Materials, STP-984, L. Kirkaldie Ed, Philadelphia, 1988, p. 55–8.
- Moore JS, Temple DM, Kirsten HAD. Headcut advance threshold in earth spillways. Bulletin of the Association of Engineering Geologists 1994;31:277–80.
- Mörén L, Sjöberg J. Rock erosion in spillway channels – A case study of the Ligga spillway. Proceedings of 11th Congress of the International Society for Rock Mechanics, Lisbon, Portugal, 2007, p. 87–90.
- Palmstrom A. Measurements of and correlations between block size and rock quality designation (RQD). Tunnelling and Underground Space Technology 2005;20:362–77.
- Palmstrom A. Characterizing rock masses by the RMI for Use in Practical Rock Engineering. Part 1: The development of the Rock Mass index (RMI). Tunnelling and Underground Space Technology 1996;11:175–88.
- Palmstrom A. RMI--a rock mass characterization system for rock engineering purposes. Ph.D. thesis, University of Oslo, Norway, 1995.
- Palmstrom A, Blindheim OT, Broch E. The Q-system – possibilities and limitations (in Norwegian). Norwegian National Conference on Tunnelling. Norwegian Tunnelling Association, Oslo, Norway, 2002, p. 41.1-41.43.
- Palmstrom A, Broch E. Use and misuse of rock mass classification systems with particular reference to the Q-system. Tunnelling and Underground Space Technology 2006;21:575–93.
- Pells SE. Erosion of rock in spillways. Ph.D Thesis, University of New South Wales, Australia; 2016a.
- Pells SE. Assessment and surveillance of erosion risk in unlined spillways. Proceeding of International symposium on Appropriate technology to ensure proper development, operation and maintenance of dams in developing countries”, Johannesburg, South Africa, 2016b, p. 269–78.
- Pells SE, Bieniawski ZT, Hencher S, Pells PJN. RQD: Time to Rest in Peace. Canadian Geotechnical Journal 2017a;54:825–34.
- Pells SE, Douglas K, Pells PJN, Fell R, Peirson WL. Rock mass erodibility. Technical Note: Journal of Hydraulic Engineering 2017b;43:1–8.
- Pells SE, Pells PJN, Peirson WL, Douglas K, Fell R. Erosion of unlined spillways In Rock - does a “scour threshold” exist? Proceeding of Australian National Committee on Large Dams . Brisbane, Queensland, Australia, 2015, p. 1–9.

- Pitsiou S. The effect of discontinuities of the erodibility of rock in unlined spillways of dams. Master's Thesis, University of Pretoria, South Africa; 1990.
- Rock AJ. A semi-empirical assessment of plung pool scour: Two-dimensional application of Annandale's Erodibility Method on four dams in British Columbia, Canada. Master's Thesis, University of British Columbia. Vancouver, British Columbia, Canada; 2015.
- Rouse H, Ince S. History of hydraulics. Iowa Institute of Hydraulic Research, State University of Iowa; 1957.
- Saeidi A, Deck O, Verdel T. Development of building vulnerability functions in subsidence regions from analytical methods. *Géotechnique* 2012;62:107–20.
- Saeidi A, Deck O, Verdel T. Development of building vulnerability functions in subsidence regions from empirical methods. *Engineering Structures* 2009;31:2275–86.
- Scoble MJ, Hadjigeorgiou J, Nenonen L. Development of an excavating equipment selection expert system, based on geotechnical considerations. Proceedings of the 40th Canadian Geotechnical Conference, Regina, 1987, p. 67–78.
- Van-Schalkwyk A. Watenavorsingskommissie: Verslag oor loodsondersoek: Die erodeerbaarheid van verskillende rotsformasies in onbeklede damoorlope., Unpublished report, University of Pretoria, South Africa (Cited in Van Schalkwayk et al., 1994); 1989.
- Van-Schalkwyk A, Jordaan J, Dooge N. Erosion of rock in unlined spillways. *Proceeding of International Commission on Large Dams*, Paris, 71 (37), 1994, p. 555–71.
- Weaver JM. Geological factors significant in the assessment of rippability. *The Civil Engineer in South Africa* 1975;17:313–6.
- Wise S. Assessing the quality for hydrological applications of digital elevation models derived from contours. *Hydrological Processes* 2000;14:1909–29.
- Wittler RJ, Annandale GW, Ruff JF, Abt SR. Prototype validation of erodibility index for scour in granular media. *International Water Resources Engineering Conference*, Memphis, Tennessee, American Society of Civil Engineers., 1998, p. 1090–5.
- Zimmerman D, Pavlik C, Ruggles A, Armstrong MP. An experimental comparison of ordinary and universal kriging and inverse distance weighting. *Mathematical Geology* 1999;31:375–90.

CHAPTER 5 – DEVELOPMENT OF A METHODOLOGY FOR DETERMINING THE RELATIVE IMPORTANCE OF ROCK MASS PARAMETERS THAT CONTROL THE HYDRAULIC ERODIBILITY OF ROCK⁸

Abstract

The methods commonly used for evaluating rock scour correlate flowing water energy and rock resistance. The latter is evaluated by using indices that are based on selected rock mass parameters. In this paper, (i) we review the existing methods used to evaluate rock scour, and we determine the committed error according to each method, and (ii) using a large existing dataset of case studies that detail eroded unlined spillways, we develop a method to determine the relative importance of the rock mass parameters that govern hydraulic erodibility. Based on this method, we find that the relative importance of the relevant rock mass parameters, from highest to lowest, are joint shear strength, the nature of the potentially eroding surface, rock block volume, joint opening, rock block shape and orientation relative to flow direction, and the rock mass deformation module. This ordering of the importance of the rock mass parameters largely agrees with that based on field observations.

Keywords: Rock mass, Hydraulic erosion, Rock mass parameters, Annandale's method, Pells's method, Kirsten's index, Erosion level.

⁸ Boumaiza, L., Saeidi, A. and Quirion, M. (2019). A method to determine the relative importance of rock mass parameters that control the hydraulic erodibility of rock. *Journal of Rock Mechanics and Geotechnical Engineering* (Submitted).

5.1. Introduction

Standard methods for evaluating rock scour⁹ correlate flowing water energy and rock resistance; these approaches include the Annandale (Annandale, 1995) and Pells methods (Pells, 2016). The flowing water energy, named the available hydraulic stream power (P_a), is the hydraulic power (expressed in kW/m²) generated by flowing water (Henderson, 1966). To evaluate the capacity of rock resistance, selected rock mass parameters are related to each other via an equation to produce an index. Certain engineering rock mass classification systems used to evaluate the rock excavatability incorporate most of the parameters that affect rock scour (Van Schalkwyk 1989; Pitsiou 1990; Moore 1991). Some rock mass characterization indices, such as the rock mass rating (*RMR*) system (Bieniawski, 1973), the Q-system (Barton et al., 1974), and Kirsten's index (Kirsten, 1988, 1982) have been tested to determine their efficacy in evaluating hydraulic rock scour. From these tests, Kirsten's index was found to be most accurate (Van Schalkwyk et al. 1994a). As such, this index has been the most commonly used index to evaluate hydraulic rock scour (Annandale, 1995; Annandale and Kirsten, 1994; Dooge, 1993; Kirsten et al., 1996; Moore et al., 1994; Van-Schalkwyk et al., 1994a, 1994b). Kirsten's index (N) (Eq. 5.1) is determined based on a selection of rock mass parameters including the unconfined compressive strength (*UCS*) of rock (M_s), rock block size (K_b), joints shear strength (K_d), and relative block structure (J_s).

⁹ In this paper, we consider the terms “scour,” “erodibility,” and “hydraulic erosion” as synonymous technical terms that describe erosion when a rock mass is submitted to flowing water energy.

$$N = M_s \cdot K_b \cdot K_d \cdot J_s \quad (5.1)$$

Kirsten (1982) adopted the Jennings et al. (1973) *UCS* classification to propose a descriptive chart that has M_s ratings ranging from 0.87 to 280. The K_b factor is the ratio of the *RQD* index (rock quality designation) to the joint set number (J_n). Given that the *RQD* index varies from 5% to 100% (Barton et al., 1974), and J_n values vary from 1 to 5 (Kirsten, 1988, 1982), the K_b rating consequently ranges from 1 to 100. The K_d factor is determined as the ratio J_r/J_a . J_r is the rating corresponding to joint roughness (from 0.5 to 4), and J_a is the rating corresponding to joint surface alteration (from 0.75 to 18). Accordingly, the K_d rating can vary between 0.03 and 5.33 (Kirsten, 1982). The J_s factor represents the effect of rock block shape and orientation relative to the flow direction. For an orthogonal fractured system, the J_s rating ranges from 0.37 to 1.5 (Kirsten, 1982). For non-orthogonal fractured systems, the J_s rating is from 0.09 to 1.38 (Boumaiza et al., 2019a, 2018). Two other indices have been developed by Pells (2016) to evaluate rock resistance capacity. The first index is *eGSI*, representing a modification of the *GSI* (geological strength index; Hoek et al. 1995) by including a new discontinuity orientation factor (E_{doa}) to represent the effect of rock block shape and orientation relative to the flow direction (Eq. 5.2). The second index is the rock mass erosion index (*RMEI*). As presented in Eq. 5.3, *RMEI* can be determined according to the relative importance factor (*RF*) and likelihood factor (*LF*). The prefixes *P1* to *P5* in Eq. 5.3 are various sets of parameters (introduced in classification system) that represent, respectively, the mechanism for detachment, the nature of the potentially eroding surface, the joints nature, the joints spacing, and the rock block shape (Pells, 2016).

$$eGSI = GSI + E_{doa} \quad (5.2)$$

$$RMEI = (RF_{P1} \cdot LF_{P1}) \cdot (RF_{P2} \cdot LF_{P2}) \cdot [(RF_{P3} \cdot LF_{P3}) + (RF_{P4} \cdot LF_{P4}) + (RF_{P5} \cdot LF_{P5})] \quad (5.3)$$

Pells (2016) assumed that the existing indices, including Kirsten's index, did not represent the erosion mechanism observed in the field. Accordingly, the *RMEI* system attempts to represent the rock mass parameters controlling the erosion mechanism, where their relative importance is assumed from field observations of unlined spillways. The most important rock mass parameters are weighted by a high *RF* value compared with those judged as less important. The kinematically viable mechanism for detachment and the nature of the potentially eroding surface are both weighted with a high *RF* value of 3, compared to the nature of the joints (*RF* = 2), joint spacing (*RF* = 1), and rock block shape (*RF* = 1). The structure of the *RMEI* system for hydraulic erosion could be considered as being similar to the Q-system (Barton et al., 1974) that was also developed from field investigations. In the *RMEI* system (Pells, 2016a), rock block size is not included directly; however, joint spacing can provide an idea of rock block size given that a greater spacing of joints begets a greater rock block volume. Joint shear strength is also not included in the *RMEI* classification, but the nature of the joint can be considered as its synonym factor given that this factor incorporates the natural condition of joints. The *RMEI* classification considers the joint spacing factor to be less important (*RF* = 1) than the nature of the joints, which is weighted as *RF* = 2. The Q-system, on the other hand, places more importance on the *K_b* factor (rating range from 1 to 100; indicating the

rock block size) than the K_d factor (rating range from 0.03 to 5.33; representing joint shear strength) (Barton et al., 1974). The discordance of the relative importance of the parameters included in these two classification systems demonstrates that the field evaluation can be greatly impacted by expert judgment. Consequently, the challenge remains to find an accurate alternative approach for determining the relative importance of rock mass parameters.

As rock scour is a highly complicated process (Bollaert and Schleiss, 2003), any assessment should begin by determining the relevant rock mass parameters applicable to its evaluation. This initial selection should then be coupled with determining the relative importance of the selected rock mass parameters. The main objective of this paper is to develop a method that determines the relative importance, via classification of the rock mass parameters governing rock scour. Our method emerges from observing the errors produced when evaluating the hydraulic rock scour using existing methods.

5.2. Background of the comparative methods

At present, dam spillway design relies largely on a “scour threshold” methods to assess the hydraulic rock erosion; these methods exist as a function of P_a and an erodibility index (Hahn and Drain, 2010; Mören and Sjöberg, 2007; Pells et al., 2015). The “scour threshold” used within a suite of methods is determined from the interpreted erosion observed for various case studies. The threshold emerges from

plotted data and a threshold line that separates case studies having observable specific scour conditions from those lacking a significant scour.

5.2.1 Background of comparative methods based on Kirsten's index

Van Schalkwyk et al. (1994a) categorized the erosion conditions of certain classes based on rock scour depth (Table 5.1). This classification was updated (Table 5.2) (Van Schalkwyk et al., 1994b) by adding the data of Moore et al. (1994). This update to the erosion classification subsequently altered the level of scour threshold lines.

Table 5.1. Classification of the erosion (Van Schalkwyk et al., 1994a).

Depth of erosion (m)	Erosion class
0	None
0–1	Little
1–5	Moderate
>5	Extensive

Table 5.2. Classification of the erosion (Van Schalkwyk et al., 1994b).

Depth of erosion (m)	Erosion class
<0.2	Negligible
0.2–0.5	Minor
0.5–2	Moderate
>2	Large

Using Kirsten's index, Annandale (1995) analyzed the data collected by Van Schalkwyk et al. (1994a) and Moore et al. (1994). By plotting this data in relation to P_a , Annandale (1995) proposed a single scour threshold line that separated scour and no-scour events. He considered scour conditions when the erosion depth exceeded 2 m, as less than 2 m of erosion is considered relatively inconsequential, as it is most often the result of loose blocks of rock being removed from the stratum surface (Annandale, 2006). Applying the same concept as Annandale (1995), Kirsten et al. (2000) incorporated data from Dooge (1993) and Moore et al. (1994) to propose an alternative scour threshold line separating scour and no-scour conditions.

Given that the scour threshold lines proposed by Annandale (1995) and Kirsten et al. (2000) are based on the same evaluation of erosion conditions (>2 m = scour, <2 m = no scour), these threshold lines can be plotted together. The concept proposed by Van Schalkwyk et al. (1994a) cannot be compared as it does not consider an erosion limit depth of 2 m (Table 1). However, the proposal of Van Schalkwyk et al. (1994b) can be compared to that of Annandale (1995) and Kirsten et al. (2000) by considering together the "negligible", "minor", and "moderate" classes (Table 5.2) as being no-scour (<2 m), and the "large" class as representing scour conditions (>2 m). The lines that demarcate the interpreted onset of scour based on Kirsten's index versus P_a are summarized in Figure 5.1.

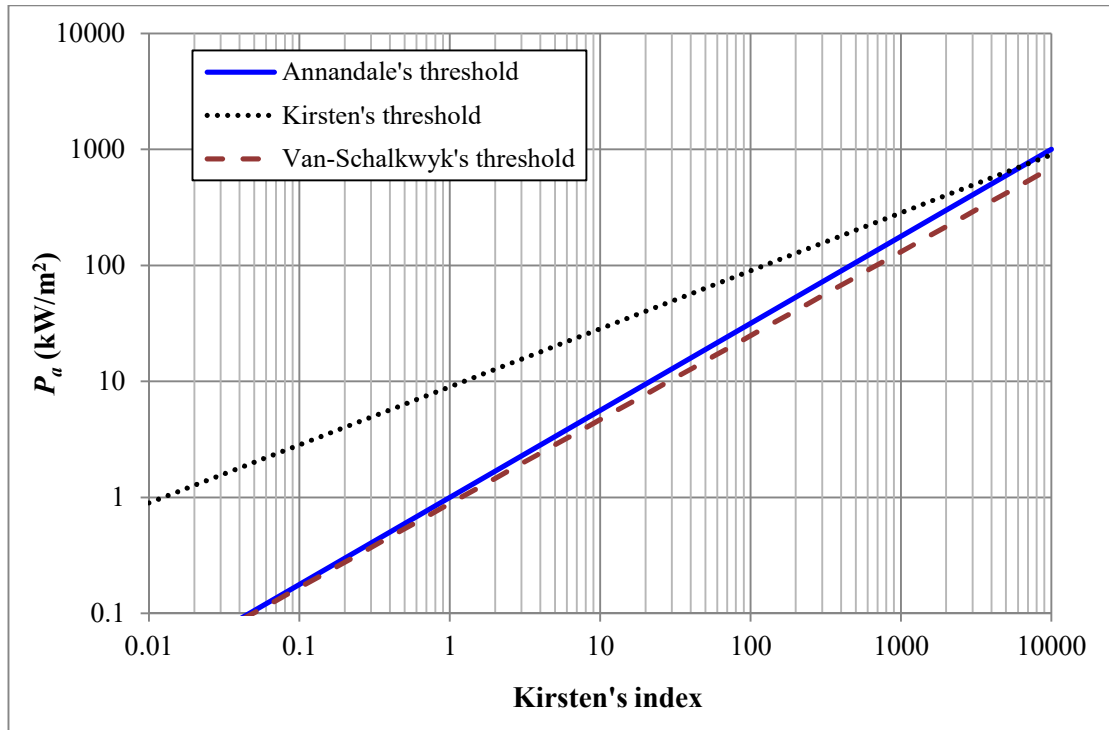


Figure 5.1. Comparison of scour threshold lines.

5.2.2 Background of the Pells's methods

Adopting the same concept of Van Schalkwyk et al. (1994b), Pells (2016) categorized the erosion conditions for certain classes by slightly modifying the depth of the eroded area. He also added information related to the extent of the eroded area (Table 5.3). Using the $eGSI$ index (Eq. 5.2) and $RMEI$ index (Eq. 5.3), Pells (2016) plotted their calculated values versus P_a to manually determine the selected erosion classes. These classes are separated by scour threshold lines, as shown in Figures 5.2 and 5.3. Figure 5.3, as proposed originally by Pells (2016), was recently modified by

Douglas et al. (2018). However, it is not clear whether an optimizing process was used to determine the placement of the updated threshold lines.

Table 5.3. Description of erosion conditions (Pells, 2016a).

Max. depth (m)	General extent (m ³ /100 m ²)	Erosion level
<0.3	<10	Negligible
0.3–1	1–30	Minor
1–2	30–100	Moderate
2–7	100–350	Large
>7	>350	Extensive

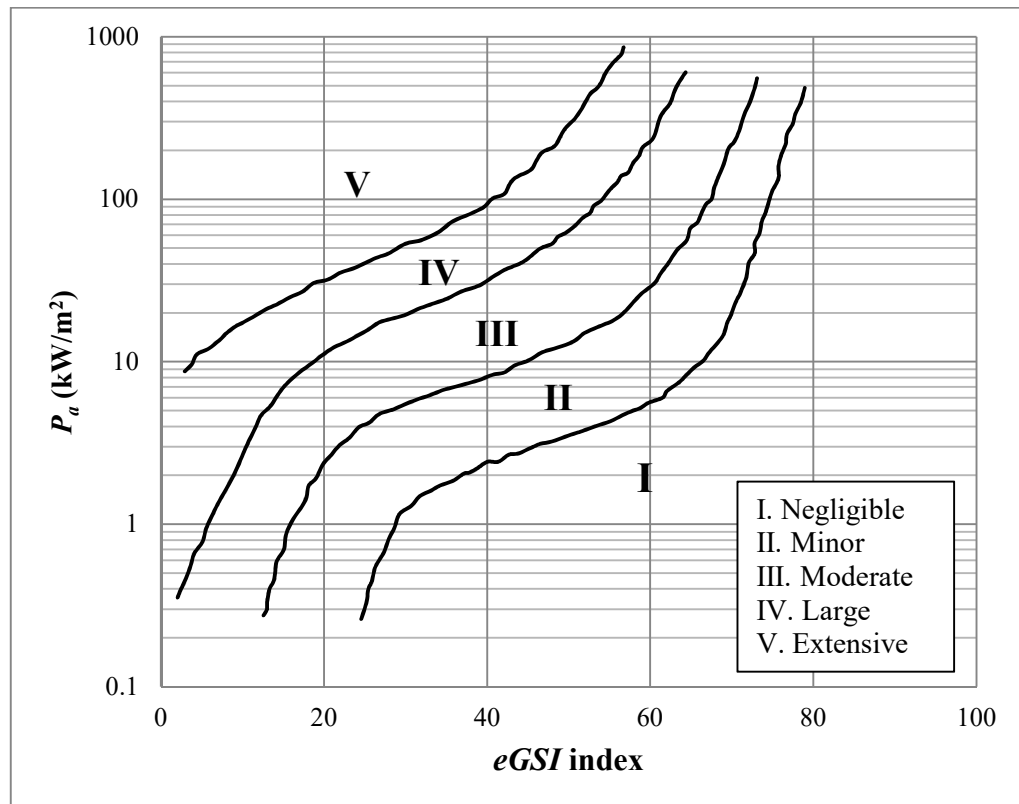


Figure 5.2. Erosion classes as determined based on the *eGSI* index (Pells, 2016).

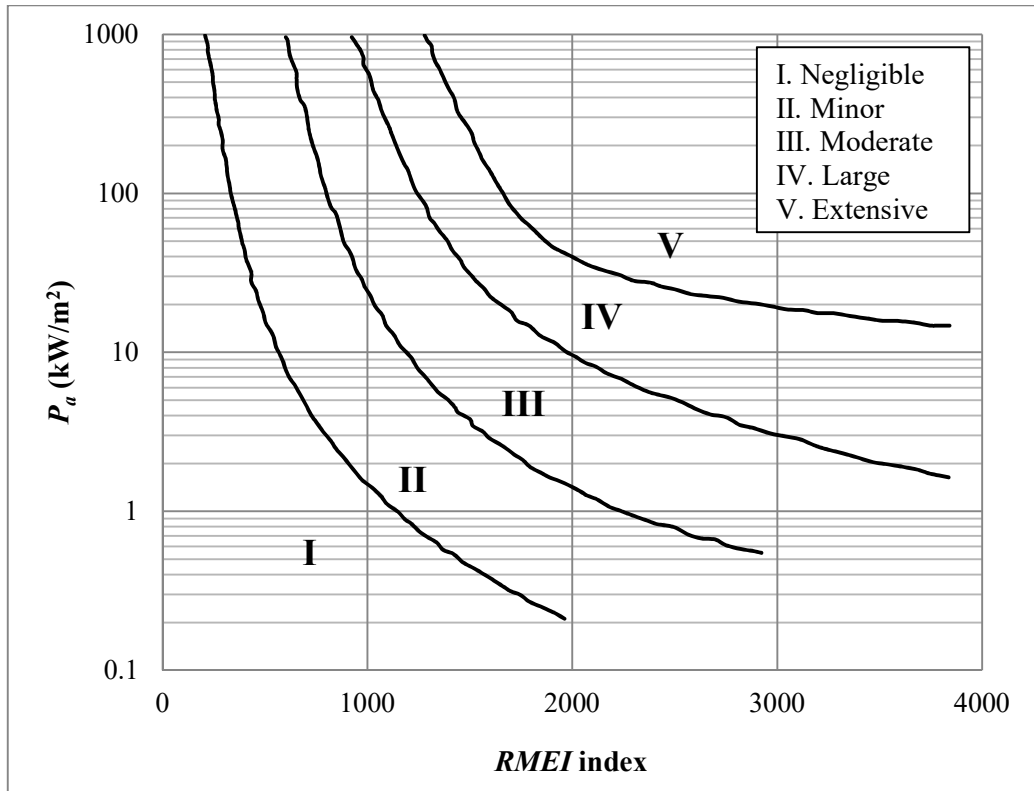


Figure 5.3. Erosion classes as determined based on the *RMEI* index (Douglas et al., 2018).

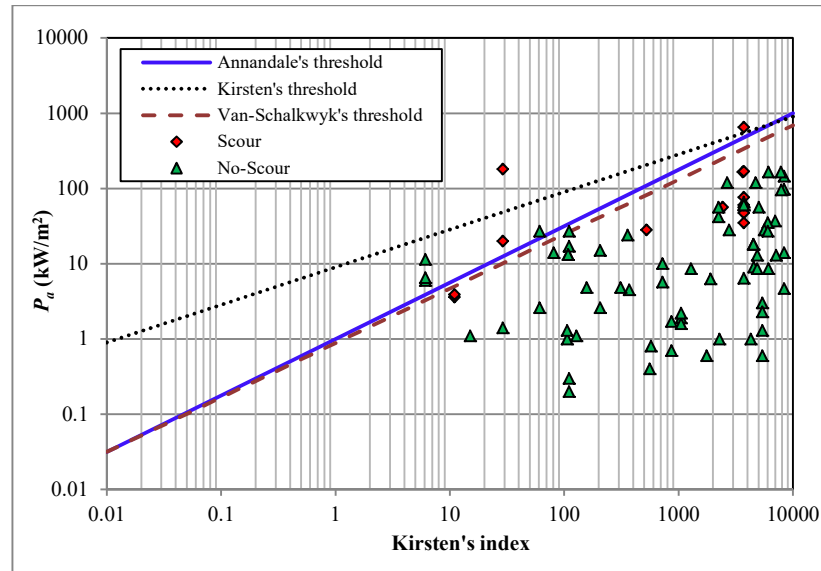
5.3. Analysis of comparative methods

Our comparative analysis includes: 1) comparing all comparative scour threshold methods (the Van Schalkwyk, Annandale, Kirsten, and Pells methods); 2) comparing the Van Schalkwyk and Pells methods; and 3) comparing the two Pells's methods separately. For this comparative analysis, we use field data from unlined spillways as collected by Pells (2016). 86 case studies provide a complete dataset for

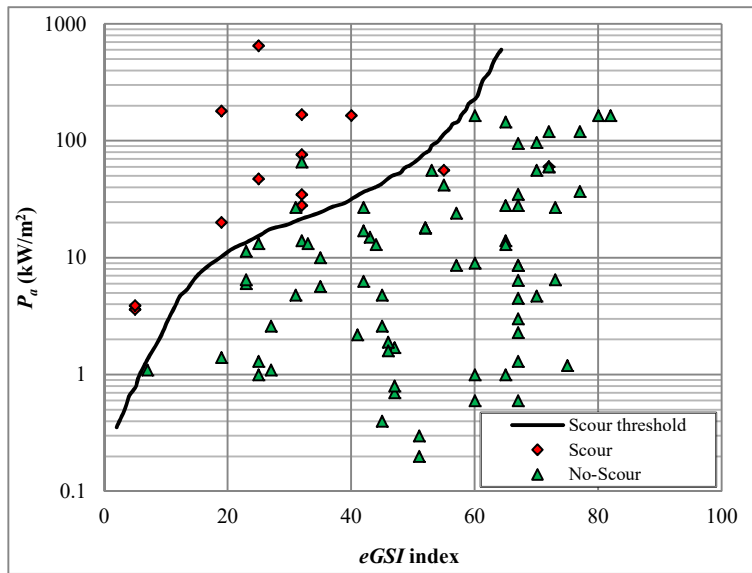
all values of the three erodibility indices (Kirsten's index, the *eGSI* index, and the *RMEI* index) being compared. The case study datasets are presented in Appendix G.

5.3.1 Comparing all methods

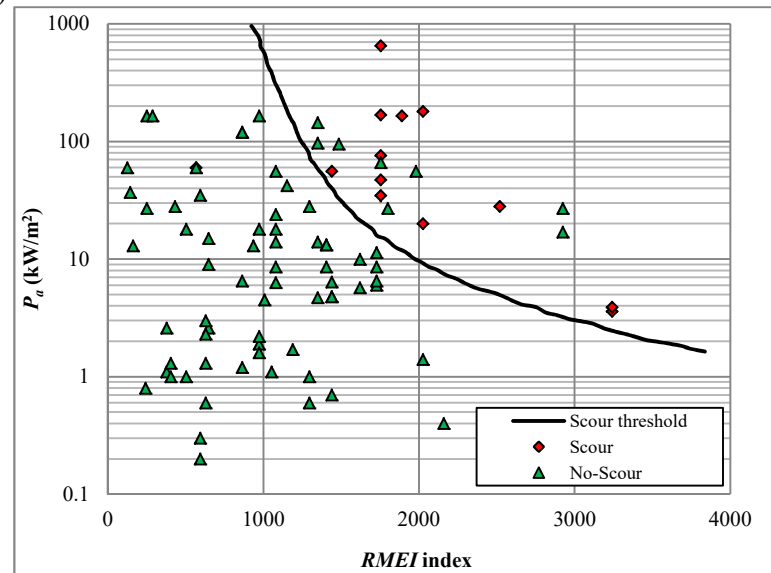
To compare the existing methods, we harmonized the different erosion classes as the Annandale and Kirsten methods are based on two scour classes, whereas the Van Schalkwyk and Pells methods are based on several scour classes. By assuming that scour conditions exist when erosion depth is >2 m (Annandale, 2006), Pells's charts (Figures 5.2 and 5.3) could be interpreted as a single scour threshold. Indeed, the erosion condition classes of "negligible", "minor", and "moderate" (Table 5.3) can be grouped to represent the "no-scour" condition as the erosion depth of these classes is <2 m. The "large" and "extensive" classes (Table 5.3) can represent the "scour" condition as their erosion depth is >2 m. Accordingly, the considered scour threshold line is that separating the "moderate" and "large" classes. As introduced in Section 2.1, the Van Schalkwyk, Annandale, and Kirsten scour thresholds can be presented together (Figure 5.1) given that scour is assumed to occur when erosion is >2 m. The 86 case studies plotted according to Kirsten's index, the *eGSI* index, and the *RMEI* index are presented in Figures 5.4a, 5.4b, and 5.4c, respectively.



(a)



(b)



(c)

Figure 5.4. Plots of the 86 case studies according to (a) Kirsten's index, (b) the $eGSI$ index, and (c) the $RMEI$ index.

We can determine the efficacy of these developed scour thresholds by the number of case studies having a poorly evaluated scour condition. Annandale and Van Schalkwyk methods differ marginally from Kirsten’s threshold (Table 5.4). Annandale’s method (Annandale, 2006, 1995), however, is the most commonly used method for evaluating hydraulic rock scour (Castillo and Carrillo, 2016; Hahn and Drain, 2010; Laugier et al., 2015; Mören and Sjöberg, 2007; Rock, 2015). We observe an improvement when we include the erodibility indices of *RMEI* and *eGSI*. These recently developed indices were developed specifically to evaluate hydraulic rock scour compared to Kirsten’s index that was initially proposed to evaluate the excavatability of earth materials.

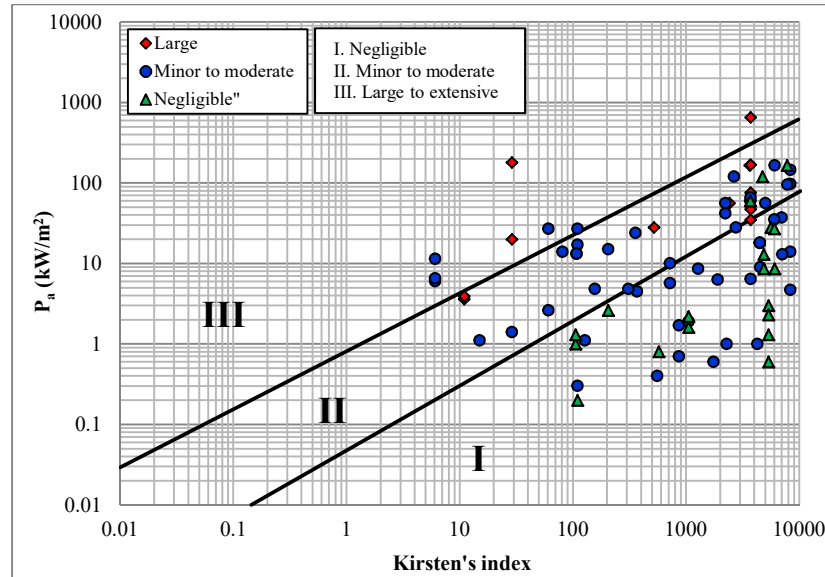
Table 5.4. Committed error calculated based on the various methods.

Method	Number of poorly evaluated case studies	Committed error (%)
Annandale, Van Schalkwyk (same threshold)	14	16
Kirsten	11	13
<i>eGSI</i>	4	5
<i>RMEI</i>	9	10

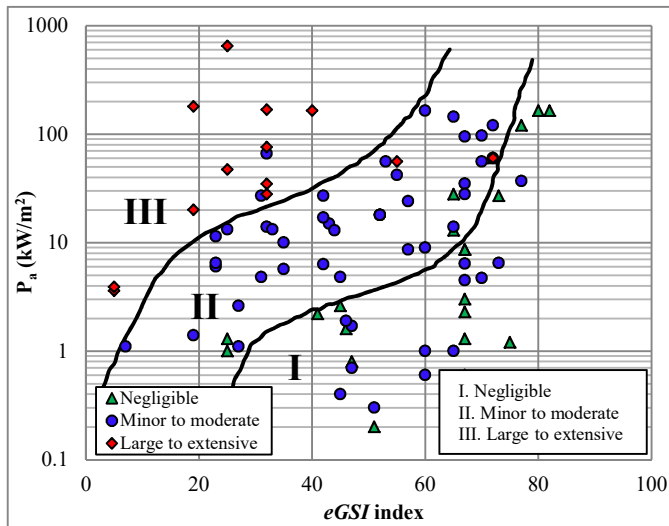
5.3.2 Comparing the Van Schalkwyk and Pells methods

As both of the proposed Van Schalkwyk’s classifications (Tables 5.1 and 5.2) and that of Pells (Table 5.3) categorize the erosion condition within a number of

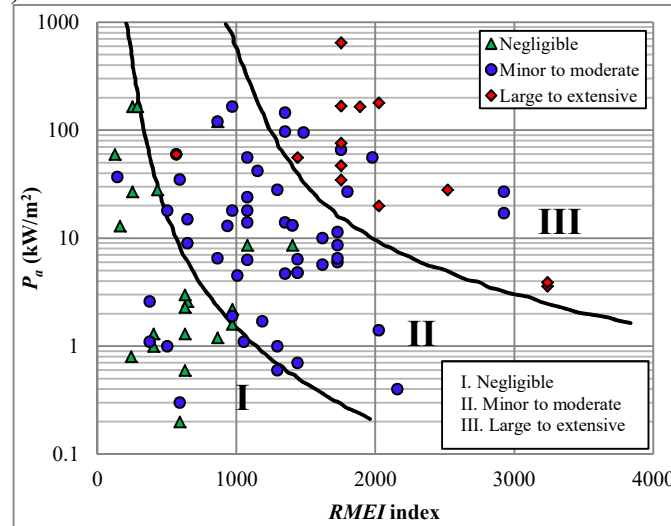
classes, comparing these methods will assess their respective efficacies when different erodibility indices (Kirsten's index, *eGSI* index, and *RMEI* index) are applied. This comparison therefore included a greater number of erosion classes than when we compared the pair of classes in Section 3.1. As the three erosion classifications (presented in Tables 5.1, 5.2, and 5.3) differ, we optimally harmonize the classification systems using Table 5.2 (Van Schalkwyk et al., 1994b; an update to Table 5.1) and Table 5.3 (Pells, 2016a). The final harmonized classification includes the classes “negligible” (<0.2 or 0.3 m depth), “minor to moderate” (0.2 to 2 m depth), and “large to extensive” (>2 m depth). The plotted data based on the Van Schalkwyk, *eGSI*, and *RMEI* methods are shown in Figures 5.5a, 5.5b, and 5.5c, respectively.



(a)



(b)



(c)

Figure 5.5. Plotted data based on (a) Kirsten's index, (b) $eGSI$ index, (c) $RMEI$ index by considering three erosion classes.

The Van Schalkwyk et al. (1994b) method produces a high committed error percentage (77%) for the “large to extensive” class (Table 5.5), while the committed error percentage was highest for the “minor to moderate” using the Pells’s methods (29%). The discordance between the Van Schalkwyk et al. (1994b) and Pells’s methods is also observed for the least committed error; the “negligible” class has the least committed error (14%) according to the Van Schalkwyk et al. (1994b) method, while the “large to extensive” class has values of 15% and 8% for the *eGSI* and *RMEI* methods, respectively. Furthermore, the “negligible” erosion condition class of Van Schalkwyk et al. (1994b) provides less committed error than those of Pells. However, the Pells’s methods provide less committed error for the “minor to moderate” and “large to extensive” erosion condition classes. For two erosion classes (“minor to moderate” and “large to extensive”), the recently developed method of Pells provides a better evaluation than that of Van Schalkwyk et al. (1994b), the latter based on Kirsten’s index. This pattern could be related to the recent indices of Pells (2016) that are especially proposed to evaluate hydraulic rock scour.

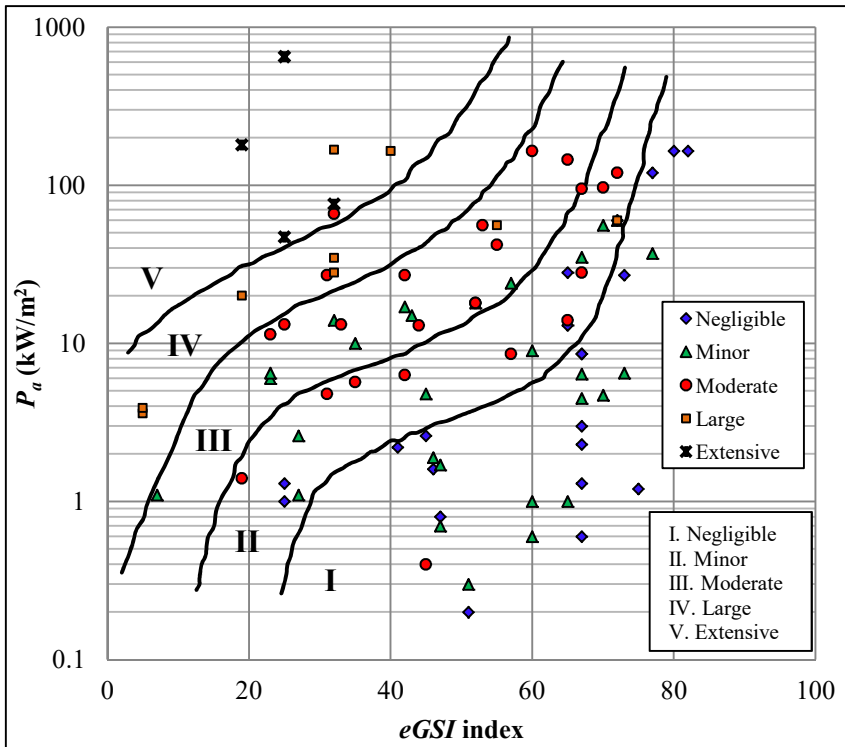
Table 5.5. Committed error calculated according to the Van Schalkwyk and the Pells’s methods (*eGSI* and *RMEI*).

Erosion class	Van Schalkwyk	<i>eGSI</i>	<i>RMEI</i>
	Committed error (%)		
Negligible	14	24	19
Minor to moderate	46	29	29
Large to extensive	77	15	8

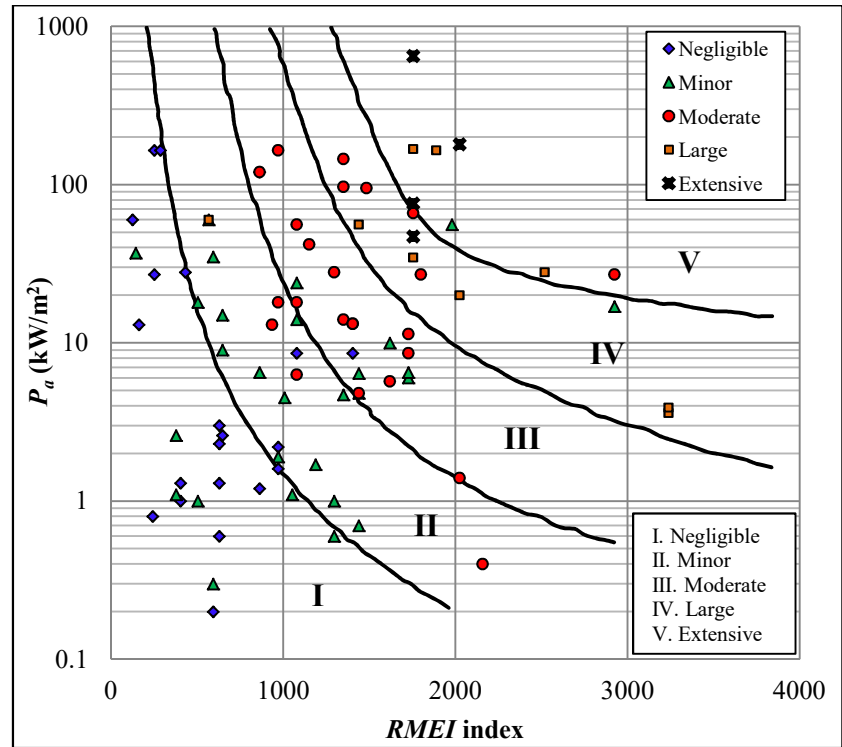
5.3.3 Comparing the Pells methods

5.3.3.1 Comparisons based on erosion classes

As the Pells's methods (*RMEI* and *eGSI*) categorize erosion condition with the same classes (Table 5.3), we can compare the committed error of each method and verify the ranking of the eventual committed error. The error is determined here using the number of case studies where the scour condition is poorly evaluated. The plotted case studies, based on the *eGSI* and *RMEI* indices, are shown in Figures 5.6a and 5.6b, respectively.



(a)



(b)

Figure 5.6. Plotted data based on the (a) $eGSI$ index and (b) $RMEI$ index with five classes.

From the plotted *eGSI* index dataset (Figure 5.6a), 42 case studies are evaluated poorly, corresponding to a committed error of 49% from all considered case studies. The plotted *RMEI* index dataset has 35 poorly evaluated case studies (Figure 5.6b), corresponding to a committed error of 41%. Overall, the *RMEI* method provides a better evaluation of the two indices. Nonetheless, the rank of the committed error is very high for both approaches (41% for *RMEI*; 49% for *eGSI*). Observing the individual erosion classes, the highest committed error is found in the “extensive” class of the *RMEI* method (63%) and in the “minor” class of the *eGSI* method (68%) (Table 5.6, Figure 5.7). Differences exist between *RMEI* and *eGSI* for the least committed error as the “negligible” class has the least committed error based on the *RMEI* method (30%), while the “large” class has the least committed error using *eGSI* (17%). The *RMEI* committed error percentage follows an upward trend, whereas *eGSI* committed error percentage follows an irregular trend between classes (Figure 5.7). Furthermore, the erosion condition classes of “negligible”, “minor”, and “moderate” using *RMEI* generate lower committed error percentages than the *eGSI* method. *RMEI*, however, has a higher committed error than *eGSI* for the “large” and “extensive” classes. Based on the observed discordance between the *RMEI* and *eGSI* methods, we can conclude that the *RMEI* and *eGSI* methods cannot be used simultaneously for assessing hydraulic rock scour in a planned unlined spillway project.

Table 5.6. Committed error calculated from the *RMEI* and *eGSI* methods.

Erosion class	<i>eGSI</i>	<i>RMEI</i>
	Committed error (%)	
Negligible	45	30
Minor	68	38
Moderate	45	36
Large	17	58
Extensive	43	63

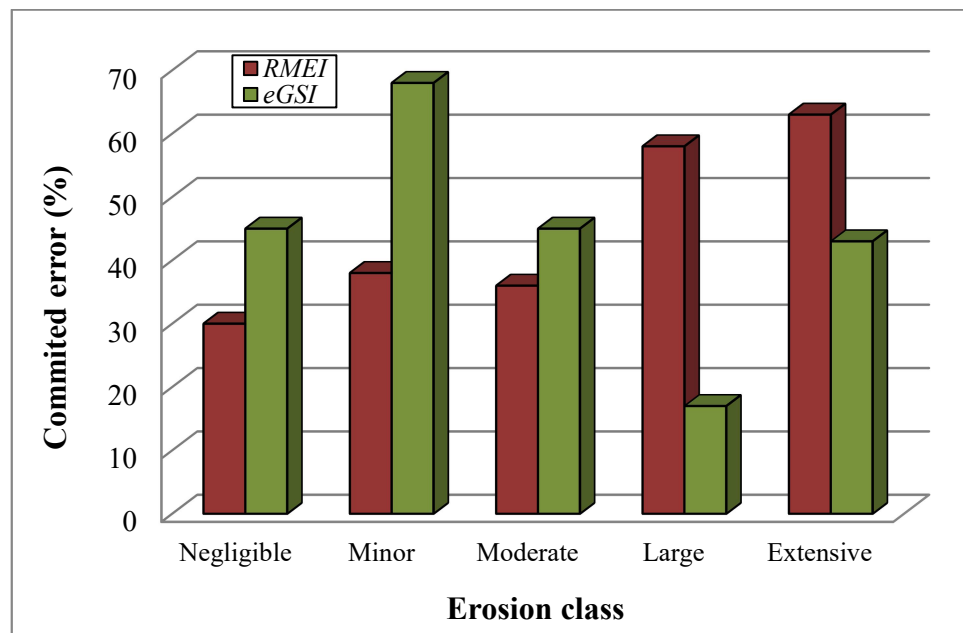


Figure 5.7. Committed errors within the different erosion classes.

5.3.3.2 Comparisons based on hydraulic stream power class

As the hydraulic rock scour mechanism is controlled by the rock mass resistance capacity and the erosive force of water, a comparative analysis is

performed by taking into account the effect of the subsequent variations of P_a . The committed error is calculated for each P_a class by determining the number of case studies where scour condition is poorly evaluated within the considered P_a class. The P_a classes for this purpose (0–2.5, 2.5–5, 5–10, 10–25, 25–50, and >50 kW/m²) are adopted from Boumaiza et al. (2019b). The calculated committed errors are illustrated in Figure 5.8.

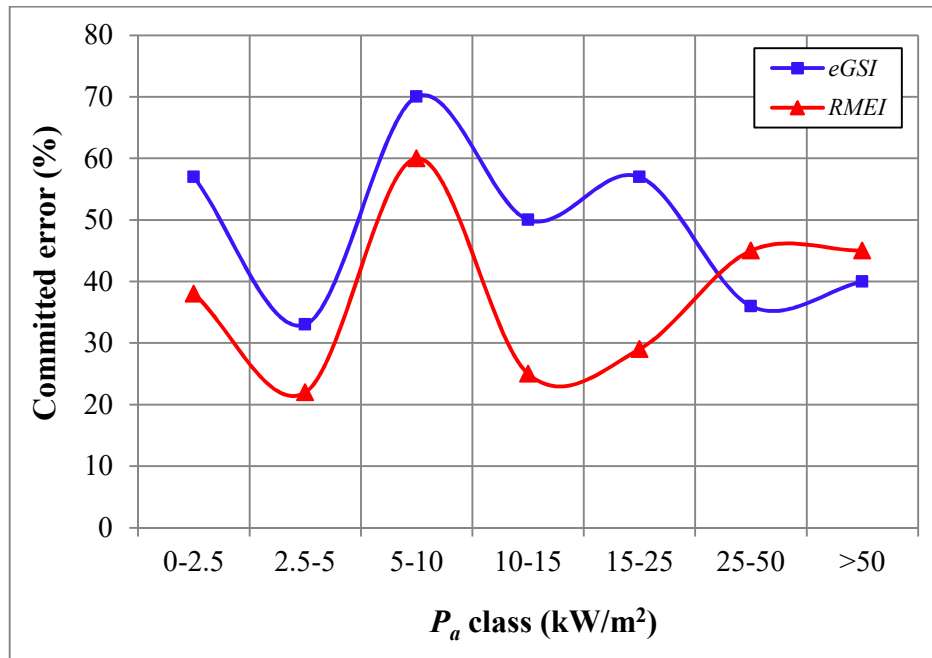


Figure 5.8. Committed errors for the various P_a classes.

In general, the $eGSI$ method generates a higher committed error than the $RMEI$ method (Figure 5.8). However, for four P_a classes (2.5–5, 5–10, 25–50, and >50 kW/m²), the committed error difference between $RMEI$ and $eGSI$ varies around 10% or less. Moreover, the P_a classes of 2.5–5 and 5–10 present a high and low committed error, respectively, for both methods, and similar values for the >50 kW/m² class. The behavior of the $RMEI$ committed error curve generally matches

that of the *eGSI* curve, and thus demonstrates a concordance between *RMEI* and *eGSI*. Thus, hydraulic conditions tend not to affect *RMEI* nor *eGSI*. If hydraulic conditions have less effect on the committed error, attention should focus more on the rock mass parameters.

A focus on rock mass parameters can improve the methods used for evaluating the hydraulic rock scour, and attempts to improve these methods must include two main steps: 1) identify the relevant rock mass parameters for evaluating hydraulic rock scour, and 2) determine the relative importance of the selected rock mass parameters. Boumaiza et al. (2019b, 2019c) analyzed a set of rock mass parameters related to hydraulic erosion and proposed a methodology that allows for specifying the relevant geomechanical parameters. Boumaiza et al. (2019b, 2019c) highlighted that hydraulic erodibility is governed by specific rock mass parameters. In the following section, we detail how to determine the relative importance of the determined rock mass parameters and present a developed method. We then compare the outcomes of this developed method with field observations.

5.4. Description of the method

The proposed method for determining the relative importance of the rock mass parameters that control the hydraulic erodibility of rock is summarized in Figure 5.9. Each methodological step is described in the following subsections.

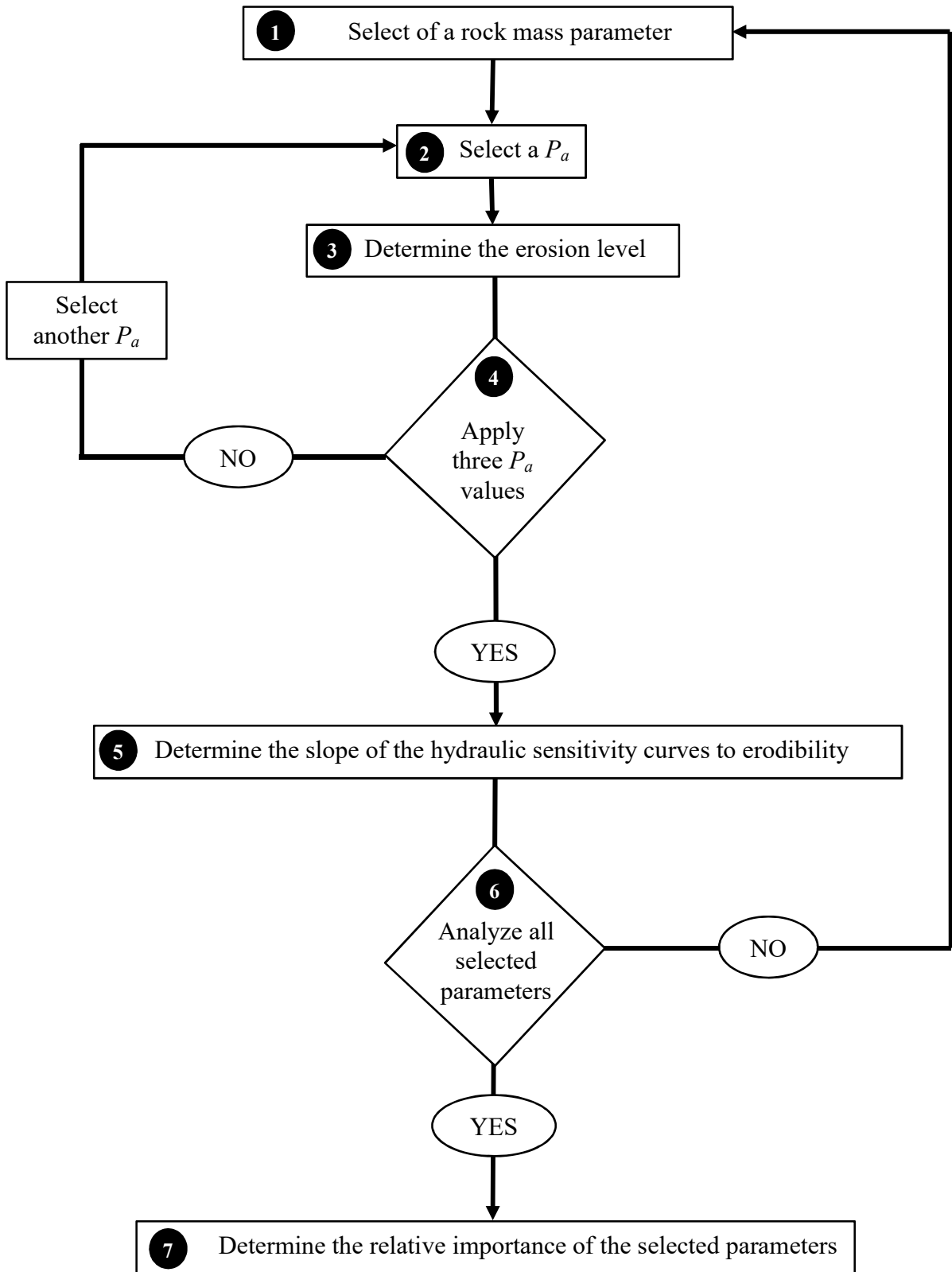


Figure 5.9. Algorithm for determining the relative importance of selected parameters.

5.4.1 Step 1 - Selecting a rock mass parameter

Using their developed method, Boumaiza et al. (2019b) examined a set of rock mass parameters to specify those parameters considered to be relevant for evaluating rock resistance to water flowing energy. Briefly, they compiled data from case studies of unlined spillways (Pells 2016). The compiled data included information on geomechanical parameters, the P_a , and the observed erosion (i.e., “negligible”, “minor”, “moderate”, “large” and “extensive”) that were labeled with an erosion level of 1, 2, 3, 4, and 5, respectively. Boumaiza et al. (2019b) assessed individually the impact of selected parameters by classifying each parameter in certain classes. As some case studies had the same class, the erosion level for a given P_a category was calculated; the identical calculation process was then run for all P_a categories and for all classes of a single rock-mass parameter. A best-fit curve representing the mean erosion level versus the average P_a was then plotted. Boumaiza et al. (2019b) considered these best-fit curves as sensitivity curves to erodibility that can be used to determine the potential erosion level at a considered value of P_a . The parameters having sensitivity curves to erodibility aligned in a consecutive sequence were considered to be relevant. The retained parameters were joints opening (J_o), joints shear strength (K_d), rock block volume (V_b), the parameter representing the block’s shape and orientation relative to the flow direction (E_{doa}), and the nature of the potential eroding surface ($NPES$).

By applying this approach of Boumaiza et al. (2019b), we can examine the rock mass deformation modulus (E_{rm}) as it is a representative parameter of a rock

mass subjected to hydraulic loading. We calculate E_{rm} of the eroded case studies using Eq. 5.4 (Hoek and Diederichs, 2006).

$$E_{rm} = E_i \left[0.02 + \frac{1-D/2}{1 + e^{((60+15D-GSI)/11)}} \right] \quad (5.4)$$

where E_i is Young's modulus of intact rock (GPa), D is the disturbance factor and GSI is the geological strength index. We use the GSI values available in Pells (2016) for the eroded case studies and assume the D factor to be 0.7 (Hoek et al., 2002). However, E_i was not reported for the eroded case studies. As both the rock type and uniaxial compressive strength of the eroded case studies are available in Pells (2016), we use Eq. 5.5 (Hoek and Diederichs, 2006) to determine E_i .

$$E_i = MR \cdot \sigma_{ci} \quad (5.5)$$

where MR is the modulus ratio that can be determined according to rock type. Depending on the rock type of the eroded case studies, the MR is determined from the compiled available data of the *RocData* software (Rocsciences, 2019). σ_{ci} is the uniaxial compression strength of intact rock. The available σ_{ci} values in Pells (2016) for the eroded case studies are used in this study. The GSI , rock type, σ_{ci} , MR , and the calculated E_i and E_{rm} are tabulated in Appendix G. As there is no existing E_{rm}

classification, we can build one by evaluating the case studies of eroded unlined rocky dam spillways (Table 5.7), taking inspiration from Fattahi et al. (2019).

Table 5.7. Proposed E_{rm} classification.

Class	E_{rm} (GPa)	Description
1	0–10	Very low deformation modulus
2	10–20	Low deformation modulus
3	20–30	Moderate deformation modulus
4	>30	High deformation modulus

As E_{rm} indicates the resistance of a rock mass to deformation, a rock mass of E_{rm} Class 1 ($E_{rm} = 0–10$ GPa), should be more sensitive to erodibility compared to other rock masses (e.g., an E_{rm} of Class 4 with E_{rm} is >30 GPa). The obtained sensitivity curves according to the E_{rm} classification (Table 5.7) are shown in Figure 5.10.

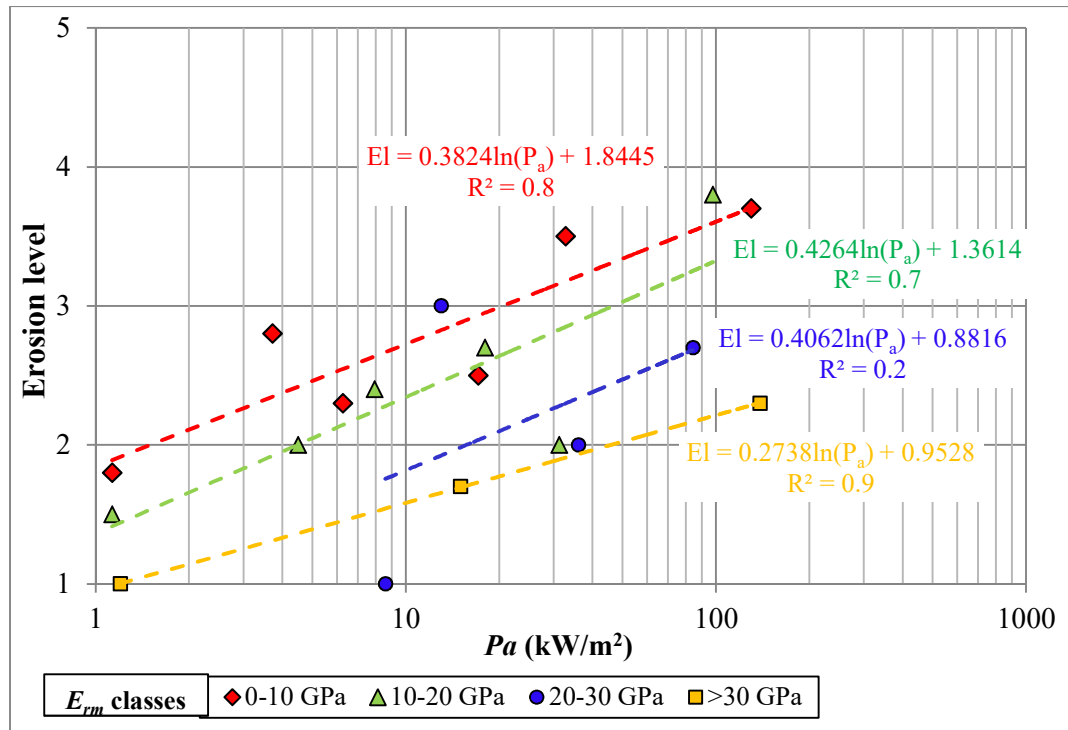


Figure 5.10. Sensitivity curves to erodibility based on E_{rm} classification. It should be mentioned that each best-fit line corresponds to symbol data points of the same color and shape (e.g., the best-fit blue line corresponds to the blue circles), and the associated equation is also of the same color.

The best-fit curves follow perfectly the E_{rm} categories (Figure 10). In fact, the case studies characterized by a lower value of E_{rm} (e.g., Class 1 rock mass with $E_{rm} = 0\text{--}10$ GPa) are more sensitive to erodibility compared to rock masses characterized by a higher value of E_{rm} (e.g., Class 4 with $E_{rm} >30$ GPa). For P_a value of 10 kW/m^2 , a Class 4 rock mass would undergo minor erosion compared to a Class 1 rock mass that would be moderately eroded. As E_{rm} sensitivity curves to erodibility are aligned in a consecutive sequence, and demonstrate a proportional relationship between E_{rm} and erosion level, E_{rm} can be considered as a relevant parameter for evaluating hydraulic rock scour. Accordingly, E_{rm} can be added to the set of relevant parameters (J_o , K_d , V_b , E_{doa} , and $NPES$) retained previously by Boumaiza et al. (2019b). We consider all of these relevant parameters to determine their relative importance in hydraulic

erosion mechanism. Each parameter is assessed individually (Steps 1–5, Figure 5.9). The process is then repeated from Step 6 to the end for the considered rock mass parameters. To explain our method, we introduce the J_o parameter into the analysis process (Steps 1–6).

5.4.2 Step 2 - Selecting a hydraulic stream power

Using the Bieniawsk (1989) J_o classification, Boumaiza et al. (2019b) proposed J_o sensitivity curves to erodibility (Figure 5.11; J_o classes are indicated in the legend). These sensitivity curves to erodibility can be used to determine the erosion level for a given P_a . In Step 2, we select a given P_a value of 2 kW/m². This value can occur in actual study cases and is selected to determine erosion level, as explained in Step 3.

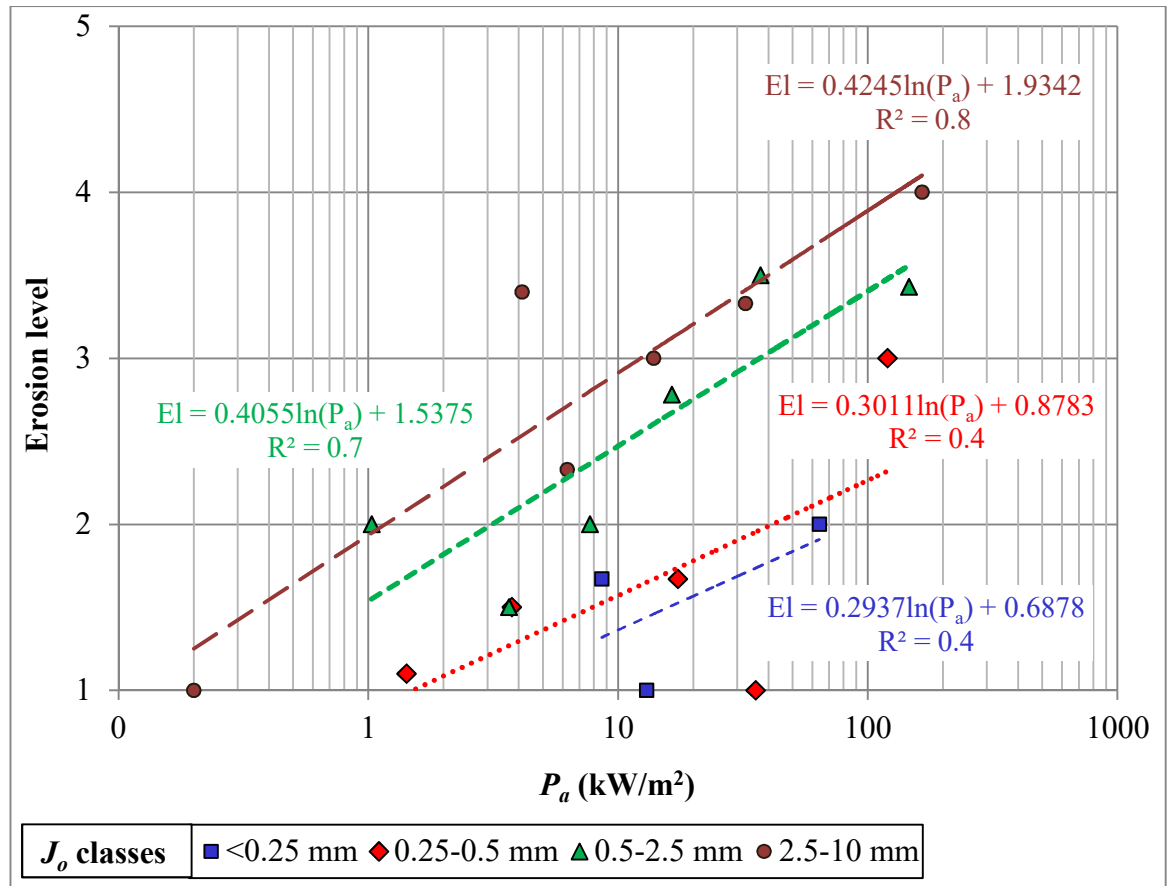


Figure 5.11. Sensitivity curves to erodibility based on J_o classification (Boumaiza et al., 2019a).

5.4.3 Steps 3 and 4 - Determining erosion level based on the selected P_a

Using Figure 5.11, the best-fit curve equation of each J_o class is used to determine the erosion level (El), where the P_a value is kept at 2 kW/m². Step 3 determines the erosion level when different J_o classes are subjected to the same P_a , and therefore provides an overview of erosion level behavior versus J_o . The same process is then repeated for the other P_a (Step 4). For this analysis, we select P_a

values of 2, 10, and 40 kW/m² to represent a range of increasing P_a . The main goal of Step 4 is identify the erosion level behavior for J_o classes when these classes are subjected to various P_a . The calculated erosion level for the subsequent J_o classes, based on the three selected P_a , are presented in Table 5.8 and Figure 5.12. It should be noted that the J_o classes <0.25 mm, 0.25–0.5 mm, 0.5–2.5 mm, and 2.5–10 mm (Table 5.8) are represented in Figure 5.12 as 0.25, 0.5, 2.5, and 10 mm, respectively.

Table 5.8. Calculated erosion level based on J_o classification.

P_a (kW/m ²)	J_o (mm)			
	<0.25 mm	0.25–0.5 mm	0.5–2.5 mm	2.5–10 mm
2 kW/m ²	0.89	1.09	1.82	2.23
10 kW/m ²	1.36	1.57	2.47	2.91
40 kW/m ²	1.77	1.99	3.03	3.50

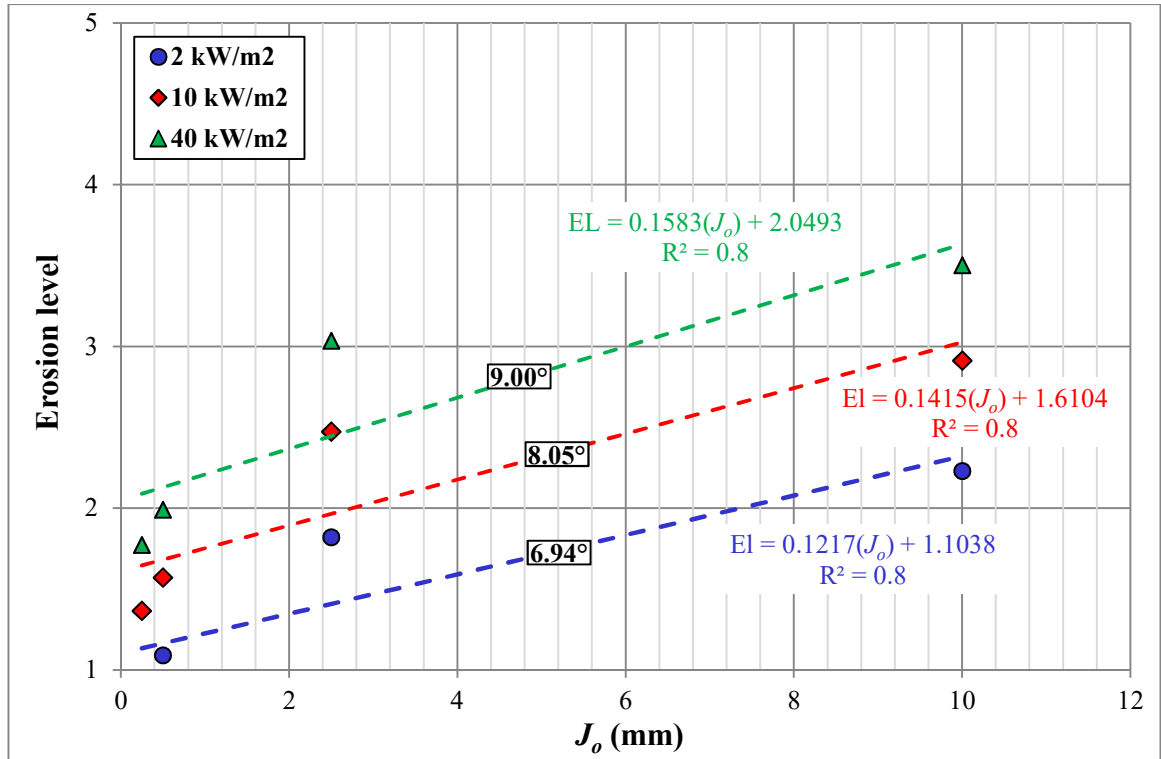


Figure 5.12. J_o hydraulic sensitivity curves to erodibility.

The best-fit J_o hydraulic sensitivity curves to erodibility represent the calculated erosion level versus J_o classes as related to the P_a value (2, 10, and 40 kW/m²). These best-fit curves (hereafter named hydraulic sensitivity curves to erodibility) illustrate a sound relationship between J_o and erosion level. When J_o increases, the erosion level becomes greater, and this pattern is observed for all three selected P_a values.

5.4.4 Steps 5 and 6 - Determining the slope of the hydraulic sensitivity curves to erodibility for the selected rock mass parameters

We then calculate the slope of the hydraulic sensitivity curves to erodibility using the equation of the best-fit curve (Figure 5.12). The calculated slopes for J_o hydraulic sensitivity curves to erodibility are proportional to P_a (Figure 5.12). The hydraulic sensitivity curve having the steepest slope is $P_a = 40 \text{ kW/m}^2$ (9°), followed by $P_a = 10 \text{ kW/m}^2$ (8.05°), and $P_a = 2 \text{ kW/m}^2$ (6.94°), respectively (Figure 5.12). The steepest hydraulic sensitivity curve includes the highest erosion levels and, consequently, corresponds to an important erosion effect compared with other lower-sloped hydraulic sensitivity curves. However, these slopes are controlled mostly by P_a .

Following the same process as that used for the J_o parameter, we analyze all the selected rock mass parameters using the sensitivity curves to erodibility (Appendix H). Each selected rock mass parameter has a specific hydraulic sensitivity curve to erodibility (i.e., specific slope), where the slope is controlled mostly by P_a . However, plotting the calculated slopes of selected parameters versus selected P_a (i.e., 2, 10, and 40 kW/m^2) provides an overview of the relative importance of each parameter. This forms Step 7 (Figure 5.9) and is detailed in the Results section.

5.5 Results and discussion

5.5.1 Determining the hydraulic sensitivity curves to erodibility

The hydraulic sensitivity curves to erodibility for the selected parameters K_d , V_b , E_{doa} , $NPES$, and E_{rm} are shown in Figures 5.13a, 5.13b, 5.13c, 5.13d, and 5.13e, respectively. The classes of the analyzed rock mass parameters are represented by average values. From Figure 5.13a, we note an inversely proportional relationship between K_d and erosion level; when K_d increases, the erosion level decreases. In Figure 5.13b, we adopt the rock block volume classification of Palmstrom (1995). As already observed for K_d , there is an inversely proportional relationship between V_b and erosion level; as V_b increases, erosion becomes less important. We adopt the E_{doa} classes in Figure 5.13c from Pells's classification (Pells, 2016a). Again, there is an inversely proportional relationship between E_{doa} and erosion level. There is a proportional relationship between $NPES$ and erosion level (Figure 5.13d), as an increase in $NPES$ produces a greater erosion level. Finally, we note an inversely proportional relationship between E_{rm} and erosion level, so that as E_{rm} decreases, erosion level increases (Figure 5.13e).

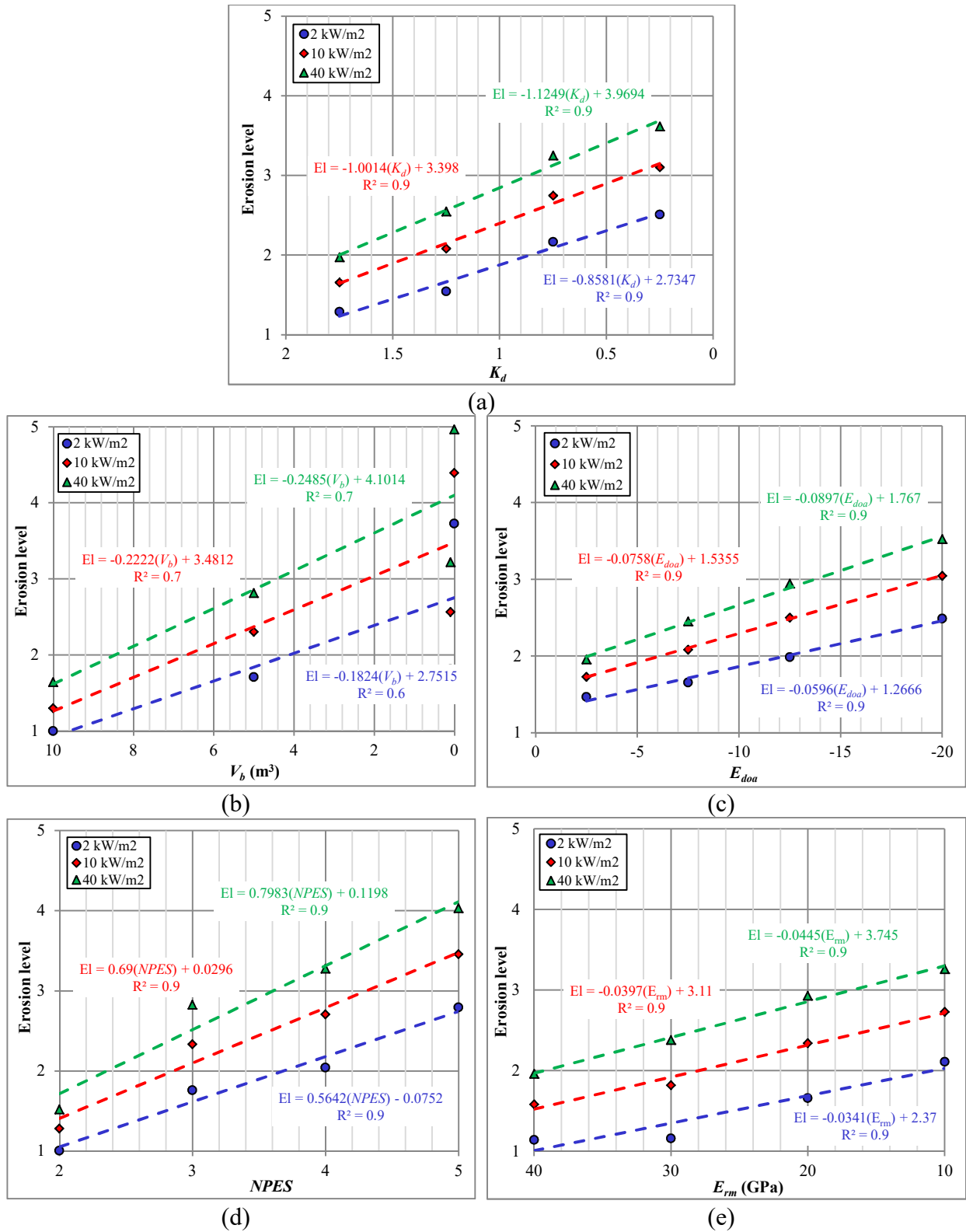


Figure 5.13. Hydraulic sensitivity curves for (a) K_d , (b) V_b , (c) E_{doa} , (d) $NPES$, and (e) E_{rm} . Note that for the hydraulic sensitivity curves of K_d , V_b , E_{doa} , and E_{rm} , the x-axis values are presented from higher to lower values.

5.5.2 Determining the relative importance of the selected parameters

To determine the relative importance of the selected parameters (J_o , K_d , V_b , E_{doa} , $NPES$, and E_{rm}), we undertake the following steps:

- 1) For each rock mass parameter, we apply the three hydraulic sensitivity curves to erodibility ($P_a = 2, 10, \text{ and } 40 \text{ kW/m}^2$) to determine the slope value of each hydraulic sensitivity curve (the calculated slopes are presented in Table 5.9);
- 2) For each rock mass parameter, the calculated slope values, corresponding to a P_a of 2, 10, and 40 kW/m^2 , are plotted as a function of these P_a values (the produced curve is named hereafter as the slope variation curve);
- 3) All selected rock mass parameters are plotted and presented together (Figure 5.14).

Table 5.9. Determined slopes of hydraulic sensitivity curves to erodibility.

	Selected parameters					
	J_o	K_d	V_b	E_{doa}	$NPES$	E_{rm}
P_a (kW/m^2)	Calculated slopes					
2	6.94°	40.63°	10.34°	3.41°	29.43°	1.95°
10	8.05°	45.04°	12.53°	4.33°	34.46°	2.27°
40	9.00°	48.36°	13.96°	5.13°	38.60°	2.55°

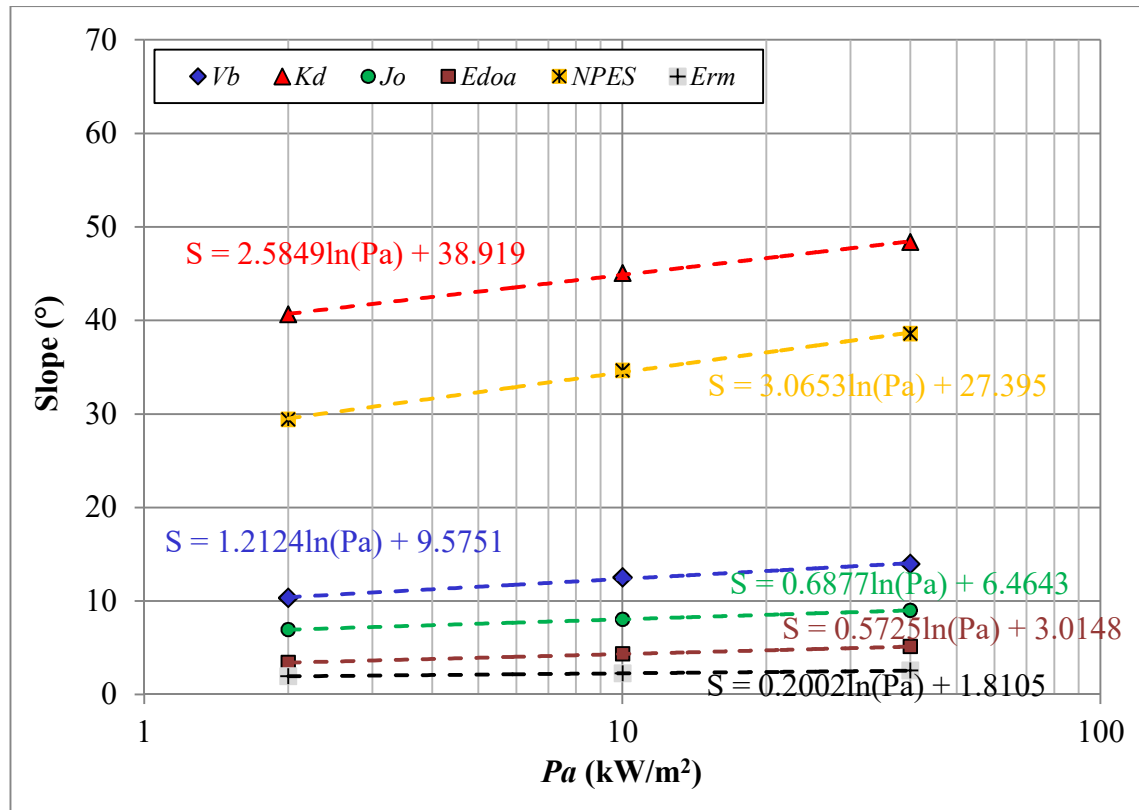


Figure 5.14. Slope variation curves of the selected parameters.

Considering the calculated slopes of hydraulic sensitivity curves to erodibility (Table 5.9 and Figure 5.14), the selected parameters (for $P_a = 2 \text{ kW/m}^2$) are ranked based on the slope of the hydraulic sensitivity curve from K_d (40.63°), $NPES$ (29.43°), V_b (10.34°), J_o (6.49°), E_{doa} (3.41°), to E_{rm} (1.95°). The same pattern is observed for $P_a = 10$ and 40 kW/m^2 . As slope results from the highest recorded erosion levels, K_d likely has a much greater role in hydraulic erosion than the other selected parameters, as based on the used P_a values (2, 10, and 40 kW/m^2). In terms of relative importance in hydraulic erodibility, the selected parameters are ranked in importance (highest to lowest) from K_d , $NPES$, V_b , J_o , E_{doa} , and then E_{rm} . On the other hand, each selected parameter presents a distinct slope variation curve (i.e., the line

connecting the calculated slopes of each parameter; Figure 5.14). Consequently, each parameter has a specific slope difference within the considered P_a interval (i.e., 2–40 kW/m²). For example, the K_d slope difference is 7.73°, corresponding to a difference between the slope of 40 kW/m² (48.36°) and 2 kW/m² (40.63°). The selected parameters can therefore be ranked in terms of slope variation rate from highest to lowest as $NPES$ (9.17), K_d (7.73), V_b (3.62), J_o (2.06), E_{doa} (1.72), and E_{rm} (0.60). This observation raises an important question as to what occurs when P_a is very high (e.g., 16 000 kW/m²; Laugier et al., 2015). In these extreme cases, $NPES$ may have a greater impact, given its steeper slope variation rate. If we extend the slope variation curves to these very (fictional) high P_a values (e.g., 100,000 kW/m²), we observe that P_a is intense, the selected rock mass parameters maintain the same sequence, and maintain their relative importance in assessing the hydraulic erodibility of rock.

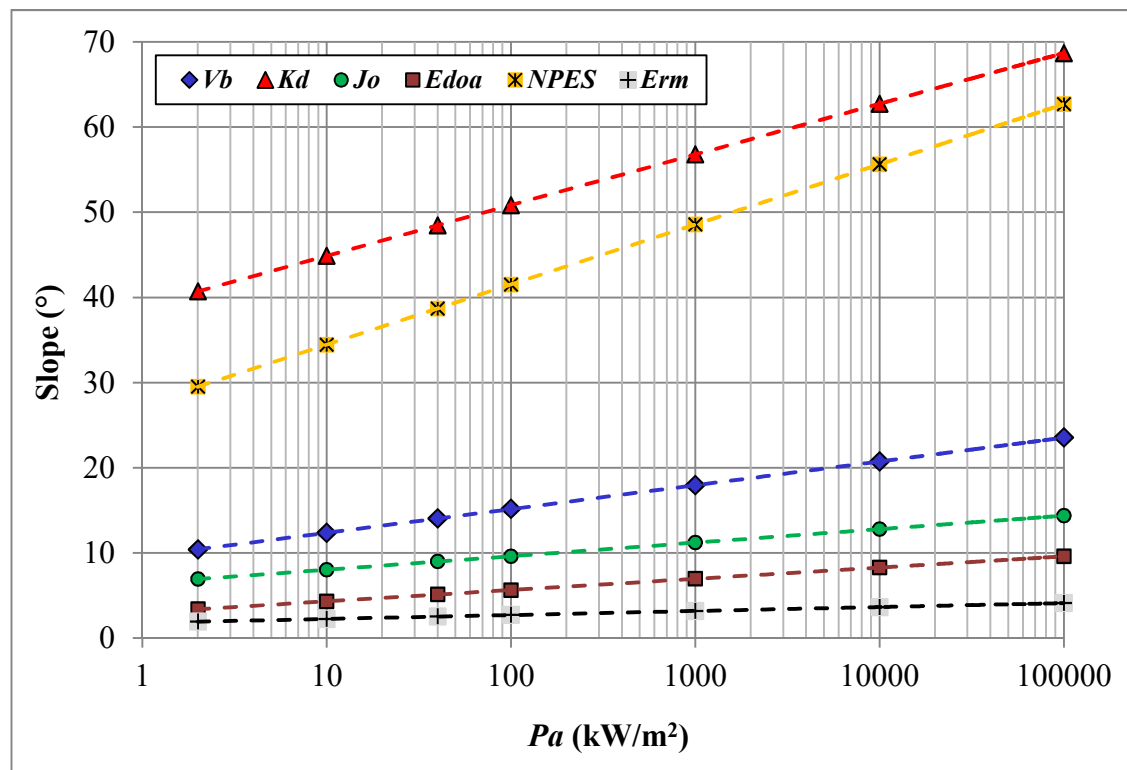


Figure 5.15. Extended slope variation curves of the selected parameters.

5.5.3 Comparison with field observations

It is difficult to directly compare the *RMEI* classification system, developed based on field observation (Pells, 2016a), with our study results for three main reasons.

1) Some analyzed parameters, such as V_b , K_d , and E_{rm} , are not included as such in the *RMEI* system;

2) The analyzed parameters are evaluated separately in our study, while in the *RMEI* system, some rock mass parameters are presented together as one factor; for example, the nature of joint factors includes joint roughness, joint aperture, and joint strength;

3) The relative importance of parameters in the *RMEI* classification system involves three levels (1 to 3), while our analysis identifies only two.

In our study, the first-level parameters include the K_d and $NPES$ that, given their steep slopes, are deemed as the most important parameters controlling hydraulic erosion (Figure 5.15). The second-level parameters include V_b , J_o , E_{doa} and E_{rm} that are relatively less important than the first-level parameters (Figure 5.15). $NPES$ is identified as one of the most important parameters, both from our method and the field observations of Pells (2016). Rock block shape, observed in the field as being relatively less important ($RF = 1$ in the *RMEI* classification system), is also determined through our analysis (as part of the E_{doa} parameter) to be less important than the first-level parameters (Figure 5.15).

In the *RMEI* classification system (Pells, 2016a), the rock block size is not included directly. However, joint spacing (included as a factor in the *RMEI* classification system) provides an idea of rock block size, given that a greater spacing of joints begets a larger rock block volume than does a tight spacing of joints. Accordingly, the joint spacing factor of the *RMEI* classification system can be compared with the V_b parameter analyzed by our method. We also determine that the joint spacing factor (V_b parameter), considered in *RMEI* classification as a less important factor ($RF = 1$), falls into the second level of parameters (Figure 5.15).

The J_o parameter is classified in the *RMEI* system as a second-level factor ($RF = 2$). In our analysis, we also find this parameter to be less important than the parameters of the first-level group. However, the J_o parameter in the *RMEI* classification system is included in the nature of the joint factor that combines joint opening and other joint conditions (i.e., joint roughness and strength). Joint roughness and strength can be considered as being synonymous with joint shear strength (K_d), which in our study is among the most important parameters. Combining the joint conditions highlights the importance of joint opening in the *RMEI* classification system. On the other hand, combining joint conditions downplays the importance of the joint roughness and strength (synonymous with K_d) that we determine as being very important parameters. This may explain the resultant committed error when the *RMEI* system is used to evaluate hydraulic rock scour (Section 2) despite *RMEI* being more sophisticated as it is based on field observations of eroded spillways. It should be noted that we could not compare the E_{rm} parameter as *RMEI* does not include this parameter or even a synonymous parameter.

5.6 Conclusion

We presented a comparative analysis of the existing methods for evaluating hydraulic rock scour, and this examination determined that existing methods are subjected to a given amount of error. As hydraulic conditions have less effect on the committed error, we focused particularly on rock mass parameters and determined the relative importance of the rock mass parameters that govern hydraulic erosion. We determined the relevance of the rock mass deformation module (E_{rm}) for evaluating the hydraulic rock scour and added E_{rm} to an existing set of relevant rock mass parameters. We then presented a methodology for identifying the relative importance of individual rock mass parameters within the set. For this, we assessed a suite of relevant parameters (K_d , J_o , $NPES$, V_b , E_{doa} , and E_{rm}) and found that the parameters could be classified in terms of their relative importance to hydraulic erodibility, from most to least important, as K_d , $NPES$, V_b , J_o , E_{doa} , then E_{rm} . This classification order generally agrees with classifications based on field observations.

Conflict of interest

The authors confirm that there are no conflicts of interest associated with this publication. Moreover, the financial support for this work did not influence its outcome.

Acknowledgments

The authors acknowledge the funding for this project from the Natural Sciences and Engineering Research Council of Canada (Grant No 498020-16), Hydro-Québec (NC-525700), and the Mitacs Accelerate program (Grant Ref. IT10008).

5.7 References

- Annandale, G.W., 1995. Erodibility. *Journal of Hydraulic Research* 33, 471–494.
- Annandale, G.W., 2006. *Scour Technology, Mechanics and Engineering in Practice*. McGraw-Hill, New York.
- Annandale, G.W., Kirsten, H.A.D., 1994. On the erodibility of rock and other earth materials. *Hydraulic Engineering* 1, 68–72.
- Barton, N., Lien, R., Lunde, J., 1974. Engineering classification of rock masses for the design of tunnel support. *Rock Mechanics* 6, 189–236.
- Bieniawski, Z.T., 1989. *Engineering rock mass classifications: a complete manual for engineers and geologists in mining, civil, and petroleum engineering*, New York: Wiley.
- Bieniawski, Z.T., 1976. Rock mass classification in rock engineering. In *Exploration for rock engineering, procedures of the symposium*. Z.T. Bieniawski, Cape Town: Balkema 97–106.
- Bieniawski, Z.T., 1973. Engineering Classification of Jointed Rock Masses. *The Civil Engineer in South Africa* 15, 343–353.
- Bollaert, E., Schleiss, A., 2003. Scour of rock due to the impact of plunging high velocity jets Part I: A state-of-the-art review. *Journal of Hydraulic Research* 41, 451–464.
- Boumaiza, L., Saeidi, A., Quirion, M., 2018. Determining rock erodibility parameter "relative block structure" for non-perpendicular hydraulic flow, in: *Proceeding of the 71st Canadian Geotechnical Conference and the 13th Joint CGS/IAH-CNC Groundwater Conference*, Edmonton, Alberta, Canada. p. 7.

- Boumaiza, L., Saeidi, A., Quirion, M., 2019a. Determining relative block structure rating for rock erodibility evaluation in the case of non-orthogonal joint sets. *Journal of Rock Mechanics and Geotechnical Engineering* 11, 72–87.
- Boumaiza, L., Saeidi, A., Quirion, M., 2019b. Development of a method for determining the relevant geomechanical parameters for evaluating the hydraulic erodibility of rock. *Journal of Rock Mechanics and Geotechnical Engineering* (in press).
- Boumaiza, L., Saeidi, A., Quirion, M., 2019c. Determining geomechanical parameters controlling the hydraulic erodibility of rock in dam spillways, in: *Proceeding of the 87th Meeting of the International Commission on Large Dams*, Ottawa, Ontario, Canada. p. 13.
- Castillo, L.G., Carrillo, J.M., 2016. Scour, velocities and pressures evaluations produced by spillway and outlets of dam. *Water* 8, 1–21.
- Cecil, O.S., 1970. Correlations of rock bolt-shotcrete support and rock quality parameters in Scandinavian tunnels. Ph.D thesis., Urbana, University of Illinois.
- Dooge, N., 1993. Die hidrouliese erodeerbaarheid van rotmassas in onbelynde oorlope met spesiale verwysing na die rol van naatvulmateriaal. Master's thesis, University of Pretoria, South Africa.
- Douglas, K., Pells, S., Fell, R., Peirson, W., 2018. The influence of geological conditions on erosion of unlined spillways in rock. *Quarterly Journal of Engineering Geology and Hydrogeology* 51, 219–228.
- Fattahi, H., Varmazyari, Z., Babanouri, N., 2019. Feasibility of Monte Carlo simulation for predicting deformation modulus of rock mass. *Tunnelling and underground space technology* 89, 151–156.
- Hahn, W.F., Drain, M.A., 2010. Investigation of the erosion potential of kingsley dam emergency spillway, in: *Proceeding of the Joint Annual Meeting and Conference of AIPG, AGWT, and the Florida Section of AIPG*, Orlando, Florida, USA. pp. 1–10.
- Henderson, F.M., 1966. *Open Channel Flow*. Macmillan. New York.
- Hoek, E., Corkum, B., Carranza-torres, C., Corkum, B., 2002. Hoek-Brown failure criterion – 2002 Edition, in: *The Fifth North American Rock Mechanics Symposium*, Toronto, Canada. pp. 267–273.
- Hoek, E., Diederichs, M.S., 2006. Empirical estimation of rock mass modulus. *International Journal of Rock Mechanics and Mining Sciences* 43, 203–215.
- Hoek, E., Kaiser, P.K., Bawden, W.F., 1995. *Support of underground excavations in hard rock*. A.A. Balkema/Rotterdam/Brookfield.

- Jennings, J.E., Brink, A.B.A., Williams, A.A.B., 1973. Revised guide to soil profiling for civil engineering purposes in South Africa. *Civil Engineering in South Africa* 15, 3–12.
- Kirsten, H.A.D., 1988. Case histories of groundmass characterization for excavatability. *Rock Classification Systems for Engineering Purposes*. American Society for Testing and Materials, STP 984 102–120.
- Kirsten, H.A.D., 1982. A classification system for excavation in natural materials. *The Civil Engineer in South Africa* 24, 292–308.
- Kirsten, H.A.D., Moore, J.S., Kirsten, L.H., Temple, D.M., 2000. Erodibility criterion for auxiliary spillways of dams. *International Journal of Sediment Research* 15, 93–107.
- Kirsten, H.A.D., Moore, J.S., Kirsten, L.H., Temple, D.M., 1996. Erodibility criterion for auxiliary spillways of dams, in: *ASAE International Meeting*, Phoenix, Arizona, No. 962099.
- Laugier, F., Leturcq, T., Blancet, B., 2015. Stabilité des barrages en crue : Méthodes d'estimation du risque d'érodabilité aval des fondations soumises à déversement par-dessus la crête, in: *Proceeding de La Fondation Des Barrages*. Chambéry, France. pp. 125–136.
- Moore, J.S., 1991. The characterization of rock for hydraulic erodibility. *SCS Technical Release - 78*, Northeast National Technical Center, Chester. PA.
- Moore, J.S., Temple, D.M., Kirsten, H.A.D., 1994. Headcut advance threshold in earth spillways. *Bulletin of the Association of Engineering Geologists* 31, 277–280.
- Mörén, L., Sjöberg, J., 2007. Rock erosion in spillway channels – A case study of the Ligga spillway, in: *Proceedings of 11th Congress of the International Society for Rock Mechanics*, Lisbon, Portugal. pp. 87–90.
- Palmstrom, A., 1995. RMI--a rock mass characterization system for rock engineering purposes. Ph.D. thesis, University of Oslo, Norway.
- Pells, S.E., 2016. Erosion of rock in spillways. Ph.D thesis, University of New South Wales, Australia.
- Pells, S.E., Pells, P.J.N., Peirson, W.L., Douglas, K., Fell, R., 2015. Erosion of unlined spillways In *Rock - does a “scour threshold” exist?*, in: *Proceeding of Australian National Committee on Large Dams*. Brisbane, Queensland, Australia. pp. 1–9.
- Pitsiou, S., 1990. The effect of discontinuities of the erodibility of rock in unlined spillways of dams. Master's thesis, University of Pretoria, South Africa.

Rock, A.J., 2015. A semi-empirical assessment of plung pool scour: Two-dimensional application of Annandale's Erodibility Method on four dams in British Columbia, Canada. Master's thesis, University of British Columbia. Vancouver, British Columbia, Canada.

Rocsciences, 2019. <https://www.rocscience.com/>.

Van Schalkwyk, A., 1989. Waternavorsingskommissie: Verslag oor loodsondersoek: Die erodeerbaarheid van verskillende rotsformasies in onbeklede damoorlope,. Unpublished report, University of Pretoria, South Africa.

Van Schalkwyk, A., Jordaan, J.M., Dooge, N., 1994a. Erosion of rock in unlined spillways, in: Proceeding of International Commission on Large Dams, Paris, 71 (37). pp. 555–571.

Van Schalkwyk, A., Jordaan, J.M., Dooge, N., 1994b. Die Erodeerbaarheid van Verskillende Rotsformasies Onder Varierende Vloeitoestande. Tech. Rep. WNK Verslag No. 302/1/95, verslag aan die waternavorsingskommissie deur die Departement of Geologie, Universiteit van Pretoria, South Africa.

CHAPTER 6 – CONCLUSIONS

Although “scour threshold line” methods are commonly used for evaluating the hydraulic erodibility of rock during the dam spillway design phase, in some cases the rock erosion is observed after spill events. This raises questions regarding the evaluation of rock erodibility potential. Inaccuracies related to the evaluation of hydraulic rock scour certainly exist when evaluating the hydraulic condition of flowing water and assessing the rock mass resistance capacity. In this thesis, particular focus is placed on the rock mass. Regarding the first objective of this thesis and starting from the fundamentals of the commonly used methods for evaluating hydraulic rock scour, it is concluded that improving knowledge of the rock mass parameters is a key step for ensuring the optimal evaluation of the rock mass resistance capacity. As hydraulic rock scour is a complex mechanism governed by a specific set of rock mass parameters, its evaluation requires refining the erodibility index.

In regard to the second objective of this thesis, the original concept of the relative block structure parameter based on an orthogonal fracture system is adjusted to propose a new rating, of the relative block structure parameter, adapted for non-orthogonal fracture systems. Furthermore, using datasets from previous case studies of eroded unlined spillways, the third objective of this thesis is achieved as a method is developed for identifying the relevant rock mass parameters to be used when evaluating the hydraulic erodibility of rock. The fourth and fifth objectives of this thesis are also attained. A comparative analysis approach evaluated the reliability of

the most common methods used for evaluating the hydraulic erodibility. Coupled with the identification of the key rock mass parameters to be used for evaluating the rock resistance capacity, a novel method is developed for determining the relative importance of rock mass parameters that govern the hydraulic erodibility of rock. All told, all objectives planned in this thesis were attained.

The most important findings of the thesis are presented below.

6.1 Determining the relative block structure rating for evaluating rock erodibility in the case of non-orthogonal joint sets

Kirsten's initial concept of relative block structure having an angle of 90° between the two joint sets, an orthogonal fracture system, represents a situation that occurs only when the direction of flow is perpendicular to the strike of the closer spaced joint set. If the direction of flow is not perpendicular, Kirsten suggested taking the apparent dip of the closer spaced joint set in the vertical plane containing the direction of flow to determine the J_s value. However, it is argued in Chapter 3 that the change of angle between the two joint sets, along the vertical plane containing the direction of flow, should also be considered. Such a situation where this angle differs from 90° (on the vertical plane containing the direction of flow) is equivalent to a flow having a direction that is effectively perpendicular to the strike of the closer spaced joint set, but in a non-orthogonal fracture system. In practice, Kirsten's index

is applied to all cases, including non-orthogonal fracture systems, by assuming a certain lack of precision in terms of assessing the rock mass resistance capacity.

Instead of applying a sole equation for determining the J_s parameter in all cases, two equations are proposed in this thesis. One equation is applied when blocks are oriented in the direction of flow, while the second is applied when blocks are oriented against the direction of flow. These two equations are used for determining the J_s parameter for the orthogonal and the non-orthogonal fracture systems as it is observed that the results obtained from two proposed equations agree perfectly with those obtained through Kirsten's concept for the orthogonal fracture system.

Non-orthogonal fracture systems reflect cases that actually occur in the field, and it is concluded that assuming an orthogonal fracture system in cases representing a non-orthogonal fracture system can create discrepancies when assessing rock mass resistance capacity.

6.2 A method for determining the relevant geomechanical parameters when evaluating the hydraulic erodibility of rock

From the review of the different rock mass parameters included in the erodibility indices used to evaluate the rock mass resistance capacity, there is no clear consensus on those rock mass parameters that are indeed relevant for evaluating the hydraulic erodibility of rock. As such, a novel method derived from existing case

studies of eroded spillways is developed in this thesis to determine the relevant rock mass parameters for evaluating the hydraulic erodibility of rock.

The UCS and J_s parameters included in Kirsten's index have no large effect on erodibility. However, the E_{doa} parameter, which can be considered as synonymous with the J_s parameter, given that it considers a rock block's shape and orientation relative to the direction of flow, was deemed to be a relevant parameter for evaluating hydraulic rock scour. A similar observation was noted for evaluating rock block size as the K_b parameter, included in Kirsten's index, was determined to be not relevant when compared to the V_b parameter. Using the rock block volume measurements can improve the characterization of rock block size and, consequently, improve the evaluation of rock resistance capacity. It is pertinent to note that an accurate evaluation of any rock mass parameter is of utmost importance. As already mentioned, the K_b and V_b parameters are both used for evaluating rock block size. However, it is demonstrated in the thesis that the V_b parameter provides a more accurate evaluation of rock block size, given its more accurate results when compared to that of K_b .

From the large suite of analyzed rock mass parameters, J_o , K_d , V_b , E_{doa} , $NPES$, and E_{rm} were retained as relevant rock mass parameters for evaluating the hydraulic erodibility of rock because they all showed a logical sequence of sensitivity curves to erodibility. Determining the relevant rock mass parameters for evaluating the hydraulic erodibility of rock is a key step in developing a new erodibility index that provides a more accurate assessment of the hydraulic erodibility of rock.

6.3 A method to determine the relative importance of rock mass parameters that control the hydraulic erodibility of rock

The comparison performed on the various “scour threshold line” methods used to evaluate hydraulic rock scour illustrated that these methods are subject to a certain level of committed error. However, the comparison between the methods based on Kirsten’s index and those proposed recently by Pells (*eGSI* and *RMEI*) has demonstrated that improvement is noted when the recently developed erodibility indices (*RMEI* and *eGSI*) are used. These new indices are recommended because they are proposed in particular for evaluating the hydraulic erodibility of rock; this is in contrast to Kirsten’s index that was proposed initially for evaluating the mechanical excavatability of earth materials. However, the efficacy of these Pells’s indices is not the same as the evaluation of rock erosion differs somewhat between these two indices.

Particular attention is given, in this study, to rock mass parameters by determining the relevant rock mass parameters for evaluating hydraulic rock scour and the relative importance of rock mass parameters that govern the hydraulic erodibility mechanism. The relative importance of the selected rock mass parameters was determined using a method developed in this study. Each rock mass parameter can be characterized effectively by a specific relative importance. The analyzed rock mass parameters are ranked in the following order: 1) K_d , 2) $NPES$, 3) V_b , 4) J_o , 5) E_{doa} , and 6) E_{rm} . This order agrees largely with that based on field observations.

Determining the relative importance of rock mass parameters is very helpful tool that can be used to judge the rock mass resistance capacity during the design phase of new unlined spillways. Indeed, spillways should be excavated in rock masses characterized by high quality values for the most important rock mass parameters that govern erosion; otherwise, the rock mass will be more susceptible to be eroded. Determining the relative importance of rock mass parameters can also be a useful step in developing a new hydraulic erodibility index that provides a more accurate assessment of rock resistance capacity.

6.4 Perspectives for future research

The topics cited below were identified during this research work as interesting research avenues that merit further investigation and research.

(1) In this thesis, the rock mass parameters were analysed individually to determine the relevant parameters for evaluating hydraulic rock scour and their relative importance within the mechanism of erosion. Determining the interactions between the various rock mass parameters during erosion is strongly recommended as a future research direction.

(2) Given the limited experimental analyses dealing with hydraulic rock scour, small-scale experimental laboratory analyses are strongly recommended for

future research. Small physical models representing unlined spillways could be developed using small-scale rock blocks and then trying to simulate the actual rock mass parameters. As a second step, the small physical model could be reproduced at a larger scale to provide more realistic analyses. These physical modes can be used to verify the findings of this thesis; for example, using the modes to confirm the rock mass parameters governing the hydraulic rock scour.

(3) Given the effectiveness of the numerical tools, numerical modeling can be envisioned using distinct element methods, such as UDEC or 3DEC, to analyse the three main issues studied in this thesis: (i) the effect of rock block's shape and orientation relative to the direction of flow, (ii) the relevant rock mass parameters for evaluating the erodibility of rock, and (iii) the relative importance of rock mass parameters governing hydraulic rock scour. Furthermore, numerical modeling is advantageous when physical model equipment cannot be easily installed.

APPENDICES

Appendix A: Description of rock mass parameters rating (Kirsten 1982)

Table A.1. Mass strength rating (Kirsten 1982)

Hardness	Identification in profile	Unconfined compressive strength (MPa)	Mass strength number (M_s)
Very soft rock	Material crumbles under firm (moderate) blows with sharp end of geological pick and can be peeled off with a knife; it is too hard to cut a triaxial sample by hand	1.7	0.87
	Can just be scraped and peeled with a knife; indentations 1 mm to 3 mm show in the specimen with firm (moderate) blows of the pick point	1.7 – 3.3	1.86
Soft rock	Can just be scraped and peeled with a knife; indentations 1 mm to 3 mm show in the specimen with firm (moderate) blows of the pick point	3.3 – 6.6	3.95
	Cannot be scraped or peeled with knife; hand-held specimen can be broken with hammer end of a geological pick with a single firm (moderate) blow	6.6 – 13.2	8.39
Hard rock	Cannot be scraped or peeled with knife; hand-held specimen can be broken with hammer end of a geological pick with a single firm (moderate) blow	13.2 – 26.4	17.70
Very hard rock	Hand-held specimen breaks with hammer end pick under more than one blow	26.4 – 53.0	35
	Specimen requires many blows with geological pick to break through intact material	53.0 – 106	70
Extremely hard rock (very, very hard rock)	Specimen requires many blows with geological pick to break through intact material	106 – 212	140
		212	280

Table A.2: Joint sets rating (Kirsten 1982)

Number of joint sets	Joint set number (J_n)
Intact, no or few joint/fissures	1.00
One joint/fissure set	1.22
One joint/fissure set plus random	1.50
Two joint/fissure set	1.83
Two joint/fissure set plus random	2.24
Three joint/fissure set	2.73
Three joint/fissure set plus random	3.34
Four joint/fissure set	4.09
Multiple joint/fissure set	5.00

Table A.3: Joint roughness rating (Kirsten 1982)

Joint separation	Condition of joint	Joint roughness number (J_r)
	Discontinuous joint/fissures	4.0
	Rough or irregular, undulating	3.0
	Smooth undulating	2.0
Joint/fissures tight or closing during excavation	Slickenside undulating	1.5
	Rough or irregular, planar	1.5
	Smooth planar	1.0
	Slickenside planar	0.5
Joints/fissures open and remain open during excavation	Joints/fissures either open or containing relatively soft gouge of sufficient thickness to prevent joint/fissure wall contact upon excavation	1.0
	Shattered or micro-shattered clays	1.0

Table A.4: Joint alteration rating (Kirsten 1982)

Description of gouge	Joint alteration number (J_a) for joint separation (mm)		
	<1 ¹	1 - 5 ²	>5 ³
Tightly healed, hard, non-softening impermeable filling	0.75	-	-
Unaltered joint walls, surface staining only	1	-	-
Slightly altered, non-softening, non-cohesive rock mineral or crushed rock filling	2	4	6
Non-softening, slightly clayey, non-cohesive filling	3	6	10
Non-softening strongly over-consolidated clay mineral filling, with or without crushed rock	3 ⁴	6	10
Softening or low friction clay mineral coatings and small quantities of swelling clays	4	8	13
Softening moderately over-consolidated clay mineral filling, with or without crushed rock	4	8	13
Shattered or micro-shattered (swelling) clay gouge, with or without crushed rock	5	10	18

1: Joint walls effectively in contact

2: Joint walls come into contact after approximately 100 mm shear

3: Joint walls do not come into contact at all upon shear

4: Values asterisked added to Barton's data

Table A.5: Relative block structure rating (Kirsten 1982)

Dip direction ¹ of the closer spaced joint set (°)	Dip angle ² of the closer spaced joint set (°)	Ratio of joint spacing (r)			
		1:1	1:2	1:4	1:8
		Values of relative block structure (J_s)			
180/0	90	1	1	1	1
In the direction of excavation	85	0.72	0.67	0.62	0.56
	80	0.63	0.57	0.5	0.45
	70	0.52	0.45	0.41	0.38
	60	0.49	0.44	0.41	0.37
	50	0.49	0.46	0.43	0.4
	40	0.53	0.49	0.46	0.44
	30	0.63	0.59	0.55	0.53
	20	0.84	0.77	0.71	0.68
	10	1.22	1.1	0.99	0.93
	5	1.33	1.2	1.09	1.03
0/180	0	1	1	1	1
Against the direction of excavation	5	0.72	0.81	0.86	0.9
	10	0.63	0.7	0.76	0.81
	20	0.52	0.57	0.63	0.67
	30	0.49	0.53	0.57	0.59
	40	0.49	0.52	0.54	0.56
	50	0.53	0.56	0.58	0.6
	60	0.63	0.67	0.71	0.73
	70	0.84	0.91	0.97	1.01
	80	1.22	1.32	1.4	1.46
	85	1.33	1.39	1.45	1.5
180/0	90	1	1	1	1

1: Dip direction of the closer spaced joint set relative to the direction of excavation

2: Apparent dip of the closer spaced joint set in the vertical plane containing the direction of excavation

3: For intact material, $J_s = 1$

4: For values of r less than 0.125, take J_s as for $r = 0.125$

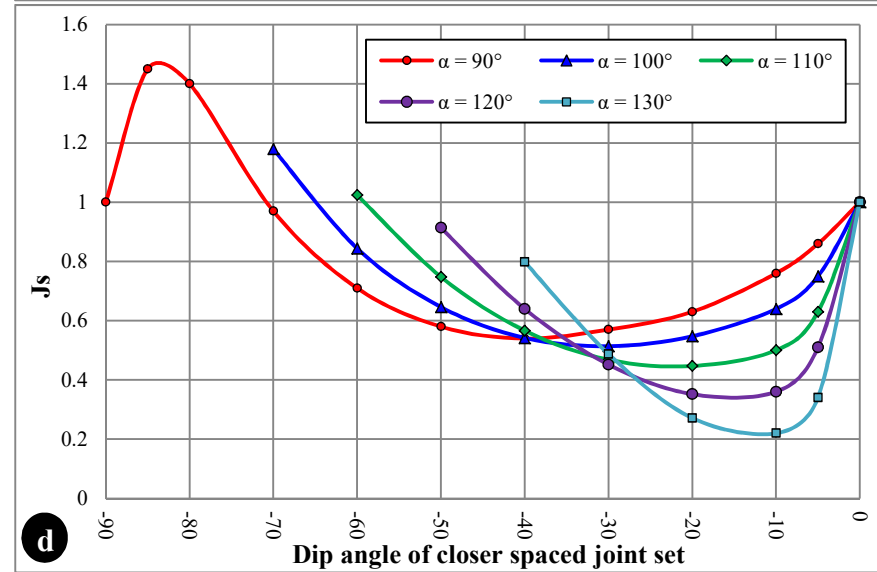
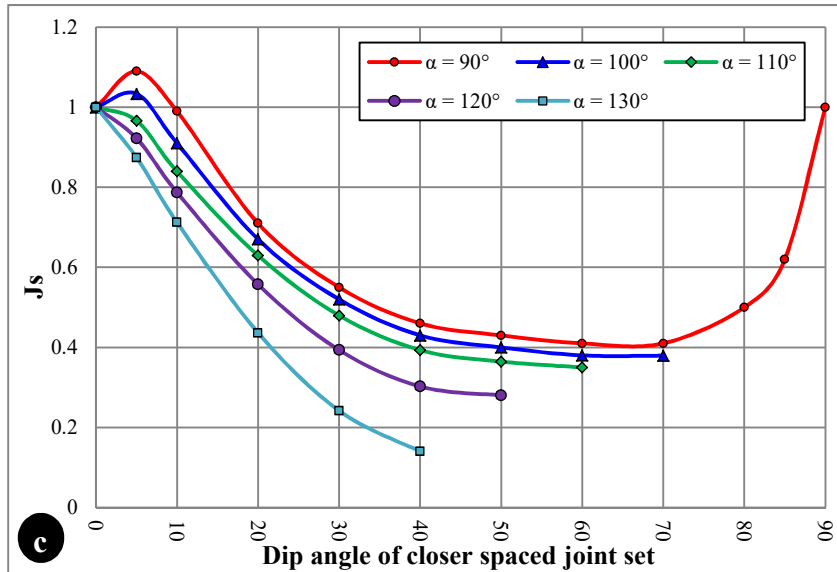
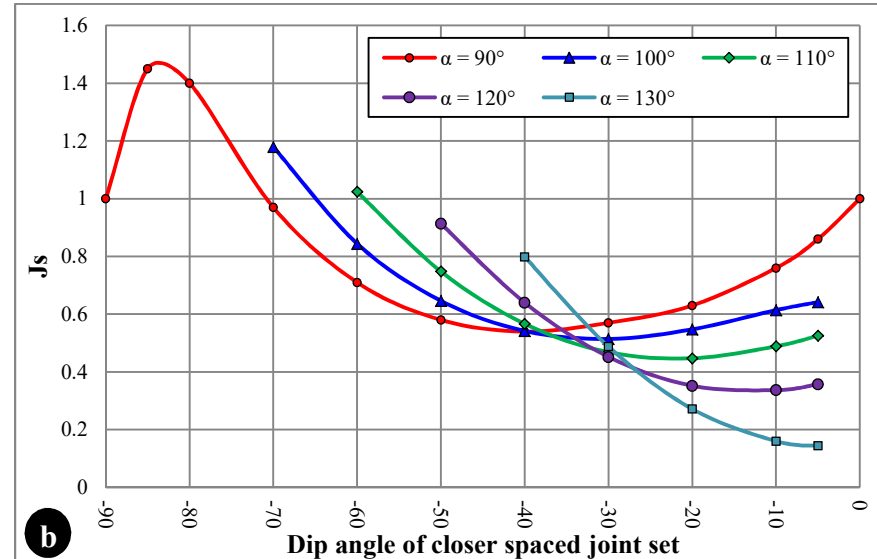
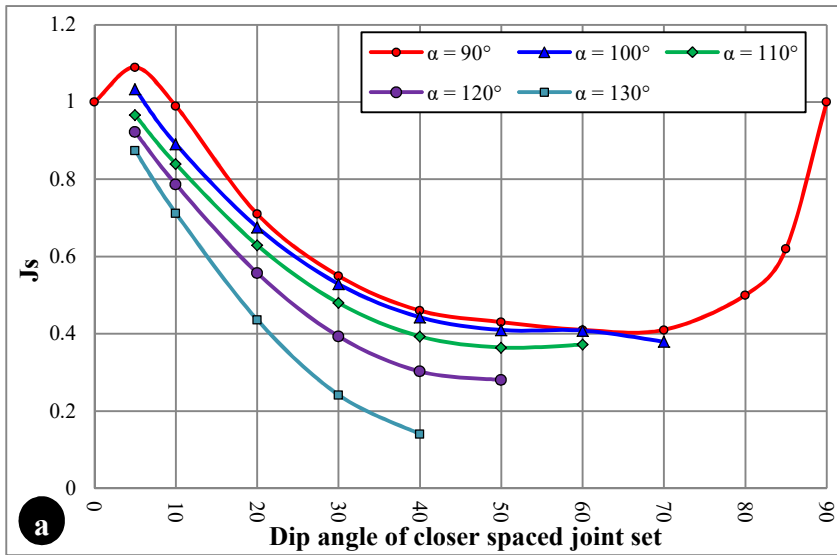
Appendix B. Relative block structure rating (Annandale 1995, 2006)

Dip direction of the closer spaced joint set (°)	Dip angle of the closer spaced joint set (°)	Ratio of joint spacing (r)				
		1:1	1:2	1:4	1:8	
		Values of relative block structure (J_s)				
In the direction of stream flow	180/0	90	1.14	1.20	1.24	1.26
		89	0.78	0.71	0.65	0.61
		85	0.73	0.66	0.61	0.57
		80	0.67	0.60	0.55	0.52
		70	0.56	0.50	0.46	0.43
		60	0.50	0.45	0.42	0.40
		50	0.49	0.46	0.43	0.41
		40	0.53	0.49	0.46	0.45
		30	0.63	0.59	0.55	0.53
		20	0.84	0.77	0.71	0.67
		10	1.25	1.10	0.98	0.90
	5	1.39	1.23	1.09	1.01	
	1	1.50	1.33	1.19	1.10	
Against the direction of stream flow	0/180	0	1.14	1.09	1.05	1.02
		1	0.78	0.85	0.90	0.94
		5	0.73	0.79	0.84	0.88
		10	0.67	0.72	0.78	0.81
		20	0.56	0.62	0.66	0.69
		30	0.50	0.55	0.58	0.60
		40	0.49	0.52	0.55	0.57
		50	0.53	0.56	0.59	0.61
		60	0.63	0.68	0.71	0.73
		70	0.84	0.91	0.97	1.01
		80	1.26	1.41	1.53	1.61
	85	1.39	1.55	1.69	1.77	
	89	1.50	1.68	1.82	1.91	
180/0	90	1.14	1.20	1.24	1.26	

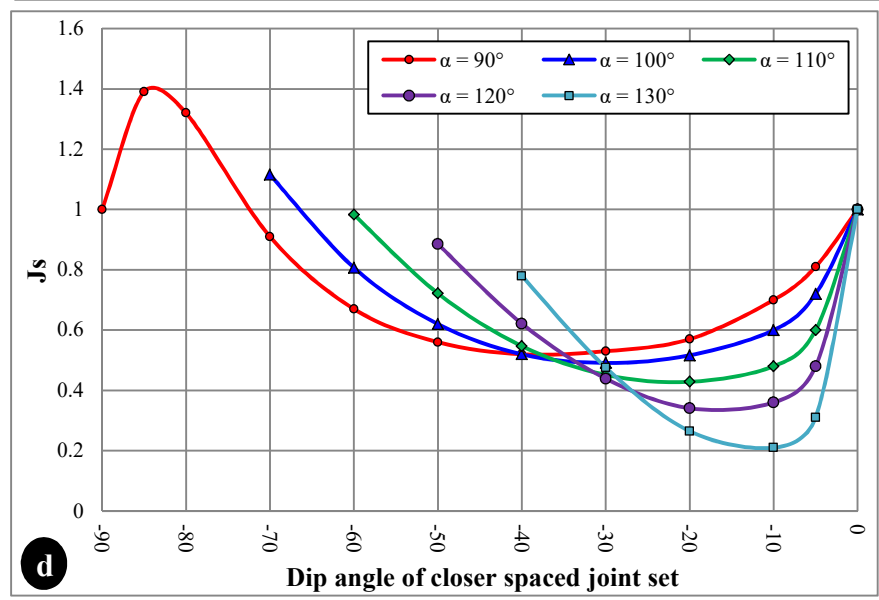
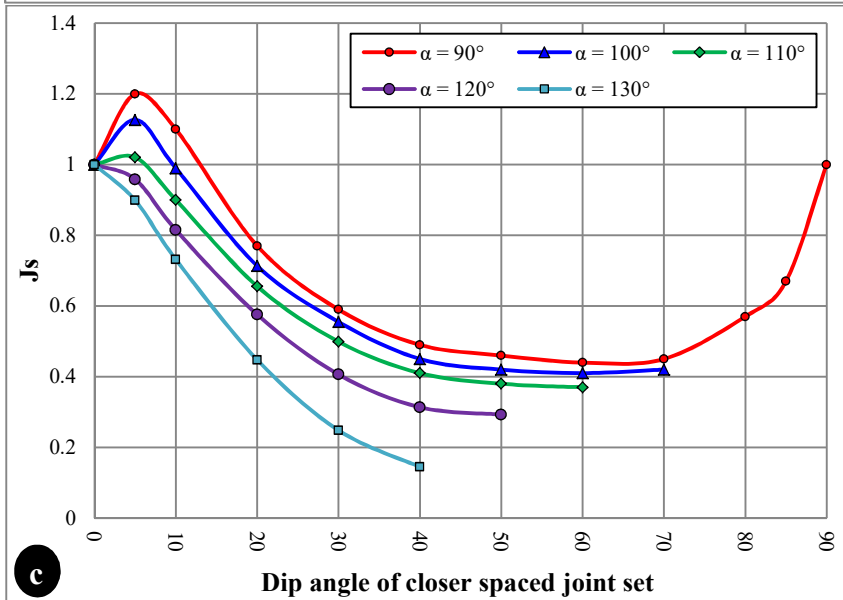
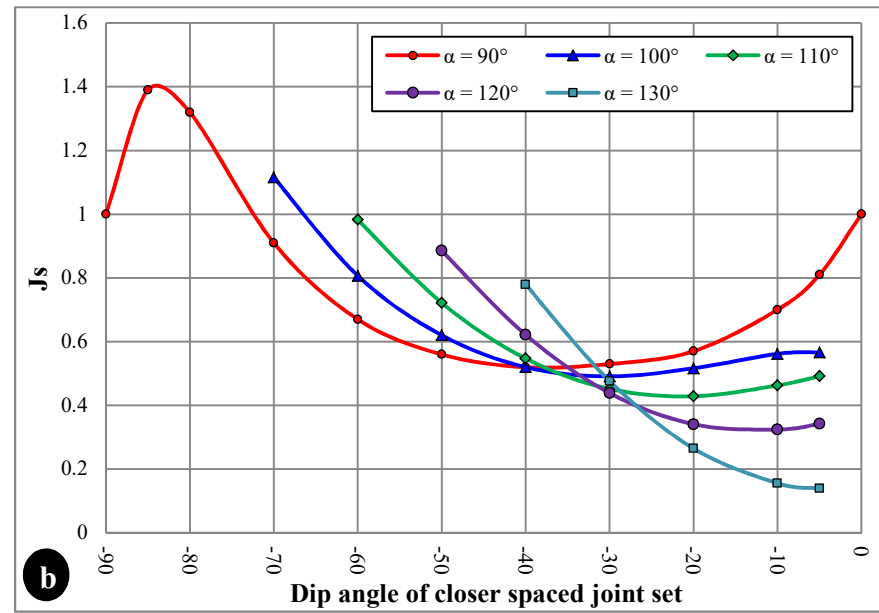
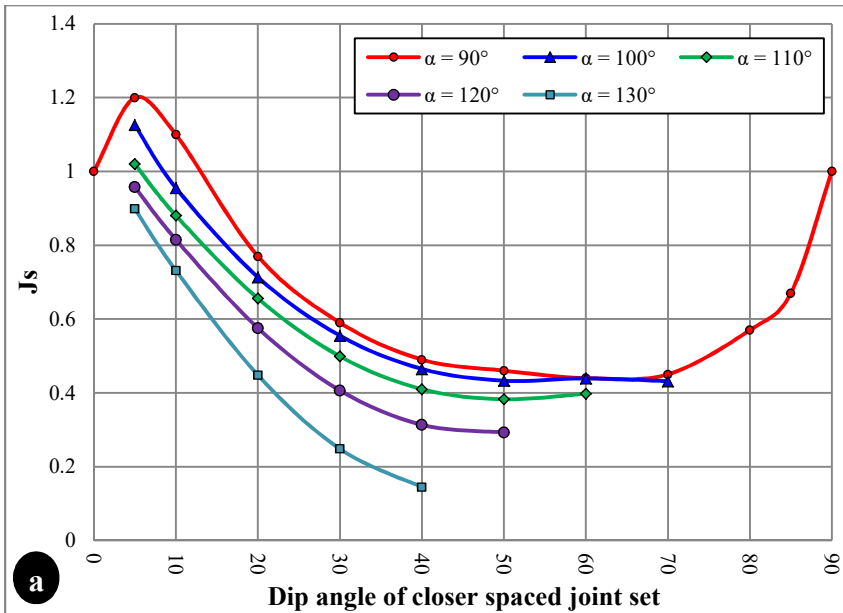
1: For intact material, $J_s = 1$

2: For values of r great than 8, take J_s as for $r = 8$

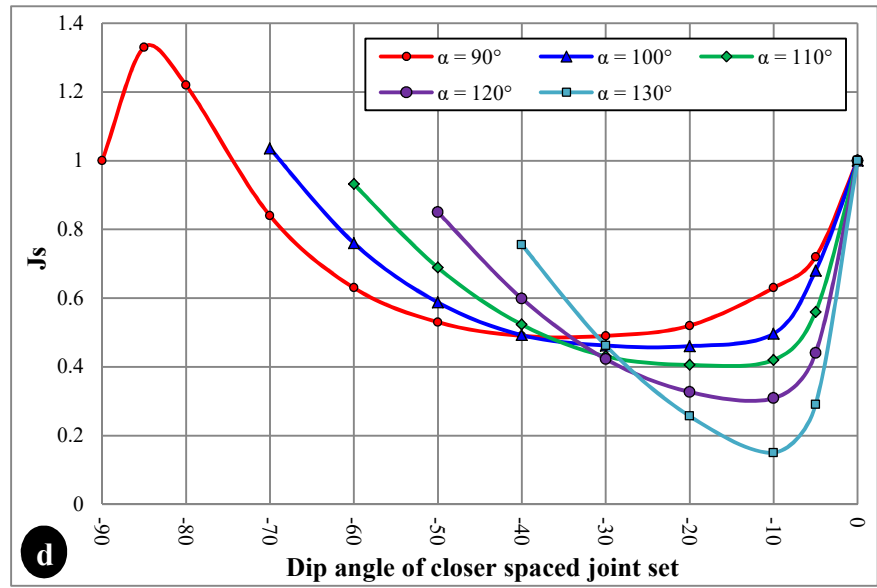
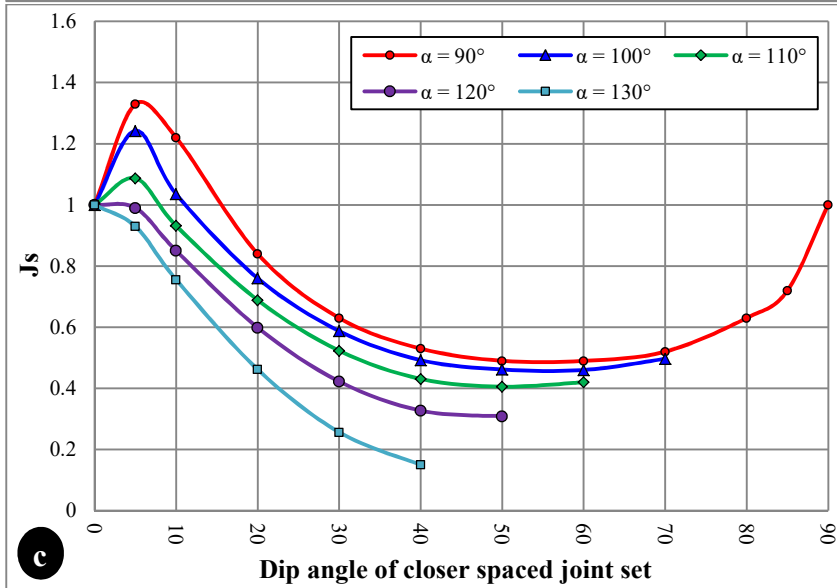
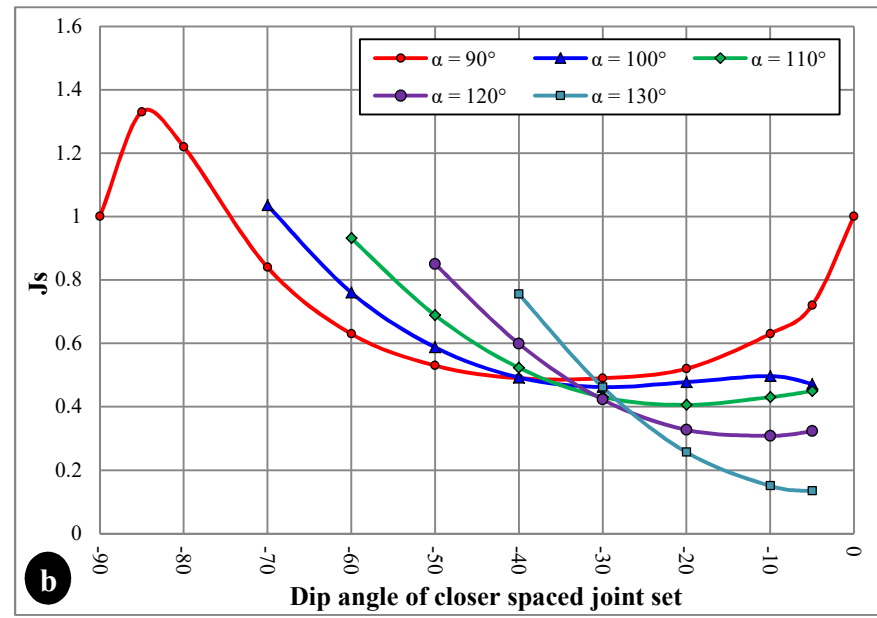
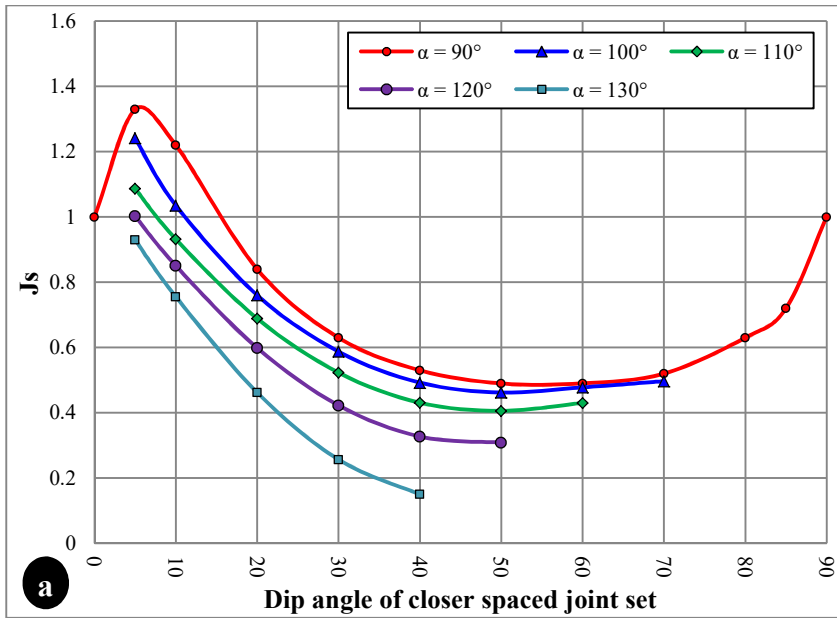
Appendix C.1 Curves before and after adjustment for a RJS of 4, 2 and 1 ($\alpha > 90^\circ$).



J_s curves when RJS = 4: a) Before adjustment-in the direction of flow; b) Before adjustment-against the direction of flow; c) After adjustment-in the direction of flow; d) After adjustment-against the direction of flow.

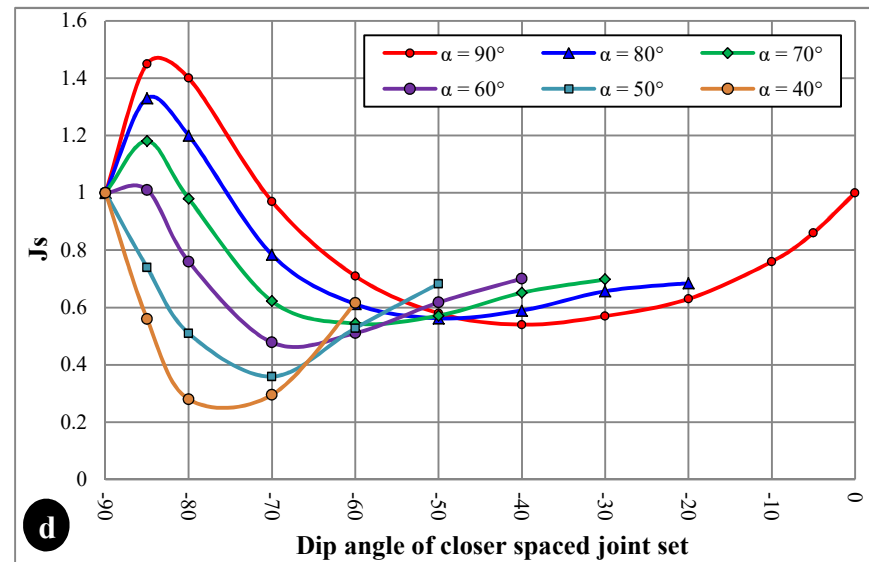
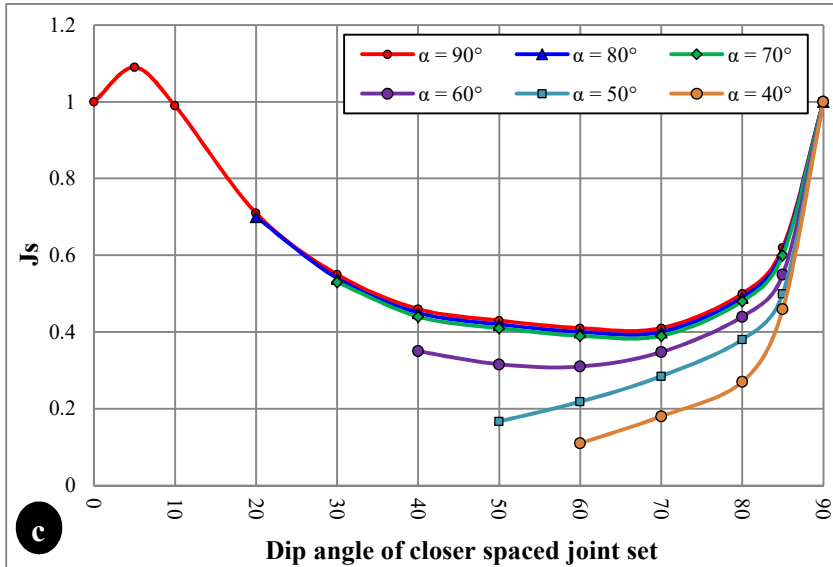
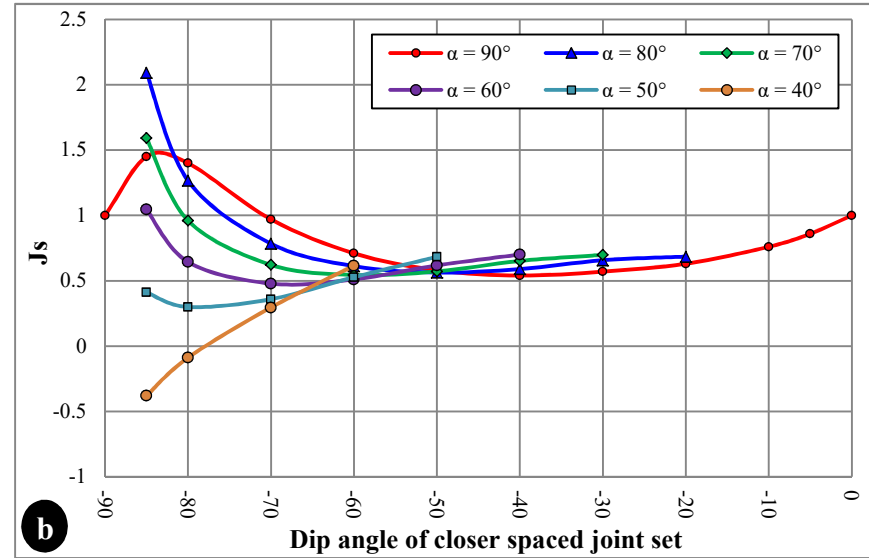
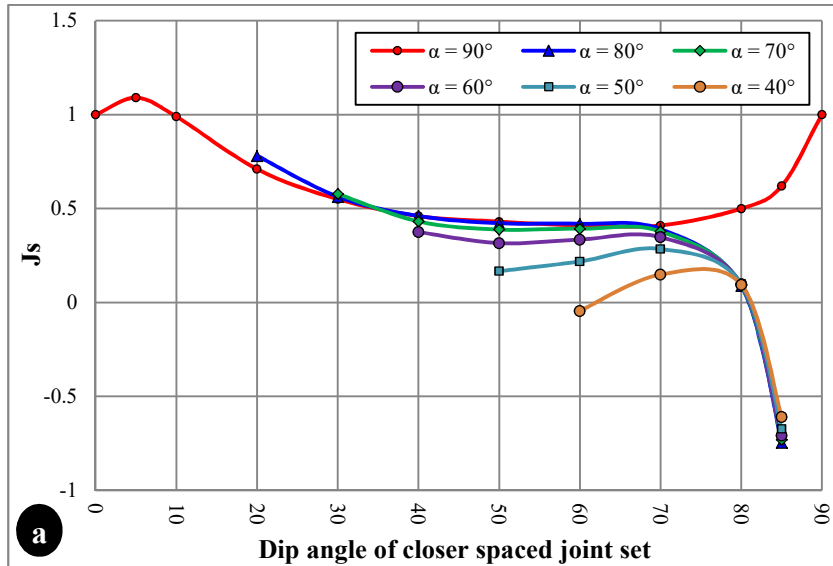


J_s curves when RJS = 2: a) Before adjustment-in the direction of flow; b) Before adjustment-against the direction of flow; c) After adjustment-in the direction of flow; d) After adjustment-against the direction of flow.

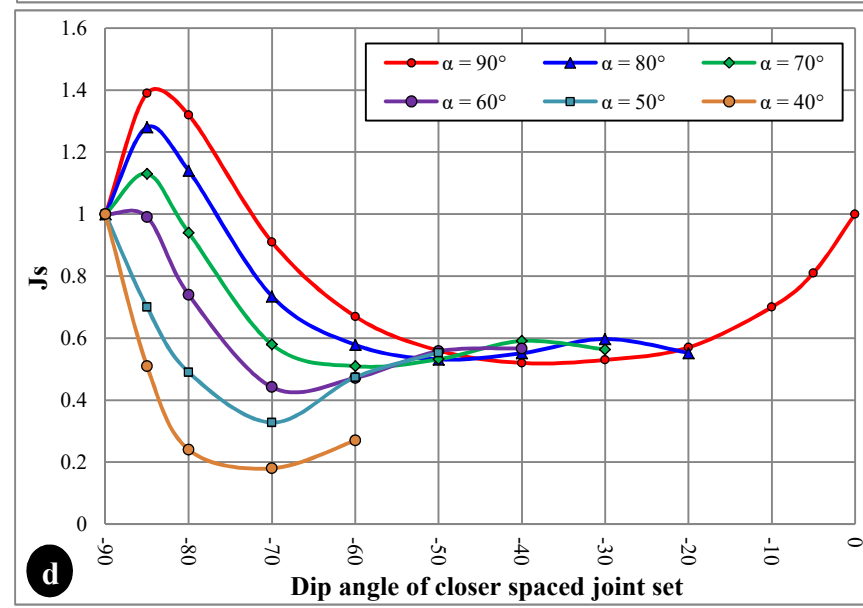
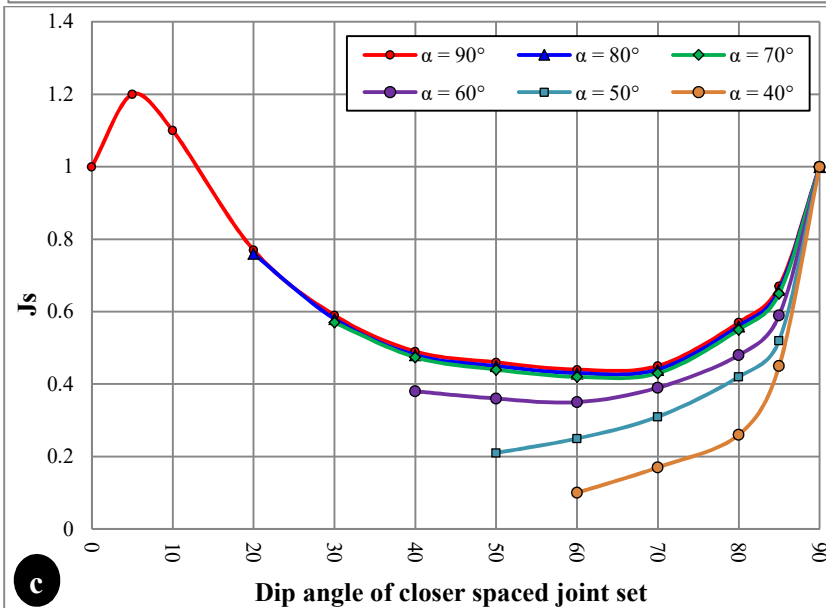
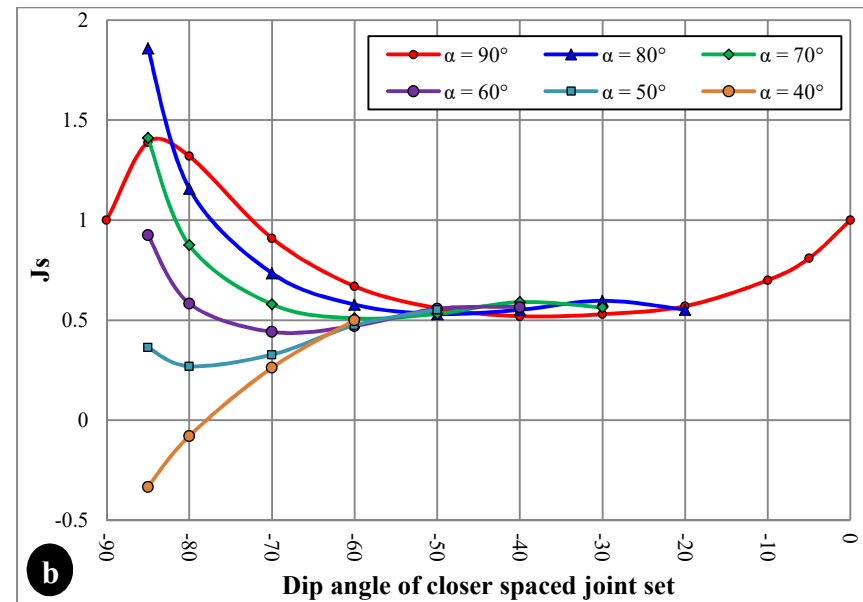
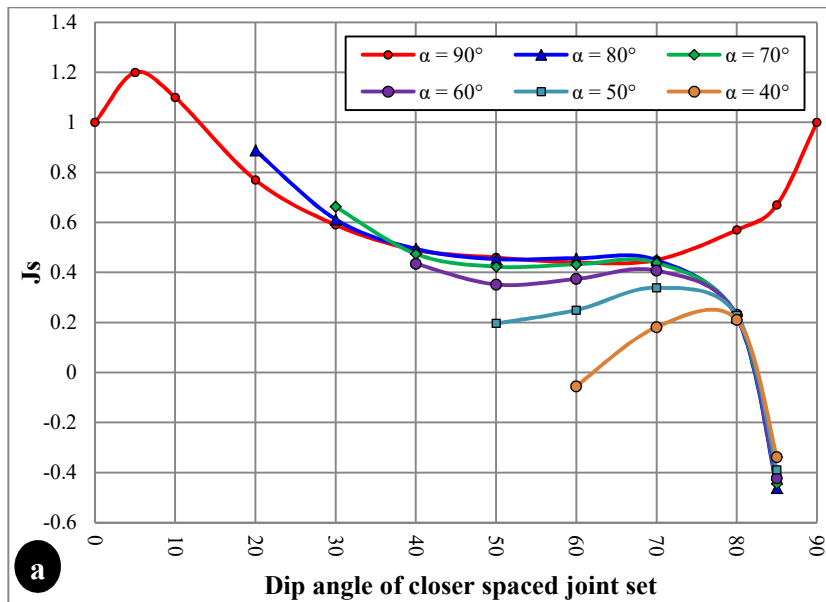


Js curves when RJS = 1: a) Before adjustment-in the direction of flow; b) Before adjustment-against the direction of flow; c) After adjustment-in the direction of flow; d) After adjustment-against the direction of flow.

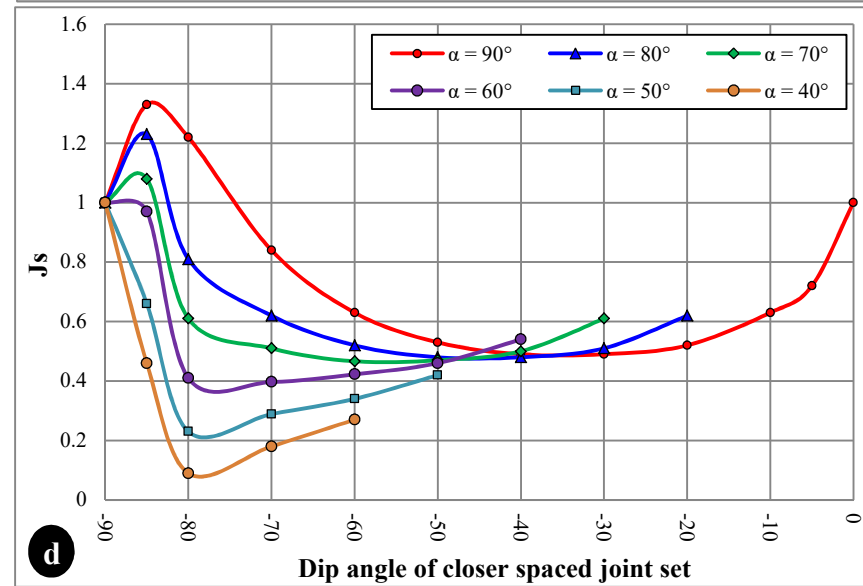
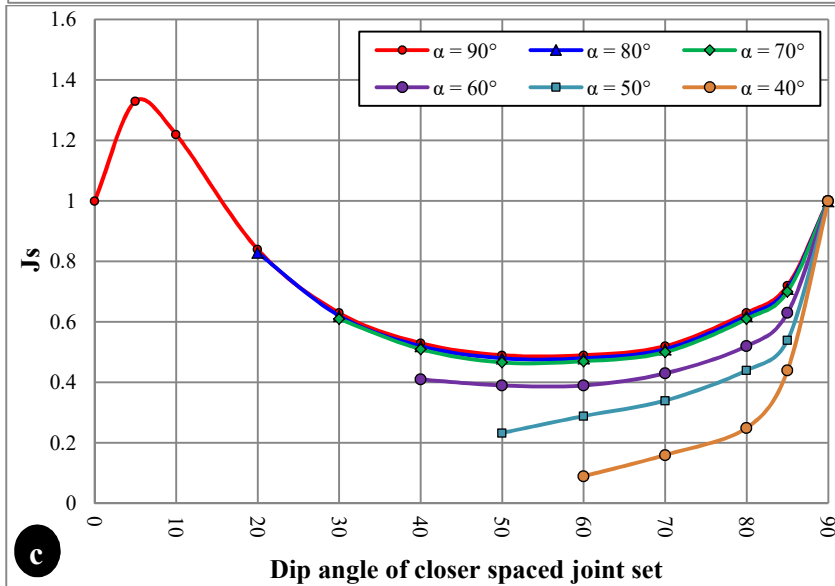
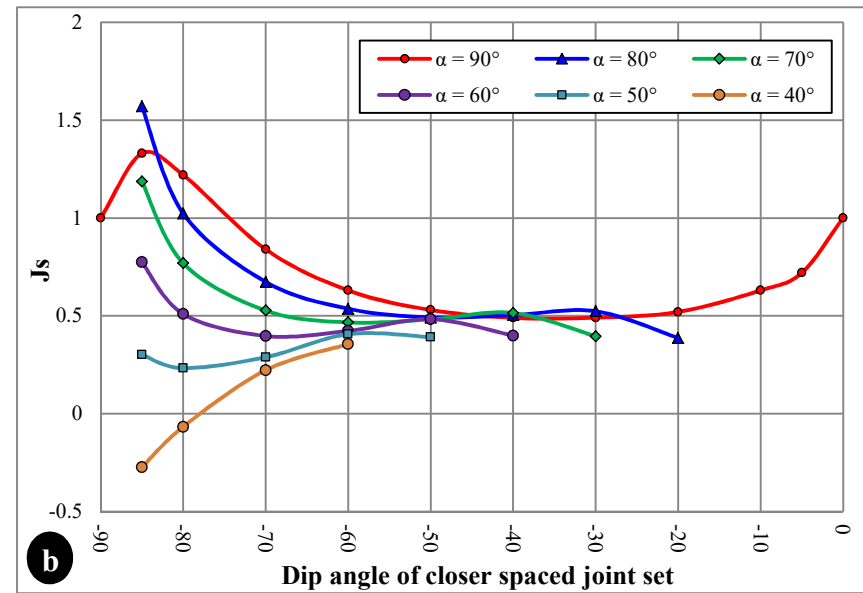
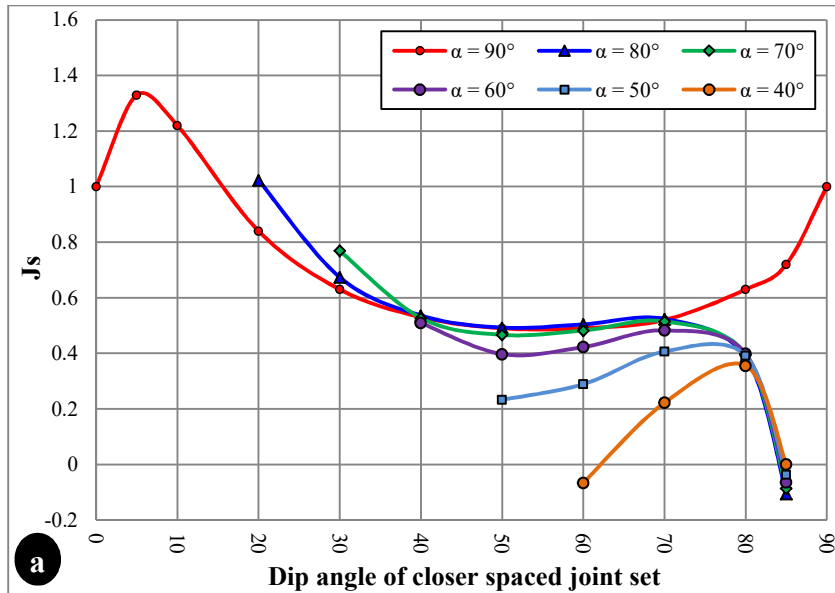
Appendix D. Curves before and after adjustment for a RJS of 4, 2 and 1 ($\alpha < 90^\circ$).



J_s curves when RJS = 4: a) Before adjustment-in the direction of flow; b) Before adjustment-against the direction of flow; c) After adjustment-in the direction of flow; d) After adjustment-against the direction of flow.



J_s curves when RJS = 2: a) Before adjustment-in the direction of flow; b) Before adjustment-against the direction of flow; c) After adjustment-in the direction of flow; d) After adjustment-against the direction of flow.



J_s curves when RJS = 1: a) Before adjustment-in the direction of flow; b) Before adjustment-against the direction of flow; c) After adjustment-in the direction of flow; d) After adjustment-against the direction of flow.

Appendix E. Summary of the data used in this study (Chapter 4)

ID	UCS (MPa)	K _b	K _a	J ₀ (mm)	J ₁	E _{doa}	NPES	Erosion condition	P _a (kW/m ²)	ID	UCS (MPa)	K _b	K _a	J ₀ (mm)	J ₁	E _{doa}	NPES	Erosion condition	P _a (kW/m ²)
Ant. 1	35	17.70	2.00	<1	0.7	-8	4	Minor	1.7	Haa.4	13	5.90	0.33	2.5-10	0.48	-15	-	Large	2
Ant. 2	35	11.74	2.00	0.1-0.5	0.7	-8	3	Negligible	0.8	Har.1	140	25.07	0.50	<1	1	-5	4	Minor	0.6
Ant. 3	35	17.70	2.00	1-2	0.7	-8	4	Minor	0.7	Har.2	140	32.61	0.50	1-2	1	-5	4	Minor	1
Ant. 4	35	27.17	2.00	2-5	1	-18	2	Moderate	6.3	Har.3	140	30.52	1.00	<1	1	-5	4	Minor	1
App.1	50	18.32	0.38	0.5-2.5	0.6	-5	3	Negligible	2.6	Har.4	140	32.61	1.00	-	1.1	-10	4	Minor	56
App.2	50	18.32	0.38	0.5-2.5	0.6	-8	3	Minor	15	Hart.1	180	20.96	1.25	0.1-0.5	0.8	-5	4	Negligible	44
Bro.1	100	25.36	1.47	1-2	1	-3	4	Minor	6.4	Hart.2	16	11.98	0.25	0.5-2.5	0.8	-15	4	Moderate	50
Bro.2	100	20.65	1.33	1-2	1	-3	4	Moderate	28	Hart.3	180	20.96	1.25	0.1-0.5	0.8	-5	4	Negligible	18
Bro.3	100	21.74	1.33	2-5	0.77	-15	4	Moderate	42	Kam.1	140	11.98	0.20	0.1-0.5	1.1	-8	4	Minor	4.5
Bro.4	100	21.74	1.33	<1	0.77	-17	4	Moderate	56	Kam.2	140	19.56	2.00	0.1-0.5	1.1	-8	2	Negligible	27
Bro.5	100	42.25	1.33	2-5	1	-10	4	Negligible	28	Kam.3	30	7.33	0.25	0.5-2.5	1.1	-8	4	Moderate	27
Bro.6	100	52.63	1.33	<1	1	-3	2	Minor	37	Kam.4	30	7.33	0.25	0.5-2.5	1.1	-25	-	Large	49
Bro.7	100	23.60	1.33	1-2	0.77	-15	4	Large	56	Kam.5	30	2.44	1.00	0.5-2.5	1.1	-5	3	Minor	14
Bur.1	280	32.61	1.25	<1	1	-3	2	Negligible	165	Kli.1	200	18.34	3.00	0.1-0.5	1	-5	3	Negligible	1.2
Bur.2	280	22.44	1.25	<1	1	-5	2	Negligible	165	Kli.2	11	3.67	0.17	2.5-10	1	-13	4	Minor	6
Bur.3	280	28.99	0.75	1-2	1	-10	3	Moderate	165	Kli.3	11	3.67	0.17	2.5-10	1	-13	4	Moderate	11.4
Bur.4	280	27.17	0.48	2-5	1	-10	3	Large	165	Kli.4	200	18.34	3.00	0.1-0.5	1	-8	3	Minor	6.5
Cat.1	140	21.20	2.50	0.1	0.5	-13	3	Minor	60	Kli.5	11	3.67	0.17	2.5-10	1	-13	4	Minor	6.5
Cat.2	140	21.20	2.50	0.1	0.5	-13	1	Negligible	60	Kun.1	140	25.36	2.00	0-3	0.85	-8	3	Minor	35
Cat.3	140	21.20	2.50	0.1	0.5	-13	3	Large	60	Mac.1	18	3.62	2.00	<1	1	-13	3	Minor	1.1
Cop.1	280	20.65	0.25	0.5-2.5	0.5	-15	4	Moderate	5.7	Mac.2	9	3.62	0.50	<1	1	-13	3	Minor	1.1
Cop.10	280	9.98	1.33	0.5-2.5	1	-25	3	Extensive	650	Mac.3	9	3.62	2.00	<1	1	-13	3	Minor	2.6
Cop.11	280	20.65	0.25	0.5-2.5	0.5	-15	4	Minor	10	Mok.1	140	25.64	1.50	0.1-0.5	1	-8	2	Negligible	0.6
Cop.12	280	22.44	1.33	0.5-2.5	1	-10	3	Moderate	97	Mok.2	70	2.44	0.17	0.5-2.5	1	-17	5	Moderate	1.4
Cop.13	280	22.44	1.33	0.5-2.5	1	-15	3	Moderate	145	Mok.4	140	25.64	1.50	0.1-0.5	1	-8	2	Negligible	1.3
Cop.2	280	22.44	1.33	0.5-2.5	1	-10	3	Minor	4.7	Mok.5	140	25.64	1.50	0.1-0.5	1	-8	2	Negligible	3
Cop.3	280	22.44	1.33	0.5-2.5	1	-15	3	Moderate	14	Mok.6	70	2.44	0.17	0.5-2.5	1	-17	5	Large	20
Cop.4	280	9.98	1.33	0.5-2.5	1	-18	3	Large	34.7	Mok.8	140	25.64	1.50	0.1-0.5	1	-8	2	Negligible	2.3
Cop.5	280	9.98	1.33	0.5-2.5	1	-18	3	Extensive	76.1	Mok.9	70	2.44	0.17	0.5-2.5	1	-17	5	Extensive	180
Cop.6	280	9.98	1.33	0.5-2.5	1	-25	3	Extensive	47.1	Moo.1	18	12.47	0.50	2-5	1	-9	3	Minor	0.3
Cop.7	280	9.98	1.33	0.5-2.5	1	-18	3	Moderate	66.1	Moo.2	18	12.47	0.50	2-5	1	-9	3	Negligible	0.2
Cop.8	280	21.20	1.33	0.5-2.5	1	-8	3	Moderate	95	Moo.3	18	12.47	0.50	2-5	1	-18	5	Moderate	27
Cop.9	280	9.98	1.33	0.5-2.5	1	-18	3	Large	168	Moo.4	18	12.47	0.50	2-5	1	-18	5	Minor	17
Dar.1	140	19.17	2.00	1-2	0.84	-13	4	Minor	18	Osp.1	40	18.32	1.25	0.1-0.5	1.15	-13	4	Negligible	1.6
Dar.2	140	19.17	2.00	1-2	0.84	-13	4	Moderate	18	Osp.2	30	3.66	0.86	0.5-2.5	1.15	-20	4	Moderate	13.2
Dar.3	140	19.17	2.00	1-2	0.84	-13	4	Moderate	18	Osp.3	40	18.32	1.25	0.1-0.5	1.15	-13	4	Minor	1.9
Dar.5	140	16.21	2.00	1-2	1	-5	4	Minor	9	Osp.4	30	3.66	0.86	0.5-2.5	1.15	-13	4	Moderate	13.2
Dar.6	140	22.12	1.50	2-5	1	-	5	Large	3.5	Osp.5	40	18.32	1.25	0.1-0.5	1.15	-18	4	Negligible	2.2
Flo.1	200	21.98	2.50	0.1-0.5	0.5	-25	-	Moderate	120	Pin.1	70	2.95	1.50	2-5	1	-10	4	Minor	4.8
Flo.2	100	1.50	1.33	0.1-0.5	0.5	-25	-	Moderate	120	Pin.2	70	4.99	0.75	2-5	0.6	-14	4	Moderate	4.8
Gar.1	13	20.00	1.00	0.1-0.5	0.44	-5	3	Negligible	1	Pin.3	70	17.70	0.60	5	0.75	-10	5	Moderate	0.4
Gar.2	13	20.00	1.00	0.1-0.5	0.44	-8	-	Minor	14	Pin.4	70	9.98	0.75	2-5	1	-18	4	Large	28
Gar.4	13	20.00	1.00	0.1-0.5	0.44	-5	3	Negligible	1.3	Row.1	280	17.46	1.00	0	1	-10	4	Negligible	13
Gar.5	13	20.00	1.00	0.1-0.5	0.44	-8	-	Minor	20	Row.2	280	25.36	1.00	1-2	1	-21	4	Moderate	13
Goe.1	140	20.96	1.00	<0.1	1	-8	-	Minor	90	Spl.1	140	25.36	1.50	0-1	0.5	-3	4	Moderate	120
Goe.2	35	4.49	0.17	>10	1	-8	-	Moderate	90	Spl.2	140	37.56	1.50	0-1	0.6	-3	4	Negligible	120
Goe.3	140	20.96	1.00	<0.1	1	-8	-	Negligible	50	Spl.3	80	10.87	0.75	1-2	0.55	-3	4	Minor	24
Goe.4	35	4.49	0.17	>10	1	-8	-	Moderate	90	Way.1	140	28.99	1.50	0.1	1	-13	4	Negligible	8.6
Goe.5	35	4.49	0.17	>10	1	-8	-	Moderate	22	Way.2	140	28.99	1.50	0.1	0.8	-13	4	Negligible	8.6
Haa.1	13	5.90	0.33	2.5-10	0.48	-15	4	Large	3.6	Way.3	140	17.46	0.75	0.1	0.7	-13	4	Moderate	8.6
Haa.2	13	5.90	0.33	2.5-10	0.48	-15	4	Moderate	0.3	Way.4	35	4.99	0.25	-	1	-18	-	Moderate	22
Haa.3	13	5.90	0.33	2.5-10	0.48	-15	4	Large	3.9										

Appendix F. Summary of V_b calculating according to the three used methods

ID	Method 1					Method 2						Method 3									
	Joint spacing of the considered joint sets			Sa	V_b	Joint spacing of the considered joint sets			Y_1	Y_2	Y_3	V_b	a_3	a_1	β	Joint spacing of the considered joint sets				J_v	V_b
	Joint set 1	Joint set 2	Joint set 3			Joint set 1	Joint set 2	Joint set 3								Joint set 1	Joint set 2	Joint set 3	Joint set 4		
Ant. 1	0.75	1	1.5	1.08	1.2714	0.75	1	3.5	47	36	76	3.7964	1.5	3.5	23.0	0.75	1	1.5	3.5	3.29	0.6484
App.1	0.4	0.13	0.4	0.29	0.0252	0.4	2	0.4	59	89	86	0.3743	0.4	2	21.4	0.4	2	0.4	-	5.50	0.1286
App.2	0.4	0.06	0.4	0.27	0.0197	0.4	2	0.4	59	89	86	0.3743	0.4	2	21.4	0.4	2	0.4	-	5.50	0.1286
Bro.1	0.35	2.5	6	2.95	25.6724	0.35	2.5	6	97	80	142	8.7240	2.5	6	22.9	0.35	2.5	6	-	3.42	0.5710
Bro.2	0.35	4	1.75	2.03	8.4067	0.35	4	1.75	30	78	85	2.6188	4	6	24.6	0.35	6	4	1.75	3.85	0.4339
Bro.3	1.5	4.5	0.06	2.02	8.2424	1.5	4.5	0.06	78	80	65	0.4639	1.5	4.5	22.3	1.5	4.5	0.06	-	17.56	0.0041
Bro.4	1.2	0.75	10	3.98	63.2033	1.2	0.75	10	26	80	75	21.5827	1.2	10	20.8	1.2	0.75	10	-	2.27	1.7895
Bro.7	1.75	3	10	4.83	112.9120	1.75	0.4	0.7	90	85	60	0.5680	0.7	1.75	22.8	1.75	0.4	0.7	-	4.50	0.2502
Bur.1	1.5	6.5	0.65	2.60	17.5760	1.5	1.75	10	76	75	24	68.8602	1.75	10	21.2	1.5	1.75	10	-	1.34	8.8590
Bur.2	1.5	6.5	0.65	2.60	17.5760	1.5	3	10	76	75	77	49.7724	10	10	27.0	1.5	3	10	10	1.20	15.6250
Bur.3	0.65	1.1	1.35	0.95	0.8574	0.65	6.5	0.65	75	77	83	2.9398	0.65	6.5	20.7	0.65	6.5	0.65	-	3.23	0.6138
Bur.4	0.65	1.1	1.35	0.95	0.8574	0.65	6.5	0.65	75	77	83	2.9398	0.65	6.5	20.7	0.65	6.5	0.65	-	3.23	0.6138
Cat.1	0.4	1.1	1.35	0.95	0.8574	0.4	1.1	1.35	87	38	76	0.9957	1.1	1.35	25.7	0.4	1.1	1.35	-	4.15	0.3597
Cat.2	0.4	1.3	1.3	1.30	2.1970	0.4	1.1	1.35	87	38	76	0.9957	1.1	1.35	25.7	0.4	1.1	1.35	-	4.15	0.3597
Cat.3	0.4	1.3	1.3	1.53	3.6050	0.4	1.1	1.35	87	38	76	0.9957	1.1	1.35	25.7	0.4	1.1	1.35	-	4.15	0.3597
Cop.1	1.3	1.3	1.3	1.30	2.1970	1.3	1.3	1.3	80	55	99	2.3092	1.3	2	24.5	1.3	1.3	2	1.3	2.81	1.1092
Cop.10	2	1.3	1.3	1.30	2.1970	2	1.3	1.3	80	55	99	3.5526	2	2	27.0	2	1.3	2	1.3	2.54	1.6506
Ant. 1	0.75	1	1.5	1.08	1.2714	0.75	1	3.5	47	36	76	3.7964	1.5	3.5	23.0	0.75	1	1.5	3.5	3.29	0.6484
App.1	0.4	0.13	0.4	0.29	0.0252	0.4	2	0.4	59	89	86	0.3743	0.4	2	21.4	0.4	2	0.4	-	5.50	0.1286
App.2	0.4	0.06	0.4	0.27	0.0197	0.4	2	0.4	59	89	86	0.3743	0.4	2	21.4	0.4	2	0.4	-	5.50	0.1286
Cop.11	1.3	1.3	1.3	1.30	2.1970	1.3	1.3	1.3	80	55	99	2.3181	1.3	2	24.5	1.3	1.3	2	1.3	2.81	1.1092
Cop.12	1.3	0.3	0.4	0.67	0.2963	1.3	1.3	1.3	80	55	99	2.3181	1.3	2	24.5	1.3	1.3	2	1.3	2.81	1.1092
Cop.13	1.3	0.55	1.6	1.15	1.5209	1.3	1.3	1.3	80	55	99	2.3181	1.3	2	24.5	1.3	1.3	2	1.3	2.81	1.1092
Cop.2	1.3	1.3	1.3	1.53	3.6050	1.3	1.3	1.3	80	55	99	2.3092	1.3	2	24.5	1.3	1.3	2	1.3	2.81	1.1092
Cop.3	1.3	1.3	1.3	1.53	3.6050	1.3	1.3	1.3	80	55	99	2.3092	1.3	2	24.5	1.3	1.3	2	1.3	2.81	1.1092
Cop.4	2	1.3	1.3	1.53	3.6050	2	1.3	1.3	80	55	99	3.5526	2	2	27.0	2	1.3	2	1.3	2.54	1.6506
Cop.5	2	1.3	1.3	1.53	3.6050	2	1.3	1.3	80	55	99	3.5526	2	2	27.0	2	1.3	2	1.3	2.54	1.6506
Cop.6	2	2	1.3	1.77	5.5140	2	1.3	1.3	80	55	99	3.5526	2	2	27.0	2	1.3	2	1.3	2.54	1.6506
Cop.7	2	1.3	1.3	1.53	3.6050	2	1.3	1.3	80	55	99	3.5526	2	2	27.0	2	1.3	2	1.3	2.54	1.6506
Cop.8	2	1.3	1.3	0.94	0.8306	2	2	1.3	55	45	102	5.5188	2	2	27.0	2	2	2	1.3	2.27	2.3106
Cop.9	2	1.3	1.3	1.13	1.4557	2	1.3	1.3	80	55	99	3.5526	2	2	27.0	2	1.3	2	1.3	2.54	1.6506
Dar.1	0.22	0.55	0.3	0.47	0.1016	0.22	0.3	0.4	97	80	45	0.0382	0.3	0.4	25.2	0.22	0.3	0.4	-	10.38	0.0226
Dar.2	0.8	0.8	0.8	0.80	0.5120	0.8	0.55	1.6	83	96	44	1.0267	0.8	1.6	23.5	0.8	0.55	1.6	-	3.69	0.4665
Dar.3	0.55	1.5	0.8	0.98	0.9508	0.55	0.55	0.3	65	48	61	0.1396	0.55	0.8	24.8	0.8	0.55	0.55	0.3	8.22	0.0447
Dar.5	0.8	0.7	0.7	0.60	0.2160	0.8	0.8	0.8	51	113	89	0.7158	0.8	0.8	27.0	0.8	0.8	0.8	0.8	6.25	0.1106
Dar.6	0.65	0.7	0.5	0.53	0.1517	0.65	1.5	0.8	128	77	101	1.0349	0.8	1.5	23.7	0.65	1.5	0.8	-	3.46	0.5754
Flo.1	0.4	1.3	1.3	1.00	1.0000	0.4	0.13	0.4	60	83	135	0.0342	0.4	0.4	27.0	0.4	0.13	0.4	-	12.69	0.0132
Flo.2	0.4	1.3	1.3	1.00	1.0000	0.4	0.06	0.4	60	83	135	0.0158	0.4	0.4	27.0	0.4	0.06	0.4	-	21.67	0.0027
Goe.1	0.4	1.3	1.3	1.00	1.0000	0.4	1.3	1.3	66	98	90	0.7472	1.3	1.3	27.0	0.4	1.3	1.3	-	4.04	0.4099
Goe.2	0.4	1.3	1.3	1.00	1.0000	0.4	1.3	1.3	66	98	90	0.7472	1.3	1.3	27.0	0.4	1.3	1.3	-	4.04	0.4099
Goe.3	0.4	1.3	1.3	1.00	1.0000	0.4	1.3	1.3	66	98	90	0.7472	1.3	1.3	27.0	0.4	1.3	1.3	-	4.04	0.4099
Goe.4	0.4	0.06	0.06	0.06	0.0002	0.4	1.3	1.3	66	70	90	0.7875	1.3	1.3	27.0	0.4	1.3	1.3	-	4.04	0.4099
Goe.5	0.4	0.06	0.06	0.06	0.0002	0.4	1.3	1.3	66	70	90	0.7875	1.3	1.3	27.0	0.4	1.3	1.3	-	4.04	0.4099
Haa.1	0.06	0.06	0.06	0.06	0.0002	0.06	0.06	0.06	102	55	109	0.0003	0.06	0.06	27.0	0.06	0.06	0.06	-	50.00	0.0002
Haa.2	0.06	0.06	0.06	0.06	0.0002	0.06	0.06	0.06	102	55	109	0.0003	0.06	0.06	27.0	0.06	0.06	0.06	-	50.00	0.0002
Haa.3	0.06	0.06	0.4	0.39	0.0578	0.06	0.06	0.06	102	55	109	0.0003	0.06	0.06	27.0	0.06	0.06	0.06	-	50.00	0.0002
Haa.4	0.06	1.3	0.4	0.80	0.5120	0.06	0.06	0.06	102	55	109	0.0003	0.06	0.06	27.0	0.06	0.06	0.06	-	50.00	0.0002

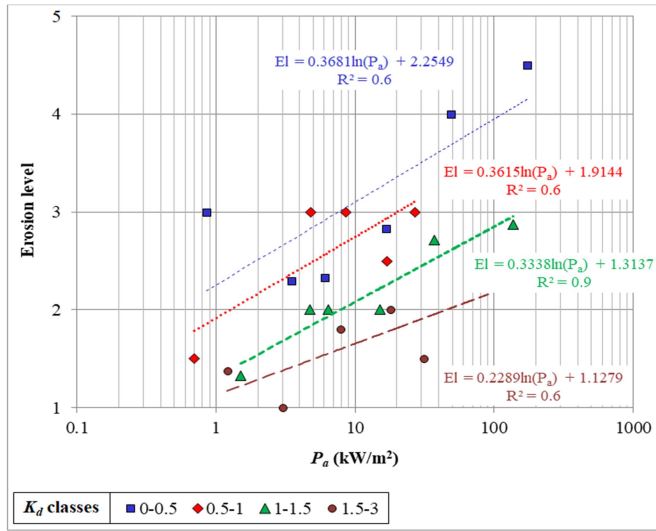
ID	Method 1					Method 2						Method 3									
	Joint spacing of the considered joint sets			Sa	V_b	Joint spacing of the considered joint sets			Y_1	Y_2	Y_3	V_b	a_3	a_1	β	Joint spacing of the considered joint sets				J_v	V_b
	Joint set 1	Joint set 2	Joint set 3			Joint set 1	Joint set 2	Joint set 3								Joint set 1	Joint set 2	Joint set 3	Joint set 4		
Har.1	0.7	0.4	1.15	0.65	0.2746	0.7	0.7	1.25	94	37	90	0.6140	0.7	1.25	23.9	0.7	0.7	0.7	1.25	5.09	0.1818
Har.2	0.7	8	1.5	3.30	35.9370	0.7	0.7	0.5	94	90	90	0.2456	0.7	0.7	27.0	0.7	0.7	0.5	-	4.86	0.2356
Hart.1	0.4	1.3	0.4	0.70	0.3430	0.4	0.06	0.4	80	84	85	0.0113	0.4	1.3	22.1	0.4	0.06	1.3	0.4	22.44	0.0020
Hart.2	0.4	1.3	1.3	1.30	2.1970	0.4	1.3	0.4	80	84	85	0.2448	1.3	1.3	27.0	0.4	1.3	1.3	0.4	6.54	0.0966
Hart.3	0.4	1.3	1.3	1.30	2.1970	0.4	1.3	0.4	80	84	85	0.2448	1.3	1.3	27.0	0.4	1.3	1.3	0.4	6.54	0.0966
Kam.1	1.3	0.4	0.4	0.40	0.0640	1.3	1.3	1.3	73	157	88	2.2081	1.3	1.3	27.0	1.3	1.3	1.3	1.3	3.08	0.9269
Kam.2	1.3	0.4	0.4	0.40	0.0640	1.3	1.3	1.3	73	157	88	2.2081	1.3	1.3	27.0	1.3	1.3	1.3	1.3	3.08	0.9269
Kam.3	0.4	0.13	0.4	0.31	0.0298	0.4	0.4	0.4	73	85	157	0.1719	0.4	1.3	22.1	0.4	0.4	0.4	1.3	8.27	0.0392
Kam.4	0.4	0.4	0.4	0.70	0.3430	0.4	0.4	0.4	73	85	157	0.1719	0.4	1.3	22.1	0.4	0.4	0.4	1.3	8.27	0.0392
Kam.5	0.4	0.4	0.4	0.70	0.3430	0.4	0.13	0.4	73	85	157	0.0559	1.3	0.13	90.0	0.4	0.13	0.4	1.3	13.46	0.0369
Kli.1	1.3	0.4	0.4	0.70	0.3430	1.3	0.4	0.4	82	151	63	0.2755	1.3	1.3	27.0	1.3	1.3	0.4	0.4	6.54	0.0966
Kli.2	1.3	0.4	0.4	0.70	0.3430	1.3	0.4	0.4	82	151	63	0.2755	1.3	1.3	27.0	1.3	1.3	0.4	0.4	6.54	0.0966
Kli.3	1.3	0.4	0.4	0.70	0.3430	1.3	0.4	0.4	82	151	63	0.2755	1.3	1.3	27.0	1.3	1.3	0.4	0.4	6.54	0.0966
Kli.4	1.3	1.3	1.3	1.17	1.5880	1.3	0.4	0.4	82	151	63	0.2755	1.3	1.3	27.0	1.3	1.3	0.4	0.4	6.54	0.0966
Kli.5	1.3	1.3	0.4	1.00	1.0000	1.3	0.4	0.4	82	151	63	0.2755	1.3	1.3	27.0	1.3	1.3	0.4	0.4	6.54	0.0966
Kun.1	0.9	8	1.5	3.30	35.9370	0.9	0.4	1.15	71	15	79	1.7234	0.9	1.15	25.4	0.9	0.4	1.15	-	4.48	0.2832
Mok.1	1.3	1.3	1.3	1.30	2.1970	1.3	1.3	1.3	90	80	80	2.2653	1.3	1.3	27.0	1.3	1.3	1.3	-	2.31	2.1970
Mok.2	0.4	1.3	1.3	1.30	2.1970	0.4	1.3	0.4	90	80	80	0.2145	0.4	1.3	22.1	0.4	1.3	0.4	-	5.77	0.1154
Mok.4	1.3	0.4	0.4	0.40	0.0640	1.3	1.3	1.3	90	80	80	2.2653	1.3	1.3	27.0	1.3	1.3	1.3	-	2.31	2.1970
Mok.5	1.3	1.3	1.3	1.30	2.1970	1.3	1.3	1.3	90	80	80	2.2653	1.3	1.3	27.0	1.3	1.3	1.3	-	2.31	2.1970
Mok.6	0.4	0.4	0.4	0.40	0.0640	0.4	0.4	0.4	90	80	80	0.0660	0.4	0.4	27.0	0.4	0.4	0.4	-	7.50	0.0640
Mok.8	1.3	0.4	0.13	0.31	0.0298	1.3	1.3	1.3	90	80	80	2.2653	1.3	1.3	27.0	1.3	1.3	1.3	-	2.31	2.1970
Mok.9	0.4	0.4	0.13	0.31	0.0298	0.4	0.4	0.4	90	80	80	0.0660	0.4	0.4	27.0	0.4	0.4	0.4	-	7.50	0.0640
Moo.1	0.4	8	1.5	3.30	35.9370	0.4	8	1.5	96	86	81	5.4844	8	20	22.8	0.4	8	20	1.5	3.34	0.6110
Moo.2	0.4	8	1.5	3.30	35.9370	0.4	8	1.5	96	86	81	5.4844	8	20	22.8	0.4	8	20	1.5	3.34	0.6110
Moo.3	0.4	0.2	0.5	0.37	0.0493	0.4	8	1.5	96	86	81	5.4844	8	15	23.7	0.4	8	15	1.5	3.36	0.6266
Moo.4	0.4	0.2	0.5	0.37	0.0493	0.4	8	1.5	96	86	81	5.4844	8	15	23.7	0.4	8	15	1.5	3.36	0.6266
Osp.1	0.4	0.4	0.13	0.31	0.0298	0.4	0.4	0.13	91	110	90	0.0221	0.4	0.4	27.0	0.4	0.4	0.13	-	12.69	0.0132
Osp.2	0.4	0.4	0.13	0.31	0.0298	0.4	0.4	0.13	91	110	90	0.0221	0.4	0.4	27.0	0.4	0.4	0.13	-	12.69	0.0132
Osp.3	0.4	0.4	0.13	0.31	0.0298	0.4	0.4	0.13	91	110	90	0.0221	0.4	0.4	27.0	0.4	0.4	0.13	-	12.69	0.0132
Osp.4	0.4	-	-	-	-	0.4	0.4	0.13	91	110	90	0.0221	0.4	0.4	27.0	0.4	0.4	0.13	-	12.69	0.0132
Osp.5	0.4	-	-	-	-	0.4	0.4	0.13	91	110	90	0.0221	0.4	0.4	27.0	0.4	0.4	0.13	-	12.69	0.0132
Pin.1	0.07	1	0.5	0.62	0.2345	0.6	0.07	0.2	90	90	127	0.0113	0.6	1	24.2	0.6	0.07	0.2	0.5	23.00	0.0020
Pin.2	0.07	0.2	0.5	0.35	0.0429	0.6	0.07	0.2	87	82	127	0.0114	0.6	1	24.2	0.6	0.07	0.2	0.5	23.00	0.0020
Pin.3	0.35	0.1	0.15	0.18	0.0062	0.35	1	0.5	52	94	120	0.2571	0.5	1	23.5	0.35	1	0.5	-	5.86	0.1170
Pin.4	0.35	0.55	0.4	3.65	48.6271	0.35	0.2	1	55	101	111	0.1162	0.5	1	23.5	0.35	0.2	0.5	1	10.86	0.0184
Row.1	0.3	3	0.45	1.20	1.7280	0.3	0.55	0.4	45	110	80	0.0910	0.55	10	20.4	10	0.3	0.55	0.4	7.75	0.0438
Row.2	10	0.2	0.45	0.48	0.1129	10	1	0.4	101	56	67	5.3397	1	10	20.7	10	1	0.4	-	3.60	0.4437
Spl.3	0.15	1	0.4	0.88	0.6892	0.15	0.1	0.15	64	56	71	0.0032	0.15	0.15	27.0	0.15	0.1	0.15	-	23.33	0.0021
Way.1	0.8	0.45	0.45	0.36	0.0480	0.8	3	0.45	116	89	78	1.2286	0.8	3	21.9	0.8	3	0.45	-	3.81	0.3968
Way.2	1.25	2	0.4	0.80	0.5120	1.25	0.2	0.45	66	65	65	0.1499	0.45	1.25	22.5	1.25	0.2	0.45	-	8.02	0.0436
Way.3	0.19	2	0.4	0.80	0.5120	0.19	0.45	0.45	94	78	50	0.0515	0.45	2	21.6	0.19	0.45	0.45	2	10.21	0.0203

Appendix G. Summary of the data used in this study (Chapter 5)

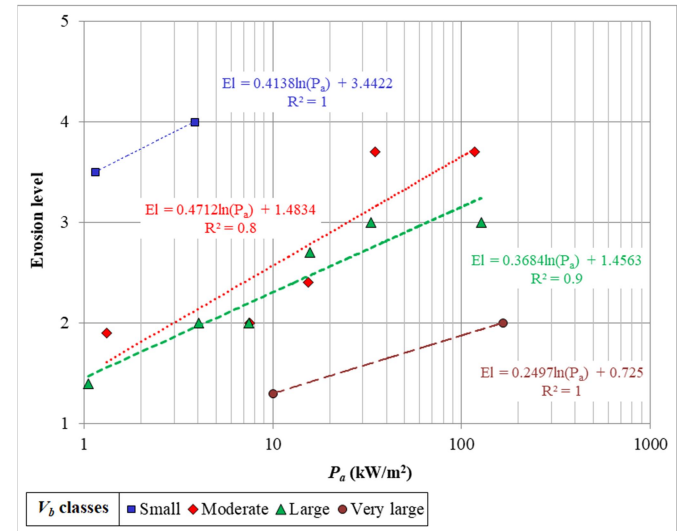
ID	GSI	Rock type	UCS (MPa)	MR	E_i (GPa)	E_{rm} (GPa)	N	eGSI	RMEI	P_a (kW/m ²)	Observed scour
Ant. 1	55	Conglomerate	35.00	350	12.25	1.81	868	47	1188	1.7	Minor
Ant. 2	55	Conglomerate	35.00	350	12.25	1.81	575	47	243	0.8	Negligible
Ant. 3	55	Conglomerate	35.00	350	12.25	1.81	868	47	1440	0.7	Minor
Ant. 4	60	Conglomerate	35.00	350	12.25	2.46	1903	42	1080	6.3	Moderate
App.1	50	Sandstone	50.00	275	13.75	1.48	206	45	648	2.6	Negligible
App.2	50	Sandstone	50.00	275	13.75	1.48	206	43	648	15	Minor
Bro.1	70	Granite	100.00	425	42.50	14.35	3721	67	1440	6.4	Minor
Bro.2	70	Granite	100.00	425	42.50	14.35	2756	67	1296	28	Moderate
Bro.3	70	Granite	100.00	425	42.50	14.35	2233	55	1152	42	Moderate
Bro.4	70	Granite	100.00	425	42.50	14.35	2233	53	1080	56	Moderate
Bro.5	75	Granite	100.00	425	42.50	17.45	5629	65	432	28	Negligible
Bro.6	80	Granite	100.00	425	42.50	20.28	7003	77	144	37	Minor
Bro.7	70	Granite	100.00	425	42.50	14.35	2425	55	1440	56	Large
Bur.1	85	Ignimbrite	280.00	400	112.00	59.67	11417	82	252	165	Negligible
Bur.2	85	Ignimbrite	280.00	400	112.00	59.67	7848	80	288	165	Negligible
Bur.3	70	Ignimbrite	280.00	400	112.00	37.81	6089	60	972	165	Moderate
Bur.4	50	Ignimbrite	280.00	400	112.00	12.02	3653	40	1890	165	Large
Cat.1	85	Dolerite	140.00	350	49.00	26.11	3706	72	567	60	Minor
Cat.2	85	Dolerite	140.00	350	49.00	26.11	3706	72	126	60	Negligible
Cat.3	85	Dolerite	140.00	350	49.00	26.11	3706	72	567	60	Large
Cop.1	50	Granite	280.00	425	119.00	12.77	724	35	1620	5.7	Moderate
Cop.10	50	Granite	280.00	425	119.00	12.77	3721	25	1755	650	Extensive
Cop.11	50	Granite	280.00	425	119.00	12.77	724	35	1620	10	Minor
Cop.12	80	Granite	280.00	425	119.00	56.79	8372	70	1350	97	Moderate
Cop.13	80	Granite	280.00	425	119.00	56.79	8372	65	1350	145	Moderate
Cop.2	80	Granite	280.00	425	119.00	56.79	8372	70	1350	4.7	Minor
Cop.3	80	Granite	280.00	425	119.00	56.79	8372	65	1350	14	Moderate
Cop.4	50	Granite	280.00	425	119.00	12.77	3721	32	1755	34.7	Large
Cop.5	50	Granite	280.00	425	119.00	12.77	3721	32	1755	76.1	Extensive
Cop.6	50	Granite	280.00	425	119.00	12.77	3721	25	1755	47.1	Extensive
Cop.7	50	Granite	280.00	425	119.00	12.77	3721	32	1755	66.1	Moderate
Cop.8	75	Granite	280.00	425	119.00	48.86	7906	67	1485	95	Moderate
Cop.9	50	Granite	280.00	425	119.00	12.77	3721	32	1755	168	Large
Dar.1	65	Gneiss	140.00	525	73.50	19.51	4515	52	504	18	Minor
Dar.2	65	Gneiss	140.00	525	73.50	19.51	4515	52	1080	18	Moderate
Dar.3	65	Gneiss	140.00	525	73.50	19.51	4515	52	972	18	Moderate
Dar.5	65	Gneiss	140.00	525	73.50	19.51	4535	60	648	9	Minor
Dar.6	75	Gneiss	140.00	525	73.50	30.18	4651	-	2700	3.5	Large
Flo.1	68	Tillite	200.00	375	75.00	23.12	5495	43	-	120	Moderate
Flo.2	38	Tillite	100.00	375	37.50	1.96	100	13	-	120	Moderate
Gar.1	30	Schist	12.61	675	8.51	0.31	106	25	405	1	Negligible
Gar.2	30	Schist	12.61	675	8.51	0.31	106	23	-	14	Minor
Gar.4	30	Schist	12.61	675	8.51	0.31	106	25	405	1.3	Negligible
Gar.5	30	Schist	12.61	675	8.51	0.31	106	23	-	20	Minor
Goe.1	76	Tillite	140.00	375	52.50	22.29	2934	69	-	90	Minor
Goe.2	38	Tillite	35.00	375	13.13	0.68	26	31	-	90	Moderate
Goe.3	76	Tillite	140.00	375	52.50	22.29	2934	69	-	50	Negligible
Goe.4	38	Tillite	35.00	375	13.13	0.68	26	31	-	90	Moderate
Goe.5	38	Tillite	35.00	375	13.13	0.68	26	31	-	22	Moderate
Haa.1	20	Sandstone	12.61	275	3.47	0.09	11	5	3240	3.6	Large
Haa.2	55	Conglomerate	35.00	350	12.25	1.81	11	5	-	0.3	Moderate

ID	GSI	Rock type	UCS (MPa)	MR	E_i (GPa)	E_{rm} (GPa)	N	$eGSI$	RMEI	P_a (kW/m ²)	Observed scour
Haa.3	55	Conglomerate	35.00	350	12.25	1.81	11	5	3240	3.9	Large
Haa.4	20	Sandstone	12.61	275	3.47	0.09	11	5	-	2	Large
Har.1	20	Sandstone	12.61	275	3.47	0.09	1757	60	1296	0.6	Minor
Har.2	20	Sandstone	12.61	275	3.47	0.09	2283	65	1296	1	Minor
Har.3	65	Dolerite	140.00	350	49.00	13.00	4269	60	504	1	Minor
Har.4	70	Dolerite	140.00	350	49.00	16.54	5024	70	1980	56	Minor
Hart.1	65	Dolerite	140.00	350	49.00	13.00	3772	75	-	44	Negligible
Hart.2	80	Dolerite	140.00	350	49.00	23.38	36	31	-	50	Moderate
Hart.3	80	Quartzite	180.00	375	67.50	32.21	3772	75	-	18	Negligible
Kam.1	46	Quartzite	15.76	375	5.91	0.49	369	67	1008	4.5	Minor
Kam.2	80	Quartzite	180.00	375	67.50	32.21	6024	73	252	27	Negligible
Kam.3	74	Sandstone	140.00	275	38.50	15.26	61	31	1800	27	Moderate
Kam.4	80	Sandstone	140.00	275	38.50	18.37	61	13	-	49	Large
Kam.5	38	Sandstone	30.00	275	8.25	0.43	81	32	1080	14	Minor
Kli.1	38	Sandstone	30.00	275	8.25	0.43	11002	75	864	1.2	Negligible
Kli.2	37	Sandstone	30.00	275	8.25	0.41	6.1	23	1728	6	Minor
Kli.3	80	Dolerite	200.00	350	70.00	33.41	6.1	23	1728	11.4	Moderate
Kli.4	35	Dolerite	10.51	350	3.68	0.16	11002	73	864	6.5	Minor
Kli.5	35	Dolerite	10.51	350	3.68	0.16	6.1	23	1728	6.5	Minor
Kun.1	80	Dolerite	200.00	350	70.00	33.41	6038	67	594	35	Minor
Mac.1	35	Dolerite	10.51	350	3.68	0.16	128	27	1053	1.1	Minor
Mac.2	75	Quartzite	140.00	375	52.50	21.55	15	7	378	1.1	Minor
Mac.3	40	Greywacke	17.70	350	6.20	0.36	61	27	378	2.6	Minor
Mok.1	20	Greywacke	8.81	350	3.09	0.08	5385	67	630	0.6	Negligible
Mok.2	40	Greywacke	8.81	350	3.09	0.18	29	19	2025	1.4	Moderate
Mok.4	74	Sandstone	140.00	275	38.50	15.26	5385	67	630	1.3	Negligible
Mok.5	35	Sandstone	70.00	275	19.25	0.86	5385	67	630	3	Negligible
Mok.6	74	Sandstone	140.00	275	38.50	15.26	29	19	2025	20	Large
Mok.8	74	Sandstone	140.00	275	38.50	15.26	5385	67	630	2.3	Negligible
Mok.9	35	Sandstone	70.00	275	19.25	0.86	29	19	2025	180	Extensive
Moo.1	74	Sandstone	140.00	275	38.50	15.26	110	51	594	0.3	Minor
Moo.2	35	Sandstone	70.00	275	19.25	0.86	110	51	594	0.2	Negligible
Moo.3	60	Sandstone	17.70	275	4.87	0.98	110	42	2925	27	Moderate
Moo.4	60	Sandstone	17.70	275	4.87	0.98	110	42	2925	17	Minor
Osp.1	60	Sandstone	17.70	275	4.87	0.98	1053	46	972	1.6	Negligible
Osp.2	60	Sandstone	17.70	275	4.87	0.98	108	25	1404	13.2	Moderate
Osp.3	58	Sandstone	40.00	275	11.00	1.96	1053	46	972	1.9	Minor
Osp.4	45	Sandstone	30.00	275	8.25	0.65	108	33	1404	13.2	Moderate
Osp.5	58	Sandstone	40.00	275	11.00	1.96	1053	41	972	2.2	Negligible
Pin.1	45	Sandstone	30.00	275	8.25	0.65	310	45	1440	4.8	Minor
Pin.2	58	Sandstone	40.00	275	11.00	1.96	157	31	1440	4.8	Moderate
Pin.3	55	Rhyolitic	70.00	400	28.00	4.13	558	45	2160	0.4	Moderate
Pin.4	45	Rhyolitic	70.00	400	28.00	2.19	523	32	2520	28	Large
Row.1	55	Rhyolitic	70.00	400	28.00	4.13	4883	65	162	13	Negligible
Row.2	50	Rhyolitic	70.00	400	28.00	3.00	7104	44	936	13	Moderate
Spl.1	75	Quartzite	280.00	375	105.00	43.11	2664	72	864	120	Moderate
Spl.2	65	Quartzite	280.00	375	105.00	27.87	4729	77	864	120	Negligible
Spl.3	75	Greywacke	140.00	350	49.00	20.12	359	57	1080	24	Minor
Way.1	80	Greywacke	140.00	350	49.00	23.38	6089	67	1080	8.6	Negligible
Way.2	60	Greywacke	80.00	350	28.00	5.62	4871	67	1404	8.6	Negligible
Way.3	80	Dolerite	140.00	350	49.00	23.38	1282	57	1728	8.6	Moderate
Way.4	80	Dolerite	140.00	350	49.00	23.38	44	2	-	22	Moderate

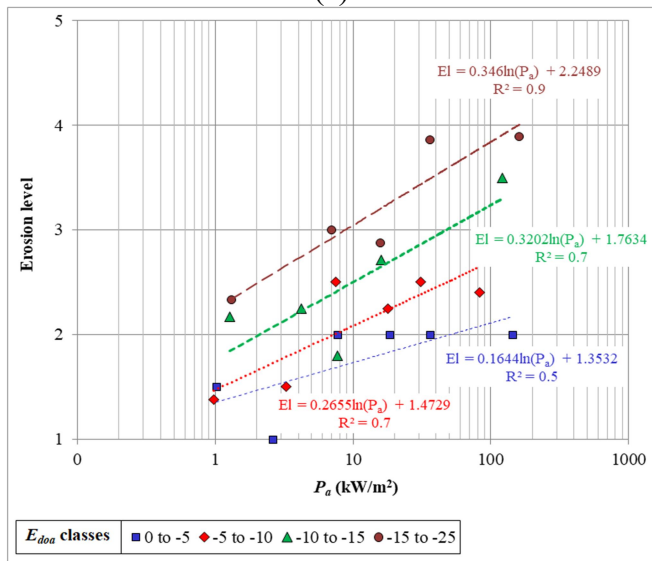
Appendix H. Sensitivity curves to erodibility based on (a) K_d , (b) V_b , (c) E_{doa} , (d) $NPES$ classifications (Boumaiza et al., 2019b)



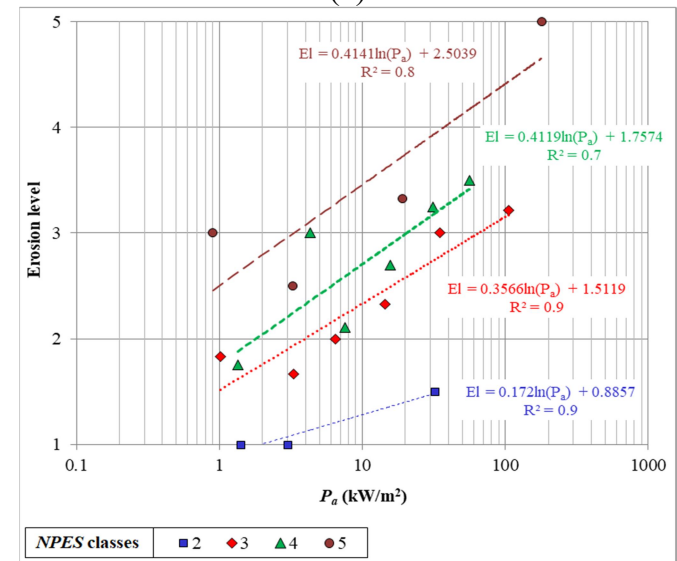
(a)



(b)



(c)



(d)